A hand is shown holding a large, clear, rectangular glass block. The block is held in a way that its three-dimensional structure is emphasized. The background is a solid teal color. The text is overlaid on the image.

Unveiling the third dimension of glass

Solid cast glass components
and assemblies for structural
applications

Faidra Oikonomopoulou

Unveiling the third dimension of glass

Solid cast glass components
and assemblies for structural
applications

Faidra Oikonomopoulou



A+BE | Architecture and the Built Environment | TU Delft BK

19#09

Design | Sirene Ontwerpers, Rotterdam

ISBN 978-94-6366-220-8

ISSN 2212-3202

© 2019 Faidra (Phaedra) Oikonomopoulou

Digital version freely available at abe.tudelft.nl

All rights reserved. No part of the material protected by this copyright notice may be reproduced or utilized in any form or by any means, electronic or mechanical, including photocopying, recording or by any information storage and retrieval system, without written permission from the author.

Unless otherwise specified, all the photographs in this thesis were taken by the author. For the use of illustrations effort has been made to ask permission for the legal owners as far as possible. We apologize for those cases in which we did not succeed. These legal owners are kindly requested to contact the publisher.

Unveiling the third dimension of glass

Solid cast glass components and assemblies for structural applications

Dissertation

for the purpose of obtaining the degree of doctor
at Delft University of Technology
by the authority of the Rector Magnificus, prof.dr.ir. T.H.J.J. van der Hagen
chair of the Board for Doctorates
to be defended publicly on
Monday, 25th of November 2019 at 15:00 o'clock

by

Faidra [Phaedra] OIKONOMOPOULOU
Master of Science in Architecture, Urbanism and Building Sciences, Delft University
of Technology, the Netherlands
Diploma of Architect Engineer, National Technical University of Athens, Greece

born in Athens, Greece

This dissertation has been approved by the promotor.

Composition of the doctoral committee:

Rector Magnificus	chairperson
Prof. ir. R. Nijssse	Delft University of Technology, promotor
Dr. ir. F. A. Veer	Delft University of Technology, promotor

Independent members:

Prof. Mr. J. D. O' Callaghan	Delft University of Technology
Prof. Dr. P. J. S. Cruz	University of Minho
Prof. Dr. ir. P. C. Louter	Technische Universität Dresden
Dr. E. Karana	Delft University of Technology
Dr. M. Prassas	Corning Incorporated
Prof. Dr. ir. A.A.J.F. van den Dobbelsteen	Delft University of Technology, reserve member

The experimental work and prototyping presented in this research has been partially funded by the *Crystal Houses Façade* project (2014 - 2016) and by two *4TU.Bouw Lighthouse* research grants (2016, 2017) awarded by the *4TU.Bouw Center of Excellence for the Built Environment*.

*To my parents,
Amalia and Spyros*

Preface

Glass!

Immediately the words *transparent*, *fragile* and *brittle* pop into one's mind. Indeed, transparency and brittleness are the two most characteristic properties of glass. Yet, what most people are unaware of, is that glass is also a *strong* material. Its mechanical properties are superior to those of (unreinforced) concrete; its compression strength is actually higher than that of many types of structural steel. Then, why don't we use it for load-bearing applications? In fact, we have just started discovering the structural potential of this intriguing material. Over the last decades, more and more full-glass structures are realized in the built environment. Due to the prevalence of the float glass industry, up to now, the design of full-glass structures has been dominated by the limited forms, shapes and dimensions feasible by virtually two-dimensional, planar elements. The casting of glass can overcome the design limitations imposed by the 2-dimensional nature of float glass. By pouring molten glass into moulds we can create solid 3-dimensional glass components of almost any shape and cross-section. Such objects can be shaped to form repetitive units for free-form full-glass structures that do not buckle due to their slender proportions, taking full advantage of the high compressive strength of glass.

Although cast glass is well explored in art and design, in the built environment the potential of this alternative manufacturing method remains still unexplored. Discouraging factors such as the meticulous and time-consuming annealing process required, the, currently, non-standardized production, the small community of producers and the corresponding high manufacturing costs, have limited cast glass to only a handful of realized architectural applications.

This thesis aims to explore both the potential and limitations of cast glass as an alternative production process for the creation of three-dimensional structural glass components and their application in the built environment. In specific, the research focuses on the development and experimental validation of two new structural design systems for self-supporting structures out of cast glass components. Either adhesively bonded, or dry interlocked, the presented structural systems with cast glass units demonstrate the structural potential of this alternative manufacturing process for glass, unveiling the third dimension of glass!

Acknowledgements

They say that the road to the PhD degree is a long and lonely journey, yet, for me, it has only been possible thanks to the support and contribution of many people in so many ways.

It was actually a chain of fortunate events and opportunities that lead me to pursue a PhD degree in structural glass, which I have to attribute first and foremost to my co-promotor Dr. ir. Fred Veer and to...the Greek God Apollo! It was actually through my thesis initiative that I came to know the potential of glass as a structural material. I had come up with the idea to design a glass shelter for the Temple of Apollo Epicourios in Peloponnese that would protect the temple from weathering and even regulate the climate conditions inside; most importantly, it would not disturb the connection of the temple with the surroundings. I can vividly recall going to Fred's office to propose the design of a shelter for the temple, made of glass and a very slender metal load-bearing structure. He said:

- *Great idea, but we will make the load-bearing structure also from glass.*
- *Is that even possible?!*
- *People will think we are crazy, but we can do it.*

And this is how I entered the world of glass. A bit by accident, a bit by luck, definitely not completely intentionally. Nonetheless, the more I read about glass as a material the more fascinated I was by it. Transparent, brittle, unpredictable and unforgiving, yet strong.

This dissertation would not have been possible if it were not for my two supervisors, Dr. ir. Fred Veer and Prof. ir. Rob Nijse. Thank you both for your unconditional trust and support and for giving me a great freedom in my research activities that helped me not only pursue this PhD degree but also evolve both as a glass expert and an academic. None of this would have been possible without you. The “constructive destruction” of glass is definitely much more fun when you are around!

Secondly, I want to acknowledge the members of my defence committee: Prof. dr. Christian Louter, prof. James O' Callaghan, prof. dr. Paulo Cruz, dr. Elvin Karana, dr. Michalis Prassas and prof. dr. Andy van den Dobbelen. Thank you all for your interest on the topic and the time you dedicated reading this manuscript.

I would also like to thank my fellow colleagues and staff members from the Department of Architectural Engineering, and in particular from the chair of Structural Design & Mechanics, for creating a friendly and stimulating environment to work in. Special thanks to Ate Snijder and Peter Eigenraam for substituting me in teaching sessions when needed and for the Bouwpub sessions after tough days of work. Thank you Joris and Andrew for always greeting me with a smile! Bo, Tessa, Linda, Barbara and Françoise you are the best! A special mention goes to dr. Thaleia Konstantinou, from the Building Product Innovation group, for being my unofficial advisor throughout this PhD journey, providing me with invaluable guidance and insights regarding the PhD process. I would also like to express my gratitude to prof. Ulrich Knaack and prof. Andy van den Dobbelen for securing the good working conditions that allowed this PhD work to flourish. Marcel Bilow, your out-of-the box thinking has always been an inspiration for both me and the MSc students we have supervised together (and thank you in advance for taking the photos in my defence)! Michela Turrin you may not remember, but you were the one who motivated me to talk to Fred for my MSc topic in glass – partially, I reached this point also thanks to you!

None of the experimental testing presented in this dissertation would have been possible without the help of Kees Baardolf, the best technician in the world. Kees, you are a true engineer and problem-solver of any test set-up or other technical issue! But most importantly, thank you Kees for making me smile even at the most stressful of times! I want to extend my gratitude to all the technicians of the Stevin Laboratory (CiTG) and the Materials Laboratory (3ME) for helping me with the testing and set-ups but also with finding cunning solutions for the most challenging technical issues. Kees van Beek, the high-tec/low-tec *laser-milk* system still impresses structural engineers around the world! Rong and Tommy I appreciate a lot your hard work in preparing the kiln-cast prototypes!

Cast glass was not the original topic of my dissertation – in fact my research was initially meant to be on something completely different: innovative glass joints. But thanks to the deep involvement in the research, development and construction of the *Crystal Houses* project, I discovered the potential of using cast glass for structural applications. That said, the third dimension of glass started to unveil thanks to the vision, passion and persistence of all parties involved in the realization of this façade, and foremost of MVRDV Architects, Gijs Rikken, Ivano Massarotto, Ronald Jorissen, Erwin ten Brincke and especially of Jack Bakker. It is thanks to Jack's determination to make this façade real that this PhD research started. The *Crystal Houses* façade is a great example of what good teamwork can achieve: An inspiring design by MVRDV and Gietermans & Van Dijk, materialized to perfection through the excellent collaboration of the architects with TU Delft, ABT consulting engineers, Wessels Zeist, Poesia and Rob Janssen from Siko B.V. Jack, thank you for providing

the apartment above the façade to Telesilla and me to stay during the façade's construction. Starting to work at 06:30 would have been extremely painful if we had to come all the way from Delft! I would like to especially thank the building crew of the *Crystal Houses* façade and particularly Richard van het Ende and the Poppe brothers, Marco and Ronald! Thank you for taking care of us, thinking along with us when technical challenges arose and for transforming the construction site to a lab. And thank you all, for having always a cheerful attitude, for your choice of good, uplifting music while building and for introducing “Salad Wednesdays” and “Sushi Mondays” at the construction site just for us!

The construction of the *Crystal Houses* façade triggered not only the formation of this PhD topic but also the idea of a circular, dry-assembled system out of interlocking cast glass components. Many MSc students have contributed to the research work of the latter through their MSc thesis works: Lida Barou, Erwin Jacobs, Giulia Frigo, Heran Young, Robert Akerboom, to just name a few. I should also mention here the impressive MSc thesis of my students Wilfried Damen and Ivneet Bhatia, showcasing the potential of cast glass for topologically optimized structural components and the use of 3D-printed sand moulds for manufacturing them. The prototype and experimental work of the presented interlocking system was only possible thanks to two consecutive *4TU.Bouw Lighthouse* grants that Telesilla and I initiated together. Thank you Siebe for promoting our work and giving us the opportunity to take this idea from conceptual to materialized! Thanks to the aforementioned research grants, Telesilla and I had the opportunity to go as guest researchers for two months to the *School of Art and Design of Southern Illinois University* (SIU) under the guidance of glass artist and professor Jiyong Lee. Our short time as guest researchers at SIU has been a milestone in the direction our research has taken. At SIU we did not only master our skills at glass casting under the guidance of Jiyong Lee, Katherine Rutecki and Joshua Hershman; it is where we discovered the potential of recycling glass waste by casting. Our first recycling trials were with the left-over art glass of the students of the Kiln-Casting studio!

I would also like to extend a big thank you to all the people and companies that helped me in the challenging task of collecting all the information and visual material presented in the literature review. I would like to thank in particular Jordi Torres, Carles Teixidor, Francesc Arbós from Bellapart and Michalis Prassas, Jean-Francois Kergaravat and Thierry Dannoux from Corning for providing me with insightful engineering input on the described projects, as well as Nakamura & NAP Architects, MVRDV and Rakow Research Library for freely providing images and drawings of projects. A big thank you goes to Vero Crickx for her valuable assistance in the layout of this book!

This PhD journey would not have been so enjoyable and rewarding if it was only research and there was no fun involved (besides breaking glass specimens...). I have been fortunate to be surrounded by great friends through this process, who were always there for me, to celebrate the good times and to hear my concerns at the bad times: Luzma, Ale, Ale Jr (Jandro), Bernat, Nadjla, Maria, Stavroula, Hyperion, Maritta, Marina, Kosta, thank you all for being there for me all these years, for the great coffees, drinks, parties, movie-nights, lunches, dinners and travels. Life is so much more fun with you guys around! Wiebke and Yasemin thank you for following me in my crazy expeditions around the world! Tommy, your positive spirit, kind heart and Italian cooking definitely made even the darkest of days brighter! Tonio, thank you for always being there for me, through all the good and the bad (*para todo mal mescal, para todo bien, tambien!*). To my friends back in Greece, but also all over the world, thank you for always making time for me, even at the shortest notice!

Last but not least, there are no words good enough to show my gratitude to my best friend, colleague, cast glass expert and paranymp, Telesilla Bristogianni. Tele, thank you for supporting me morally at the hardest of times, both as a friend and as a colleague, for taking over every time I would give up, for being my “partner in crime” throughout this PhD journey, for making together the structural cast glass dream team! You have been a sister to me – it does not come as a surprise that many people mistake us for twins!

Finally, I would like to thank my family for their unconditional support and love. Mom, thank you for encouraging me to make the step further every time I would hesitate and for hearing all my worries, from the most serious to the most ridiculous ones. Dad, thank you for dedicating endless hours proof-reading my papers and the entire PhD and for your incredible patience since I was still a kid, when you had to sit and listen to me repeating the whole history book each and every year! Apollon, my dear brother and paranymp, I am very curious to see you dressed in a toxedo!

Σας ευχαριστώ όλους!

Φαίδρα

*If you work with hot glass and its natural properties,
it begins to look like something that came from the sea.*
Dale Chihuly

Contents

Preface	7
Acknowledgements	9
Summary	21
Samenvatting	25

1 Introduction to the research 33

1.1	Problem definition	34
1.1.1	Glass as a structural material	34
1.1.2	Cast glass as a structural material: Potential and limitations.	37
1.2	Research questions and aims	41
1.3	Objectives	42
1.4	Research Methodology	43
1.5	Societal and Scientific Relevance	45
1.6	Outline of the dissertation	46

2 Material compositions and production methods for solid cast glass components 51

2.1	Introduction	52
2.2	Types of Glass	53
2.3	Prevailing glass manufacturing processes and current dimensional limitations	55
2.3.1	Float glass	56
2.3.2	Extruded glass	58
2.3.3	3D-printed glass	62
2.3.4	Cast glass	65
2.4	Casting and annealing process	68
2.4.1	Prevailing casting processes	68
2.4.2	Annealing Process	69
2.4.3	Measuring stresses in cast glass objects	73

- 2.5 **Mould types** 74
- 2.6 **Strength of cast glass** 79
- 2.7 **Discussion** 86

3 **Overview of large-scale non-architectural cast glass applications** 91

- 3.1 **Introduction** 91
- 3.2 **The giant telescope mirror blanks** 94
 - 3.2.1 The design of a honeycomb structure 94
 - 3.2.2 Reducing post-processing: Spin casting 94
- 3.3 **Radiation-shield lead blocks** 97
- 3.4 **Art pieces** 98
- 3.5 **Discussion** 99

4 **Overview of realized examples in architecture using structural cast glass blocks** 107

- 4.1 **Introduction** 108
- 4.2 **Principles of structural system employing solid cast blocks** 110
 - 4.2.1 Solid glass vs hollow blocks 110
 - 4.2.2 Structural systems employing cast glass blocks 112
- 4.3 **Solid glass block envelopes with supportive substructure** 113
- 4.4 **Adhesively bonded blocks** 116
- 4.5 **Interlocking components** 124
- 4.6 **Discussion** 127

5 **An adhesively-bonded cast glass system for the Crystal Houses façade** 133

- 5.1 **Introduction** 136
- 5.2 **The case study** 136
- 5.3 **Methodology** 140

5.4	Materials	140
5.4.1	Selection of Adhesive	140
5.4.2	Defining the optimum thickness range of the adhesive	142
5.4.3	Choice of glass	146
5.5	Experimental	149
5.5.1	Test specimens	149
5.5.2	Set-up of compression tests on single blocks	151
5.5.3	Set-up of compression tests on glass pillars out of adhesively bonded glass blocks	151
5.5.4	Set-up of 4-point bending tests on glass beams out of adhesively bonded glass blocks	153
5.5.5	Set-up of 4-point bending test of glass architrave	154
5.5.6	Impact and vandalism test set-up	156
5.5.7	Set-up of thermal shock test on single blocks	157
5.6	Results and Discussion	158
5.6.1	Compressive tests on single blocks	158
5.6.2	Compressive tests on columns out of adhesively-bonded glass blocks	160
5.6.3	4-point bending tests on adhesively bonded beams	162
5.6.4	4-point bending test on adhesively bonded glass architrave	165
5.6.5	Impact and vandalism test	167
5.6.6	Thermal shock tests on individual blocks	169
5.7	Conclusions	170
6	Learning by building – Challenges & Innovations during the construction of the Crystal Houses façade	177
6.1	Introduction	180
6.2	Manufacturing and quality control of the glass blocks	181
6.2.1	Manufacturing process of the glass bricks	181
6.2.2	Quality control of the glass bricks	186

6.3	Construction of the glass brick wall	188
6.3.1	Construction site set-up	188
6.3.2	Levelling the starting bonding surface	189
6.3.3	Bonding Process	191
6.3.4	Construction and installation of the architraves	195
6.3.5	Transition layer between standard and glass masonry	195
6.3.6	Boundary connections of the façade	197
6.3.7	Installation and bonding of the cast glass window and door frames	198
6.3.8	Maintenance	200
6.4	Conclusions	201
6.5	Recommendations	204

7 Interlocking cast glass components: Main principles 209

7.1	Introduction	211
7.2	Methodology	211
7.3	Definition and mechanical principles of interlocking structures in architecture	212
7.3.1	Definition	212
7.3.2	Enhanced resistance of the assembly against crack propagation	214
7.3.3	Improved mechanical properties due to inverse scale effect	214
7.3.4	Redundancy - tolerance to missing components	215
7.3.5	Out-of-plane behaviour	215
7.3.6	Buildability and Reversibility	216
7.3.7	Global constraint	217
7.3.8	Use of soft interlayer as intermediary	217
7.4	Establishment of design criteria	217
7.4.1	Design criteria related to interlocking principles	219
7.4.2	Design criteria related to glass casting	220
7.5	Interlocking designs and prototypes	222
7.5.1	Prototype manufacturing	222
7.5.2	Interlocking geometries	224
7.5.3	Assessment and selection of interlocking topology	227

7.6	Properties of dry-interlayer	229
7.7	Potential for a circular use of glass and recycling of glass waste	234
7.7.1	Reversibility of the structure and reuse of the components	234
7.7.2	Recycling of discarded (waste) glass	235
7.8	Conclusions	241
8	Experimental and numerical investigation of an interlocking system out of osteomorphic cast glass components	247

8.1	Introduction	250
8.2	Methodology	250
8.3	Experimental	251
8.3.1	Materials	251
8.3.2	Interlayer testing under compressive static load	254
8.3.2.1	Method	254
8.3.2.2	Results	256
8.3.2.3	Series [1]: Load Calibration	258
8.3.2.4	Series [2]: Compression testing of 3 mm thick interlayers	258
8.3.2.5	Series [3]: Compression testing of 6 mm thick interlayers	263
8.3.3	Conclusions on Interlayer material	267
8.3.4	Shear tests on osteomorphic blocks with different amplitude height	269
8.3.4.1	Method	269
8.3.4.2	Results	271
8.4	Numerical investigation of the interlocking geometry of the osteomorphic blocks	277
8.4.1	Model set-up	277
8.4.2	Results	284
8.5	Conclusions	288
8.5.1	Conclusions from the interlayer testing under static load	288
8.5.2	Conclusions from the out-of-plane shear testing of assemblies with various amplitudes	289
8.5.3	Conclusions from the numerical modelling	291
8.6	Recommendations	291

9 Conclusions 297

- 9.1 Introduction 297
- 9.2 Answers to the sub-questions 298
- 9.3 Main research question 307

10 Recommendations 315

- 10.1 Introduction 315
- 10.2 Limitations of the research 315
- 10.3 Recommendations for further research 317
 - 10.3.1 Recommendations on the adhesively bonded glass system 317
 - 10.3.2 Recommendations on the interlocking cast glass system 318
 - 10.3.3 Possible other applications 319
 - 10.3.4 Investigating the strength of cast glass 319
 - 10.3.5 Circular cast glass components out of glass waste 320
 - 10.3.6 Development of cost-effective fabrication methods 321
 - 10.3.7 Optimizing the geometry of the components with respect to the properties of glass 321
 - 10.3.8 Improving the thermal performance of cast glass structures 322

- Appendix 326
- References 327
- List of Tables 333
- List of Figures 335
- Curriculum Vitae 343

Summary

Glass as a material has always fascinated architects. Its inherent transparency has given us the ability to create diaphanous barriers between the interior and the exterior that allow for space and light continuity. Yet, we are just starting to understand the full potential, properties and characteristics of glass as a material. Only in the last decades did we discover the structural potential of glass and started to use it, besides as a cladding material, also for load-bearing applications thanks to its high compressive strength. Indeed, at present the structural applications of glass in architecture are continuously increasing, yet they are dominated by a considerable geometrical limitation: the essentially 2-dimensionality imposed by the prevailing float glass industry. Although glass panels can stretch more than 20 m in length, the maximum monolithic thickness by this manufacturing method remains a mere 25 mm. As a result glass structures are currently dominated by virtually 2-dimensional, planar elements and confined to the limited shapes that can be achieved by those.

This research focuses on the exploration of cast glass as a promising, 3-dimensional construction material in architecture. The main aim of this research is therefore to investigate the potential, as well as the constraints, of cast glass components for the engineering of transparent, 3-dimensional glass structures in architecture.

By pouring molten glass into moulds, solid 3-dimensional glass components of virtually any shape and cross-section can be made. Owing to their monolithic nature, such components can form repetitive units for the construction of free-form, full-glass structures that are not sensitive to buckling. Such structures can take full advantage of the high compressive strength of glass, sparing the necessity of additional supporting elements. To achieve cast glass structures, it is essential to use an intermediate material between the individual glass components that contributes to the structure's stiffness, ensures a homogeneous load distribution and prevents early failure due to concentrated stresses triggered by glass-to-glass contact. To maximize transparency, this intermedium should be colourless and any additional substructure should be minimized.

Accordingly, the main scientific contribution of this research work is the design, development and experimental investigation of two distinct systems for self-supporting envelopes of maximized transparency: An adhesively bonded glass block system, using a colourless adhesive as an intermedium and a dry-assembly, interlocking cast glass block system, employing a colourless dry interlayer. Although,

in this work, both systems have been developed for self-supporting envelopes, the results can be used as a guideline for further structural applications of cast glass components in compressive elements, such as columns, arches and bending elements, such as beams and fins.

At present, the load-bearing function of cast glass in architecture remains an uncharted field. Discouraging factors such as the lengthy annealing process required, the to-date non-standardized production and the corresponding high manufacturing costs, have limited cast glass to only a few realized architectural applications. As a result, there is a lack of engineering data and a general unawareness of the potential and risks of employing cast glass structurally. Hence, in order to accomplish the research goal, all pertinent aspects of a cast glass structure should be tackled, ranging from cast glass's production method to practical implications when building with cast glass. These distinct aspects are addressed through the formulation of the research sub-questions, which in turn define the different chapters of this dissertation. Accordingly, the presented work is divided in four parts.

Part I provides the *Introduction to the Research*, and aims at giving a brief summary of the involved challenges, identify the research gap and introduce the research questions and the research methodology.

Part II focuses on the *Theoretical Framework of the Research*. It lays the foundations for this dissertation and contributes to the scientific field of structural glass by providing the first comprehensive literature review and state-of-the-art overview of cast glass structural applications. Initially, the material compositions and production methods for solid cast glass components are explored. Then, to address both possibilities and limitations in the size and form of cast glass components, an overview and critical assessment of the largest produced monolithic pieces of cast glass is made. Given the limited published scientific output on this specific field, an extensive field research was conducted in order to derive the relevant data. The discussed examples, although coming from different fields of science and art, provide great insight into the practical implications involved in casting as a manufacturing method. Subsequently, a separate chapter gives an overview of the state-of-the-art in cast glass structural applications in architecture. Aiming on providing the reader with an holistic overview of the structural potential of cast glass in architectural applications, this chapter includes the synopsis, feasibility assessment and comparison of not only the realized structural design systems but also of the adhesively-bonded and dry-assembly interlocking systems developed in this dissertation. Special attention is given to the advantages and disadvantages of the connection method of each -existing and developed in this dissertation- structural design system with solid glass blocks.

Following the findings of the literature review and field research, Part III, consisting of four chapters, presents the *design and experimental investigation of two distinct, novel structural systems out of cast glass components*, developed for self-supporting envelopes. Part III can be considered the main scientific outcome of this dissertation. Firstly, the research, development and experimental validation of an adhesively bonded system utilizing solid cast glass blocks is presented. Numerous full-scale prototypes are made and tested in order to comprehend the structural behaviour of the adhesively bonded glass assembly. A separate chapter explores the main challenges and innovations and defines the construction requirements necessary for the realization of the investigated system at the *Crystal Houses Façade* in Amsterdam. An important conclusion is that such an adhesively bonded system requires an extremely high dimensional accuracy both in the fabrication of the glass blocks and in the entire construction, and has an irreversible nature, which in turn results in a meticulous and unsustainable construction. Based on the aforementioned challenges, a new concept for glass structures out of dry-assembled interlocking cast glass components is developed that tackles the integral limitations of the adhesively-bonded system. An entire chapter is dedicated to the principles, the establishment of design criteria and to the preliminary exploration and assessment of different interlocking cast glass shapes that can yield an interlocking cast glass system of satisfactory structural performance. Following, the last chapter of this part concerns the experimental and numerical investigation of this second system. The effect of various parameters in the structural behaviour of the system is explored through the production of scaled prototypes and their experimental validation. A numerical model further explores the correlation of the various geometrical parameters of the interlocking geometry to the structural behaviour of the system.

Finally, Part IV presents an *integrated discussion of the research results*, summarizing and discussing the main outcomes of the dissertation. Initially, responses to the research questions are given in order to assess the particular findings. Based on the conclusions, further recommendations are made, firstly for overcoming the limitations of the presented research, following by general suggestions on a wider range of the aspects of cast glass that can be explored and contribute to its structural applicability.

The findings of this dissertation prove the feasibility of the discussed systems and can serve as solid guidelines for further applications.

The research presented in this work has been positively received by the international architectural and engineering community. In specific, the presented adhesively-bonded cast block system, which was realized at the *Crystal Houses façade*, received numerous awards by the structural engineering community, including

the *Outstanding Innovation Award 2016* by the Society of Façade Engineers and the *Glass Innovation Award 2016* from the Bouwend Nederland association. Still, the *Crystal Houses façade* is but the first real-scale prototype of the developed adhesively bonded system. The actual construction of the façade provided invaluable feedback on the engineering challenges and construction requirements involved in such a system, giving room for new suggestions. This triggered the development of the second presented system with interlocking glass blocks as a reversible, easily assembled solution. The interlocking cast glass block system, initiated within TU Delft and funded partially by a 4TU.bouw grant is yet to be applied in practice. Prototypes of this research, using recycled cast glass components, have been exhibited in international fairs such as the *Venice Design 2018*, the *Dutch Design Week 2018* and *Salone del Mobile 2019* and are currently displayed at the material collection of the *Vitra Design Museum* at the *Vitra Schaudapot*. The project was also nominated for the *New Material Award 2018* under the title *Re³ Glass*.

Even though cast glass has, so far, been rarely applied in structural applications, the development of new building systems and their experimental validation presented in this work provide a strong basis for further developments and applications in a range of compressive structures. At present, the most considerable drawbacks hindering the marketability of cast glass components are (a) the cost barriers imposed by their customized production and application and (b) the lack of standardized strength data and building guidelines. Thus, even if cast glass elements have proved to be suitable structural components, several economic aspects and logistics need to be tackled, and performance issues need to be further explored, in order to make cast glass a competitive manufacturing method to float production for structural components.

Samenvatting

Het materiaal glas heeft architecten en ingenieurs altijd gefascineerd. De inherente doorzichtigheid van glas biedt de mogelijkheid om een grens te scheppen tussen de binnenkant en de buitenkant van een gebouw. Het biedt echter ook de mogelijkheid ruimte en licht op deze grens in elkaar te laten overvloeien. We beginnen ons nu pas de mogelijkheden van glas als bouw materiaal te realiseren en worden ons bewust van de goede materiaalkundige eigenschappen die dit prachtige materiaal biedt.

De laatste decennia is duidelijk geworden dat het transparante en brosses materiaal glas een zeer hoge druk sterkte kan bereiken waardoor het mogelijk is glas niet alleen te gebruiken als ramen in de gevel, maar ook als een dragend materiaal voor muren, kolommen, vloeren en liggers. De constructieve toepassingen van glas nemen jaar na jaar toe, maar worden beperkt door de 2 dimensionale uitgangsvorm van het "float" glas dat het meest gebruikelijke materiaal voor glas is. Hoewel tegenwoordig panelen van 20 m lang gemaakt kunnen worden is de dikte beperkt tot maximaal 25 mm. Het gevolg is dat momenteel de glas architectuur gedomineerd wordt door 2-dimensionale platen met alle beperkingen die inherent zijn aan deze grondvorm.

Dit onderzoek is er op gericht de mogelijkheden van gegoten glas objecten te verkennen om een 3-dimensionale vormgeving mogelijk te maken. Het hoofdonderzoek concentreert zich op het bepalen van de mogelijkheden en onmogelijkheden van gegoten glas in de architectonische bouwtechniek.

Door gesmolten glas in mallen te gieten kunnen 3-dimensionale objecten van vrijwel iedere vorm of doorsnede worden gemaakt. Door hun solide aard kunnen deze elementen gestapeld of gekoppeld worden tot knik resistente constructie onderdelen.

Om constructies te maken uit gegoten glas is een intermediair tussen de glazen delen onderling nodig. Dit voorkomt brosses breuk van glazen onderdelen door spanningsconcentraties ten gevolge van lokaal glas/glas contact. Het intermediair zal transparant moeten zijn om de transparantie van de gehele constructie niet aan te tasten.

De bijdrage aan de Technische Wetenschap van dit onderzoek is het ontwerpen en valideren door experimenteel onderzoek van twee verschillende constructieve systemen die maximale transparantie geven. Het eerste systeem is een verlijmd systeem van glazen blokken met een transparante kleurloze lijm. Het tweede systeem

is gebaseerd op, niet verlijmde maar, in elkaar grijpende glazen blokken met een transparant kleurloos intermediair. Beide systemen zijn ontwikkeld om dragende, hoog transparante muren en gevels te kunnen bouwen. De resultaten van dit onderzoek kunnen gebruikt worden als een richtlijn voor het constructief gebruik van gegoten glazen elementen die primair op druk belast worden, maar ook op buiging belast kunnen worden.

Op dit moment is het gebruik van gegoten glas als constructiemateriaal een nieuwe toepassing. Beperkende factoren zoals het lange spanningsvrij gloeien van grote gegoten glazen elementen, de niet gestandaardiseerde productieprocessen en de daaraan gekoppelde hoge productie kosten; hebben als gevolg dat slechts een handvol toepassingen van gegoten glas in de architectuur gerealiseerd zijn.

Hierdoor zijn er enerzijds weinig technische gegevens voorhanden en is er anderzijds een gebrek aan bewustzijn van de mogelijkheden van gegoten glas.

Om de onderzoeksdoelstelling te bereiken is het dus nodig alle relevante aspecten van de gegoten glazen constructie te behandelen. Beginnende met de productie en verwerking van het gesmolten glas zelf tot de aspecten van de praktische uitvoering van het bouwen met gegoten glas elementen.

Deze zaken worden behandeld door het formuleren van onderzoeks(sub)vragen , die in de verschillende hoofdstukken opeenvolgend worden behandeld. Het proefschrift als geheel is hierdoor verdeeld in vier delen.

Deel I is de inleiding tot het onderzoek en geeft een kort overzicht van de uitdagingen, beschrijft het kennis deficit en de daaruit volgende onderzoeksvragen en onderzoeksmethodologie.

Deel II omvat het theoretisch grondwerk van dit onderzoek en vormt de basis voor dit proefschrift. Het bevat ook een literatuuroverzicht en een "state of the art"-document van het gebruik van gegoten glas in de architectonische bouwtechniek. Glas samenstellingen en verwerkingstechnieken voor gegoten glas worden eveneens behandeld. Hieruit volgen de beperkingen aan vorm en afmeting van gegoten glazen componenten. Een overzicht van de grootste, gerealiseerde, gegoten glazen componenten wordt gegeven als voorbeeld van wat kan, maar wat voor massaproductie (nog) niet praktisch is. Deze extreme voorbeelden geven echter een goed inzicht in de praktische problemen bij het gieten van glas.

Het laatste hoofdstuk van deel II geeft een overzicht van gegoten glas toegepast in de architectonische bouwtechniek. Hierbij wordt gekeken naar alle aspecten

waaronder de verbindingen om de lezer een volledig beeld te geven van de “state of the art”.

Deel III bevat vier hoofdstukken en geeft als geheel een beeld van het ontwerpen, en de validatie door experimenteel onderzoek, van twee verschillende systemen om gegoten glazen elementen samen te stellen tot dragende muren.

Deel III is in essentie de bijdrage die dit proefschrift maakt aan de Technische Wetenschap. Allereerst wordt het onderzoek en de validatie van het systeem van verlijmde glazen blokken beschreven. Meerdere prototypes op schaal 1/1 zijn vervaardigd en beproefd om het constructief gedrag van het verlijmde glas blok systeem te bepalen.

Het volgende hoofdstuk van deel III gaat over de uitvoering van de *Crystal Houses façade* in Amsterdam met dit systeem en de lessen die daarbij geleerd zijn.

Een belangrijke conclusie was dat verlijmen geen economische en duurzame methode voor het maken van gevels en muren. Het derde hoofdstuk van deel III gaat over de principes en ontwerpcriteria voor een systeem waar de stenen in elkaar grijpen, waarbij voldoende sterkte en stijfheid is voor constructieve toepassingen.

Het vierde hoofdstuk van dit deel beschrijft het experimenteel onderzoek voor de validatie van het systeem van in elkaar grijpende blokken. Diverse aspecten van het systeem zijn onderzocht op een aantal schaal niveaus. Een eindige elementen analyse (FEA) is gebruikt om diverse aspecten van de geometrie van in elkaar grijpende stenen te onderzoeken en conclusies over de toepasbaarheid te kunnen trekken. Ook zijn diverse mogelijke prototypes van verschillend vormen van in elkaar grijpende stenen vervaardigd. Tot slot: deel IV is een geïntegreerde analyse en discussie van de resultaten, het omvat de belangrijkste uitkomsten van het onderzoek samen en gaat ook in op mogelijke toepassingen. Ook wordt in dit deel verkregen antwoorden op de onderzoeksvragen worden behandeld.

Op basis van de uitkomsten van het onderzoek worden aanbevelingen gedaan, allereerst hoe het huidige onderzoek vervolgd moet worden en daarna hoe verder gekeken moet worden naar de constructieve toepassing van gegoten glas.

Dit proefschrift toont de praktische toepasbaarheid van de onderzochte systemen aan en kan ook gebruikt worden als een richtlijn van hoe deze systemen toegepast kunnen worden in de praktijk.

Het onderzoek is positief ontvangen in de internationale architectonische en bouwtechnische gemeenschap. Het verlijmd systeem, gebruikt in de *Crystal Houses* façade, heeft meerdere prijzen ontvangen zoals de *Outstanding Innovation Award* van de Society of Façade Engineers in 2016 en de Glass Award Innovatie 2016 van de vereniging Bouwend Nederland.

De *Crystal Houses* façade was echter het eerste 1:1 prototype van een dergelijke gevel. Het bouwen van dit prototype heeft onschatbare informatie opgeleverd en heeft geleid tot een bewuste keuze voor in elkaar grijpende blokken als bouw systeem in plaats van verlijmd blokken. Het systeem van in elkaar grijpende blokken is (wordt) ontwikkeld aan de TU Delft, voor een beperkt deel bekostigd uit door een 4TU bouw subsidie. Prototypes van deze systemen zijn tentoongesteld op *Venice Design 2018*, *the Dutch Design Week 2018* en *Salone del Mobile 2019*. Onder de naam *Re³ Glass* is het genomineerd voor de *New Material Award 2018*.

Hoewel gegoten glas nog zelden gebruikt is in de architectonische bouwtechniek, geeft dit proefschrift aan dat er een goede basis is voor toekomstig gebruik in een aantal toepassingen waar het primair op druk wordt belast.

Hoewel gegoten glas zonder meer geschikt is voor een groot aantal bouwkundige toepassingen, moeten de constructieve eigenschappen nog goed gedocumenteerd en vastgelegd worden. Ook moeten diverse productieproblemen opgelost worden waardoor het systeem gegoten glazen stenen kosten effectiever wordt en dan een goed alternatief kan bieden voor float glas voor constructieve toepassingen.



Sculpture made by glass shards by artist *Marta Klonowska* exhibited at the *Corning Museum of Glass*

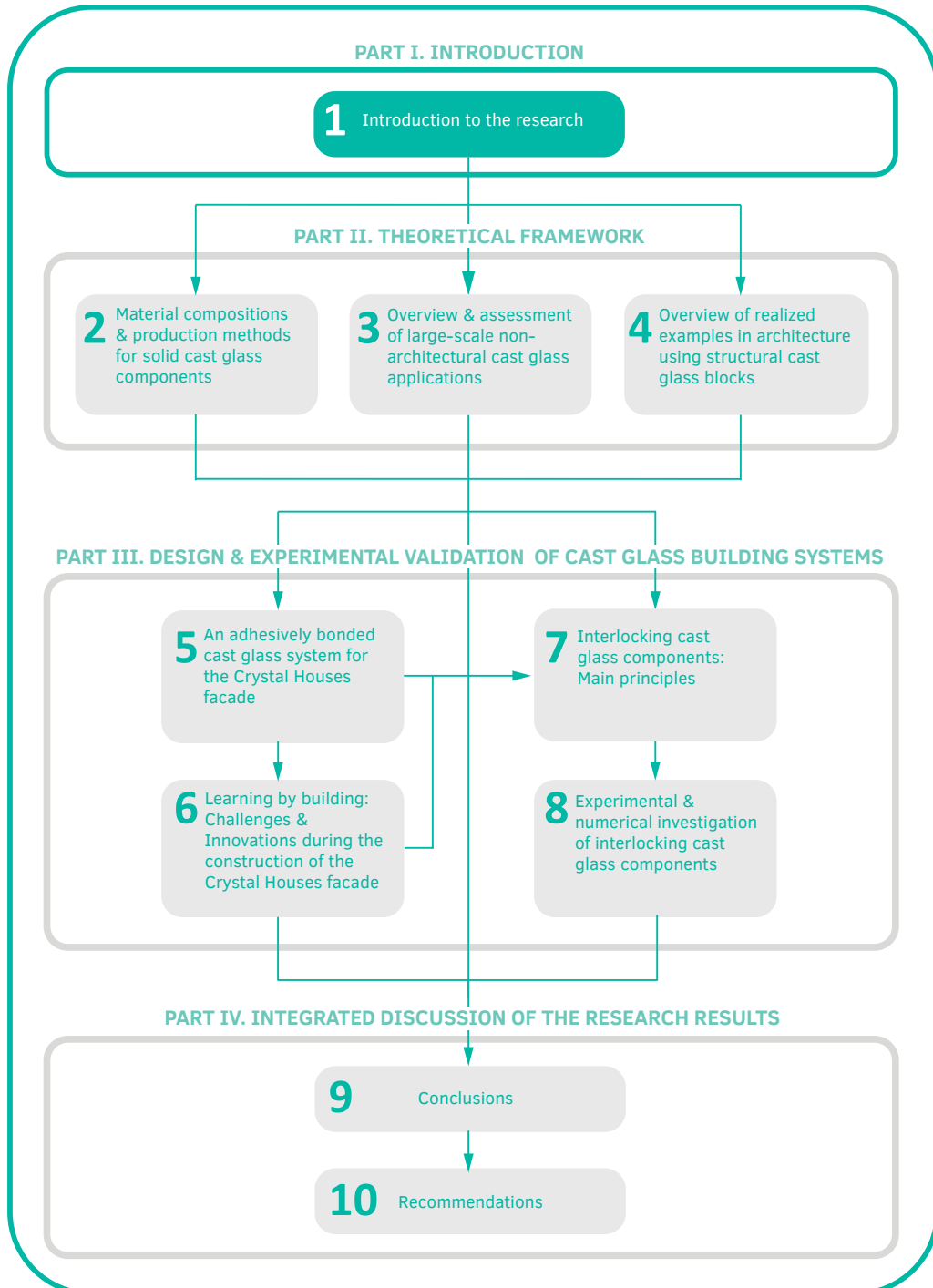
*The bird, the bee, the running child
are all the same to the glass sliding door.*

Demetri Martin [Comedian]

*“Architecture is the masterly,
correct and magnificent play of volumes
brought together in light, (...)
the history of architecture was the history
of the struggle for the window.”*

Le Corbusier

Exploring the third dimension of glass



Solid cast glass components and assemblies for structural applications

1 Introduction to the research

Innovations in glass technologies and engineering over the last decades have altered the way we perceive glass. Combining transparency, durability and a compressive strength exceeding that of concrete and even structural steel, glass has evolved in the engineering world from a brittle, fragile material to a reliable structural component with high compressive load-carrying capacity. At present, the structural applications of glass in architecture are constantly increasing, yet with a considerable geometrical limitation: although glass's fabrication boundaries have been continuously stretching so far, glass structures are still dominated by the limited shapes which can be generated by the combination of the virtually 2-dimensional, planar elements produced by the float industry. Whereas glass panels in float production can stretch more than 20 m in length, the width is restricted to 3.21 or 4.5 m and the maximum commercial thickness is only 25 mm (Lyons 2010; Schittich et al. 2007; Patterson 2011).

Cast glass can overcome the design limitations imposed by the 2-dimensional nature of float glass. By pouring molten glass into moulds, solid 3-dimensional glass components of almost any shape and cross-section can be obtained¹. Such objects can be shaped to form repetitive units for free-form full-glass structures that do not buckle due to their slender proportions, thus taking full advantage of the high compressive strength of glass; a solution little explored so far. Discouraging factors such as the meticulous and time-consuming annealing process required, the to-date non-standardized production, and the corresponding high manufacturing costs, have limited cast glass to only a handful of realized architectural applications. Consequently, there is a lack of engineering data and a general unawareness of the potential and risks of building with cast glass as a structural material. The load-bearing function of cast glass in architecture remains an unmapped field.

¹ At present, the largest monolithic pieces of cast glass made -in terms of dimensions- are the blanks of the Giant Magellan Telescope. Each honeycomb disk is 8.4 m in diameter, ranges between 0.43 – 0.89 m in thickness and weighs 16 t. The aforementioned mirror blank together with other characteristic examples of massive cast glass components are presented and discussed in detail in Chapter 3.

Scope of this research is to explore the structural potential and limitations of solid cast glass components and introduce cast glass as a promising construction material in architecture, indicating both the potential and limitations of this alternative production process for glass in buildings. To achieve this, the research focuses on the development and experimental validation of two new design concepts for self-supporting envelopes made almost entirely of cast glass components: adhesively bonded and interlocking cast glass components.

1.1 Problem definition

1.1.1 Glass as a structural material

According to the *Oxford Dictionary*, glass is a “*hard, brittle substance, typically transparent or translucent, made by fusing sand with soda and lime and cooling rapidly. It is used to make windows, drinking containers, and other articles*”.

Indeed, transparency and brittleness are the two most well-known properties of glass and the ones that have defined the majority of its applications. Yet, glass has another inherent property that has allowed us to go beyond its traditional use as an infill material, and conceive it as a structural building material: Glass exhibits a compressive strength (stated as 1000 MPa for float soda-lime glass by (Saint Gobain 2016; Weller et al. 2008; Ashby, Jones 2006)) higher than that of most conventional building materials, including concrete and even many types of structural steel². This property together with technological advances that have increased the safety of glass elements -namely the tempering and lamination process- have allowed glass to evolve from a brittle, fragile material to a material for creating structural components with high compressive load-carrying capacity. Indeed, over the last decades glass has been applied for various structural components, such as beams, columns, walls,

² Several guidelines and specifications exist on the strength of structural steel and concrete, with variable values according to the material composition. As an indication, according to (Job, Ramaswamy 2007) a typical high performance concrete has a compressive strength of 85 MPa and according to (Sarkisian 2012) for a typical ultra-high performance concrete the value is 110 MPa. For a typical high-strength structural steel, the yield strength is approx. 450 MPa (Granta Design Limited 2015; Sarkisian 2012), but higher values are also reported.

facades, staircases and even entire envelopes (Fig. 1.1) (Wurm 2007; Nijssse 2003; Schittich et al. 2007). In the quest of maximum transparency, glass's structural boundaries have been continuously stretching (Albus,Robanus 2015). The glass sheets are constantly becoming larger and the connections less, both in size and number (O' Callaghan,Marcin 2009). The long pursued architectural desire for a totally transparent, almost dematerialized structure is finally feasible.



FIG. 1.1 The Apple Store in New York by EOC Engineers

Still, due to the prevalence of the float glass industry, the design of full-glass structures is dominated by the limited forms, shapes and dimensions feasible by virtually two-dimensional, planar elements: either orthogonal or cylindrical in shape and supported by glass fins and beams or braced against buckling using slender, non-glass components. At present, glass panes can stretch more than 20 m in length, yet, their maximum standardized thickness does not exceed 25 mm in float production (Lyons 2010; Schittich et al. 2007; Patterson 2011)³. Such a disproportional slenderness ratio renders float glass panes virtually 2D elements that

³ Actually, 25 mm thick float glass is produced to a limited extent. An example of float glass produced in 25 mm thickness is by *Linea Azzurra* of AGC (AGC 2019). Float glass is usually manufactured up to 19 mm in thickness (Wurm 2007).

are susceptible to buckling, preventing the use of glass's full compressive capacity, although it is at least an order of magnitude higher than its tensile strength. In essence, a float glass element, even when loaded in compression, will eventually fail due to the initiation of tensile stresses at significantly lower values than its stated compressive strength.

Cast glass can escape the design limitations imposed by the virtually 2D nature of float glass. By pouring molten glass into moulds, solid three-dimensional glass components of considerably larger cross-sections and of virtually any shape can be obtained. Owing to their monolithic nature, such components can form repetitive units for the construction of three-dimensional, self-supporting glass-structures that are not sensitive to buckling, sparing the necessity of additional supporting elements. Certainly, solid cast glass components are a promising solution for engineering pure glass structures of high transparency (Fig. 1.2) that take full advantage of glass's compressive strength.



FIG. 1.2 The Crystal Houses façade in Amsterdam by *MVRDV Architects*, made of adhesively bonded glass blocks. Source: *Daria Scagliola and Stijn Brakke*.

Nonetheless, at present, little and rather sporadic exploration has been made in the use of casting as a manufacturing method for structural glass components in architecture. To a certain extent this is attributed to the existence of only a few realized examples of self-supporting structures from solid cast glass elements. The, so far, limited demand has in turn led to the absence of a standardized manufacturing process, to a lack of consistent engineering data and to a general unawareness of the potential of cast glass in structural applications in architecture.

The aim of this research is to bridge the knowledge gap on the use of cast glass in structural components in architecture, and introduce the potential and limitations of this alternative production process. To accomplish this, the current research focuses on the application of solid cast glass components in self-supporting envelopes with no additional, visible, substructure. Accordingly, the research evolves around the design and experimental validation of two new building concepts for self-supporting envelopes purely from cast glass components: adhesively bonded and interlocking cast glass structures.

1.1.2 **Cast glass as a structural material: Potential and limitations.**

In theory, casting enables us to create monolithic glass elements of any form and cross-section (Fig. 1.4). Such an immense forming potential combined with the high compressive strength of glass offers endless possibilities in the design of monolithic, entirely transparent, structural glass members, e.g. storey-high glass columns (Fig. 1.3) or even entire glass envelopes. Nevertheless, in practice, casting glass in volumes of such a scale requires a meticulous and excessively time-consuming annealing process that can jeopardize the marketability of the components and render them financially unaffordable. To this end, the choices of glass composition, overall dimensions, mass and form of the object are key factors for the total annealing time.

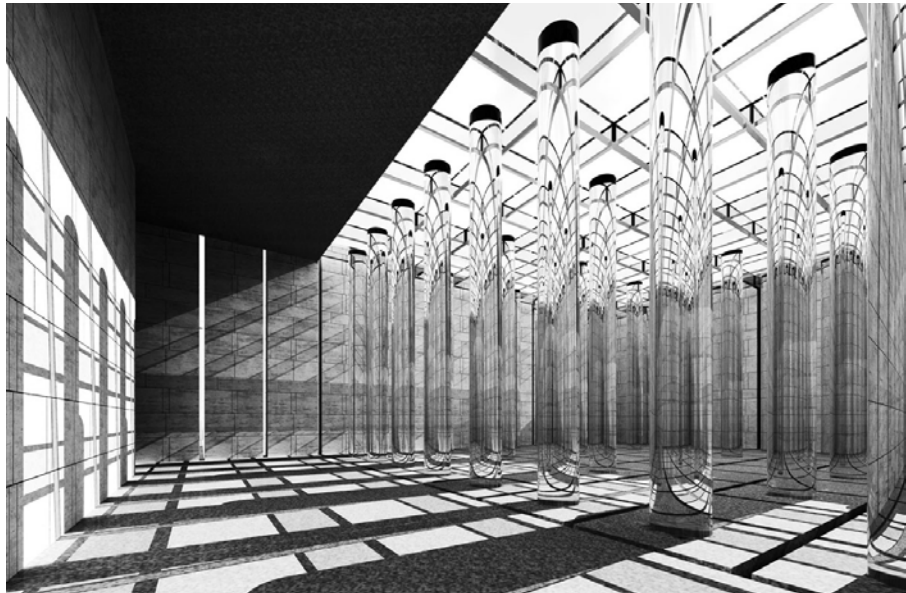


FIG. 1.3 Illustration of *Giuseppe Terragni* and *Pietro Lingeri*'s unrealized design for the *Danterium* (1938). Can we cast such solid, transparent glass columns? Source: archeyes.com



FIG. 1.4 Glass casting (hot-pouring)

In specific, based on its composition, commercial glass can be divided into six main families/types: Soda-lime, borosilicate, lead, aluminosilicate, 96% silicate and fused silica glass. Each glass family differs not only in composition, but also in the resulting material properties (Shand, Armistead 1958). Out of these properties, the thermal expansion coefficient plays a key role in determining the cooling rate of the glass component. For example, the considerably higher thermal expansion coefficient ($9 \cdot 10^{-6}/K$) of soda-lime glass compared to that of borosilicate glass ($3.1 - 6 \cdot 10^{-6}/K$) results in an annealing time that can be more than double in duration. A comparison between the annealing time of the 8.4 kg and 70 mm x 200 mm x 300 mm borosilicate block of the *Atocha Memorial* and the 7.2 kg and 65 mm x 210 mm x 210 mm soda-lime block of the *Crystal Houses* demonstrates this clearly. The latter, although smaller in both dimensions and weight requires circa 36–38 h of annealing (Oikonomopoulou et al. 2017a); almost double the time required for the comparably bigger block of the *Atocha Memorial* which needed 20 h (Goppert et al. 2008).

Mass is another critical aspect. The bigger the component, the exponentially longer the annealing time. This has been well demonstrated in the fields of astronomy and art (Fig. 1.5), where the largest monolithic cast glass objects, made until now, have been manufactured. The 5 m in diameter and 15 tons in weight honeycomb mirror of the *Mt. Palomar Observatory* required 10 months of controlled cooling to remove any residual stresses that could lead to the eventual cracking of the component (Zirker 2005). The *Opposites of White* drum-shaped cast sculptures by artist *Roni Horn*, each 50.8 cm high by 142 cm diameter, required 4 months of controlled annealing to prevent the generation of residual stresses respectively (Kroller-Muller Museum 2007).



FIG. 1.5 Solid glass sculptures by artist *Roni Horn*.

A substantially lighter structure can greatly reduce the annealing time, allowing for the fabrication of larger components in considerably reduced time. This is well illustrated by the evolution in the casting of the blanks of the *Giant Telescope Mirrors* over time, discussed in chapter 3.2. By employing smart geometry, i.e. a honeycomb structure, the four times heavier and more than triple in diameter blank of the *Giant Magellan Telescope* required 4 times less annealing time than a 2.5 m in diameter solid disk.

If the above mentioned parameters are considered and incorporated from the design stage, structurally efficient cast glass components can be made of various shapes and forms. Currently, there are only a few realized projects utilizing solid cast glass components in a structural way. The most representative projects are the envelopes of the *Atocha Memorial* (Schober et al. 2007), the *Crown Fountain* (Hannah 2009) and the *Optical House* (Hiroshi 2013), discussed in Chapter 4. Another characteristic example is the *Crystal Houses* (Oikonomopoulou et al. 2017a; Oikonomopoulou et al. 2015b), the research and development of which are an integral part of this dissertation, presented in Chapters 5 and 6.

In all four projects, cast glass elements have been limited to a size comparable to the one of standard rectangular terracotta bricks, so that they can be manufactured with an economically feasible annealing schedule. Owing to their substantial cross-sectional area and monolithic nature, solid glass bricks have great potential as structural elements in architecture: They can form repetitive units for the construction of three-dimensional glass structures that are not sensitive to buckling and thus, can take full advantage of glass's high compressive strength, sparing the necessity for an additional supporting structure. Yet, due to the lack of standardized structural specifications and strength data on transparent adhesives, the majority of such projects so far rely on a supporting substructure to ensure rigidity and prevent buckling. Such solutions not only compromise the resulting level of transparency but also do not take full advantage of the inherent strength of glass.

Prior to this dissertation the only realized example of an adhesively bonded, self-supporting, cast glass structure was the *Atocha Memorial*, where solid glass blocks bonded by a transparent UV-curing adhesive form a cylindrical construction. The cylindrical geometry of the *Memorial* plays a key role to the structure's stiffness, eliminating in this case the necessity of additional steel elements for its support (Schober et al. 2007) and allowing for a more elastic (and less rigid) adhesive compared to the one applied at the *Crystal Houses* façade.

From all the above, it is evident that there is still great room for exploration in the field of structural cast glass in architecture; particularly towards creating self-

supporting or even load-bearing structures purely from cast glass components that circumvent the use of opaque reinforcement elements. Furthermore, little exploration has been made so far on the shaping potential of cast glass in the realized projects. The cast glass components of the realized architectural projects copy the design language of common terracotta masonry bricks – just as many of the marble decorative details in Greek temples are reminiscent of the older wooden connections. Yet, glass as a material has different properties and manufacturing process, compared to standard masonry, stone or concrete, which sequentially call for different forms. The shape of cast glass components can be further improved towards both a more cost- and time-efficient production and assembly combined with an enhanced structural performance.

The current research therefore focuses on broadening the knowledge and spectrum of structural systems made of solid cast glass components in architecture. Accordingly, the structural potential of cast glass is examined from the unit level to the entire structure. To prove the feasibility of cast glass as a structural material, different systems for self-supporting envelopes made of cast glass components are developed, designed and experimentally validated. To exhibit the structural capacity of glass, the goal is to attain glass structures of maximum transparency and of minimum additional elements such as connectors. The following section provides an overview of the research aspects and the applied methodology.

1.2 Research questions and aims

Scope of this research is to develop and experimentally validate new design concepts, from the component's form to the overall structural system that can lead to fully transparent, self-supporting building envelopes made of solid cast glass components. The main research question can be formed as follows:

What is the potential of using cast glass elements as structural components for the generation of self-supporting envelopes without the need of opaque reinforcement elements?

The research can be further divided into the following sub-questions:

- 1 What are the main practical implications and limitations of employing casting for structural glass elements? (Chapter 2)
- 2 In what ways can different glass recipes, geometry and fabrication methods affect the manufacturing process and thus the feasibility and marketability of the resulting component, as suggested by relevant pre-existing applications in other fields? (Chapters 2 & 3)
- 3 Which are the current structural systems employed for creating self-supporting structures out of cast glass components? Which are the main advantages and drawbacks of each system? What is the buildability of these systems and which design principles do the glass components follow? (Chapter 4)
- 4 What is the structural potential and which are the main factors that influence the structural performance of an adhesively bonded cast glass system? (Chapter 5)
- 5 Which are the main engineering challenges involved in an adhesively bonded cast glass system for structural applications? (Chapter 6)
- 6 Which are the main engineering advantages, principles and design criteria for creating a dry-assembly, interlocking cast glass structure? (Chapter 7)
- 7 What is the potential of an interlocking system out of cast glass blocks for structural applications in architecture and which are the main factors that influence its structural performance? (Chapter 8)

1.3 Objectives

The objective of this research is to design, develop and validate via experimental testing new design concepts for fully-transparent, self-supporting structures (i.e. envelopes, walls) in architecture utilizing solid cast glass components. Aim is to explore the structural potential of cast glass in architectural applications from the level of the unit to the entire structure.

1.4 Research Methodology

Fig. 1.6 provides an illustration of the methodology of this thesis. Towards developing new design concepts for self-supporting structures of cast glass components, initially an extended literature study and field research is conducted on the commonly applied glass types/compositions and their properties, casting production methods and mould types. Characteristic examples of cast glass structures, not only in the field of architecture but also in other areas such as astronomy and art, are analysed and assessed with comparative data charts, in order to exhibit both the limitations and the potential of cast glass. Accordingly, preliminary conclusions are drawn that help establish design criteria.

Subsequently, design proposals are made regarding the component's form, structural system and type of connection or bonding media.

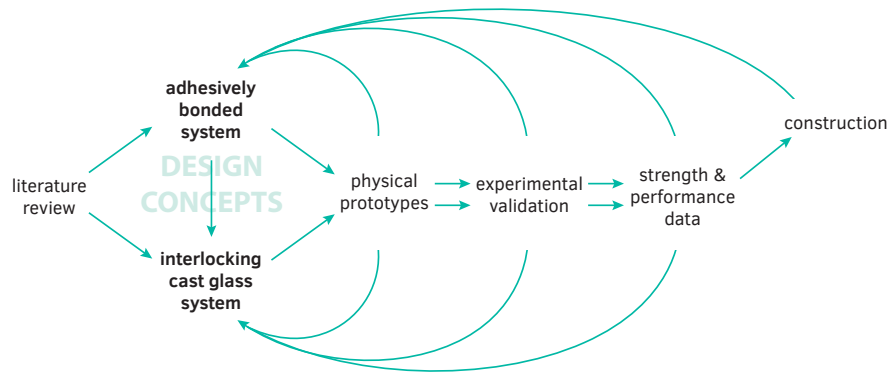


FIG. 1.6 Methodology diagram of the thesis.

The main body of the dissertation presents the research, development and experimental validation of 2 different design concepts: an adhesively bonded glass brick system and a system out of dry-assembly, interlocking cast glass components. The former is developed and eventually applied in a real case-study, the *Crystal Houses façade* in Amsterdam designed by MVRDV. The author of this dissertation has been deeply involved in the research, development and construction of the realized adhesively bonded cast brick façade. Having the opportunity to be at the frontline of realizing this cutting-edge project was a unique learning process. It has been a long, challenging, often stressful, yet rewarding and irreplaceable experience

to observe one's research scaling up from a few bonded bricks to, eventually, a 10 x 12 m façade that received several engineering and architectural awards. Having spent more than 18 months in research and 7 entire months at the construction site as a quality control engineer gave the author a rare insight in all the practical implications involved in such a project. The *Crystal Houses façade*, bonded by a rigid, colourless adhesive of virtually zero thickness, manifests the potential of cast glass in architecture but also points out the engineering challenges resulting from a permanent construction of extreme accuracy and intensive and meticulous labour. Achieving the desired dimensional accuracy and visual performance proved to be an even bigger challenge than obtaining the desired structural performance.

It was the engineering challenges and irreversible nature of this system that have led to the second design concept: Interlocking cast glass components that are stacked with the aid of a transparent dry interlayer, circumventing the use of adhesives. This allows for a reversible, reconfigurable, recyclable and easily-assembled structure that circumvents the aforementioned challenges and results as well to a more sustainable construction system: eventually the components can be easily demounted and recycled again, as they are contaminant-free. This system is yet to be applied in reality, but can be a promising answer for future inspiring structures, from small-scale furniture to full-glass columns and complete building envelopes.

Integral part of the research is the fabrication and engineering of full-scale prototypes and the experimental validation of the final design concepts. Numerous physical prototypes have been made to assess various critical aspects for the feasibility of the proposed systems. These include among others the visual performance, ease of fabrication, ease of assembly and end of life scheme of the proposed design concepts and corresponding glass components. To evaluate and quantify the structural behaviour of the presented systems, series of prototypes have been experimentally tested until failure so that statistical data can be derived regarding each proposed system's performance.

As already mentioned, the described adhesively bonded glass block system has been developed in collaboration with, and support by, the industry. All conducted experiments are made with industrially fabricated glass blocks of high dimensional accuracy. The provided results can be used as design guidelines for future applications. The second, interlocking system was developed within research context only and was funded through a *4TU.bouw* research grant and self-funding. Thus, all experiments conducted are made utilizing manually fabricated glass blocks at the *Glass & Transparency Lab*. These blocks present considerably lower dimensional tolerances and surface quality compared to the ones produced by the industry, which can have a significant influence in the structural performance of such a

system. Hence, in this case, the experiments aim to provide a qualitative comparison of different variables that influence the system but should not be used as strength values. To provide further insight on the effect of these factors in the structural behaviour and capacity of such a system, a numerical model has also been made. Compared to the presented adhesively bonded system, the interlocking system is still under development and further research is necessary for its real application in the built environment.

Still, the findings of both concepts prove their feasibility and highlight their advantages and drawbacks. Based on the results, suggestions are made for future research directions towards the further exploration of the potential of cast glass in structures.

1.5 Societal and Scientific Relevance

The applicability of glass in structures is continuously ascending, as the transparency and high compressive strength of the material render it the optimum choice for realizing diaphanous structural components that allow for both light transmittance and space continuity. Yet, so far, engineers and architects alike tend to think of glass as a virtually 2D, brittle material susceptible to buckling and spontaneous failure. In this direction, this research aims to introduce a new method for building with glass that enables the realization of safe, self-supporting full-glass structures that can take full advantage of the compressive strength of glass. By casting, solid glass elements of high transparency and strength can be made, offering a vast potential in the realization of 3D transparent elements and structures that so far have been considered unrealistic. Glass is no more a 2D material but a three-dimensional solid. Despite glass's brittleness, solid glass components are robust, have an improved buckling resistance due to their geometry and are hence, safe to use. Moreover, a solid glass block has competitive or even superior compressive strength to that of conventional building materials such as concrete and steel (see Chapter 1.1). Thus, this research aims as well to introduce a shift in the mentality of structural engineering by introducing cast glass as a new building material. To this end, experimental work is conducted in order to provide scientific data on both the performance of cast glass components as well as on the performance of the developed structural systems employing these cast glass components. This data can be used as a guideline for the applicability of the developed systems in reality.

Taking into account that the construction and logistics of a project involving cast glass components can face the most critical aspects for its feasibility, the actual construction of the *Crystal Houses* façade provides great insight on the engineering challenges involved in such a system. The real application of the developed system provides valuable input for the development of a second, demountable glass system that circumvents the use of adhesives and the relevant challenges, allowing for an easily-assembled and reversible structure. Such a system in turn can result in great reduction in the involved costs, construction time and most importantly, lead to a more sustainable, circular solution compared to an adhesively bonded structure. More specifically, in the developed interlocking, dry-assembly glass system, the reuse of the cast glass components is addressed as a design guideline, as well as the use of waste glass as raw material. Moreover, the design for disassembly of this novel system allows the easy reuse, repurpose or recycle of the components at the end of life of the specific application.

1.6 Outline of the dissertation

Fig. 1.7 presents the outline of this dissertation. The dissertation consists of 4 parts, each with a specific focus. Part I provides the *Introduction to the Research* and contains the current Chapter 1. Part II focuses on the *Theoretical Framework* of the research, which includes Chapters 2–4. In specific, Chapter 2 focuses on the main materials and production methods for cast glass. Following, Chapter 3 provides an overview and comparative assessment of existing large-scale non-architectural cast glass applications. Finally, Chapter 4 discusses the structural use of cast glass in architecture through both existing projects and the systems developed in this research. Part III presents the *design and experimental validation* of the two structural systems developed within the framework of this study. In specific, Chapter 5 focuses on the research, development and experimental validation of an adhesively bonded system utilizing solid cast glass blocks. The investigated system has been successfully applied to the *Crystal Houses Façade* in Amsterdam. Chapter 6 discusses all the challenges and innovations necessary for the realization of the façade. Based on the aforementioned challenges, a new concept for glass structures out of dry-assembled interlocking cast glass components is presented in Chapter 7. Chapter 8 provides the numerical and experimental validation of the interlocking glass system. Finally, Part IV, comprising Chapters 9 and 10, presents an *integrated discussion of the research results*. This part provides the conclusions from the

research, a discussion on the production and design aspects of cast glass structural components for other applications besides self-supporting envelopes, as well as recommendations for future studies.

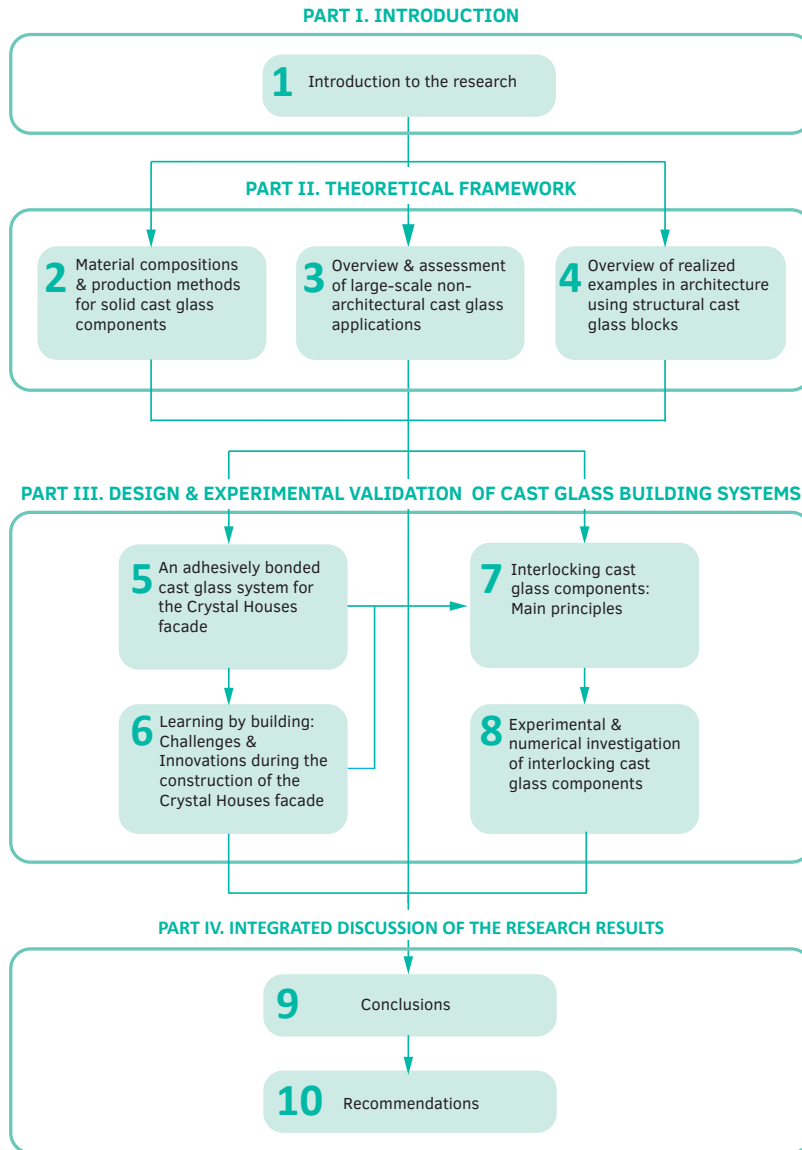


FIG. 1.7 Research strategy scheme / dissertation outline



Casting of soda-lime glass blocks at *Poesia* Factory in Italy

Casting

To give a shape to (a substance) by pouring in liquid or plastic form into a mould and letting harden without pressure

Definition by the Merriam-Webster Dictionary

[1] An object at or near finished shape obtained by solidification of a substance in a mould.

[2] Pouring molten metal into a mould to produce an object of desired shape.

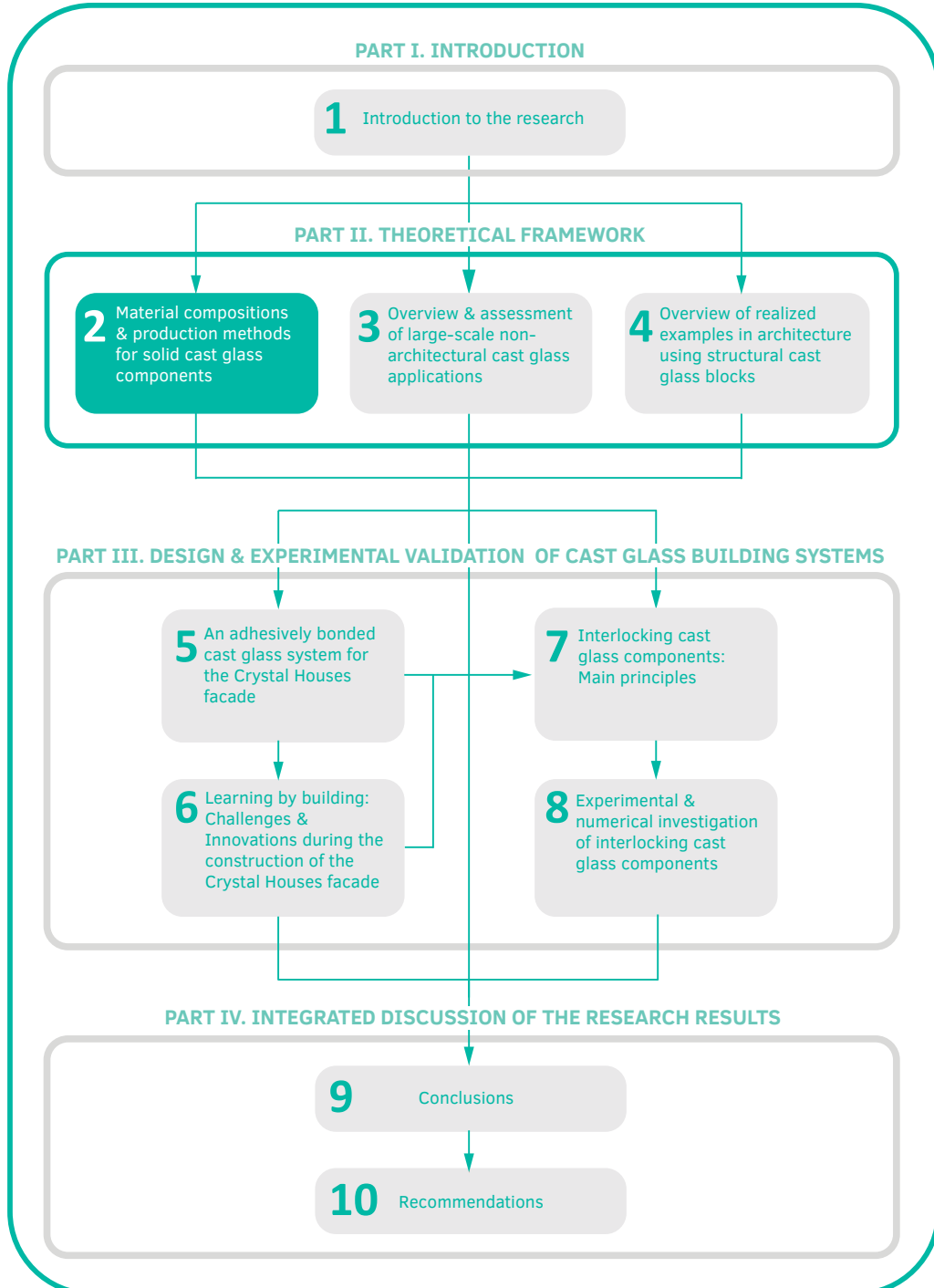
Definition by the Engineering Dictionary

Casting method

Casting is a method where a solid material is dissolved, heated to suitable temperature (generally treated to change its chemical structure), and is then added into a mould or cavity, which keeps it in a proper form during solidification. As a result, in just one step, complex or simple designs can be created from any material that can be dissolved. The end product can have nearly any setting the designer needs.

Definition by the Engineering Articles
(www.engineerinigarticles.org)

Exploring the third dimension of glass



Solid cast glass components and assemblies for structural applications

2 Material compositions and production methods for solid cast glass components

Overview of the current production methods and chemical compositions of cast glass⁴

Glass can be made by different manufacturing processes and by numerous of varied recipes that in return provide the material with different properties. Owing to their workability in lower melting temperatures and the corresponding decreased manufacturing costs, soda-lime and borosilicate glass types are preferred for cast glass applications in structures. Glass can be cast in two ways: primary and secondary casting. In primary casting, glass is molten from its primary raw ingredients, whereas in secondary casting, solid existing pieces of glass are re-heated until the (semi-) liquid mass can flow and be shaped as desired. The main process of primary casting is hot-forming (melt-quenching) and of secondary casting is kiln-casting. The principal difference between the two methods, besides the initial state of glass, is the required infrastructure. In hot-forming, molten glass from a furnace is poured into a mould and is then placed in another, second furnace for annealing. In contrast, kiln-casting employs a single kiln for the melting of the (already formed) glass into the moulds and for the subsequent annealing process and requires lower operating temperatures. In both methods the annealing process is similar. The annealing schedule is influenced by numerous factors that cannot be easily simulated as a complex non-linear time dependent multi-variable analysis is required. As a result the annealing schedule of large 3-dimensional cast units is commonly empirical. Different mould types, disposable or permanent, can be used for casting glass objects. The choice of mould mainly depends on the production volume and desired level of accuracy of the

⁴ This chapter has been published as part of the review article: Oikonomopoulou F., Bristogianni T., Barou L., Veer F., Nijse R. The potential of cast glass in structural applications. Lessons learned from large-scale castings and state-of-the art load-bearing cast glass in architecture. Journal of Building Engineering, vol.20, 2018.(Oikonomopoulou et al. 2018c)

glass product, and is in practice usually cost and time driven. Currently, there is no standard to determine the design strength of solid cast glass objects for structural applications in architecture. Based on the assumption that the increased volume of cast glass can lead to a higher amount of randomly distributed flaws in the meso-structure, the bending strength of cast glass is expected to be comparable but slightly less than that of standard float glass.

2.1 Introduction

Cast glass may have been the oldest form of glass-making, yet, at present it is rarely employed for architectural applications. This chapter serves as an introduction to casting as a manufacturing process for glass. Accordingly, the most common glass and mould types are presented and the main casting processes are described. The annealing process is explained, highlighting the different factors that can influence the annealing schedule of a cast object. Finally, the properties of cast glass as a structural material are discussed in comparison to standard float glass.

2.2 Types of Glass

Based on its composition, commercial glass can be divided into six main families/ types: soda-lime, borosilicate, lead, aluminosilicate, 96% silicate and fused silica (quartz) glass. Table 2.1 presents the typical chemical composition and characteristic applications of each glass type. An extensive description of the different glass types can be found in (Shelby 2005; Shand, Armistead 1958).

TABLE 2.1 Approximate chemical compositions and typical applications of the different glass types as derived from (Shand, Armistead 1958).

Glass type	Approximate Composition	Observations	Typical applications
Soda-lime (window glass)	73% SiO ₂ 17% Na ₂ O 5% CaO 4% MgO 1% Al ₂ O ₃	Durable. Least expensive type of glass. Poor thermal resistance. Poor resistance to strong alkalis (e.g. wet cement)	Window panes Bottles Façade glass
Borosilicate	80% SiO ₂ 13% B ₂ O ₃ 4% Na ₂ O 2.3% Al ₂ O ₃ 0.1% K ₂ O	Good thermal shock and chemical resistance. More expensive than soda-lime and lead glass.	Laboratory glassware Household ovenware Lightbulbs Telescope mirrors
Lead silicate	63% SiO ₂ 21% PbO 7.6% Na ₂ O 6% K ₂ O 0.3% CaO 0.2% MgO 0.2% B ₂ O ₃ 0.6% Al ₂ O ₃	Second least expensive type of glass. Softer glass compared to other types. Easy to cold-work. Poor thermal properties. Good electrical insulating properties.	Artistic ware Neon-sign tubes TV screens (CRT) Absorption of X-rays (when PbO % is high)
Aluminosilicate	57% SiO ₂ 20.5% Al ₂ O ₃ 12% MgO 1% Na ₂ O 5.5% CaO	Very good thermal shock and chemical resistance. High manufacturing cost.	Mobile phone screens Fiber glass High temperature thermometers Combustion tubes
Fused-silica	99.5% SiO ₂	Highest thermal shock and chemical resistance. Comparatively high melting point. Difficult to work with. High production cost.	Outer windows on space vehicles Telescope mirrors
96% silica	96% SiO ₂ 3% B ₂ O ₃	Very good thermal shock and chemical resistance. Meticulous manufacturing process and high production cost.	Furnace sight glasses Outer windows on space vehicles

Soda-lime is the most common and least expensive glass type (Corning Museum of Glass 2011d). It features limited resistance to high temperatures and to rapid temperature fluctuations. Borosilicate glass, i.e. silicate glass with minimum 5% boric oxide, has a considerably lower thermal expansion coefficient which increases the resistance to thermal shocks and reduces annealing time. Lead glass has a high percentage of lead oxide (min. 20% of the batch) and is relatively soft. It has a lower working temperature than soda-lime and is the second least expensive option. It is favoured for cast glass art as it is much softer to grind and polish than soda-lime (Thwaites 2011). Due to its ability to absorb X-rays, lead glass is employed as well for nuclear block applications. On the downside lead glass has limited thermal shock and high temperature resistance to and is susceptible to scratching due to its softness; thus it is not considered suitable for architectural applications. Aluminosilicate glass, 96% silica glass and fused silica glass can sustain much higher operating temperatures and heat shocks than borosilicate glass; however they require significantly more energy for their production due to the considerably higher temperatures required for their forming, (Table 2.2), which in turn increase substantially the manufacturing cost⁵.

TABLE 2.2 Approximate properties of the different glass types of Table 2.1 based on (Shand, Armistead 1958)*. Mean Melting Point at 10 Pa.s as stated by (Martlew 2005).

Glass type	Mean melting Point at 10 Pa.s*	Softening Point	Annealing Point	Strain Point	Density	Coefficient of Expansion 0°C - 300°C	Young's Modulus
	[°C]	[°C]	[°C]	[°C]	Kg/m ³	10 ⁻⁶ /°C	GPa
Soda-lime (window glass)	1350-1400	730	548	505	2460	8.5	69
Borosilicate	1450-1550	780	525	480	2230	3.4	63
Lead silicate	1200-1300	626	435	395	2850	9.1	62
Aluminosilicate	1500-1600	915	715	670	2530	4.2	87
Fused-silica	>>2000	1667	1140	1070	2200	0.55	69
96% silica	>>2000	1500	910	820	2180	0.8	67

* These values are only given as a guideline of the differences between the various glass types. In practice, for each glass type there are numerous of different recipes resulting into different properties.

⁵ The considerably higher operating temperatures also lead to a significantly reduced life-span of the furnace that further increases the manufacturing costs. Communication with the industry (AGC Belgium) has suggested that a furnace used for melting aluminosilicate glass has approximately half the life-span compared to a furnace used to melt soda-lime glass due to the faster deterioration of the refractory material. For a clear depiction of the difference in the required operating temperatures, refer to Fig. 2.18: Approximate viscosity versus temperature curves plot for the most characteristic glass families described in tables 2.1 and 2.2 based on (Shand, Armistead 1958). 2.16 which shows the viscosity versus temperature curves for the most characteristic glass families described in Tables 2.1 and 2.2.

Hence, such glasses are used in specialized applications, such as mobile telephone screens (aluminosilicate) and spaceship windshields (fused-silica)(Corning Museum of Glass 2011a).

Owing to their reduced cost and comparatively easier manufacturing process and post-processing, soda-lime, borosilicate and lead glass are currently prevailing for castings of standardized or large monolithic glass objects. Due to its reduced hardness lead glass is not recommended for architectural applications. Subsequently, for cast glass applications in architecture, soda-lime and borosilicate glass are the prevailing types.

In the experimental part of this research, soda-lime silica glass is chosen for the manufacturing of prototypes, since, it is the most common and least expensive glass type in the building industry⁶.

2.3 Prevailing glass manufacturing processes and current dimensional limitations

Based on its manufacturing process, glass for building industry applications can be shaped as a flat, extruded or solid element. From these methods, float glass is the prevailing type in the building industry. An additional, yet currently only developed within research context, manufacturing method for glass is 3D-printing. Below, the main processes and the corresponding current dimensional limitations for each manufacturing method are briefly presented. It can be concluded that cast glass is the only manufacturing method at present that allows for the creation of solid glass components with a considerable cross-section in 3 dimensions.

⁶ Soda-lime glass is a more economic option compared to borosilicate glass due to the already considerably higher demand and vast availability of this type of glass and the corresponding raw material. Also, owing to its lower melting point, soda-lime glass requires less energy to be produced, which further decreases the involved manufacturing costs.

2.3.1 Float glass

Flat glass is currently the prevailing type of glass for the building industry. At present, 90% of the flat glass is produced by the float glass method (Bourhuis 2014). The main advantages of this process, introduced in 1959 by the *Pilkington Brothers*, is its relatively low cost, wide availability, superior optical quality glass and large size of glass sheets. A schematic representation of the (soda-lime) float glass process can be seen in Fig. 2.1.

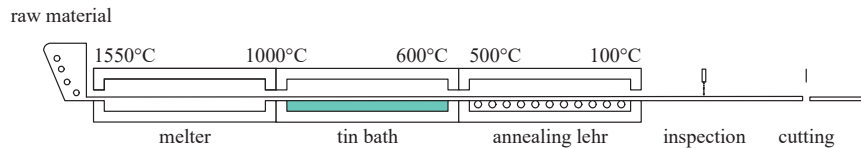


FIG. 2.1 Schematic illustration of the float production process by (Louter 2011) based on (Wörner et al. 2001).

In this continuous float glass process the raw materials are melted in a furnace at $\sim 1550^\circ\text{C}$. The molten glass is poured at $\sim 1100^\circ\text{C}$ onto a bath of molten tin. Being less dense, the glass floats and forms a continuous glass ribbon (approximately 6 mm thick) with perfectly smooth surfaces of the desirable thickness (Fig. 2.2). The thickness of the glass can be adjusted through top rollers in standard thicknesses between 2 and 25 mm⁷.

Upon leaving the tin bath the glass has cooled down to $\sim 600^\circ\text{C}$. At this temperature range glass has become a solid ribbon which is drawn into a cooling oven, the annealing lehr. In the annealing lehr the solid glass ribbon is carried on rollers over a length up to 150 m so that it is slowly and controllably cooled down to 100°C , preventing the generation of residual stresses. Once the glass has left the annealing lehr it is inspected by an automated process for visual defects, which are subsequently removed in the cutting process. Finally, the glass is cut to its final size by automated diamond wheels. The sides of the glass ribbon are also slightly cut to

⁷ Float glass is produced in standard thicknesses of 2, 3, 4, 5, 6, 8, 10, 12, 15, 19 and 25 mm. In practice, the thickness (for building applications) ranges from 4 to 19 mm. 25 mm thick glass is rarely produced (for example currently in Europe only the Cuneo float line of AGC produces 25 mm thick glass). Reasons include the comparatively much slower cooling and annealing process and complications with the cutting of the excessive edge of the float ribbon.

remove any marks of the rollers used to adjust its thickness in the tin bath (Bricknell 2010). The standard float glass size is 6 x 3.21 m (Fig. 2.3), but larger (oversized) plates (Fig. 2.4) can be obtained as well⁸. Yet, the maximum commercial thickness of the float glass panels remains 25 mm.

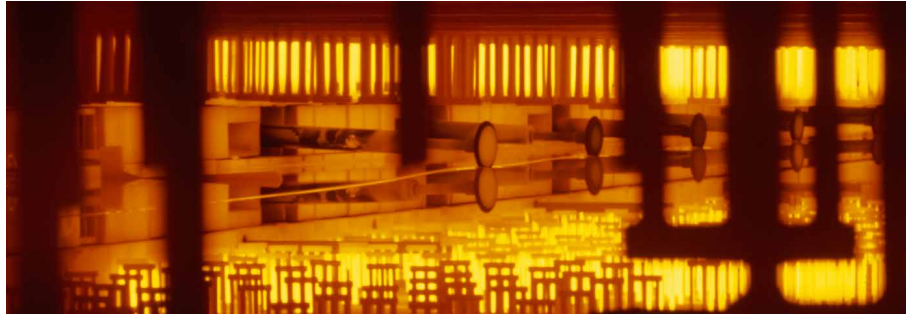


FIG. 2.2 Float glass ribbon within the tin bath. Source: <https://www.skyre-inc.com/applications/hydrogen-recycling/>



FIG. 2.3 Glass structure out of standard float panels up to 6 m in length by *EOC Engineers* in Philadelphia, USA.

⁸ The maximum size of float glass panels has been continuously increasing over the last years (Callaghan, Marcin 2009). Currently oversized plates up to 20 m in length and 4 m in width can be obtained.

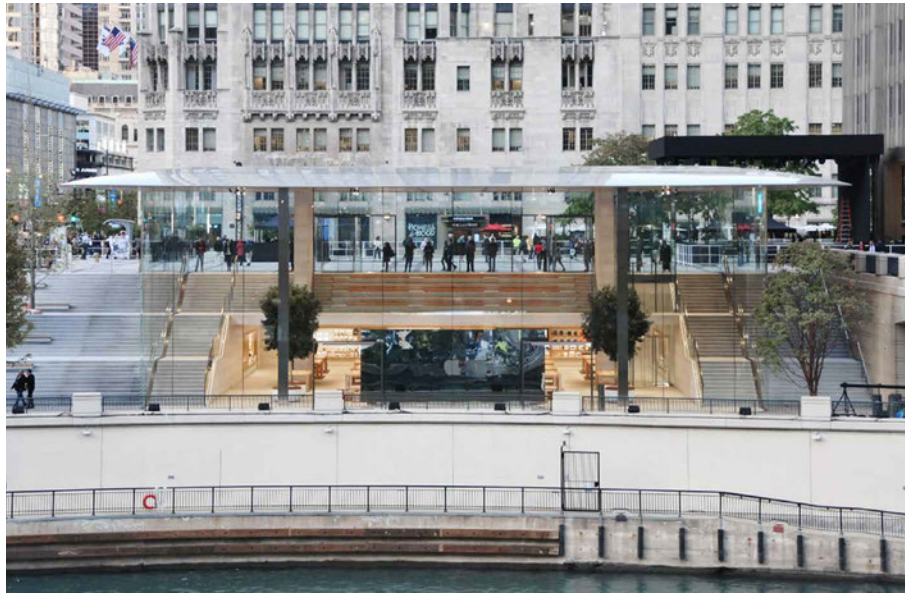


FIG. 2.4 The *Apple Store* in Chicago by *EOC Engineers*. Panels are 3 m wide and up to 10 m in height. Source: *EOC Engineers*.

2.3.2 Extruded glass

Glass extrusion is used to produce glass profiles such as (thin wall) tubes, rods or other glass elements with a constant cross-section. Extruded glass profiles are mainly used in interior architecture, art, design and lighting solutions. Extrusion can be used for glasses with a steep viscosity curve, increased tendency to crystallize and/or a considerably high softening point, such as silica glass (Roeder 1971). Extrusion is an economical method for producing various types of full or hollow profiles with sharp-edged cross sections for industrial use (Pfaender 2012). The most common method for a continuous drawing of tubing is the *Danner process* (Fig. 2.5): A continuous strand of molten glass flows onto a rotating, slightly downward pointing mandrel. Air is blown down a shaft through the middle of the mandrel, creating a hollow space in the glass as it is drawn off the end of the mandrel by a tractor mechanism. The diameter and thickness are controlled by regulating the air flow rate and the speed of the drawing machine. This process allows for a wall thickness of up to 10 mm (Haldimann et al. 2008). After being redirected horizontally, the solidifying tube is transported on a roller track to the pulling unit and is cut into sections of, typically, 1.5 m in length.

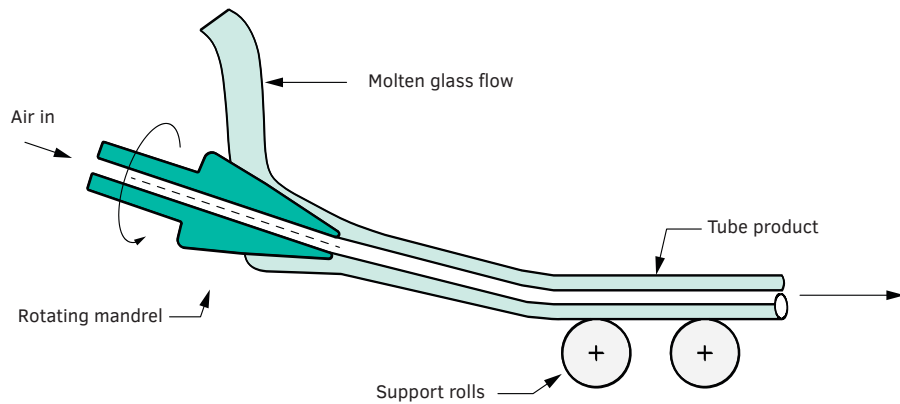


FIG. 2.5 Principle of the Danner process.

The more recent centrifuging process allows for the production of relatively large sections and non-rotationally symmetrical items by spinning: Molten glass is fed into a steel mould that rotates at the required speed. At high speeds, the glass can assume almost cylindrical shapes. When the glass has sufficiently cooled, rotation stops and the glass is removed. This process is more expensive than the Danner production method.

Another important process is the *Vello process*, which has a similar output as the *Danner process*. Molten glass from the furnace flows downward through an orifice (ring). The hollow space in the glass is maintained by a pipe with a conical opening located within the ring. The tube, which is still soft, is redirected horizontally and is drawn off along a roller track, cooled and cut as in the aforementioned process.

Currently, the leading manufacturer of extruded glass profiles is *SCHOTT AG*. The profiles come in a standardized length of 1.5 m but can be customized up to 10 m in length. At present, the standard production of *SCHOTT AG* includes hollow tubes up to 465 mm in diameter and 7 mm thick and solid rods up to 30 mm in diameter (SCHOTT AG 2017).

A great example of the architectural potential of glass rods is the window installation for the *S.C. Johnson Building* in USA (Fig. 2.6), designed by American architect *Frank Lloyd Wright*. The structural potential of the rods has been exhibited in the design and testing of a glass bundle (Fig. 2.7) by (Oikonomopoulou et al. 2017b) which was later applied in the glass truss bridge (Fig. 2.8) as described in (Snijder et al. 2018).



FIG. 2.6 Extruded hollow tubes used at the facade of the *Johnson Building* in USA.

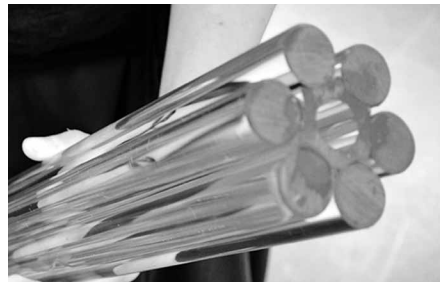
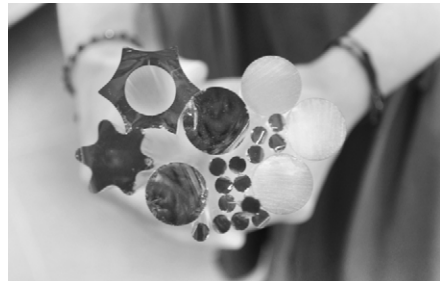
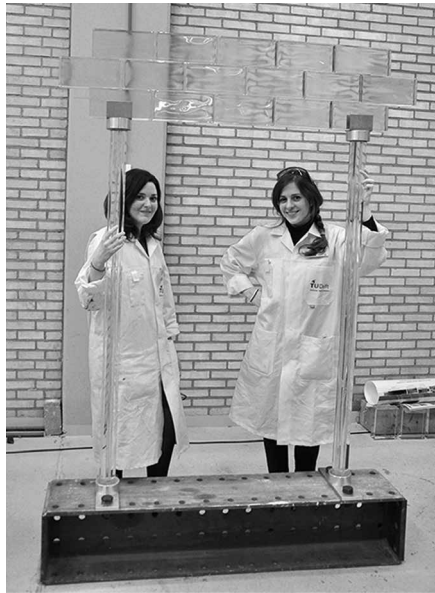


FIG. 2.7 Left: 1.5 m long bundled glass columns at *TU Delft Glass Lab*. Top right: Extrusion profiles made by *SCHOTT AG*. Bottom right: A bundled glass column made of adhesively bonded extruded profiles developed by (Oikonomopoulou et al. 2017b).

For the *GlassTec 2018 Fair* the *TU Delft Glass & Transparency Group*, in collaboration with *Arup*, *SCHOTT AG* and *RAMLAB* developed two novel glass structures utilizing glass rods and tubes: A *glass swing* (Fig. 2.9), created from glass struts, each composed of five glass rods that are pre-stressed by an internal (central) steel bar (Snijder et al. 2019) and a *glass sandwich floor* (Fig. 2.10), where the core elements are extruded glass tubes. The engineering of the latter was based on the concept for glass sandwich panels developed by (Vitalis et al. 2018).

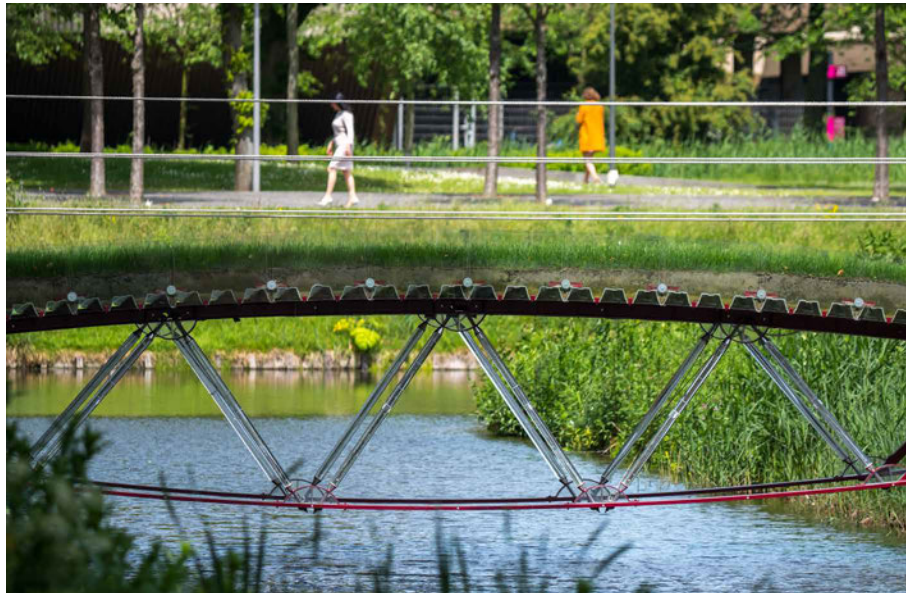


FIG. 2.8 The glass truss bridge at the TU Delft campus made of extruded glass profiles as described in (Snijder et al. 2018).



FIG. 2.9 The glass swing developed by (Snijder et al. 2019) from TU Delft, in collaboration with Arup, SCHOTT AG and RAMLAB for the GlassTec 2018 exhibition.



FIG. 2.10 The glass sandwich floor developed by the *TU Delft Glass & Transparency Lab*, in collaboration with *Arup* and *SCHOTT AG* exhibited at *GlassTec 2018*.

2.3.3 3D-printed glass

3D-printing of glass is still in an infant stage of development. A glass 3D-printing method (G3DP) for optically transparent soda-lime and coloured glass has been recently developed by the *Mediated Matter Group* in collaboration with the *Department of Mechanical Engineering* and *Glass Lab* of *MIT*. The platform is based on a dual heated chamber concept. The upper part acts as a Kiln Cartridge; it operates at $\sim 1040^{\circ}\text{C}$ and pours the molten glass through a nozzle to the desired shape (Fig. 2.12). The object is built within the lower annealing chamber⁹ which keeps the glass hot enough so that the next layer of structure would adhere to it while the glass can cool down controllably (Klein 2015) (Fig. 2.11).

⁹ The temperature of the annealing chamber is set at 480°C , slightly below the glass annealing temperature of 515°C , since the glass heat radiation contributes to an increase of the environmental temperature (Klein 2015).

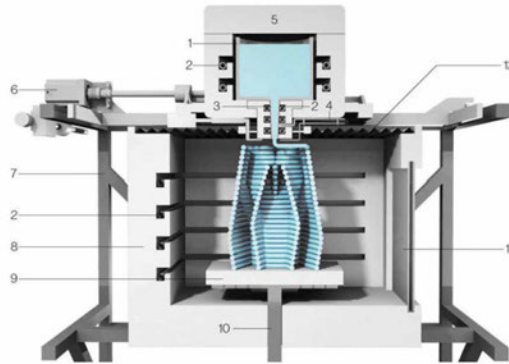


FIG. 2.11 Rendered cross-section of the Kiln Cartridge by (Klein 2015). 1. crucible 2. heating elements 3. nozzle 4. thermocouple 5. removable feed access 6. stepper motor 7. printer frame 8. print annealer 9. ceramic print plate 10. z-driven train 11. ceramic viewing window 12. insulating skirt.

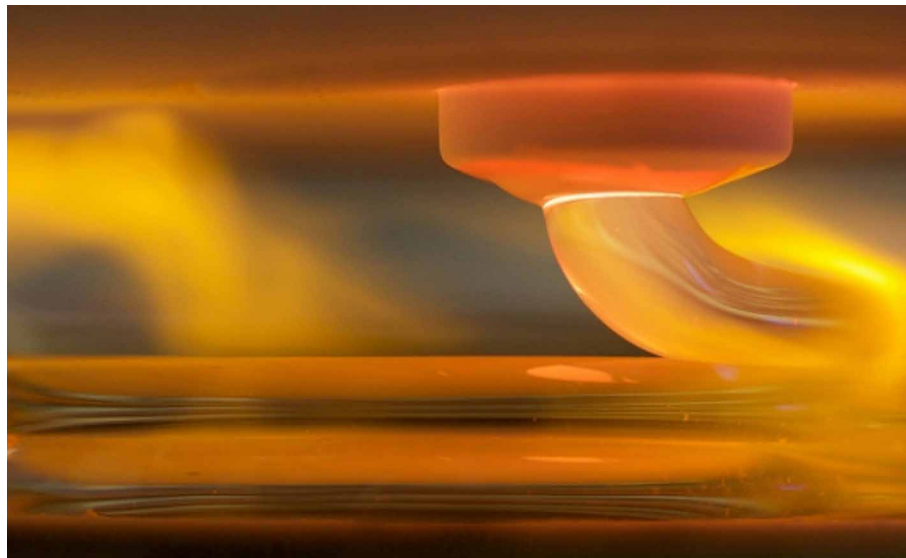


FIG. 2.12 Glass 3D-printing nozzle. Source: Steven Keating.

The process was further developed to a larger-scale additive manufacturing technology (G3DP2) for building components made of silicate glass with tuneable and predictable mechanical and optical properties. G3DP2 includes a digitally integrated thermal control system to accompany the various stages of glass forming and a 4-axis motion control system permitting flow control, spatial accuracy and precision and faster production rates with continuous deposition of up to 30 kg of molten glass (MIT Media Lab 2018). The potential of the new method has been demonstrated by the construction of a series of 3m-tall free-standing, pre-stressed

glass columns consisting of 15 segments each (Fig. 2.13 and Fig. 2.14). The columns do not carry any weight other than their own in the installation. 3D-printing of glass has a high potential in creating components with variable thicknesses and complex inner features. Nonetheless, it faces the same challenges with the annealing of glass objects (discussed in detail in Chapter 2.4) as cast glass. In consequence, 3D-printing of (soda-lime) glass can only occur within a highly controlled annealing chamber: the glass object has to be cooled down to room temperature in a slow and controlled way to release permanent stresses associated with thermal gradients that otherwise would lead to the spontaneous breakage upon cooling. Hence, the glass object is confined to the size of the annealing chamber.



FIG. 2.13 3m tall glass prototypes out of 3D-printed segments. Source: *Paula Aguilera, Jonathan Williams and The Mediated Matter Group.*



FIG. 2.14 An array of 3D-printed glass components prepared in a 3x5x3 array ordered for assembly. Source: *The Mediated Matter Group.*

2.3.4 Cast glass

Cast glass is currently the only method that allows for the creation of 3-dimensional glass objects of a substantial, monolithic cross-section and/or of complex geometry. By pouring molten glass into moulds, solid 3-dimensional components can be made of virtually any size. Moulds can be either disposable out of a soft material such as silica plaster or permanent ones out of steel or graphite. There are two main processes for cast glass: primary casting and secondary casting: In the former, glass is founded as a hot liquid from its raw materials, whereas in the latter, glass already formed in solid pieces is remolten to a temperature where it can flow and be shaped to the desired object.

Glass casting has been commonly used in the fields of art and astronomy. Currently the largest monolithic cast glass objects are the mirror blanks of the Giant Telescopes. Characteristic examples include the *Giant Magellan Telescope* blanks, each 16 t in weight and the *Hale Telescope* blank (Fig. 2.15), weighing 20 t¹⁰. Cast glass has been so far employed in structural applications in architecture in the form of solid blocks, commonly between 2 - 8.4 kg in weight. Characteristic examples are the *Atocha Memorial*, *Crown Fountain*, *Optical House* and the *Crystal Houses*¹¹. Same as with 3D-printing glass the main obstacle with cast glass of considerable dimensions is the time-consuming annealing process. As an example, the successful annealing of the aforementioned *Hale Telescope* blank required 10 months. Table 2.3 provides an overview of the current glass fabrication methods with applications in the building industry.

The current size limitations in the float and extruded processes result in virtually 2-dimensional glass objects of high slenderness ratio. 3D-printed and cast glass are thus, at present, the only methods that can result in essentially, free-form, 3-dimensional glass elements of a substantial thickness. These two processes follow the same basic principle: Molten glass is poured to form a glass object that cools controllably to room temperature into an annealing chamber or kiln. The fundamental difference is that in casting, glass is poured into a mould of the desired shape, whereas in 3D-printing, glass is directly deposited as a viscous fluid that forms a continuous layered construction. On account of the layered nature of a 3D-printed object the overall transparency is compromised. The biggest drawback though of 3D-printing glass is that it is, at present, approx. 30 times slower than

¹⁰ For a more in-depth analysis of the largest cast glass monolithic objects please refer to Chapter 3.

¹¹ For a more in-depth analysis of the existing glass structures with cast blocks please refer to Chapter 4.

cast (and pressed) glass (Klein 2015). Advantages of 3D-printing include the mass-customization and design freedom of the final object. To this end, under the assumption of fully developed processes for 3D-printing and casting of glass, the former would be preferred for customized solutions and the latter for the mass fabrication of identical units. Nevertheless, the creation of cheap, disposable moulds¹² can render cast glass a competitive solution for customized components as well that also exhibit a higher level of transparency compared to 3D-printed ones.

Overall, it can be concluded that casting provides currently the greatest freedom in the volume and size of the resulting glass object.

TABLE 2.3 Overview of existing glass fabrication methods for building components and their current size limitations.

Glass process	Optical Characteristics	Main type of glass applied	Standard size [mm]	Thickness [mm]
Float	Smooth Transparent	Soda-lime	3210 x 6000 ^a	2-25
Extruded	Smooth Transparent	Borosilicate Silica	1500-10000 in length	Hollow: 460 Ø Solid: 300 Ø
3D-printed	Layered Transparent	Soda-lime	currently up to 30 kg	currently approx. 30 mm ^b
Cast	Smooth Transparent	Soda-lime Borosilicate Lead	currently up to 20000 kg ^c	n/a

^a The max. panel size is continuously stretching. At present, up to 20 m long panels have been produced.

^b Based on the work of (Klein 2015)

^c Weight of the Hale Telescope monolithic glass blank. For more information please refer to chapter 3.2.

¹² An overview and discussion on the different mould types for cast glass can be found in Chapter 2.5

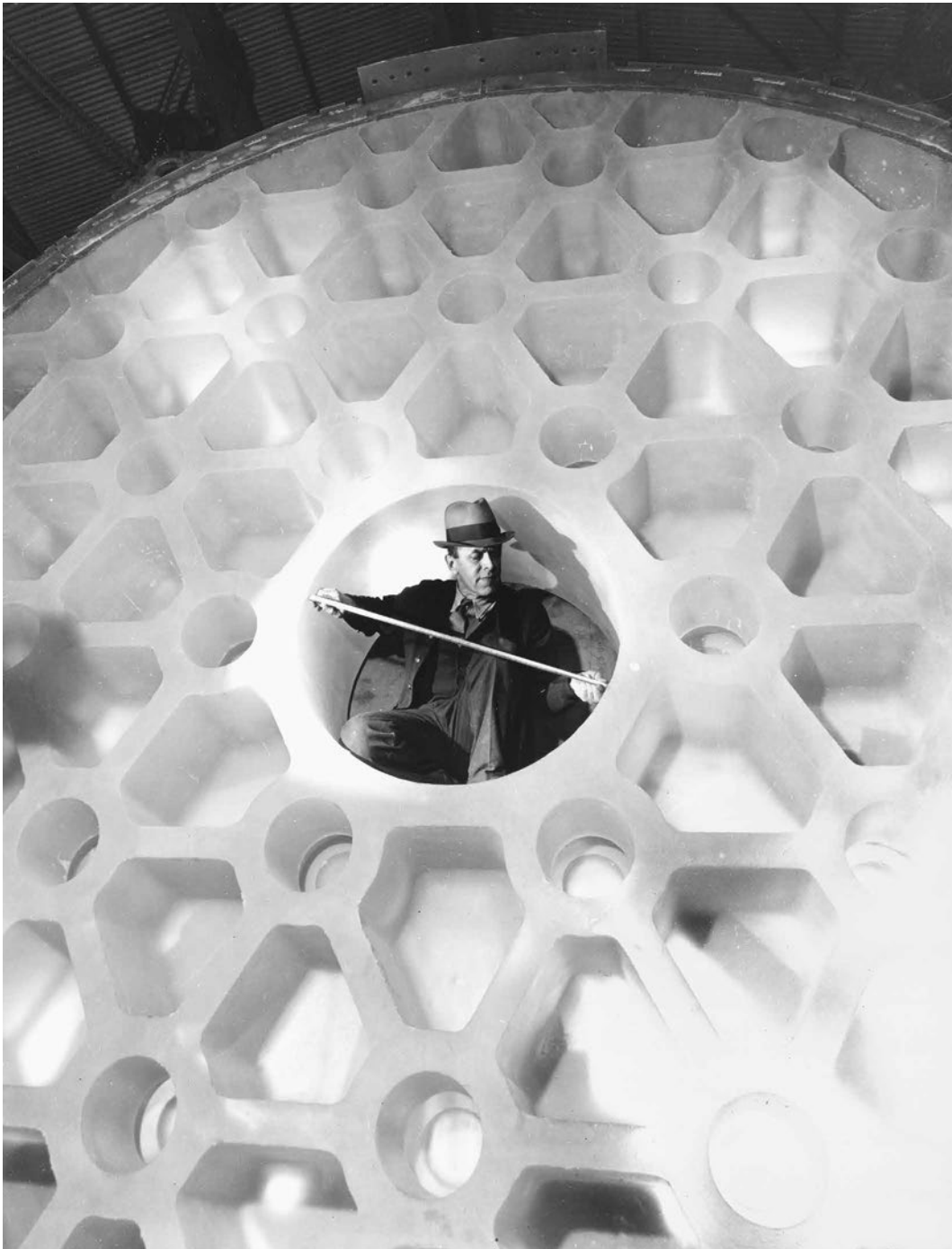


FIG. 2.15 The cast glass blank of the Hale Telescope. Image credits: Collection of the *Rakow Library*, *The Corning Museum of Glass*.

2.4 Casting and annealing process

2.4.1 Prevailing casting processes

According to the starting state of glass, glass casting can be divided into primary and secondary casting. In primary casting, glass is founded as a hot liquid from its raw ingredients, whereas in secondary casting, glass already formulated in solid pieces (i.e. sheet, rods, marbles, grains, powder) is re-heated until it can flow and be shaped as desired (Cummings 2002). Thus, the secondary process requires lower operating temperatures compared to those for founding glass.

The main process of primary casting is hot-forming (melt-quenching) and of secondary casting is kiln-casting (Fig. 2.16). The principal difference between the two methods, besides the initial state of glass, is the required infrastructure. Kiln-casting employs a single kiln for the melting of the (already formed) glass into the moulds and for the subsequent annealing process (Bristogianni et al. 2017). In contrast, in hot-forming, molten glass from a furnace is poured into a mould and is then placed in another, second furnace for annealing.



FIG. 2.16 Left: Primary casting method (hot-forming). Right: Secondary casting method (kiln-casting).

2.4.2 Annealing Process

In both methods, the annealing process is similar. Initially glass is heated until it is viscous enough to flow into the mould. The viscosity of the glass at that point is expected to be between 10 and 10^3 Pa.s, defined as melting temperature and working point of glass correspondingly (Martlew 2005). Once the mould is filled, the glass is rapidly cooled to a few degrees (typically around 20°C) below its softening point¹³. This rapid cooling stage, named quenching, is essential for preventing a crystal molecular arrangement of the melt (see Fig. 2.17). During this phase, the glass's relatively low viscosity allows any induced thermal stress to relax to a negligible amount immediately (Shelby 2005). When the glass temperature drops below the softening point, the viscosity of glass is sufficient for it to retain its shape and not deform under its own weight¹⁴ (Shand 1968). At this point the annealing process of the object starts, aiming at eliminating any possible differential strain and preventing the generation of internal residual stresses during further cooling¹⁵. The cast glass should be maintained for adequate time at the annealing point to release any existing strains and then cooled at a sufficiently slow rate to prevent the generation of residual stresses when the glass temperature has reached equilibrium (Shand, Armistead 1958). At this temperature range, stress can be relieved due to the viscous flow of the material that allows for molecular rearrangements. In particular, at the annealing point stress relief can occur within a few minutes; whilst towards the strain point it requires a few hours¹⁶ (Bray 2001). Effectively, below the strain point, stress is unable to relax in time and is considered permanent (Watson 1999). When the temperature of the entire object has dropped below the strain point, it can cool at a faster pace until ambient temperature, yet adequately slow to avoid breakage due to thermal shock (Shand, Armistead 1958). Fig. 2.17 provides a

¹³ The softening point is defined as the temperature at which the heated glass, supported at each end, begins to sag under its own weight. It must be stressed that even with the exactly same glass, this temperature can slightly vary according to the weight and thickness of the object to be annealed (Bray 2001).

¹⁴ For crystals, transition from solid to liquid occurs exactly at the melting temperature (T_m). Unlike crystals glass has no fixed melting point. Instead it gradually softens and stiffens as the temperature changes. The viscosity of the glass changes with temperature (Schott AG 2004). In this study wherever melting temperature is referred to, it actually concerns a temperature range where viscosity of glass corresponds to approximately 10 Pa.s

¹⁵ At this point, in the hot-pouring method the cast object is placed into the annealing oven.

¹⁶ A small amount of residual stress is acceptable for the majority of glass types, but for optical glass in particular it should be reduced to the minimum. This means that optical quality glass of considerable thickness such as the one required for the giant telescope mirrors, discussed in chapter 3, may require several months of annealing. For example, the Mt Palomar telescope lens, was cooled from 500°C - 300°C at the rate of 1°C a day drop (Cummings 2001).

typical curve for viscosity as a function of temperature for soda-lime glass, indicating the above discussed key temperature points (strain, annealing, softening, working). In Fig. 2.18 the viscosity versus temperature curves of the most characteristic glass families can be seen. A schematic diagram of a typical annealing scheme for soda-lime glass based on (Shand, Armistead 1958) is shown in Fig. 2.20.

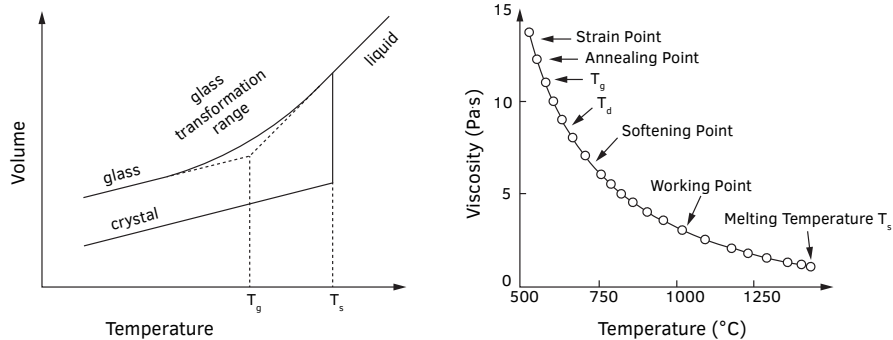


FIG. 2.17 Left: Schematic representation of the volume's dependence on temperature for a glass and a crystalline material. During the cooling process from a liquid to a solid, glasses do not convert to a crystalline state. Right: Typical curve for viscosity as a function of temperature for a soda-lime-silica melt (NIST Standard No. 710). Defined viscosity points are indicated on the figure. Source: (Shelby 2005).

During the annealing range, the magnitude of the resulting internal stresses is largely determined by the temperature difference between the warmest and coolest parts of the glass. This in turn is related to the amount of surfaces exposed to cooling, the type of glass and its coefficient of expansion, the thickness of the section (Fig. 2.19) and the amount of residual stress required (Shand, Armistead 1958). Accordingly, round or ellipsoid shapes and equal mass distribution are key aspects for the prevention of residual stresses¹⁷ and are thus preferred over sharp, pointy edges and shapes with uneven volume distribution where internal residual stresses can concentrate due to inhomogeneous shrinkage.

Nonetheless, in practice, the necessary heat transfer for achieving the desired temperature difference is influenced by various factors, challenging to accurately simulate, such as: the element's shape and mass distribution, the amount of surfaces exposed to cooling, the amount of other thermal masses in the furnace, even the

¹⁷ Variations in the thickness of a glass object result in different temperatures within the glass that in turn lead to different shrinkage rates within the component causing strain.

geometry and characteristics of the furnace itself (Watson 1999). For example, a piece of flat glass resting on a kiln shelf with only one side exposed would need twice the annealing time than a piece of glass with both sides exposed would require¹⁸. Castings almost completely enclosed within a mould tend to cool more homogeneously: the mould material functions as an insulating material that restricts the heat loss, reducing considerably the differential between exterior and interior temperatures of the glass (Bray 2001). In contrast, in castings made in open moulds (discussed in chapter 2.4), the top, exposed surface tends to cool considerably faster than the surfaces in contact with the mould¹⁹.

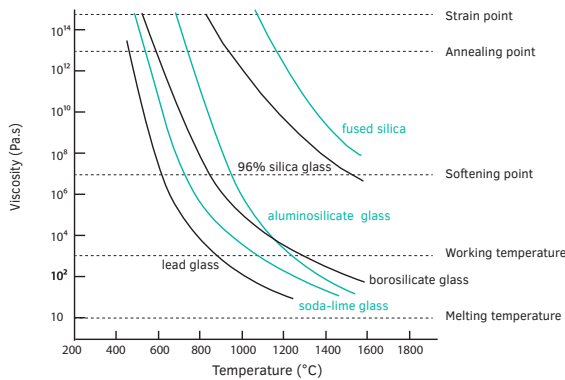


FIG. 2.18 Approximate viscosity versus temperature curves plot for the most characteristic glass families described in tables 2.1 and 2.2 based on (Shand, Armistead 1958).

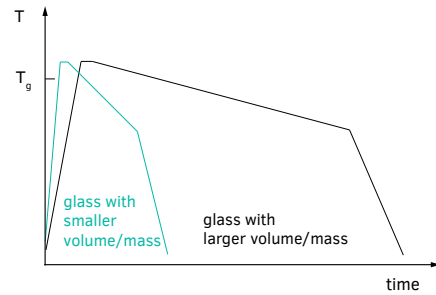


FIG. 2.19 Schematic representation of the annealing temperature as a function of time for glasses of different volume by (Schott AG 2004).

Numerous guidelines exist in the scientific and industrial literature on the annealing cycle of cast objects. Characteristic annealing guidelines based on the glass's thickness, by glass manufacturing companies such as *Gaffer* and *Bullseye* have been developed according to the annealing schedule (Fig. 2.20 and Table 2.4) proposed by (Shand, Armistead 1958) and can be found in the Appendix. (Cummins 2001) and (Bray 2001) provide a comprehensive explanation for the annealing cycle of cast glass artefacts. However, such guidelines are often tailored to specific circumstances

¹⁸ According to (Cummins 2001) the thickness of the glass is always the part furthest away from an outside surface. In this way it is considered as annealing from one side only, effectively doubling the thickness and thus the minimum acceptable annealing time.

¹⁹ A simple solution to this problem employed by glass artists is to cover the open area of the mould with a slab made of an insulation material such as ceramic fibre, once the glass approaches its annealing point.

and include unclear assumptions (Watson 1999). Thus, even though in theory the desired heat transfer can be calculated, in practice, due all the above mentioned parameters, the annealing schedule of large 3-dimensional cast units is often empirical, based on practical experience (Cummins 2001; Watson 1999).

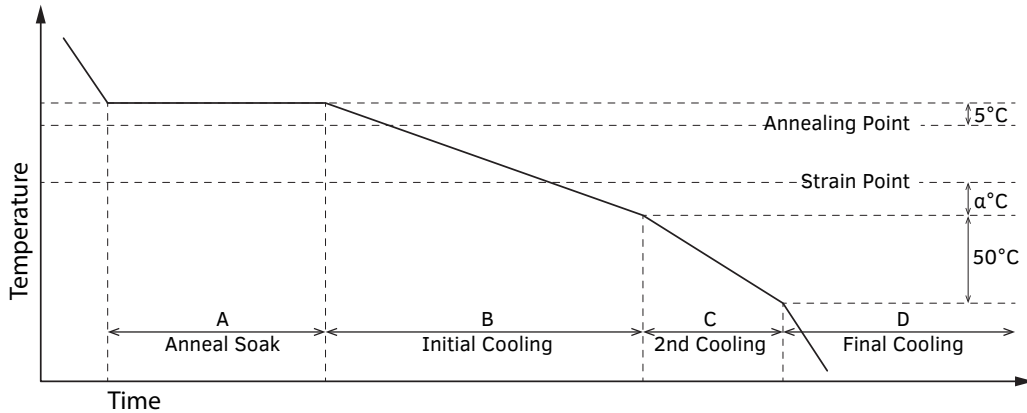


FIG. 2.20 Typical annealing scheme for commercial soda-lime glasses.

TABLE 2.4 Typical annealing scheme for commercial soda-lime glass based on Fig. 2.20, adapted from (Shand, Armistead 1958).

Expansion Coef. of Glass per °C	Glass Thickness [mm]	Cooling on one side					Cooling on two sides				
		A	B		C	D	A	B		C	D
		Anneal soak	Initial cooling (annealing)		2 nd cooling	Final cooling	Anneal soak	Initial cooling (annealing)		2 nd cooling	Final cooling
	Time [min]	Temp. [°C]	Cool rate [°C/min]	Cool rate [°C/min]	Cool rate [°C/min]	Time [min]	Temp. [°C]	Cool rate [°C/min]	Cool rate [°C/min]	Cool rate [°C/min]	
33*10 ⁻⁷	3.2	5	5	12	24	130	5	5	39	78	400
	6.3	15	10	3	6	30	15	10	12	24	130
	12.7	30	20	0.8	1.6	8	30	20	3	6	30
50*10 ⁻⁷	3.2	5	5	8	16	85	5	5	26	52	260
	6.3	15	10	2	4	21	15	10	8	16	85
	12.7	30	20	0.5	1	5	30	20	2	4	21
90*10 ⁻⁷	3.2	5	5	4	8	50	5	5	14	28	140
	6.3	15	10	1	2	11	15	10	4	8	50
	12.7	30	20	0.3	0.6	3	30	20	1	2	11

2.4.3 Measuring stresses in cast glass objects

In solid cast components with a considerably larger thickness than standard float glass plates, an accurate through-the-entire-thickness stress measurement by a *Scattered Light Polaroscope (SCALP)* stress-meter (using the current hardware/software) is not yet fully possible²⁰. In such cases, the effectiveness of annealing is normally qualitatively evaluated with the use of a polariscope. If the glass element is subjected to stress, it exhibits optical anisotropy. This corresponds to two refractive indices, which result in the presence of isochromatic fringes (coloured patterns) when polarized light passes through the component (see Fig. 2.21, right) (McKenzie, Hand 2011).



FIG. 2.21 Qualitative analysis of strain concentration by polarization test. Bricks such as the ones shown on the right have a clear indication of residual stresses. Elements with grey-scale spectral composition, such as the one on the left, have low residual stresses.

(Shribak 2015) provides an extended analysis of the interference colours seen through polarization. For small retardance the brightness of the region increases, first with a white spectral composition at 200nm. As the retardance increases,

²⁰ Over the last few years elaborate equipment has been developed for determining the stress levels in glass bottles and containers. Such polarimeters like the *StrainScope®* by *Ilis* can indicate the level of mechanical stress in the examined glass objects. Nonetheless, a measuring equipment specialized in 3D cast glass objects is yet to be developed and would ideally require a 3D-scanned model of the object that can accurately indicate the magnitude of the residual stresses and the existence of flaws or inclusions at all locations.

colours start to appear beginning with yellow, then red, blue and green. The colour changes in this sequence three more times until the retardance reaches 2000nm. Then the interference colours turn white again and the retardance can no longer be reliably determined using the region's spectral composition. A continuous presence of only black and white subsequently signifies low residual stresses (see Fig. 2.21, left). Accordingly, glass without any stress will appear completely dark (Schott AG 2004). If the specimen presents besides black only grey-scale spectral composition, it has low residual stresses. When the colour spectrum appears the amount of stress is higher but cannot be quantified.

2.5 Mould types

Table 2.5 summarizes the characteristics of the prevailing mould types available for glass casting, illustrated in Fig. 2.22. The choice of mould mainly depends on the production volume and desired level of accuracy of the glass product, and is cost and time driven. Therefore, disposable moulds are more efficient for single component or small batch castings, as they are significantly cheaper than the permanent mould alternatives. For disposable moulds (Fig. 2.23), the level of achieved accuracy and maximum melting temperature can vary, from cheap investment silica-plaster moulds for castings below 1.000 °C to milled alumina-silica fiber ceramics of top performance. In both cases though, the glass surface in contact with the mould will acquire a translucent, rough skin that requires post-processing for a transparent result. Due to the brittle nature of these moulds, quenching is not recommended, thus their common application is in kiln-casting.

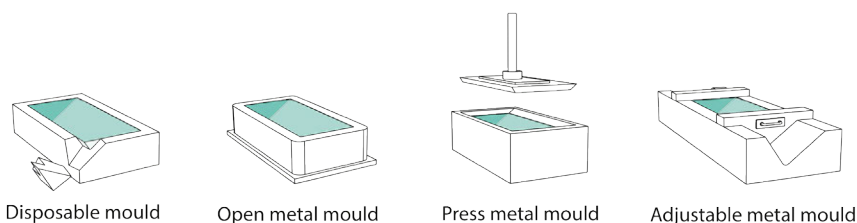


FIG. 2.22 Illustration of the most common mould types.

TABLE 2.5 Characteristics of prevailing mould types for glass casting

Characteristics	Mould type						
Reusability	Disposable		Permanent				
Material	Silica Plaster	Alumina-silica fiber	Steel/Stainless steel			Graphite	
Adjustability	-	-	Adjustable	Fixed	Pressed	Adjustable	Fixed
Production method	Investment casting/ lost-wax technique	Milling	Milling/cutting and welding			Milling/ grinding	
Manufacturing costs	Low	High	Moderate to high			High	
Top temperature	900-1.000°C	≈1.650°C	≈1.200°C/1.260°C			unknown	unknown
Glass annealing method	Mould not removed for annealing		Mould usually removed for annealing but can also remain if high accuracy is required			Mould removed for annealing	
Release method	Immerse in water	Water pressure	Release coating necessary (ex. Boron Nitride)			Release coating necessary	
Level of precision	Low/moderate	High	Moderate/High	High	Very high	Moderate/High	High
Finishing surface	Translucent/rough	Translucent/rough	Glossy. Surface chills may appear if the mould is not properly pre-heated			Glossy with surface chills	
Post-processing requirements	Grinding and polishing required to restore transparency and increase accuracy		Minimum or none post-processing required			Minimum to moderate post-processing required	
Applicability	Single component/low volume production		High volume production			High volume production	

For a series production, permanent moulds from steel or graphite (Fig. 2.24) are preferred in combination with the melt-quenching technique that is considerably more time-efficient than kiln-casting. With such moulds, significantly increased dimensional accuracy can be obtained, especially in the case of pressed-moulds. A high level of surface detailing can also be achieved with the use of graphite moulds. To avoid further deviations, the mould should not be removed during the annealing stage, situation only possible with steel. The coating of the steel mould with a release agent –usually boron nitride or graphite- is therefore crucial for the easy release of the glass component. The permanent moulds can be adjustable if required (Fig. 2.25), to allow for shape flexibility, but this compromises the level of accuracy. Overall the resulting surface is glossy and transparent and, in relation to the allowed tolerances, minimum or no post-processing is required - provided that the moulds have been properly preheated prior to casting.

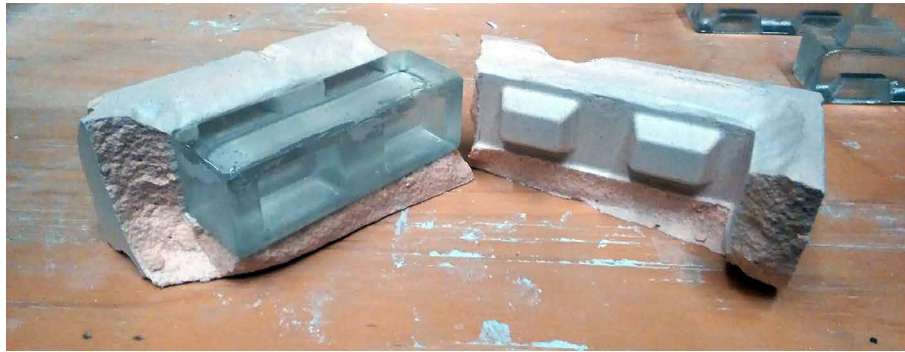


FIG. 2.23 Disposable mould out of plaster and silica sand.

Inadequate preheating of the moulds increases the risk of surface chills at the glass, especially in the case of graphite moulds. Finally, although the complexity of the shape is not a significant cost-affecting factor for disposable moulds, it does increase the price of steel and graphite moulds. For complex projects that require numerous, different, yet accurately cast components, novel solutions need to be developed. A promising affordable mould solution for customized glass components of high accuracy can be found in the 3D-printed sand moulds developed by *Arup* and *3Dealize* (Niehe 2017) for the casting of complex and individually produced steel nodes (Fig. 2.26). Sand casting, which comprises a template (typically made of wood) that is pressed into the sand to make a clear impression, is commonly used by glass artists as a cost-efficient mould solution for casting glass. This technique of low accuracy, however, is not used to produce building elements. Nonetheless, the development of automated, customized 3D-printed sand moulds of high accuracy,²¹ can revolutionize the way we design and produce cast glass elements. 3D-printers of sand, such as the ones used by *3Dealize* and *ExOne*, are already employed for the production of sand casting moulds for metal objects (aluminium, steel, iron and magnesium) of high accuracy and complex geometries (ExOne 2019). Research on the use of 3D-printed sand moulds for glass casting by (Flygt 2018) and (Bhatia 2019; Damen 2019) have so far yielded promising results (Fig. 2.27), suggesting that this method can indeed be used as a cost-effective solution of high accuracy for the casting of customized solid glass components or/and of components of complex geometry (e.g. topologically optimized).

²¹ Based on personal communication with *3Dealize*, 3D-printed sand moulds by *3Dealize* have a size accuracy of ± 0.1 mm, defined by the grain size of the sand. 3D-printed sand moulds are currently used for the metal (aluminium, steel, iron, brass, bronze) casting of perplexed components, mainly for the automotive, aerospace, pump and machine industry.

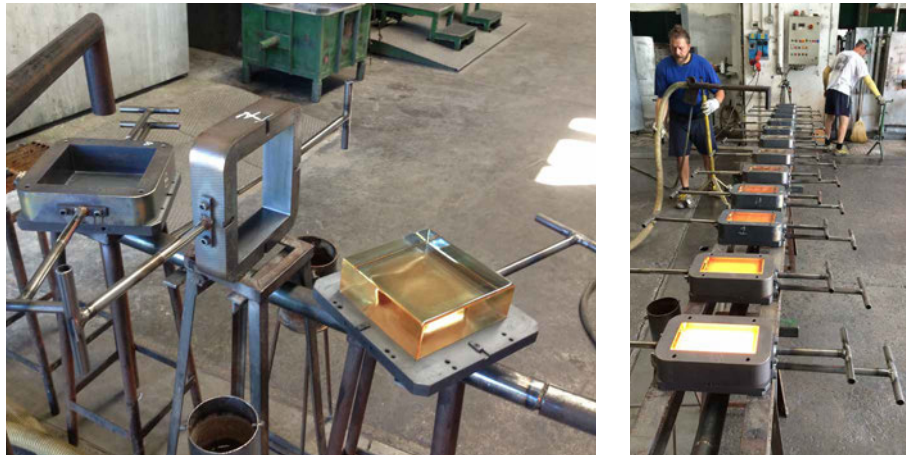


FIG. 2.24 High precision open steel moulds used for the manufacturing of the glass blocks for the *Crystal Houses* façade.



FIG. 2.25 Adjustable graphite mould at *John Lewis Glass Studio* for the components of the *Ice Falls* project by *James Carpenter*.



FIG. 2.26 Cast steel node, designed by Arup, made in 3D-printed sand mould. Source: Arup/Davidfotografie.

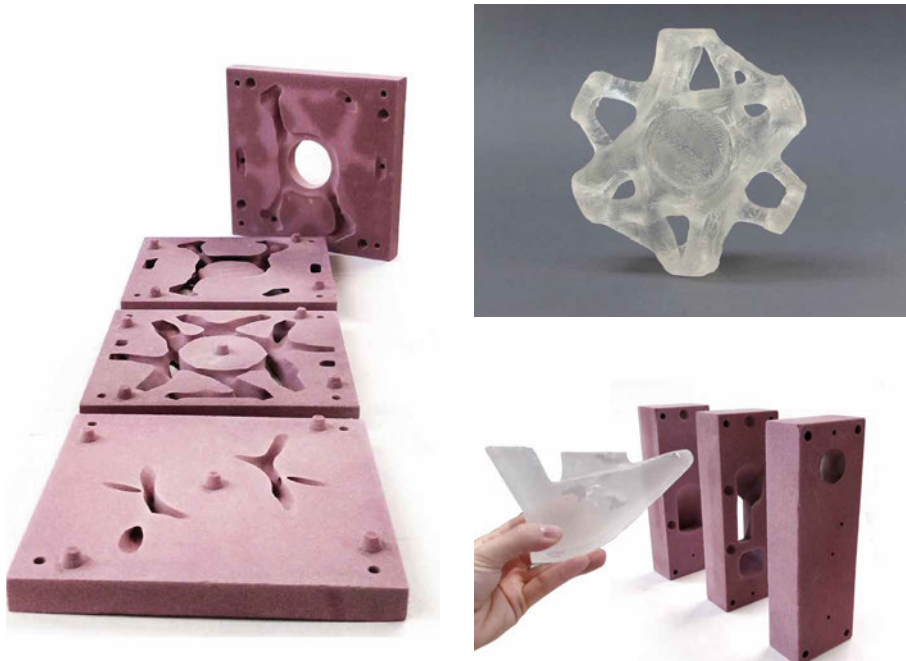


FIG. 2.27 3D-printed sand moulds produced by ExOne and the resulting cast glass components for a topologically optimized cast glass grid-shell node by (Damen 2019) (left and top right) and for a structurally optimized cast glass column by (Bhatia 2019) (bottom right).

2.6 Strength of cast glass

A selection of material properties of typical soda-lime silicate and borosilicate glass, the two most prevailing types of cast glass in architectural applications, is presented in Table 2.5. Glass is a brittle material. It has a comparable density to that of concrete and a Young's modulus similar to that of aluminium. Glass does not consist of a geometrically regular network of crystals, but of an irregular 3-dimensional distribution of rings or arches (broken rings)²² composed of at least 3 tetrahedral modules²³ -each composed of one silicium (Si) atom and four oxygen (O) atoms (SiO_4) - and intermediate alkaline parts (see Fig. 2.28). Thus, glass is an amorphous material. As an amorphous material it presents no crystallographic density variation and no phase boundaries at which the light rays are scattered, thus, it is transparent.

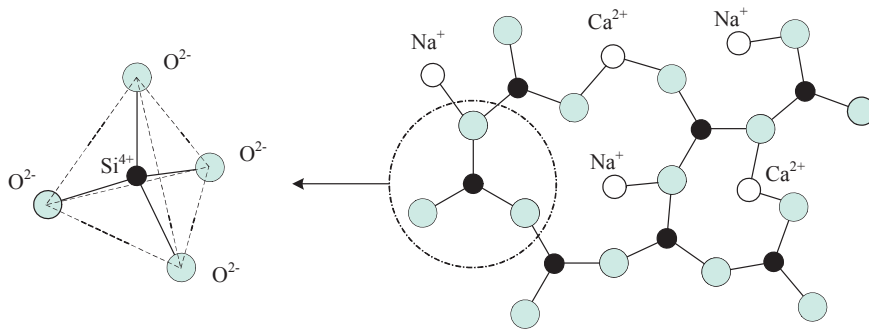


FIG. 2.28 Schematic representation of the structure of soda-lime silica glass based on (Louter 2011). Left: 3D schematic representation of a tetrahedral module built from one silicium and 4 oxide atoms. Right: 2D schematic representation of the irregular network of soda-lime silica glass.

The random molecular structure has no crystallographic slip-planes or dislocations to allow macroscopic plastic flow before failure (Overend et al. 2007). Hence, glass exhibits an almost perfectly elastic, isotropic behaviour and brittle failure at

²² A regular ring can be composed of up to 8 tetrahedral units. Where rings are combined due to a non-bridging oxide atom this can be higher; although the local structure is then no longer ring shaped.

²³ This statement refers to soda-lime glass, which is the most commonly applied in the built environment. For example, in borosilicate glass the modules are trihedral.

normal temperature. In theory, glass's strength can be defined by the forces of the interatomic bonds. Based on *Orowan's* stress formula, the failure stress σ_m of a material is given by:

$$\sigma_m = \sqrt{\frac{E\gamma}{r_0}}$$

where:

E = Young's modulus

γ = fracture surface energy

r_0 = equilibrium spacing of the atoms

Accordingly, the theoretical strength of typical silica glass (E = 70 GPa; $\gamma = 3 \text{ Jm}^{-2}$; $r_0 = 0.2 \text{ nm}$) amounts to 32 GPa (Shelby 2005). This strength is, however, of no practical relevance for structural applications. In practice, the tensile bending strength of annealed soda-lime glass is effectively 3 orders of magnitude lower. According to EN 572-1:2004 the characteristic bending strength is 45 MPa. This reduction of strength was attributed by (Griffith 1921) to the presence of randomly distributed pre-existing microscopic flaws and geometrical defects which act as stress concentrators. Due to the inability of glass to redistribute stresses by plastic deformation, a small flaw or inclusion can result in local stresses that exceed the theoretical strength, causing the fracture of the glass. Hence, fracture of glasses is governed by the presence of (Griffith) flaws.

TABLE 2.6 Properties of standardized soda-lime and borosilicate glass according to EN572-1:2004

	Symbol	Units	Soda-lime	Borosilicate glass
Density	ρ	Kg/m ³	2500	2200-2500
(Knoop) Hardness	HK _{0,1/20}	GPa	6	4.5-6
Young's modulus	E	GPa	70	60-70
Poisson's ratio	ν	-	0.22-0.24	0.2
Thermal expansion coefficient	α_T	10 ⁻⁶ /K	9	Class 1: 3.1-4 Class 2: 4.1-5 Class 3: 5.1-6
Specific thermal capacity	c_p	J·kg ⁻¹ ·K ⁻¹	720	800

In particular, a glass element will fail as soon as the stress intensity due to tensile stresses at the tip of a flaw reaches its critical value. The strength of a glass specimen

is related to the depth of the critical flaw²⁴. A larger flaw depth or a sharper flaw leads to lower strength. The flaws display a time-dependent behaviour when loaded in tension due to stress corrosion in the glass. In the presence of humidity or water, flaws grow slowly when exposed to a positive crack opening stress²⁵. Accordingly, a glass specimen stressed below its momentary strength will still fail after the time necessary for the most critical flaw to grow to its critical size at that particular stress level (Haldimann et al. 2008). Overall, the stress intensity/time dependant crack growth rate depends on several parameters and is extremely variable²⁶.

Subsequently, the tensile strength of glass is not a material constant, but it depends on multiple aspects, i.e. on the condition of the surface, the size of the glass element, the action history (intensity and duration), the amount of residual stress and the environmental conditions. Accordingly, the higher the load, or the longer the load duration and/or the deeper the initial surface flaw, the lower the effective tensile strength is (Haldimann et al. 2008). As flaws do not grow or fail when in a purely compressive stress field, the compressive strength of glass is considerably higher than its tensile strength. Nevertheless, the compressive strength of glass is not governing virtually any of the structural applications of the material. Glass will always fail due to exceeding local tensile stresses. Even when a glass element is loaded in compression, peak tensile stresses will develop due to buckling or due to the Poisson's ratio effect long before the compressive strength is reached.

Geometrical defects and flaws are already present during the production process of the material but can be further introduced due to scratching, impact, debris, chemical attack, thermal stresses, etc. Even contact with another piece of the same glass or with metal objects used in the handling and transportation process is sufficient for generating flaws.

Flaws in glass can be divided in 3 regional categories: surface, edge and inclusions (Fig. 2.29). The edge finishing has the major effect on the effective strength of glass (Molnár et al. 2012) due to the more severe surface damage at the edge, result of the cutting and machining process. Thus, the inherent tensile strength of the edge of

²⁴ At the direction perpendicular to the tensile stress vector.

²⁵ The chemical process associated with stress corrosion can be explained by the classical stress corrosion theory, which embodies the chemical reaction of a water molecule with silica at the (stressed) crack tip. This chemical reaction both sharpens and lengthens the crack tip, which leads to an increase in stress around that area.

²⁶ For an in-depth reading on the fracture strength of glass elements please refer to (Overend et al. 2007; Haldimann et al. 2008).

a glass pane is generally lower than the strength away from the edge (Louter 2011). Flaws at the surface of glass have as well a significant effect on the effective strength of the material, especially if the surface is directly loaded. Defects at the meso-structure (inner volume) can also lead to early failure. Based on the assumption that the flaws are randomly distributed over the glass surface, the chance of the presence of a large critical flaw, meaning a lower failure strength, increases with increasing specimen size (Louter 2011) – this is called the inverse scale effect.

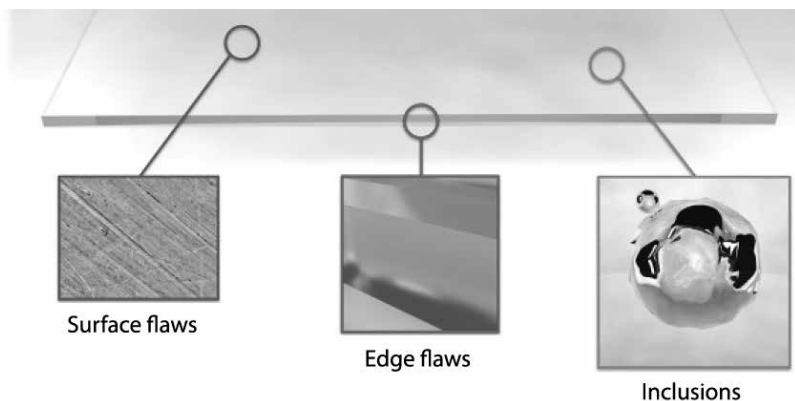


FIG. 2.29 Main glass flaw regional categories. Source: (Molnár et al. 2012)

Flaws in the meso-structure are distinguished by (Bartuška 2008) in three categories (Fig. 2.30):

- gaseous inhomogeneities (bubbles or seeds)
- crystalline inclusions (stones)
- glassy inhomogeneities (cords or striae).

Cords or striae are defined by *ASTM (American Society for Testing and Materials)* as glassy inclusions with optical properties differing from the glass matrix. They may be caused by insufficient stirring of the molten material or a chemical reaction in the furnace. Hence, striae is of different composition or may be a result of incomplete fusion of the material. Cords may have different expansion properties to the base glass, which in the occurrence of thermal stresses can lead to failure. At present, there is no extensive physiochemical study of cords and stones. Little regarding their compositions and origins is known.

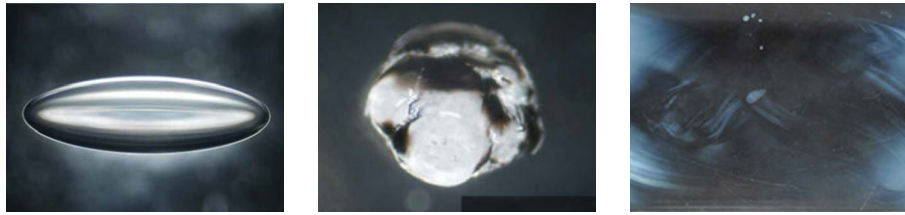


FIG. 2.30 Inclusion flaws in glass. From left to right: Bubbles, stones and cord. Source: (Molnár et al. 2012) and own image (right).

Crystalline inclusions (stones) are imperfectly melted material compounds that are not amorphous. They have a slightly different density than the base glass and exhibit different mechanical properties, different thermal expansion coefficient and almost no light transmittance ability. Such inclusions can be generated due to remains from the batch that have not been completely melted, wall material with low solubility (refractory wall contamination), particles from the surrounding atmosphere, devitrification processes and crystallization. Characteristic examples of inclusions are the nickel sulphide (NiS)²⁷ inclusions and the refractory wall traces that have been accidentally embedded in the finished glass. NiS inclusions or stones of foreign matter (such as refractory brick) can cause excessive internal stresses in glass due to the differential volume change during thermal expansion/contraction that can further lead to failure.

Air bubbles (seeds) can be generated by various sources, such as the decomposition of the raw materials, nucleation growth, chemical, electrochemical and mechanical reactions. Bubbles that remain in glass can lead to stress concentrating defects (Bartuška 2008). (Molnár et al. 2012) proved numerically that a 1 mm in length bubble could generate a significant strain peak in the glass.

Several standards²⁸ exist on the physical and mechanical properties of typical soda-lime float glass (Table 2.6). In contrast, there is no standard yet regarding the strength of solid cast glass objects. It is assumed that the cast and float manufacturing processes of glass lead to closely comparable mechanical properties. With proper annealing and processing, the chemical compositions are virtually identical and the occurrence of defects such as air bubbles is limited. In the *Material*

²⁷ NiS inclusions result from the presence of nickel contaminants in the glass melt reacting with sulphur, most likely from the furnace fuel.

²⁸ An overview of the relevant European and US standards can be found in Chapter 1 at (Haldimann et al. 2008).

Science Selection Software CES EduPack, cast glass objects from either soda-lime or borosilicate have virtually equal strength values (Table 2.7) compared to float elements of the same glass composition (Granta Design Limited 2015).

TABLE 2.7 Strength values of standardized float/cast soda-lime and borosilicate glass by CES Edupack Program (Granta Design Limited 2015).

	Symbol	Units	Soda-lime	Borosilicate glass
Fracture tensile strength [†]	$f_{gl,t}$	MPa	30-35	22-32
Fracture compressive strength	$f_{gl,c}$	MPa	300-420	260-350

[†] The values regarding the characteristic strength of glass can greatly vary according to the literature source used. For example, according to (O' Regan 2014) the characteristic tensile strength of soda-lime glass is 45 MPa. According to (Saint Gobain 2016; Ashby, Jones 2006; Weller et al. 2008) float soda-lime glass has a compressive strength of 1000 MPa, whereas (Oikonomopoulou et al. 2017b) has conducted experiments with borosilicate glass with a nominal compressive failure stress of 500 MPa.

Nonetheless, in cast objects of considerably larger thickness, the manufacturing process is more difficult to control and has not been yet standardized; a current implication is the often empirical and manual production of cast glass in comparison to the mature, automated float glass production line (Bristogianni et al. 2019). Thus, the number and size of randomly distributed critical defects is anticipated to be higher²⁹. In particular, the increased volume of cast glass results in more geometrical defects and inclusions in the meso-structure, such as seeds, stones and cord. Often, small air bubbles are visible by the naked eye in cast glass prototypes. A float glass containing such bubbles would have been discarded³⁰. However, as the surface/edge area remains confined in dimensions, it is expected that the amount of defects at the surface or close to the edge of the cast object are marginally increased compared to float glass, mainly due to the non-standardized/non-automated production process and quality control (Fig. 2.31). Post-processing of the surface/edges of the cast elements can greatly minimize the effect of such flaws, which greatly influence

²⁹ An extra implication is that currently a thermal or chemical tempering process has not yet been successfully developed for cast glass. This is a downside given that strengthened float glass is commonly applied in structural glass practice, and thus the cast glass product has a comparatively lower strength at the moment.

³⁰ According to (ASTM 2008) gaseous inclusions of max. 2 mm in diameter and with a min. separation of 600 mm are allowed in a 6 mm thick float glass. For Optical Glass the standards on gaseous inclusions are considerably more strict: As an example, SCHOTT AG permits a 0.55 mm max. allowable diameter of a single bubble in combination with more restrictions regarding the total volume of the glass (SCHOTT Advanced Optics 2013), whereas OHARA allows a max. cross section of bubbles of <0.03 mm²/100 cm³ (Ohara 2019).

the introduction of peak stresses. Flaws in the meso-structure are considered less prevailing as long as they do not disrupt the glass network in a crucial manner. Taking the above into account, cast glass is anticipated to present a comparable yet reduced bending strength compared to standardized float glass.

In summary, casting remains a non-standardized manufacturing process for structural components in the built environment, resulting as well to a non-standardized quality. Hence, in order to avoid excessive safety factors and over-dimensioning of the components, structural applications of cast glass are currently experimentally validated.

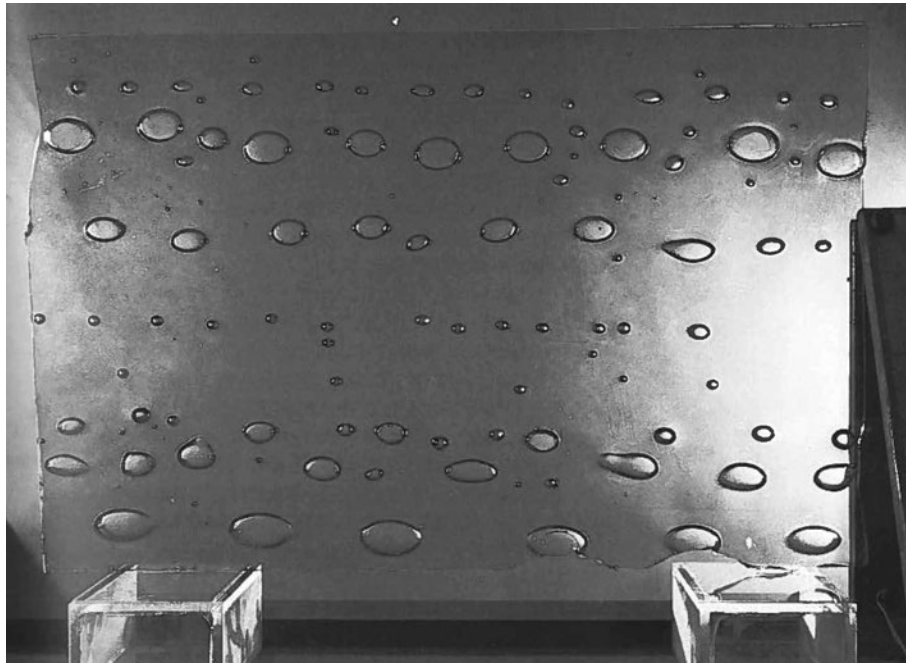


FIG. 2.31 Early piece of float glass from the *Pilkington* archive demonstrating large bubbles across the entire ribbon prior to the introduction of a fully standardized/automated process and a strict automated control of flaws and inclusions. Over the last decades, float glass has seen great developments in both infrastructure and control technology. Yet, for cast glass these aspects still remain at an earlier stage of development. Source: (Bricknell 2010)

2.7 Discussion

This chapter has sought to give an overview of the current prevailing manufacturing methods of glass, with respect to the built environment, and argue upon the potential of cast glass for building components in architectural applications.

From the presented manufacturing methods, float glass is the most prevailing one and is widely used in architecture. Nonetheless, monolithic, substantially 3-dimensional glass elements can only be achieved by 3D-printing and casting of glass. Both of these processes are relatively new for architectural applications and follow the same basic principle of molten glass being poured to form an object. The object is then controllably cooled to room temperature within an annealing kiln. Under the assumption of fully developed processes for 3D-printing and casting of glass, the former would be preferred for customized solutions and the latter for the mass fabrication of identical units. Nevertheless, the fabrication of cheap, disposable moulds can render cast glass a competitive solution for customized components as well. Overall, at present, casting provides the greatest flexibility with respect to the volume and size of the resulting glass object.

There are two main methods of casting glass: *primary casting*, which includes hot-pouring, and *secondary casting*, such as kiln-casting. The former is generally used for mass production of components while the latter is used for customized ones and requires less operating temperatures. In both processes the same annealing process is followed. The annealing schedule of an object is largely influenced by the thermal expansion coefficient of glass and the objects' thickness and mass distribution. However, more indirect factors, such as the set-up of the objects within the annealing kiln, the kiln's geometry, the type of mould, etc. further influence the annealing scheme, rendering it difficult to be accurately calculated. Thus, although several guidelines from glass manufacturers exist, the annealing schedule of large 3-dimensional objects is, in practice, still largely based on the empirical experience of the manufacturer.

A considerable obstacle in the structural application of cast glass is the lack of standardized strength data and of a standardized control process for the flaws. These exist for the float glass process but the increased volume and non-automated control of flaws in cast glass components is expected to have an effect on the strength of the resulting elements. It is anticipated though that since the mass that is comparatively increased compared to float glass is the meso-structure, the existence of critical surface flaws remains limited. Hence, the tensile strength of cast glass is anticipated to be comparable but less than that of float.



First casting attempt of the 5m in diameter borosilicate glass blank for the *Mt. Palomar Observatory*, displayed at the *Corning Museum of Glass*.

Transparent (of a material or article)

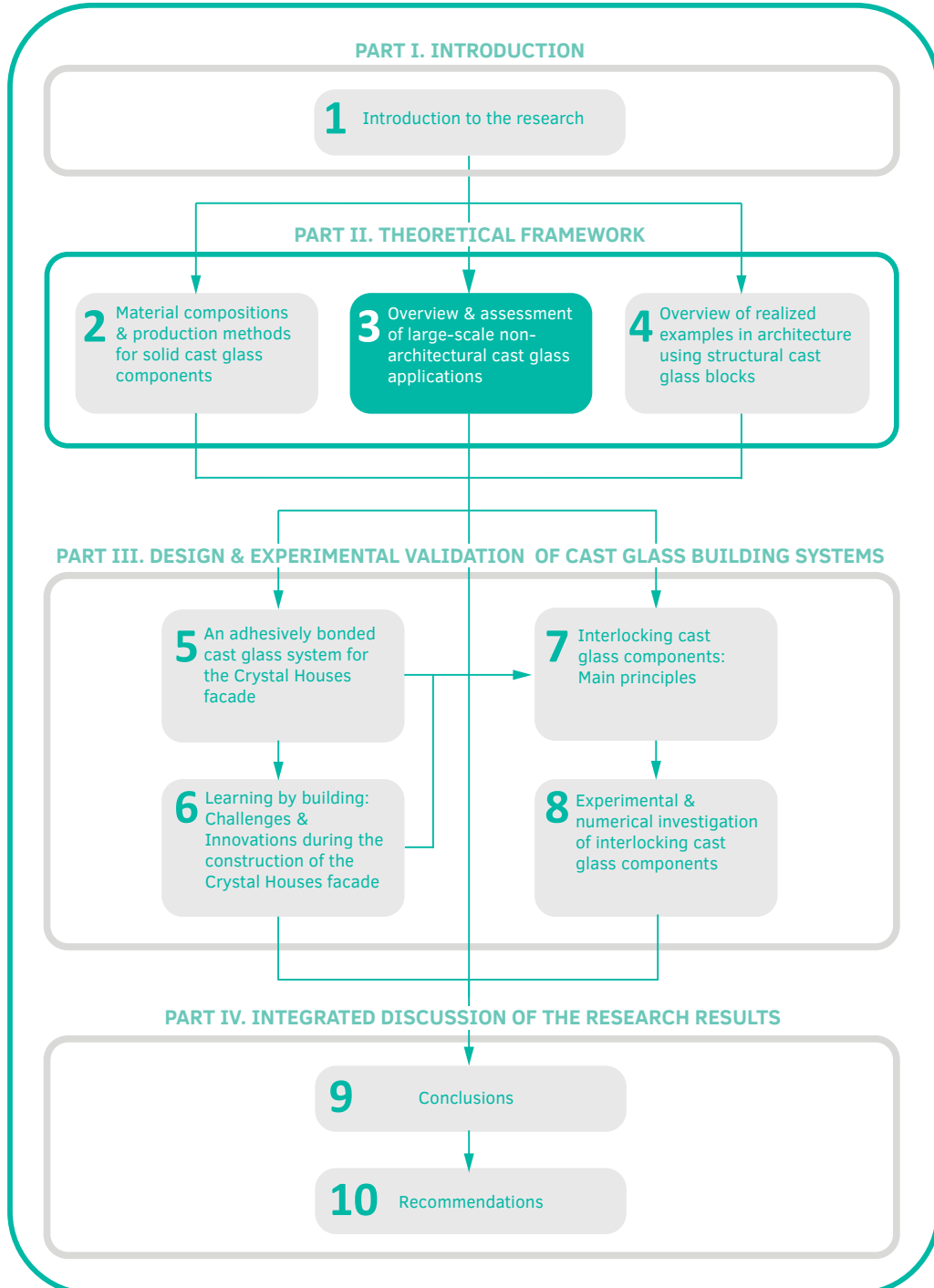
allowing light to pass through so that objects behind can be distinctly seen.

Origin of the word transparent

Late Middle English: from Old French, from medieval Latin transparent- 'shining through', from Latin transparere, from trans- 'through' + parere 'appear'.

Definition by the Oxford Dictionary

Exploring the third dimension of glass



Solid cast glass components and assemblies for structural applications

3 Overview of large-scale non-architectural cast glass applications

Overview of the state-of-the-art cast glass applications in other fields³¹.

To address both the possibilities and limitations in the size and form of cast glass components, an overview of the largest monolithic pieces of cast glass ever made is presented in this chapter, from giant telescope mirrors and nuclear glass blocks to massive artefacts. Weighing several tons each, these cast glass pieces are assessed with comparative charts of technical data collected from literature, industry and field research, regarding their geometry, materialization, manufacturing method and annealing process. The data highlight not only the potential but also the practical implications involved due to the meticulous and time-consuming casting and annealing process of three-dimensional glass elements. Learning from the extreme, proposals are made for optimizing the size, shape and casting process of cast glass components suitable for architectural applications.

3.1 Introduction

Cast glass is in fact the oldest method of glassmaking. Beads and other small objects made of molten glass cast in moulds, date back to more than 2000 B.C in Mesopotamia. (The Corning Museum of Glass 2001). Pyrotechnology was already

³¹ This chapter has been published as part of the review article: Oikonomopoulou F., Bristogianni T., Barou L., Veer F., Nijse R. The potential of cast glass in structural applications. Lessons learned from large-scale castings and state-of-the art load-bearing cast glass in architecture. Journal of Building Engineering, vol.20, 2018.(Oikonomopoulou et al. 2018c)

so developed in the Roman times that allowed for the casting of monolithic glass blocks weighing several tons. An 8.8 t rectangular glass slab with dimensions of 3.40 m x 1.95 m x 0.50 m, dating back to the 5th century AD (Corning Museum of Glass 2011c), has been discovered in the remains of a primary glassmaking furnace in *Beth She'arim*, Israel³². Such glass slabs were broken into smaller chunks and transported to secondary workshops to be fashioned into objects (Oxbow Books 2015).

At present, the telescope mirrors of giant ground-based telescopes (Corning Museum of Glass 2011c) comprise the largest monolithic pieces of cast glass in the world. These mirrors span several meters and typically employ a honeycomb structure to ensure the desired stiffness while considerably reducing their multi-ton weight. Other large-scale applications include pieces of art and lead glass blocks for nuclear applications. Below, some of the largest monolithic pieces of cast glass ever made are presented and are assessed with comparative charts of technical data collected from literature, industry and field research, regarding their geometry, materialization, manufacturing method and annealing process.

³² In the specific slab, the raw material used contained an excess amount of lime, which led to the partial crystallization of the glass that turned it opaque. Probably the lack of transparency was the reason this slab was left in situ, considered as a large defective piece (Corning Museum of Glass 2011c).

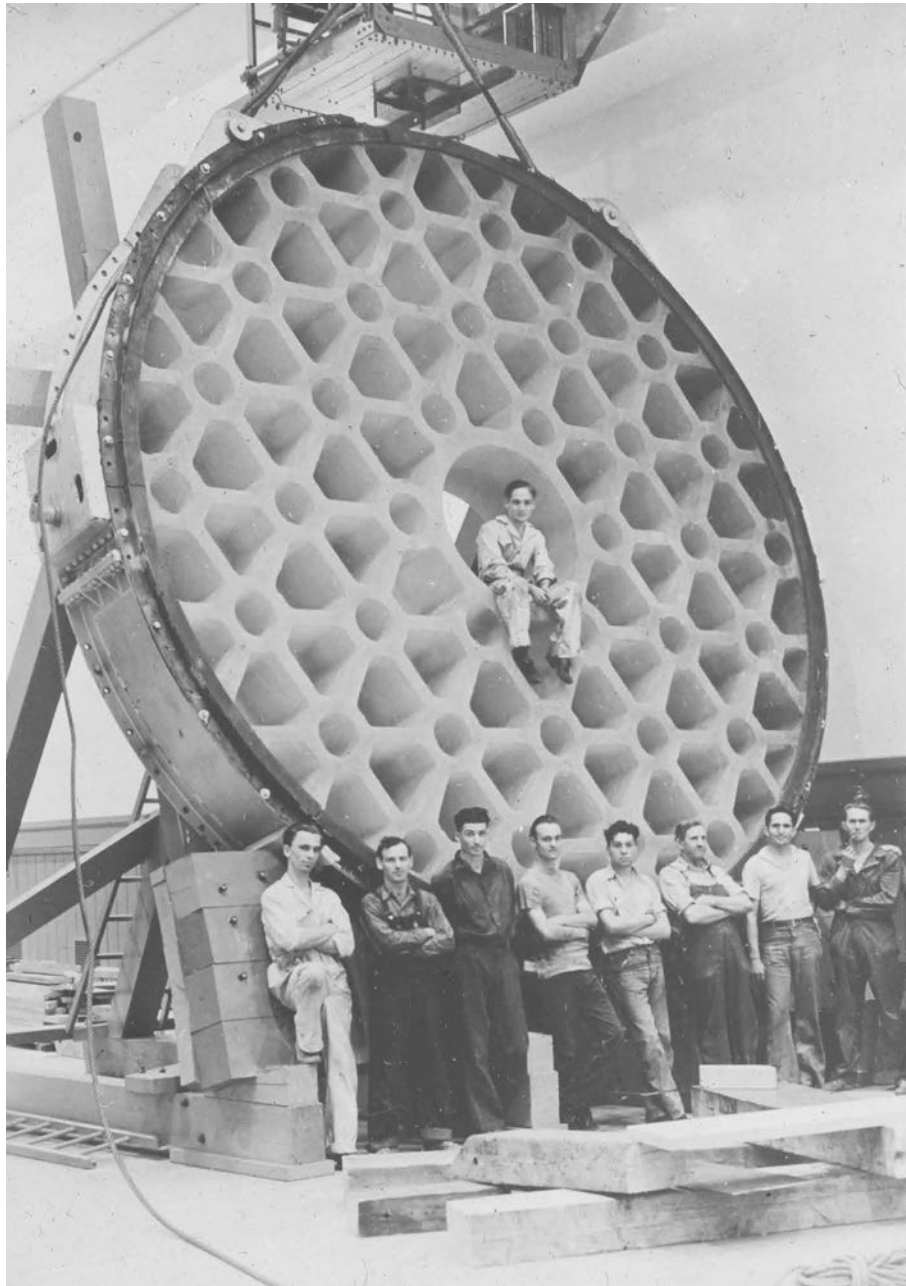


FIG. 3.1 The 5 m glass mirror blank of the *Mt. Palomar* telescope. Source: Collection of the Rakow Research Library, The Corning Museum of Glass (number: 1000093965).

3.2 The giant telescope mirror blanks

3.2.1 The design of a honeycomb structure

Nowadays, the largest monolithic pieces of cast glass are the mirrors of giant ground-based telescopes (Corning Museum of Glass 2011c). Spanning several meters these multi-ton parabolic-shaped mirrors typically employ a honeycomb structure to ensure the desired stiffness while significantly reducing their weight. Besides, a thinner blank with supportive ribs adjusts to temperature fluctuations more rapidly and anneals considerably faster (Zirker 2005). The first mirror using honeycomb geometry is the 5 m blank of the Hale telescope for the *Mt. Palomar Observatory* (Fig. 3.1), cast in 1936³³ by *Corning* using *Pyrex*[®] glass. A new glass blend at the time, *Pyrex*[®] would allow the mirror to expand and contract considerably less than regular glass, reducing distortion. The supporting ribs were formed by introducing silica firebrick (ceramic) cores in the mirror's steel mould. A special furnace was built to heat the glass to 1482 °C, so that it could successfully flow between the cores (Zirker 2005)³⁴. The honeycomb mirror of 15 t in weight, had to remain approximately 10 months in an electrically heated annealer to be properly annealed (Corning Museum of Glass 2011b; Palomar Observatory 2018). The flat top surface of the mirror was ground afterwards to the desired parabolic shape in a process lasting more than a decade.

3.2.2 Reducing post-processing: Spin casting

The meticulous and time-consuming process of obtaining the desired concave shape by grinding had to be revised in the next decades. The 2.4 m in diameter mirror of the *Hubble* telescope for example, was realized in 1979 by fusing a thin faceplate, a back plate, rings and a honeycomb lattice core into a single unit out of *Ultra Low*

³³ Until that time telescope mirrors were made as solid glass disks; the largest measuring 2.5 m in diameter and requiring a year of annealing (Zirker 2005).

³⁴ Here, the second attempt to cast the mirror is described. In the first unsuccessful attempt, the steel bolts that held the firebricks in place melted due to the intense heat of the molten glass, allowing the firebricks to float, ruining the disk (Caltech 2017).

Expansion (ULE®) glass (Fig. 3.2). Through slumping a concave front surface was created, reducing greatly the polishing needed³⁵. Even so, 3 years of post-processing were required to achieve the desired precision.



FIG. 3.2 Fused-silica prototype of the *Hubble* blank at the *Corning Museum of Glass*.

In the 1980's a new method for making monolithic, parabolic-shaped telescope mirrors whilst minimizing post-processing was employed: Spin-casting (Zirker 2005). By melting and annealing the glass into a spinning mould a parabolic shape can be directly obtained, saving several tons of glass and reducing considerably the annealing and post-processing time. Spin-casting is employed for the current manufacturing of the seven honeycomb blanks of the *Giant Magellan Telescope*. Spanning 8.4 m in diameter each, these mirrors are the largest contemporary monolithic cast glass pieces. To allow for the constant rotation of the glass during both its melting and annealing, the mirrors are kiln-cast in a rotating furnace. Specifically, a disposable mould out of silica-alumina fibre core boxes with a hexagonal cross-section, is built within a rotating kiln (Fig. 3.3). Silica-alumina fibre

³⁵ During the fusing process, the whole assembly was supported at its centre and the outer rim was allowed to slump, creating a convex backside and concave front. The same technology, called hex seal, was used to produce the 8.3 m blank of the *Subaru Telescope* and the 8.1 m blanks of the *Gemini 8-M Telescopes*.

is able to withstand both the heat and the pressure of the casting process, yet it can crumble easily with water pressure after the mirror is annealed. The mirrors are fabricated using *E6 borosilicate glass* by *Ohara*. Compared to *Pyrex*[®], E6 glass expands and contracts considerably less, melts and flows easily at reasonably low temperatures and has a competitive price (Zirker 2005). Approximately 20 t of pre-sorted glass chunks are laid on the top of the cores, then the furnace is sealed and the temperature slowly rises to 1180 °C. As the glass liquefies the kiln rotates at a constant speed of 6.8 rpm. While spinning, the mirror takes the desired concave shape to an accuracy of 0.25 mm and then finally solidifies through a 3 month annealing process - considerably faster compared to the previously analysed examples. The cast blank requires 3 years to acquire its final shape- same timeframe needed for the four times smaller *Hubble mirror blank*.

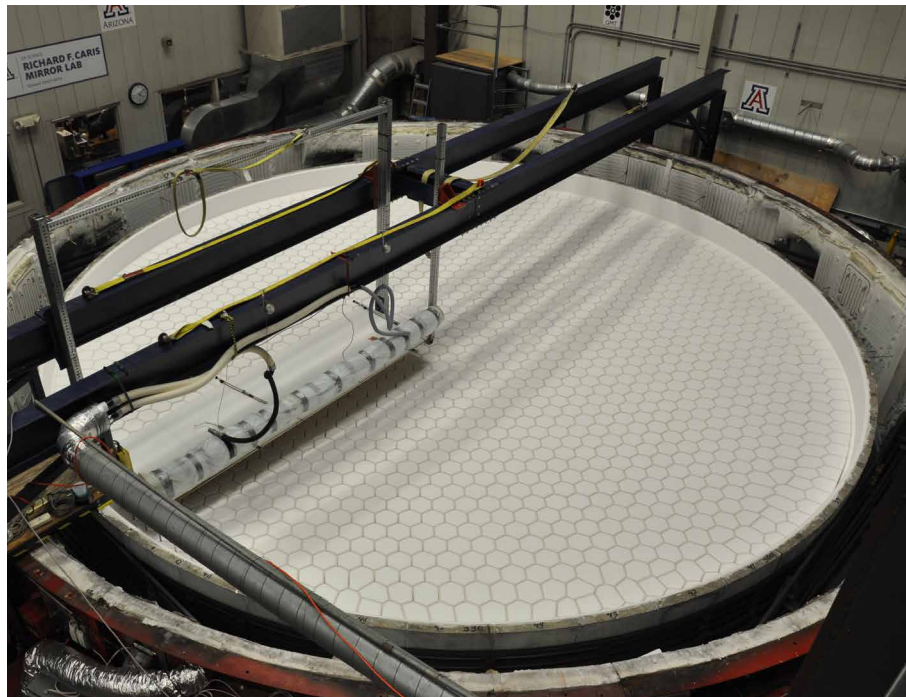


FIG. 3.3 Disposable mould for the blanks of the *Giant Magellan Telescope* built within the bottom part of the rotating kiln at the *Steward Observatory* in Arizona.

3.3 Radiation-shield lead blocks

Apart from the mirror blanks, some of the largest contemporary monolithic cast glass pieces are made for radiation-shields (Fig. 3.4). These glass pieces, measuring up to 1.4 m x 1.4 m x 0.4 m and weighing about 4.5 t are made of glass with a high content of lead (PbO). With PbO ranging between 33% and 70%, these blocks have an increased density, between 3220 kg/m³ and 5180 kg/m³ (Corning 2018). The casting process followed by *Corning* at the *Fontainebleau Factory* for the production of such blocks is as follows: A pre-heated open steel mould, coated with refractory paper liner, is set on a moving table inside a thermally controlled kiln. The glass is delivered by gravity from a tube in a continuous stream. To avoid the creation of cords, the table moves down at constant speed calculated from the glass flow and mould dimensions. When the target glass thickness is reached the mould is transferred from the kiln into a static furnace for annealing. The glass surface is still convex as viscosity impedes a perfect fill at the mould corners. The block is therefore re-heated marginally over the softening point to reduce viscosity and allow for optimal filling. Once ready the annealing cycle starts to cool the block gradually to room temperature within the mould. A block of 64% PbO lead glass and 300 mm thickness requires approximately 1 month of annealing, whereas a 400 mm thick block requires 2 months respectively (Kergaravat 2017).

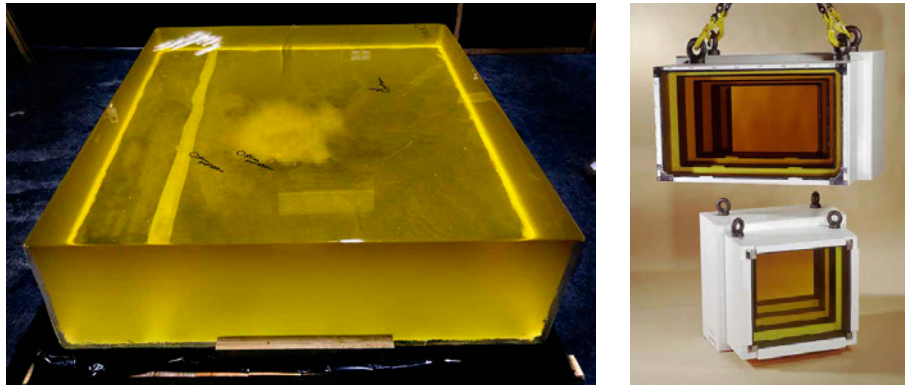


FIG. 3.4 Right: Lead glass block. Left: Radiation shield made of multiple lead blocks. Source: *Corning Fontainebleau*.

3.4 Art pieces

Art is another field employing big cast blocks exhibiting the variety of shapes we can achieve through glass casting. Numerous glass artists, such as *Karen Le Monte*, *Roni Horn* and *David Ruth* (Fig. 3.5 and Fig. 3.6), have worked with considerably sized cast glass components. Perhaps the largest monolithic cast glass sculpture is the “*Pink Tons*” by *Roni Horn*. The 4.5 t solid cube presents internal cracks, probably generated due to improper annealing. Nonetheless, little information can be found regarding the annealing schedule and process of such art pieces.



FIG. 3.5 Solid glass sculptures by artist *Roni Horn*



FIG. 3.6 A human-scale cast glass piece by artist *Karen Le Monte* at the *Corning Museum of Glass*

A challenging and well-documented example of cast glass art is the block for the *Denis Altar* in France, cast as well in *Corning's* facilities at *Fontainebleau*. The 1.42 m x 1.42 m x 0.28 m block is made with *Corning 7056* optical glass and weighs approximately 1.4 t. The block had to perfectly fit to the profile of the supporting stone (Fig. 3.7), requiring a high bottom surface accuracy. To achieve this, the glass block was initially cast rectangular with all sides flat in a large metal container, coated with non-stick refractory paper. The piece required roughly one month of annealing. Then the stone surface was imprinted on the glass: A plaster mould with the desired pattern loaded by 500 kg was set at room temperature on the glass. The assembly was slowly reheated to its softening point (690°C) and kept at that temperature for a month for the pattern to be imprinted. The block was then slowly cooled down to room temperature within another month.

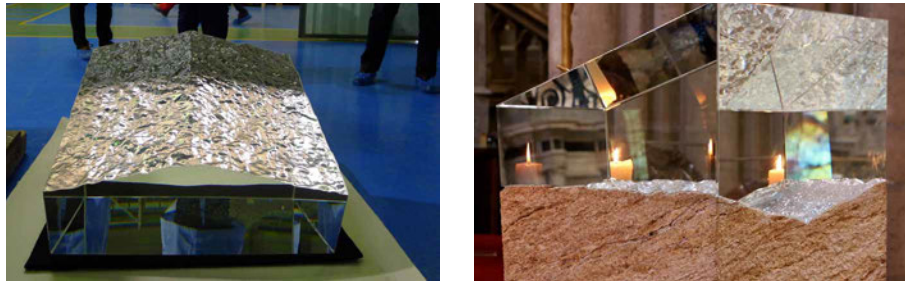


FIG. 3.7 The 1.4 t cast component of the *Denis Altar*. Source: *Thierry Dannoux, Corning*

3.5 Discussion

Table 3.1 summarizes the characteristics of the above discussed examples. Cast glass objects of such scale give us insight into both the potential and the practical limitations of glass casting. The bigger the component, the exponentially longer the annealing time is. An annealing time of several months may be acceptable for astronomical research, yet it would render a cast glass component financially unjustifiable for architectural and structural applications.

TABLE 3.1 Dimensions and characteristics of some of the largest cast glass components made. Data for the telescope mirrors as provided by (Angel 1988; Zirker 2005).

Application	unit	Hale Telescope Mirror	Giant Magellan Telescope mirror	Nuclear Glass Blocks	Dennis Altar glass slab
Dimensions	mm	Ø 5080	Ø 8417	1400x1600	1420x1420
Thickness	mm	660 (when cast)	Max:894 Min:437	400	280
Geometry		Honeycomb disc	Honeycomb disc	Rectangular massive block	Rectangular massive block
Glass type		Pyrex®	E6 borosilicate glass	Corning® RSG52 (70 PbO%)	Corning® 7506 (alkali-borosilicate)
Density	g/cm ³	2.23	2.18	5.22	2.29
Component weight	t	20 (14.5 after polishing)	16	4.5	1.4
T _{batch melt}	C°	1482	1180	1500	1495
Exp. Coeff.	1/°C	32.5x10 ⁻⁷	28x10 ⁻⁷	82.8x10 ⁻⁷	51.5x10 ⁻⁷
Mould type		Steel mould with silica firebrick cores bolted with steel bolts	Base: SiC baselites lined with aluminosilicate refractory fiberboard Cores: Carborundum Carbofrax SiC	Adjustable steel mould with refractory paper liner	Steel mould with refractory paper liner
Casting method		Hot-pouring Annealing within mould	Spin-(kiln) Casting Annealing within mould	Hot-pouring within kiln Annealing within mould	Hot-pouring Reheating above softening point to imprint pattern
Annealing time	months	~10	~3	~2	~1 (total production time 3 months)
Post-processing		Grinding and polishing (10 years)	Grinding and polishing (3 years)	Slicing to size and polishing	Polishing

Hence, the choice of glass, casting method and overall geometry greatly influences the annealing time and safeguards the component's marketability. For example, compared to the *Hale* blank, the mirror blanks of the *Giant Magellan Telescope* present significantly larger overall dimensions (Fig. 3.8); nonetheless, the substantially lighter structure (table 3.1, Fig. 3.9) and the choice of glass with a lower coefficient of thermal expansion considerably reduce their total annealing time.

Such smart geometry could also be implemented in cast components for architectural, load-bearing purposes. For example, compared to solid ones, glass blocks following the honeycomb principle would be sufficiently rigid, but faster to produce and lightweight, facilitating transportation and handling.

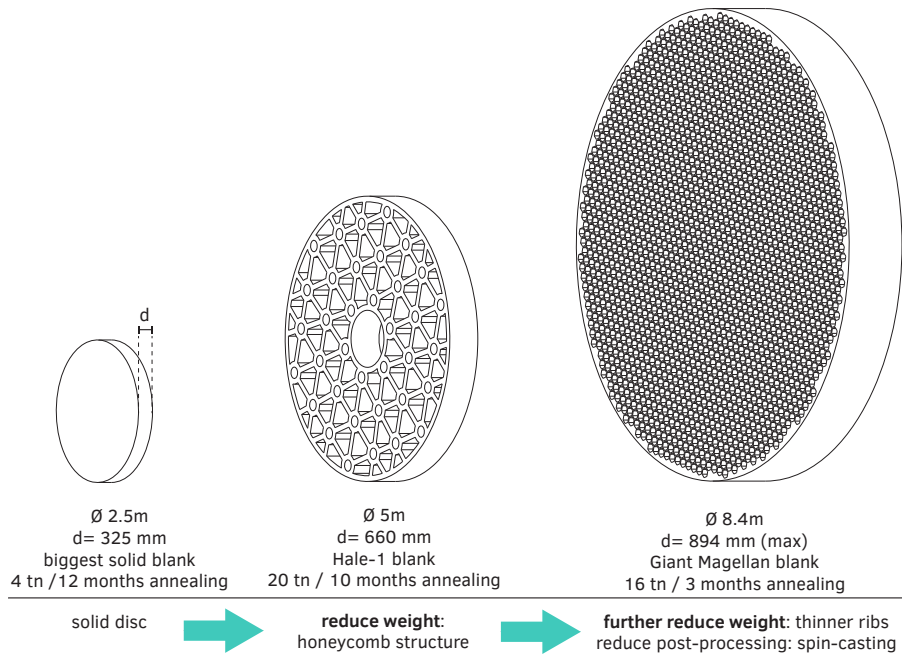


FIG. 3.8 Evolution of the cast mirror blanks in size and annealing times (Zirker 2005) due to smart geometry and improved manufacturing process.



FIG. 3.9 Segment of the *Giant Magellan's* blank at the *Steward Observatory*, Arizona.

The casting method can also reduce the required post-processing, decreasing the manufacturing costs and production time as well.

As for unique, more elaborate or variable components, singular disposable moulds are preferable over reusable adjustable ones.

The above case-studies also illustrate the importance of a homogeneous mass distribution to avoid uneven cooling. The presented examples also highlight the influence of the critical dimension, namely the thickness, to the total annealing time: i.e. an increase of 100 mm (from 300 mm to 400 mm) in the thickness of the massive lead glass radiation absorbing blocks doubles the annealing time.

Lastly, art applications indicate the possibilities of further shaping a component through a specific heating treatment. These include the creation of the desired finished surface but also the minimization of the capillary effect at the components' edges. Nevertheless, such a process would significantly delay the overall production.

In summary, there are many factors influencing the total annealing time of a cast glass component; geometry being the most decisive. If these parameters are controlled from the design stage, structural and efficient cast glass components can be made of various shapes and forms.

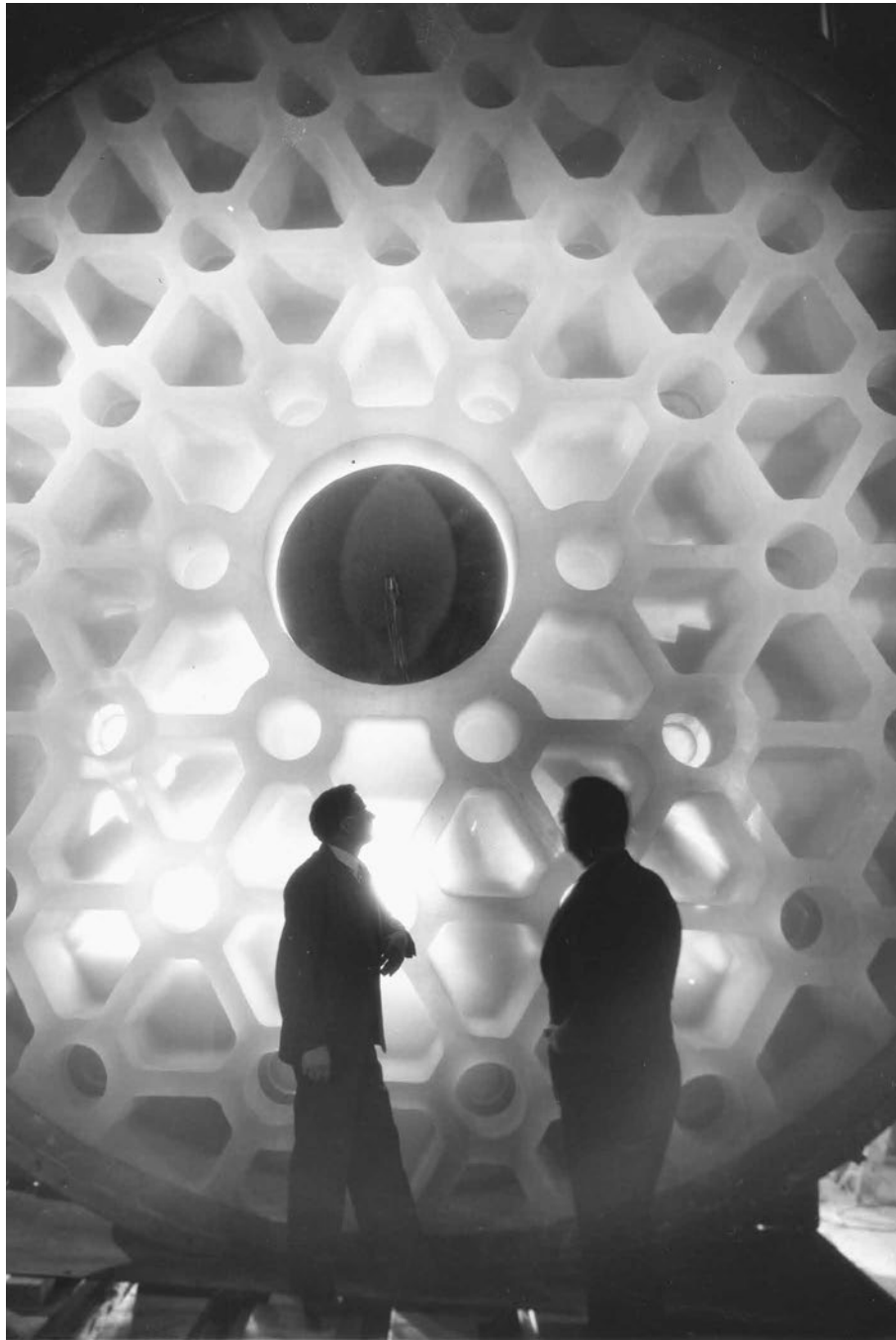
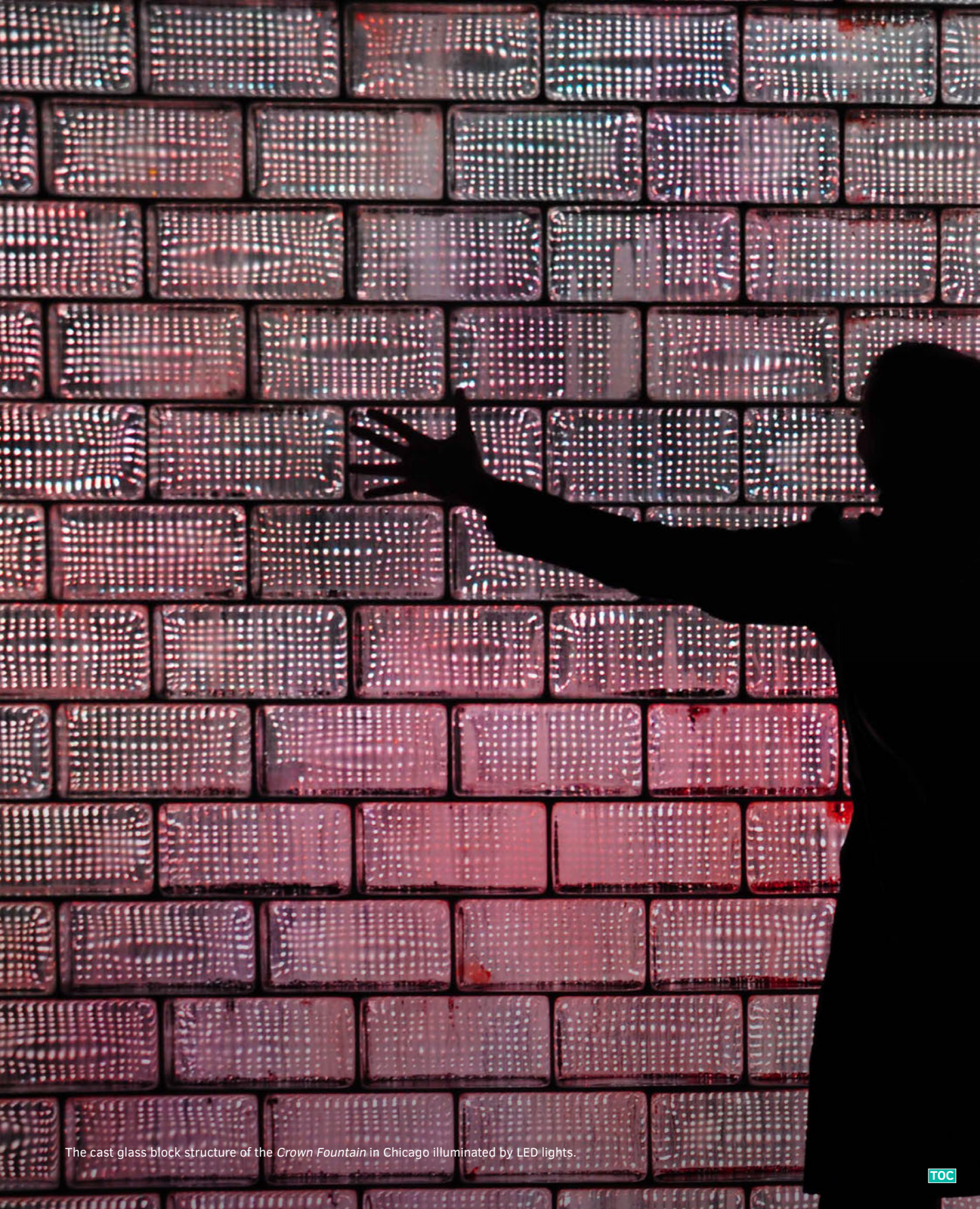


FIG. 3.10 The 5 m glass mirror blank of the *Mt. Palomar Hale* telescope. Source: Collection of the Rakow Research Library (number: 1000093961)



The cast glass block structure of the *Crown Fountain* in Chicago illuminated by LED lights.

Brittleness

The tendency of a metal or material to fracture without undergoing appreciable plastic deformation

Definition by the Engineering Dictionary

Brittle [adjective]

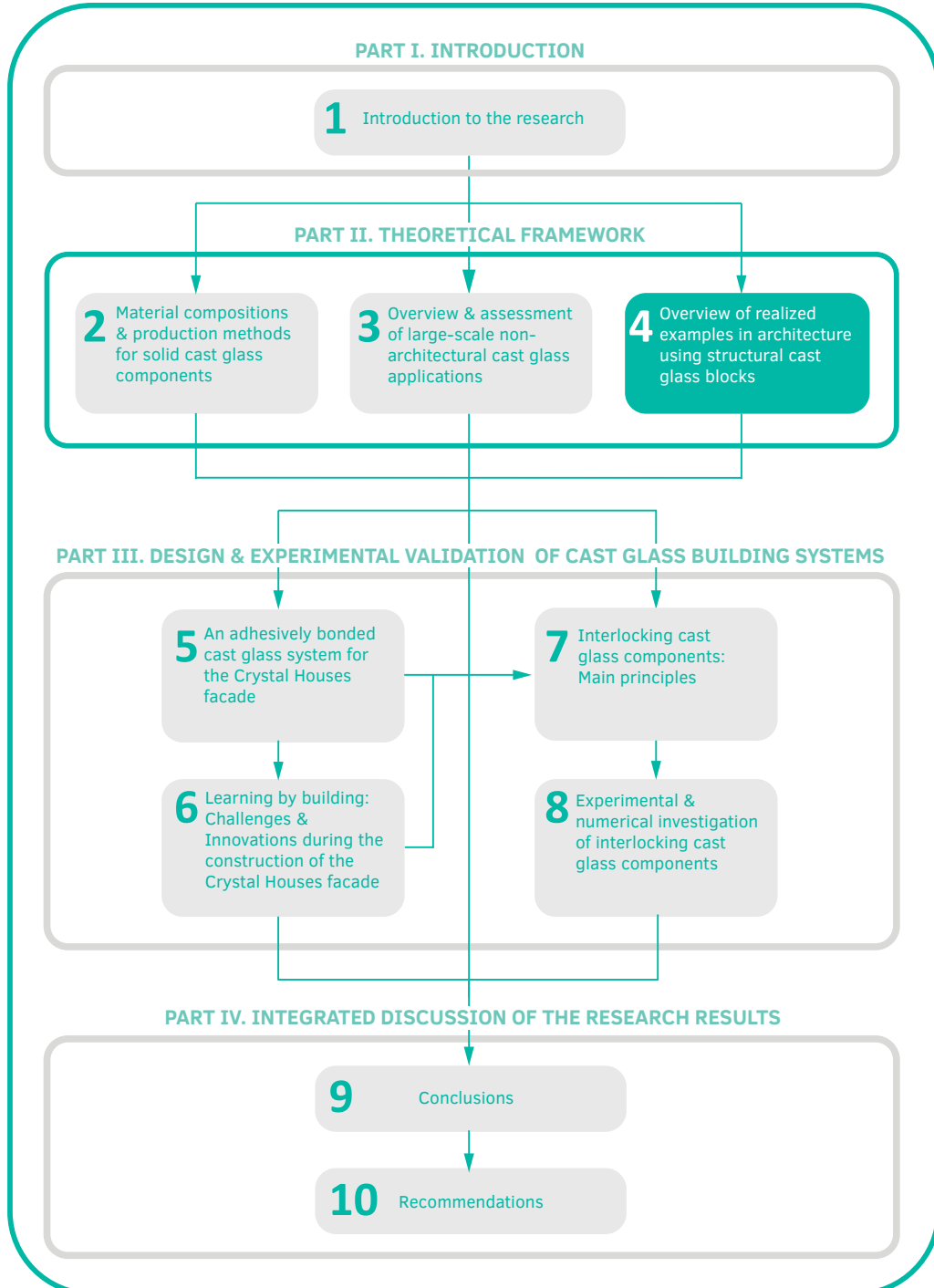
[1] Hard but liable to break easily

[2] (of a person's voice) Unpleasantly hard and sharp and showing signs of instability or nervousness.

[3] Appearing decisive or cheerful but unstable or nervous within.

Definition by the Oxford Dictionary

Exploring the third dimension of glass



Solid cast glass components and assemblies for structural applications

4 Overview of realized examples in architecture using structural cast glass blocks

Overview of the current state of the art as well as the investigated in this thesis building systems employing cast glass components³⁶

In view of the meticulous and lengthy cooling process discussed in the previous chapters, in architectural applications solid cast glass components have been commercialized up to the size range of standard masonry bricks. Owing to their large cross-sectional area, solid glass bricks are promising structural components that can fully exploit glass's compressive strength. By forming repetitive components, self-supporting, 3-dimensional all-glass structures of undisturbed transparency can be achieved. Nonetheless, at present, little and rather sporadic exploration has been made in the use of casting as a manufacturing method for structural glass in architecture. To a degree, this is attributed to the existence of only a few realized examples of self-supporting structures made of solid cast glass elements. The, so far, limited demand has in turn led to the absence of a standardized manufacturing process, to a lack of consistent engineering data and to a general unawareness of the potential of cast glass in structural applications in architecture. Currently, including the contribution of this dissertation, there are 3 structural systems employed for creating self-supporting structures out of cast glass components: (a) with a metal substructure, (b) adhesively bonded blocks, (c) interlocking glass blocks. The former two have been applied in real structures, whereas interlocking glass blocks are for the first time introduced as a building system through this dissertation. In this chapter, the 3 concepts are briefly presented, analyzed and

³⁶ This chapter has been published as part of the review article: Oikonomopoulou F., Bristogianni T., Barou L., Veer F., Nijse R. *The potential of cast glass in structural applications. Lessons learned from large-scale castings and state-of-the art load-bearing cast glass in architecture*. Journal of Building Engineering, vol.20, 2018.(Oikonomopoulou et al. 2018c)

evaluated in terms of manufacturing, structural system, level of transparency, ease of assembly and disassembly.

4.1 Introduction

At present the non-standardized, virtually manual, manufacturing process of solid glass blocks and the lack of substantial research on their assembly and structural performance have limited their structural application in only a few built architectural examples. To ensure the desired stability and stiffness of the glass assembly, such envelopes currently employ either a supportive substructure or a rigid structural adhesive (Fig. 4.2). The most characteristic case studies are the envelopes of the *Atocha Memorial* (Schober et al. 2007), the *Crown Fountain* (Hannah 2009), the *Optical House* (Hiroshi 2013) and the *Crystal Houses* (Oikonomopoulou et al. 2017a) (Fig. 4.1). Table 4.1 contains a summary of each project's characteristics. The research, development and realization of the *Crystal Houses* façade forms an integral part of this work and is extensively discussed in Chapter 5 and Chapter 6. The research, development and realization of the adhesively-bonded system triggered the design of a third structural concept, comprising dry-assembled, interlocking cast glass components. The principles and experimental validation of this proposed system are presented in Chapter 7 and Chapter 8. The interlocking system is yet to be realized in construction. This chapter, aiming to give a broad overview of all the current systems, therefore provides a synopsis of the realized systems, as well as of the systems developed in this dissertation.

Finally, it should be noted that structures employing hollow glass blocks or solid glass blocks that are, in essence, non-load-bearing remain out of the scope of this research. Thus, architectural projects where cast glass has been applied as façade cladding will not be analysed, yet, some inspiring projects in this field worth mentioning here are the *Ice Falls* and the *Periscope Window* by (James Carpenter Design Associates Inc 2018) and the art installation *Qwalala* by artist *Pae White* (*Domus* 2017).



FIG. 4.1 Characteristic examples of structures employing cast glass blocks: The *Atocha Memorial* (left), *Crystal Houses* (centre), and the *Crown Fountain* (right).

TABLE 4.1 Overview of the characteristics of realized self-supporting envelopes using solid cast glass components.

Project	Optical house	Crown fountain	Atocha memorial	Crystal house
Location	Hiroshima Japan	Chicago Illinois, USA	Madrid Spain	Amsterdam The Netherlands
Envelope dimensions [m]	8.6 x 8.6	12.5 x 7 x 4.9	8 x 11	10 x 12
geometry	Flat envelope	Cube	Elliptical cylinder	Flat envelope
Structural system	Supportive substructure	Supportive substructure	Adhesively bonded	Adhesively bonded
Number of blocks	6000	22500	15600	7500
Size of blocks [mm]	235 x 50 x 50	127 x 254 x 51	300 x 200 x 70	210 x 210 x 65 210 x 157.5 x 65 210 x 105 x 65
Number of different blocks	1	1	1	3
Weight of block [kg]	2.2	4.5	8.4	7.2 / 5.4 / 3.6
Total weight [t]	13	50.6	130	40.5
Type of glass	Borosilicate	Low-iron soda-lime	Borosilicate	Low-iron soda-lime
Annealing time	unknown	unknown	20 h	8-38 h (size dependent)
Type of mould	Press steel mould	Open steel mould	Press steel mould	Open steel mould
Post-processing	no	Polishing in one side	no	Polishing 2 faces to ± 0.25 mm precision

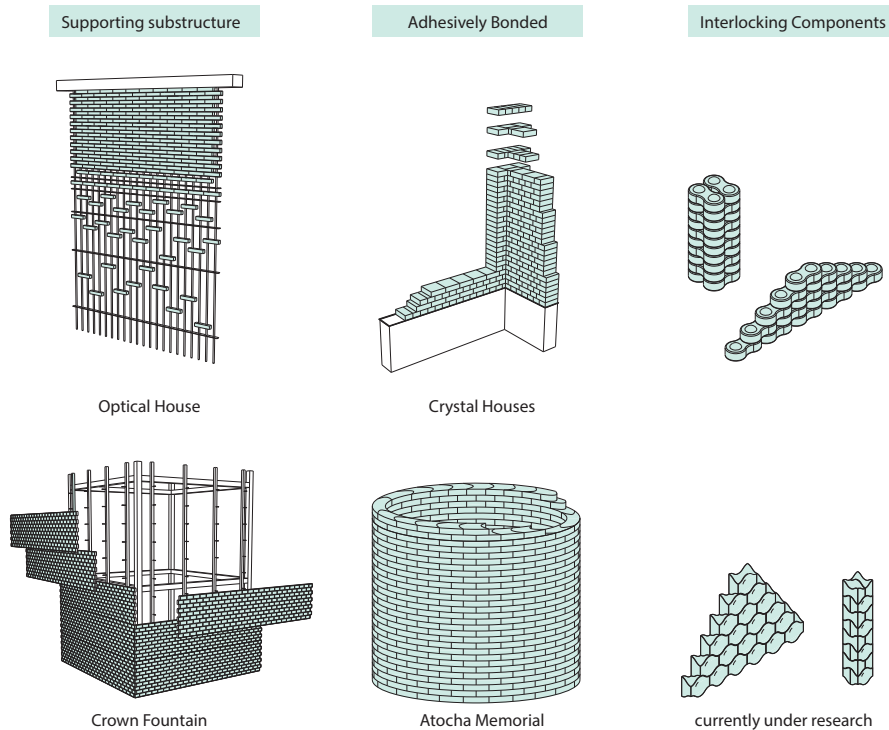


FIG. 4.2 Illustration of the structural systems currently developed for structures using cast glass components.

4.2 Principles of structural system employing solid cast blocks

4.2.1 Solid glass vs hollow blocks

Glass blocks are commonly produced in a hollow form, fabricated by thermally fusing two shallow rectangular cups along their open faces. A sealed interior air chamber is formed that gives the glass block its thermal and acoustic insulating properties (Murray 2013). Regarding transparency, hollow bricks can be completely

colourless. However, the block's multiple layers (glass – air – glass) result in severe optical distortion of objects observed through it. Fig. 4.3 illustrates how each light ray passing through a block is reflected and redirected within every media, producing a visual obscuration dependant on surface texture and angle of view. Hollow glass blocks are further considered unsuitable as load bearing components due to their relatively low stated resistance to compressive load (given as 6 MPa in *ISO 21690:2006*). While ceramic masonry bricks with comparable failure loads are used as load bearing elements, the low wall thickness of hollow glass blocks risks internal buckling and failure from the vertical load of the stacked wall; hence the increased risk renders them unsuitable as load bearing components for solid load bearing walls. Accordingly, a separate supporting structure is required if hollow blocks are used. Usually, in small structures the blocks are embedded in a steel rod reinforced cement-based mortar. In large-scale structures, elaborate metal systems are required to carry the loads of the structure. Good examples include the *Maison Hermes* (Murray 2013) and the *Maastricht Academy of Arts* (Wiel Architects 2014). Hollow glass blocks are considered non-loadbearing and therefore will not be further discussed in this research.

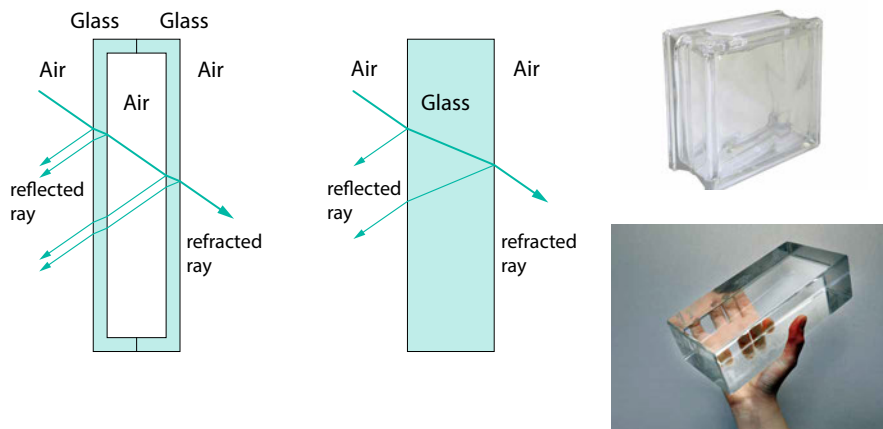


FIG. 4.3 The transition of the light rays through multiple media in a hollow glass block results in much more distortion compared to a solid glass block.

In contrast, solid glass blocks present a much higher compressive strength, typically over 200 MPa, which allows them to be used as loadbearing components. Solid glass blocks are produced by pouring liquid glass into a steel mould. Each block is then cooled down controllably for many hours – duration depending on the dimensions of the block – to avoid cracks due to unequal temperatures between the surface and

the core (Christoph, Knut 2008) and to prevent the development of any pre-stress in the block. In comparison to hollow blocks, solid blocks have similar transparency but significantly less optical distortion. Their monolithic mass implies a constant refraction index that results in the redirection of the light rays only at the two external surfaces and hence, causing less distortion of objects projected behind them (Fig. 4.3). Solid blocks, however, exhibit a reduced thermal resistance compared to hollow ones. Owing to their inferior thermal insulation properties, as well as to a noticeably higher manufacturing cost and a non-standardized manufacturing process, solid glass blocks have, so far, rarely been employed for exterior glass walls, despite their load-bearing capacity.

4.2.2 Structural systems employing cast glass blocks

As previously mentioned, a supporting structure is required when hollow glass blocks are used in a facade of considerable dimensions because of their low load-bearing capacity. Due to the lack of standardized structural specifications and strength data on transparent adhesives, the majority of projects using solid glass blocks are also dependent on pre-tensioned steel reinforcement to ensure rigidity and prevent buckling. Nevertheless, to obtain an entirely transparent visual result, opaque reinforcement elements should be avoided. This can be achieved either through the use of a transparent, structural adhesive or through an interlocking geometry of the blocks in combination with an intermediate medium that prevents peak stress concentrations due to glass-to-glass contact.

The overall geometry of the structure can further contribute to its stability and stiffness. For example, in the *Atocha Memorial* solid glass blocks bonded by a transparent UV-hardening adhesive form a cylindrical tube which contributes greatly to the structure's stiffness, eliminating the necessity of additional steel elements for its support (Christoph, Knut 2008).

In summary, there are currently 3 structural systems employed for creating self-supporting structures out of cast glass components:

- 1 With a metal substructure
- 2 Adhesively bonded blocks
- 3 Interlocking glass blocks

Prior to this research, the prevailing solution was the first one, employing a metal substructure, and there was only one example of an adhesively bonded glass

block structure. This thesis has contributed to the field of structural cast glass by developing and experimentally validating the lateral two solutions: Adhesively bonded and interlocking glass blocks. All three concepts are briefly discussed in the following sub-chapters.

4.3 Solid glass block envelopes with supportive substructure

In this system, a supportive metal substructure carries the tensile forces and ensures the desired stiffness and buckling resistance, allowing the glass assembly to perform mainly under compression. The most characteristic realized examples using this principle are the *Crown Fountain* and the *Optical House*. In specific, the 8.6 m x 8.6 m envelope of the *Optical House* (Fig. 4.4) consists of 6000 solid blocks, with through holes between top and bottom sides (Fig. 4.5), whereby pass the rods of a pre-tensioned vertical mesh, consisting of 75 stainless steel rods suspended from a steel beam (Fig. 4.6) encased in reinforced concrete (Hiroshi 2013). The mesh withstands the lateral forces, while the glass carries its own weight. Two vertical steel fins further serve against wind loads. In this way, a façade of high slenderness is obtained. The rods are connected with stainless steel flat bars (40 mm x 4 mm) that seat within the 50 mm thick glass blocks at 100 mm intervals, to reduce lateral stresses directed to the glass blocks (Fig. 4.6 and Fig. 4.7). The resulting structure is mortar-free (Hiroshi 2013). Borosilicate glass was opted for the glass blocks, due to its increased optical qualities compared to soda-lime (The Architectural Review 2012).

The *Crown Fountain* (Fig. 4.8) employs a different system, a combination of pre-assembled glass block grates connected to a stainless steel internal frame, which carries both vertical and lateral forces (Hannah 2009). Each of the 2 towers of 12.5 m x 7 m x 4.9 m employs a total of 11250 cast glass blocks, pre-assembled in grates of approx. 250 units, stacked and welded together. All forces are transferred by an embedded steel T-profile frame to the base via a zigzag pattern. The lateral stability of the tower is enhanced by Ø13 mm rods anchored to the structure and triangular corner brackets. The blocks were made using melt-quenching and an open, high-precision steel mould. This resulted in blocks that needed to be polished only on one side. Approximately 350 blocks were produced per day over a period of 4 months.



FIG. 4.4 The Optical House. Source: Koji Fujii / Nacasa & Partners Inc.



FIG. 4.5 Cast glass block unit of the Optical House. Source: Hiroshi Nakamura & NAP.



FIG. 4.6 Assembly of the *Optical House*. Source: Hiroshi Nakamura & NAP.

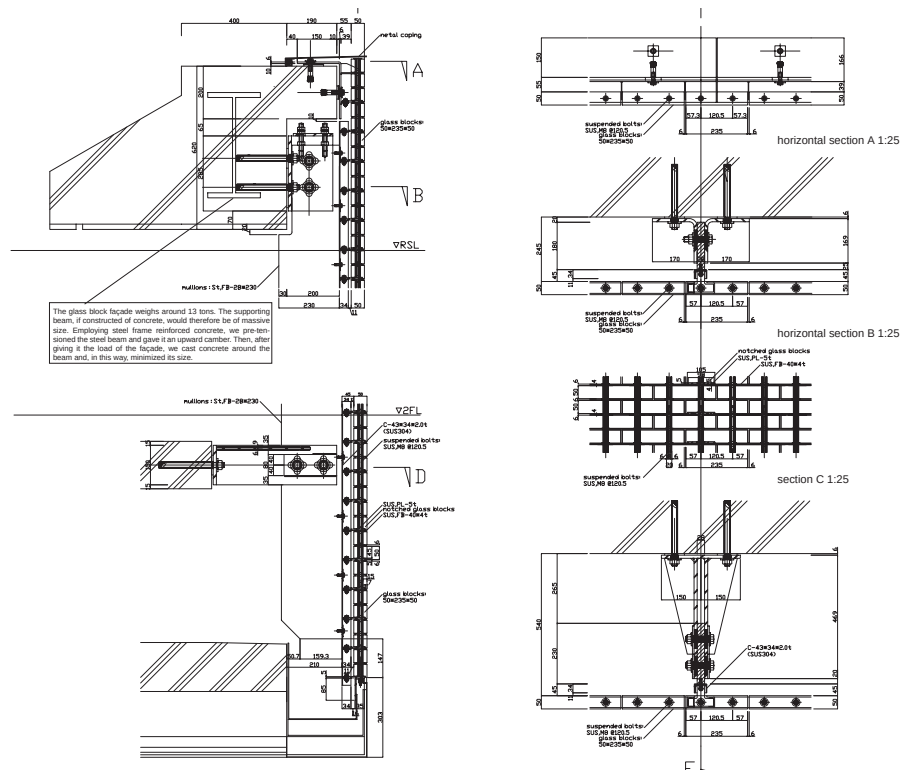


FIG. 4.7 Detail drawings of the *Optical House*'s glass block system. Drawing courtesy: Hiroshi Nakamura & NAP.

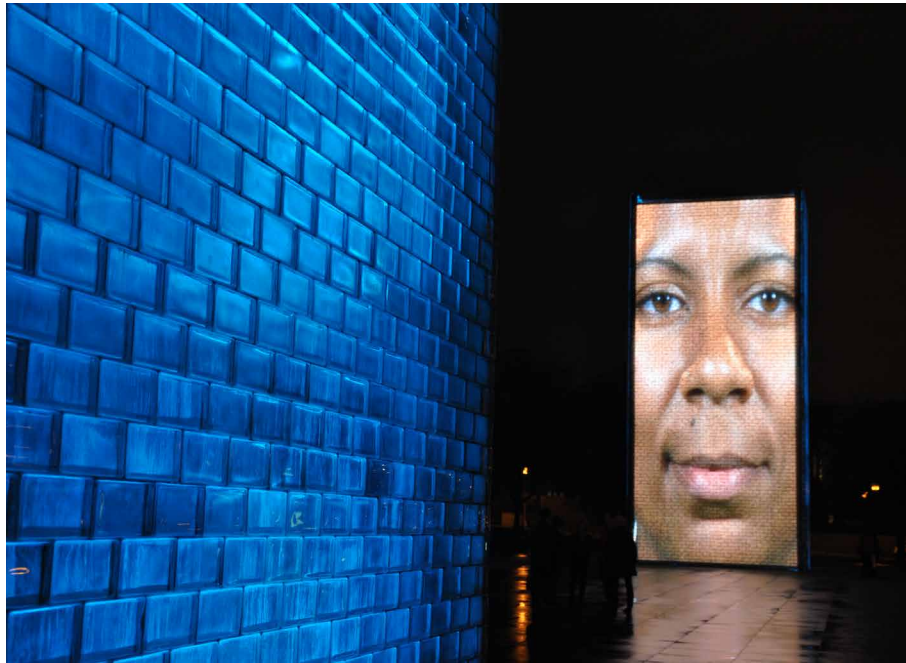


FIG. 4.8 The two *Crown Fountain* towers at night.

4.4 Adhesively bonded blocks

An entirely transparent cast glass structure can be built by bonding the glass blocks together with a colourless rigid structural adhesive. In this way material-compatible, low-stress and permanently resistant connections are established. In such a system, the mechanical properties of the adhesive are equally critical to the ones of the glass blocks; it is their interaction as one structural unit that defines the system's structural behaviour. The most favourable structural performance is when adhesive and glass fully cooperate and the assembly behaves as a single rigid unit under loading, resulting in a homogeneous load distribution (Oikonomopoulou et al. 2017a). Thus, rigid adhesives, such as acrylates and epoxies are necessary to ensure the desired bond strength. Two good examples of adhesively bonded glass envelopes from cast glass components are the *Atocha Memorial* and the *Crystal Houses*.

The *Atocha Memorial* (Fig. 4.9), approximately elliptical in plan and 11 m high, is built from 15600 glass borosilicate blocks bonded together with a 2 mm thick transparent UV-curing adhesive (Schober et al. 2007). To obtain the cylindrical shape of the monument (Fig. 4.10) by a single block geometry, a customized cast glass component was designed, convex on one side and concave on the other (Fig. 4.11). The curvature turns the glass wall into a shell structure of increased stiffness, sparing the necessity of a substructure. The glass roof is connected to the glass block structure in a rigid way to constrain the upper free edge and prevent the ovalisation of the section (Goppert et al. 2008).



FIG. 4.9 The *Atocha Memorial*. Source: *Esaú Acosta (FAM Arquitectura y Urbanismo)*

The glass elements are subject to high temperature fluctuations in Madrid, resulting in high surface tensions. Therefore, borosilicate glass was opted for the fabrication of the blocks due to its comparably lower thermal expansion coefficient than soda-lime. By casting borosilicate glass in high precision press steel moulds, the required ± 1 mm tolerance was met, guarantying the applicability and uniformity of the selected adhesive without the need for post-processing (Goppert et al. 2008). The annealing time for each brick was 20 h.

The special characteristics of the adhesive required the construction of an envelope using a UV-filtering tent for protection against solar radiation, dust and adverse weather conditions (Fig. 4.12). Both temperature and humidity levels were controlled. Prior to construction, various tests were performed to validate the

structural performance of the adhesive-glass assembly. According to the structural calculations, almost the entire contact area of the blocks had to be bonded. At the same time overflow had to be minimized. A special bonding method was developed, to distribute the adhesive in the right amount and prevent the trapping of air bubbles.

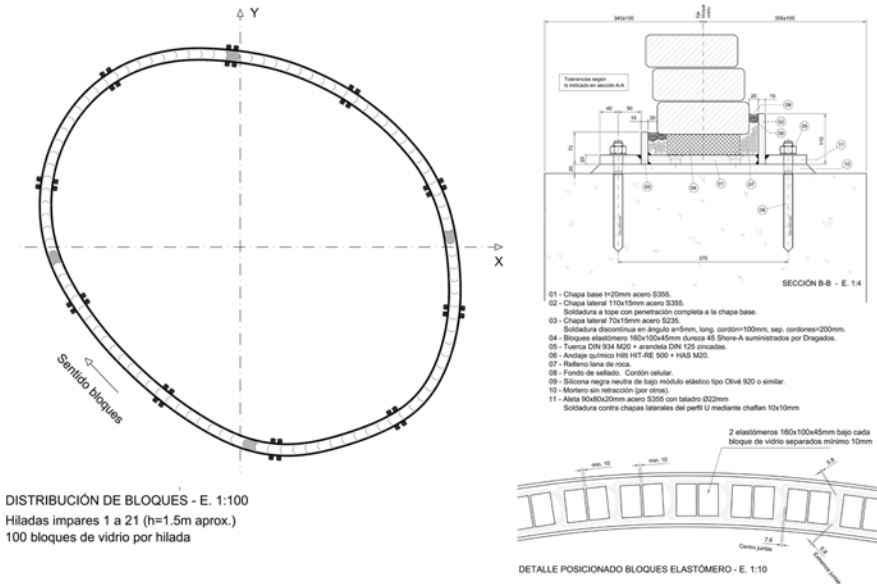


FIG. 4.10 Plan and details of the Atocha Memorial glass structure. Source: Bellpart.



FIG. 4.11 Glass block unit of the Atocha Memorial.

Logistics of the project were also challenging. Two 10 h shifts were established with 11 specialized workers per shift, 6 days per week, for the cleaning, bonding by UV-curing and external sealing of the blocks one by one, resulting in 500-600 glued blocks per day (Goppert et al. 2008).



FIG. 4.12 Construction of the Atocha Memorial. Source: Bellapart, SAU.

The *Crystal Houses* is another characteristic example of an adhesively bonded, highly transparent glass block envelope, made as an accurate yet completely transparent reproduction of the previous, 19th century masonry brick façade (Oikonomopoulou et al. 2015a). The research and development of this adhesively bonded system is part of this dissertation and is discussed in detail in Chapter 5 and Chapter 6. Based on the brick modules of the original façade, the 10 m x 12 m transparent elevation employs more than 6500 solid glass bricks, of 3 different sizes (Table 4.1), reinterpreting the traditional brickwork; while massive cast glass elements reproduce the classic timber door and window frames. Towards the top, terracotta bricks intermingle with glass ones, gradually transforming the glass elevation to a traditional brick façade (Fig. 4.13 and Fig. 4.15). The architects' desire for unimpeded transparency, rendered as sole solution the creation of an entirely self-supporting adhesively-bonded glass brick system (Oikonomopoulou et al. 2015b).

Research and testing of various adhesive types by (Oikonomopoulou et al. 2015b) led to the eventual selection of *Delo Photobond 4468*; a colourless, UV-curing, one-component acrylate, designed for high strength bonding between glass components.



FIG. 4.13 *Crystal Houses* façade, Site elevation. Source: MVRDV architects

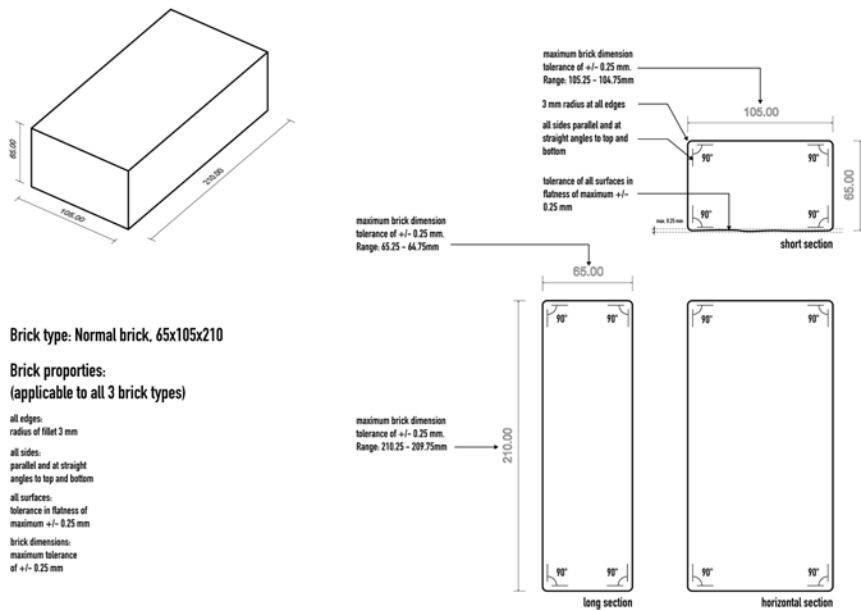


FIG. 4.14 Diagram indicating the properties and dimensional accuracy of a normal-size glass brick for the *Crystal Houses* façade project. Source: MVRDV architects.



FIG. 4.15 Left: 3D visualization of the *Crystal Houses* façade by MVRDV Architects. Right: The realized façade.

Structural experiments indicated the application thickness of the adhesive layer for an optimum bond strength to be between 0.2–0.3 mm. In addition, the construction of 4 architectural wall mock-ups by (Oikonomopoulou et al. 2015b) with tolerances ranging from ± 0.25 mm to ± 0.5 mm in the height and flatness of the bricks indicated that tolerances above ± 0.25 mm result in an uneven spread of the adhesive that can greatly affect the structural performance. Moreover, the visual result of the transparent wall is disturbed due to induced air gaps in the adhesive layer. The relatively low viscosity of the specific glue allowed a homogeneous bonding only at the horizontal surfaces of the glass bricks; the vertical joints, approx. 1 mm in width, were left open, allowing as well for thermal expansion. Accordingly, it was determined that the glass blocks' top and bottom surfaces should be flat within ± 0.25 mm (Fig. 4.14 and Fig. 4.16) (Oikonomopoulou et al. 2015b).

The thickness of each construction layer had to be confined within the same dimensional accuracy, as any accumulated deviation larger than the required bonding thickness could lead to uneven and improper bonding. The demand for this remarkably high level of accuracy and transparency, introduced various challenges in the engineering and construction of the façade. The required ± 0.25 mm tolerance influenced the selection of glass recipe and mould as well. Soda-lime glass and open high precision moulds were chosen to prevent an unnecessary increase in production

costs as the high required accuracy would necessitate the mechanical post-processing of the block's bonding surfaces anyway (Oikonomopoulou et al. 2017a). Depending on the block's size the annealing time ranged between 8–38 h. The 65 mm thickness of the blocks hindered an accurate stress measurement by a *Scattered Light Polariscopes* stress-meter; instead a qualitative analysis of strain concentration was made using cross polarization (Fig. 4.17).

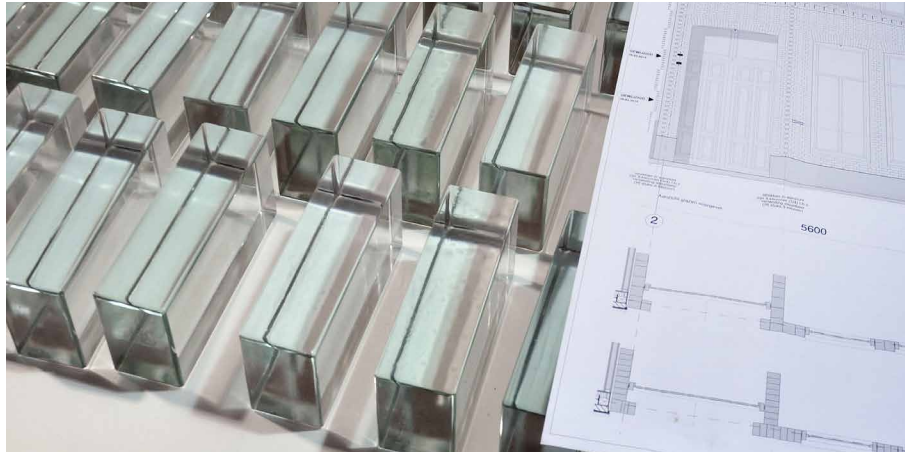


FIG. 4.16 Solid glass blocks used for the construction of the *Crystal Houses* façade.

Eventually the horizontal, bonding surfaces of the blocks were CNC polished to meet the desired precision. Structural tests and architectural mock-ups by (Oikonomopoulou et al. 2015b) suggested the bonding of the complete contact surface between blocks. Through the uniform application of the adhesive both a homogeneous load distribution and maximized transparency are attained. To eliminate defects in the adhesive layer that would deeply affect the final visual result, a customized bonding method was developed, using custom-designed self-reinforced polypropylene forms for controlling the flow, spread and amount of the adhesive (Fig. 4.18).

(Oikonomopoulou et al. 2017a) discusses the complex logistics of the project, which are similar but more stringent as for the *Atocha Memorial* project. The 8 times less allowable thickness of the adhesive, introduced a significantly higher complexity level of the manual bonding process that called for a highly skilled crew and a strictly controlled construction. A 12 h working schedule was established, 5 days per week. 7-9 highly skilled workers bonded and sealed on average 80-100 blocks per day under the supervision of 2 quality control engineers and the construction site supervisor. The entire build-up of the façade took 7 months.

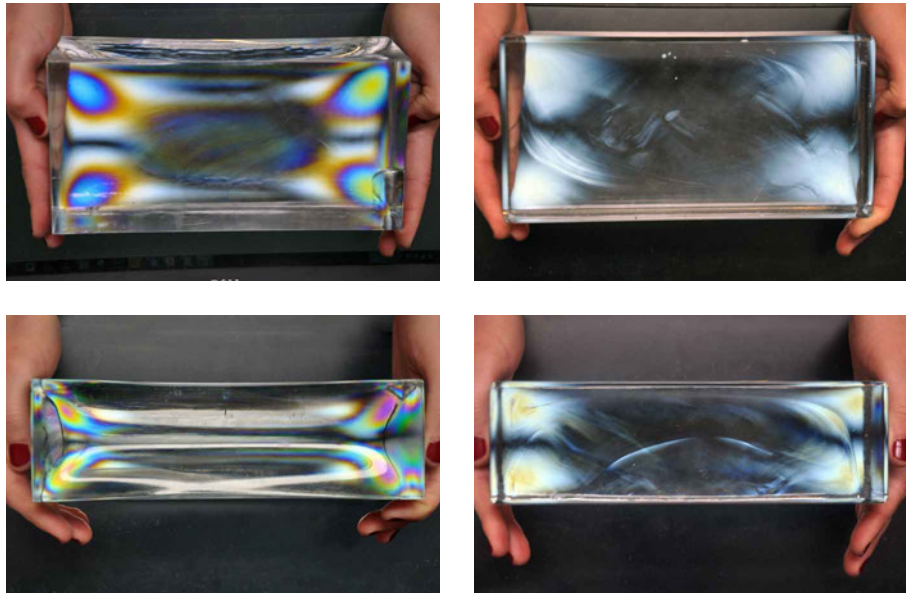


FIG. 4.17 Qualitative stress analysis through cross polarization. Bricks with clear indication of stresses (left) were discarded. Specimens with no visible strain concentration (right) were employed in the façade.



FIG. 4.18 Bonding and curing of the adhesive at the *Crystal Houses* façade.

4.5 Interlocking components

This third, new concept – that is an integral part of this dissertation and is yet to be realized in an actual construction – explores the potential of full-glass compressive structures, such as envelopes, walls and columns from interlocking cast glass components. The research and development of interlocking cast glass components is presented in detail in chapters 7 and 8 of this dissertation. In this system, the overall stability is achieved through compression provided by the construction's self-weight combined with the interlocking geometry that restrains lateral movements, resulting to a structure with minimal, if any, metal framing. The suggested system proposes the use of a dry, colourless interlayer, such as Polyurethane Rubber (PU) or Polyvinyl Chloride (PVC), as an intermediate medium between the glass units (Fig. 4.19).



FIG. 4.19 Prototype of a 3 mm thick, cast interlayer from PU70 (Oikonomopoulou et al. 2018).

This allows for a demountable structure that enables the circular use of the glass components: they can be retrieved intact and reused or, eventually, recycled as they are not contaminated by foreign substances such as coatings or adhesives. Moreover, the dry interlayer prevents stress concentrations due to glass-to-glass contact and compensates for the inevitable dimensional tolerances in the cast units' size (Oikonomopoulou et al. 2018a). So far, various geometries, dry interlayers and

structural applications have been explored and experimentally tested by the *Glass & Transparency Group of TU Delft*. In particular, (Aurik 2017; Snijder et al. 2016; Aurik et al. 2018) studied a dry-assembled arched glass masonry bridge interlocking in one direction (Fig. 4.20). All other research projects focus on systems that confine the movement in both axial and transverse direction. (Akerboom 2016) studied the realization of a glass column out of solid interlocking cast components. The column's cross-section was optimized based on its structural capacity and performance. (Barou et al. 2016) proposed an interlocking system for flat, self-supporting envelopes using a brick inspired by the *LEGO®* block (Fig. 4.21, left). (Frigo 2017; Jacobs 2017; Oikonomopoulou et al. 2018a) further developed the interlocking brick concept, suggesting more curved geometries and an equal mass distribution, in respect to the manufacturing process of cast glass and towards an increased shear capacity. Numerical modelling of the resulting osteomorphic block (Fig. 4.21, centre, right) presented in (Jacobs 2017) indicated that geometrical parameters such as amplitude and block height can have a significant influence on the system's failure mechanism and ultimate load-carrying capacity in shear.



FIG. 4.20 Visualization (top) and a tested glass block prototype (bottom) of the dry-stacked glass arch bridge concept developed by (Snijder et al. 2016).

Although there are not sufficient experimental results to derive statistical data, they suggest that interlocking cast glass components can be a promising solution for future structural applications. An important input from this research is the development of units featuring more organic shapes with curved geometries (Fig. 4.22 and Fig. 4.23), avoiding sharp edges to prevent residual stress concentrations, fitting the characteristics and peculiarities of cast glass as a construction material (Oikonomopoulou et al. 2018a).



FIG. 4.21 Evolution of interlocking cast glass blocks towards more curved geometries of equal mass distribution. From left to right: interlocking glass brick inspired by the *LEGO*[®] block by (Barou et al. 2016), osteomorphic block by (Jacobs 2017) and osteomorphic blocks by (Oikonomopoulou et al. 2018a)



FIG. 4.22 Physical prototypes of a two-component interlocking geometry by (Oikonomopoulou et al. 2018b).



FIG. 4.23 Physical prototypes of different interlocking geometries by (Oikonomopoulou et al. 2018b).

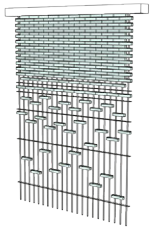
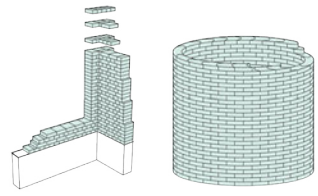
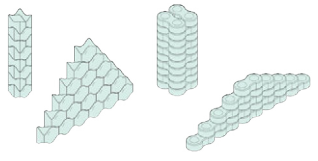
4.6 Discussion

The comparative charts of Table 4.2 lead to general conclusions regarding the applicability of cast glass in load-bearing structures in architecture. Due to the lack of sufficient and comparable technical data, the thermal and acoustic performance of the presented solid cast glass applications³⁷ have been excluded from this dissertation.

All realized projects have been made using primary casting, and typically employed a singular block geometry of simple rectangular form and less than 10 kg in weight. Either borosilicate or soda-lime glass are employed, depending on the weather conditions per location, and specifically the anticipated temperature differentials, and the required dimensional accuracy.

³⁷ In general, solid glass blocks exhibit a reduced thermal and acoustic resistance compared to hollow glass blocks. The latter, due to the air cavity, exhibit an increased thermal resistance and can reduce sound transmission. On the other hand, due to the aforementioned air cavity, hollow glass-blocks are considered non-load-bearing and cannot be applied in structural applications.

TABLE 4.2 Design principles of the different structural systems employing cast glass components

1. Additional substructure	2. Adhesively bonded glass structure	3. Interlocking cast glass units
Tensile forces are carried by a metal substructure	Homogeneous load transfer in the glass assembly via rigid adhesive	Stiffness is obtained by the interlocking geometry
		
Dry-assembly/ adhesively bonded	Adhesively bonded	Dry-assembly
Interlayer accommodates size deviations	Adhesive's thickness requires high precision in unit size	Interlayer compensates for size deviations
Easily assembled	Meticulous, intensive labour of high precision	Easily assembled
Compromised transparency	High transparency	High transparency
Reversible	Non-reversible	Reversible

Although primary casting requires higher working temperatures, it is considered a more cost-effective method for the production of numerous identical units.

Also, as described in Chapter 2, the glass type, overall dimensions, form and volume of the object are key-factors for the total annealing time. Thus, smaller-sized and simple-shaped objects are preferred. For example, the solid glass bricks of 3.6 kg weight used in the *Crystal Houses* façade required 8 h of annealing, whereas components of double the volume (and critical dimension) and 7.2 kg weight, required an annealing cycle of 36–38 h respectively (Oikonomopoulou et al. 2017a). The annealing time can be further reduced if borosilicate glass is employed instead of soda-lime due to its improved thermal expansion coefficient (table 2). A comparison between the 8.4 kg block of the *Atocha Memorial* and the 7.2 kg block of the *Crystal Houses* demonstrates this clearly. The former, although larger in dimensions and weight, required almost half the annealing time than the latter.

A limited mass also facilitates the transportation, installation and handling processes. Moreover, a repetitive component geometry is essential for simplifying the production and assembly and for limiting the manufacturing costs, owing to a limited amount of moulds and a standardized production process.

Regarding the overall shape, little exploration has been made of the forms that can be achieved by cast glass in the realized projects (Fig. 4.24). Only the research conducted in interlocking components (and included in this dissertation) shows a greater potential in developing non-orthogonal shapes matching the properties of glass.

There are currently, including the contribution of this thesis, 3 developed structural systems for making self-supporting cast glass structures, employing: (1) a supportive substructure, (2) a stiff, colourless adhesive and (3) an interlocking geometry and a dry interlayer.

Whereas the first solution compromises the overall level of transparency and the second solution results in an irreversible, non-recyclable and challenging construction of intensive and meticulous labour, the interlocking cast glass components can tackle the limitations imposed by both previous systems. Nonetheless, this solution has yet to be realized and be validated in practice.

Lastly, a crucial aspect that can greatly influence the performance of the structure is its overall geometry. Flat geometries or walls of high-slenderness have limited resistance to lateral loads and buckling and call for more challenging solutions than geometries with inherent stability such as closed shapes.

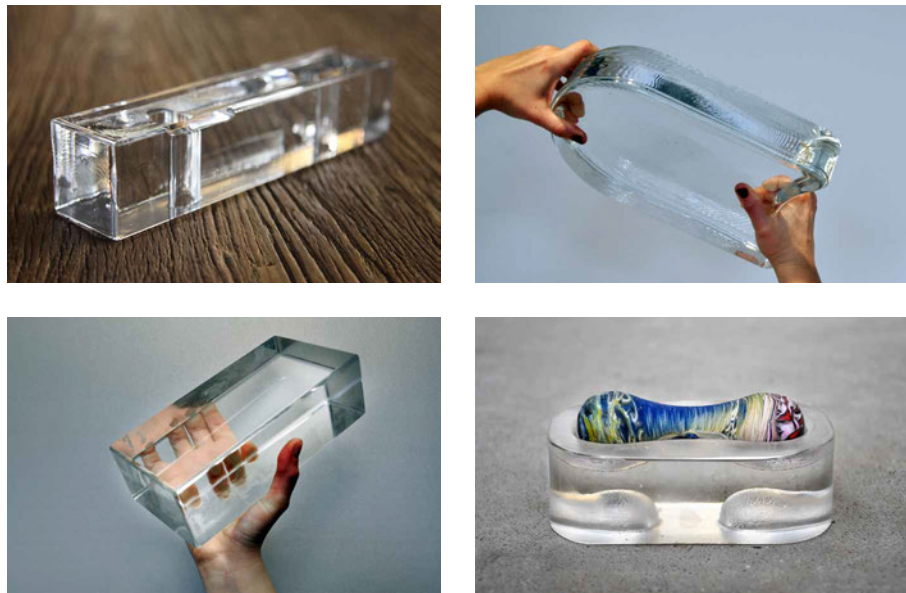


FIG. 4.24 Top left to bottom right: Glass block units employed in the *Optical House*, *Atocha Memorial*, *Crystal Houses* façade and the interlocking research.



Adhesively bonded soda-lime glass blocks at the *Crystal Houses* facade

Adhesive

A substance used for sticking objects or materials together; glue

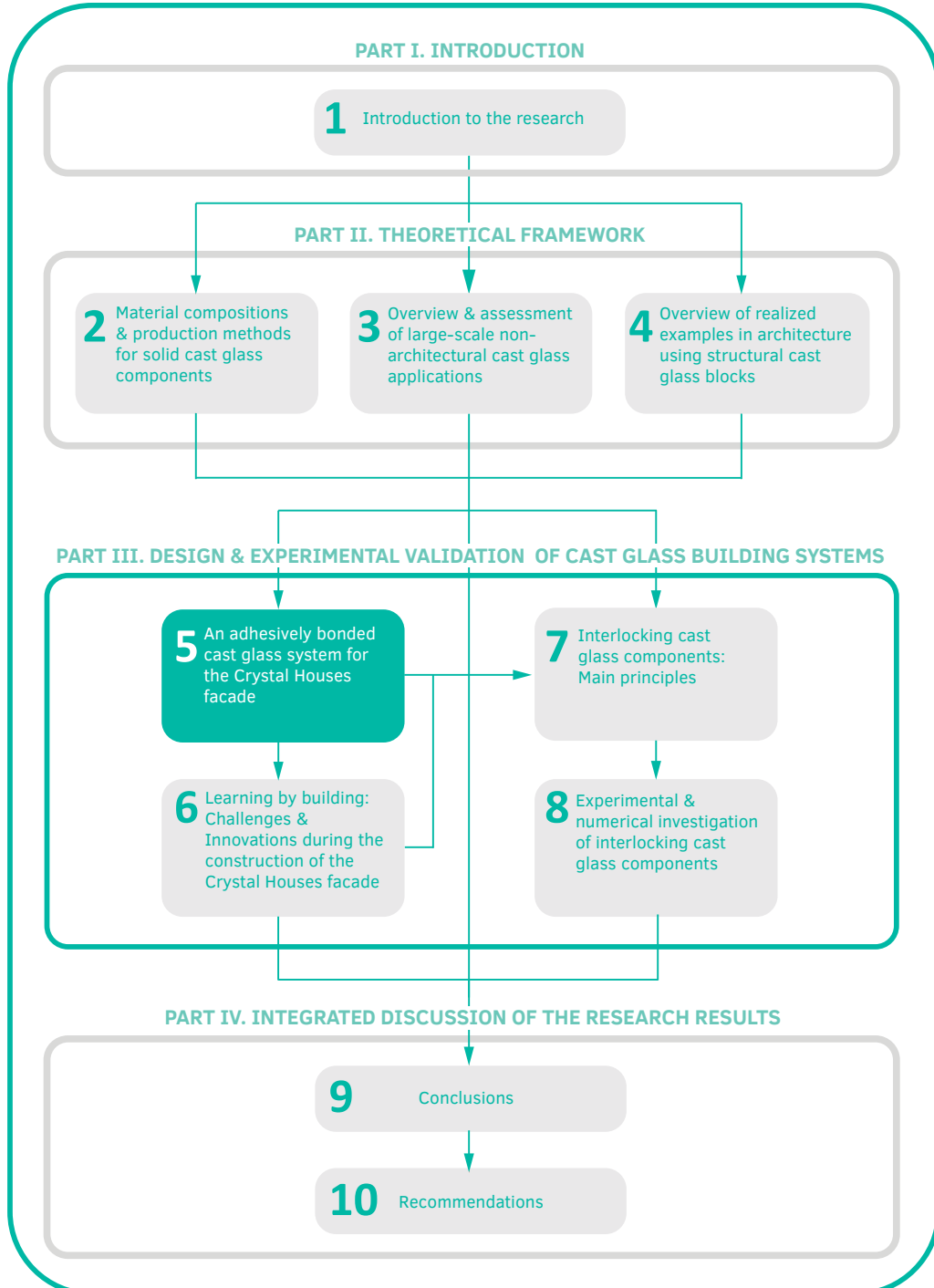
Definition by the Oxford Dictionary

Glue

A sticky substance that is used for joining things together permanently, produced from animal bones and skins or by a chemical process

Definition by Cambridge Dictionary

Exploring the third dimension of glass



Solid cast glass components and assemblies for structural applications

5 An adhesively-bonded cast glass system for the Crystal Houses façade

Design principles and experimental validation of an adhesively bonded system utilizing cast glass components³⁸.

Chapter 4 provided an overview of the three structural systems utilizing cast glass components in architecture, including a brief overview of the work presented in this dissertation. This chapter presents the design principles and experimental work for the first of the two systems explored in this work: a transparent, adhesively-bonded glass block system designed for self-supporting envelopes. The proposed system was developed for the *Crystal Houses* façade in Amsterdam, designed by MVRDV Architects. The system is exclusively constructed by solid cast glass blocks, bonded with *DELO Photobond 4468*, a colourless, UV-curing adhesive. This allows for a system of an increased transparency, sparing the necessity of an opaque substructure. In contrast with previous realized projects, solid soda-lime glass blocks are used rather than borosilicate ones.

Initially, several architectural prototypes, comprising glass elements of different tolerance ranges, are built to evaluate the visual performance and the thickness of the adhesive that allows for an even spread. The prototypes indicate that a homogeneous bond thicker than 0.3 mm cannot be obtained by the selected adhesive due to the latter's flow properties and low viscosity. Based on the adhesive's optimum application thickness, it is determined that the glass blocks' top and bottom surfaces should be flat within 0.25 mm for guaranteeing an even adhesive layer of the highest strength.

³⁸ This chapter has been published as Oikonomopoulou F., Veer F.A., Nijse R., Baardolf K. *A completely transparent, adhesively bonded soda-lime glass block masonry system*. *Journal of Façade Design and Engineering* 2014. (Oikonomopoulou et al. 2015b)

The structural verification of the system is demonstrated by physical testing of prototypes in compression, 4-point bending, hard-body impact and thermal shock. Compressive tests on individual blocks highlight the need for proper detailing and uniform load distribution of the system. Compressive tests on columns made of adhesively bonded glass blocks further confirm that strict size tolerances are essential for maximizing the load-bearing capacity of the system: specimens with larger size deviations fail in considerably lower stress values than specimens with smaller size deviations. Furthermore, series of 4-point bending tests on adhesively bonded glass beams demonstrate that the chosen adhesive enables the glass brick wall to behave monolithically under such loading when the adhesive is applied in a constant layer of the optimum thickness.

Overall, the results show that the adhesively bonded glass block structure can provide the required structural performance, but only if strict tolerances are met in the geometry of the glass blocks so that the chosen adhesive can be evenly spread in a constant thickness.

Credits

4-point bending tests conducted in collaboration with

- Telesilla Bristogianni,
Faculty of Civil Engineering & Geosciences, TU Delft

Technical support and assistance

- Kees Baardolf - *prototype construction & preparation of test set-ups*,
Stevin II Laboratory, Faculty of Civil Engineering & Geosciences, TU Delft
- Marco & Ronald van de Poppe – *assistance in construction of wall mock-ups*

Test facilities

- *Compression tests, Impact & Vandalism Test*
Stevin II Laboratory,
Faculty of Civil Engineering & Geosciences, TU Delft
- *4 point-bending tests*
Materials Laboratory,
Faculty of Mechanical, Maritime & Materials Engineering

Research Supervisors

- Rob Nijse,
Faculty of Civil Engineering & Geosciences, TU Delft
- Fred A. Veer,
Faculty of Architecture & the Built Environment, TU Delft

Architectural Design

- MVRDV

Co-Architect

- Gietermans & Van Dijk

Glass brick manufacturer

- Poesia

Adhesive Consultant

- Siko B.V. - Rob Janssen

5.1 Introduction

This chapter focuses on the research, development and experimental validation of an adhesively-bonded solid glass block self-supporting system. The proposed system has been developed for the *Crystal Houses* façade in Amsterdam, designed by *MVRDV* and successfully completed in 2016. The architectural concept behind the façade is the creation of an accurate yet completely transparent reproduction of the previous 19th century elevation of the building of 10m x 12m in dimensions. In turn, the façade is exclusively constructed by solid glass blocks, bonded by a colourless, stiff adhesive. Soda-lime glass is opted for the fabrication of the glass blocks due to cost reasons. Given the insufficient, if any, guidelines on such an adhesive application, research is conducted on choosing a suitable adhesive for the bonding of the blocks that allows for the desired visual and structural performance and for a relatively quick construction. Several architectural prototypes are built to evaluate the visual performance and to investigate the optimum thickness range of the adhesive, and correspondingly to determine the allowable size deviations of the glass blocks. The structural performance of the adhesively bonded glass block assembly is evaluated through a series of experimental tests of real size prototypes. In specific, physical prototypes are tested in compression, 4-point bending, hard-body impact and against thermal shock. The experimental work and the results are discussed in sections 5.5 and 5.6.

5.2 The case study

The novel glass masonry façade has been designed and engineered to replace the brick façade of a former townhouse in Amsterdam, aiming to preserve the city's traditional architectural style and historical ensemble. Designed by the *MVRDV* architectural studio (www.mvrdv.nl), the innovative façade follows the original 19th century elevation down to the layering of the bricks and the details of the window frames, but is stretched vertically to comply with updated zoning laws and allow for increased interior space (*MVRDV Architects 2016*) (Fig. 5.1). Based on the brick modules of the original masonry façade, the 10 m x 12 m elevation consists of more than 6500 solid glass bricks, each 210(± 1) mm thick by 65(± 0.25) mm high by 105/157.5/210 (± 0.25 mm) wide, reinterpreting the traditional brickwork and the

characteristic architraves above the openings; while massive cast glass elements reproduce the classic timber door and window frames. As it ascends, terracotta bricks intermingle with glass ones, gradually transforming the glass elevation to the traditional brick façade of the upper floor (Fig. 5.2). The end result is a building that will stand out, and at the same time will naturally blend into the urban fabric of the historic street.

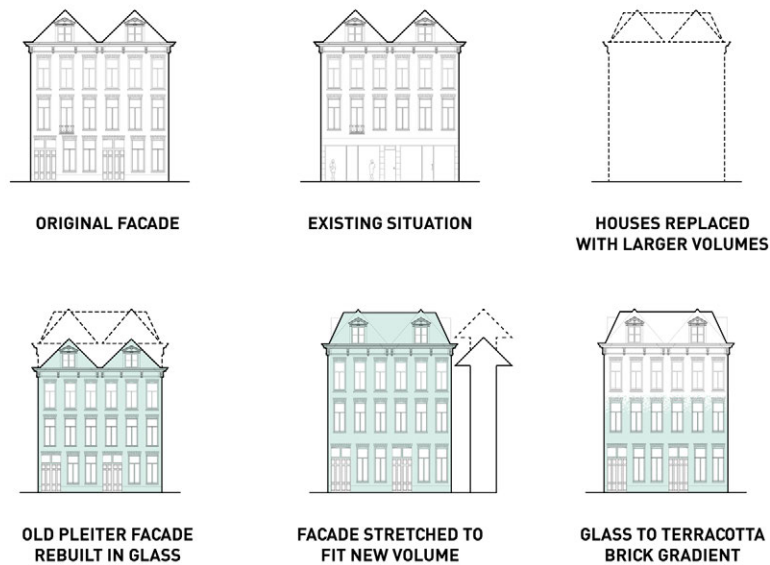


FIG. 5.1 Illustration by MVRDV of the concept behind the *Crystal Houses* façade.

The architects' desire for unimpeded transparency excluded the use of a metal substructure, rendering the choice for an entirely self-supporting glass brick system as a necessary and so far unique solution. In specific, the lower 10 m of the facade comprise mainly cast glass solid blocks. At the highest part of the elevation, the glass blocks intermix with conventional terracotta bricks in a limited zone until the first array of solely clay bricks appears (Fig. 5.2). Above this array, a steel beam covered with terracotta bricks is placed to support the upper, traditional brick facade. The beam is connected to the slab of the second floor allowing for the independent construction of the 10 m high glass block wall. From that point up a conventional brick facade with cavity is constructed (Fig. 5.2).



FIG. 5.2 Left: 3D visualization of the *Crystal Houses* façade by MVRDV Architects. Right: The realized façade.

In principle, a bearing wall of the aforementioned size comprising exclusively solid glass bricks is feasible owing to the compressive strength of glass (stated between 400–600 MPa for uniaxial loading by (Fink 2000) and 300–420 MPa by (Granta Design Limited 2015) and the considerable cross-section of the solid glass bricks (210 mm) that allow the façade to carry its own weight and have an enhanced buckling resistance³⁹. The lateral stability of the façade is guaranteed by 4 buttresses, each 5.5. m tall, erected towards the interior by interlaced glass bricks, resulting in a continuous relief glass envelope of increased rigidity (Fig. 5.3). Due to the higher density of glass compared to masonry, the glass facade, weighs approximately 25% more than a standard masonry facade of the same dimensions. This 25% difference of dead load necessitates a heavier foundation.

Besides the use of glass bricks, the main difference between the old and new masonry system is that the glass wall's thickness is covered by the width of one brick

³⁹ In comparison, a wall of the same dimensions comprising hollow glass blocks would require a supporting sub-structure. Their reduced thickness results in internal buckling or stress concentrations that in turn lead to a relatively low stated resistance in compressive load (defined as low as 6 MPa in ISO 21690:2006 by (International Organization for Standardization 2006)).

(210 ± 0.25 mm) instead of two, as is the case in normal masonry (Fig. 5.4). This was specifically chosen to eliminate unnecessary joints that can affect both the structural and optical performance/clarity of the glass structure. Accordingly, to reproduce the isodomic brick modulus of the historic facade, all glass blocks present the same width (210 ± 0.25 mm) and height (65 ± 0.25 mm) but are cast in 3 different length sizes (105, 157.5 and 210 ± 0.25 mm).

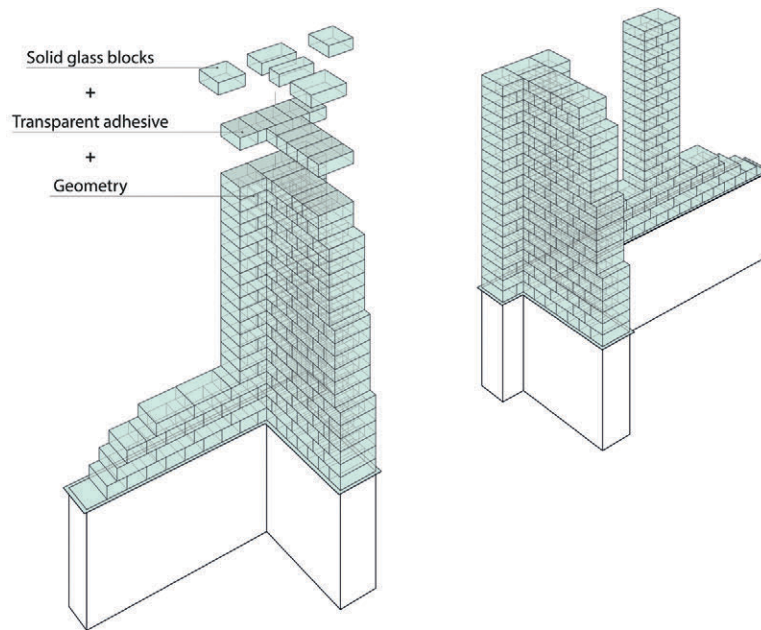


FIG. 5.3 Schematic illustration of the applied buttress system.

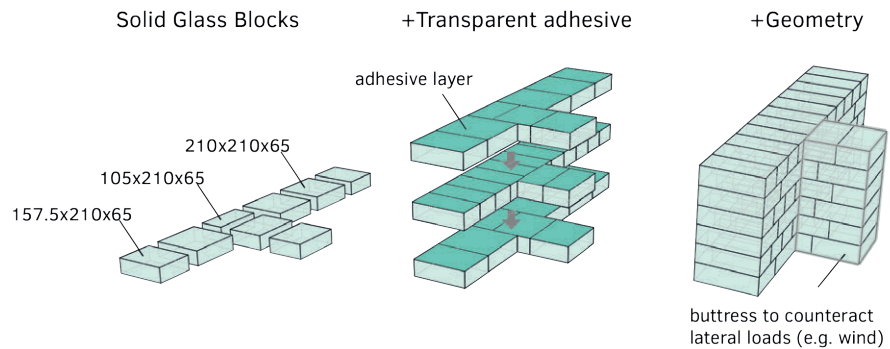


FIG. 5.4 Basic structural scheme of the proposed system

5.3 Methodology

The limited realized examples of self-supporting structures out of solid glass blocks and the lack of standardized structural specifications and building guidelines for such an adhesive application necessitated an holistic research on the materialization and engineering of the façade. Hence, based on the specific application, both the choice of glass recipe and adhesive are investigated and argued upon. The validation of the system is done through a series of experiments that aim to explore both the visual and the structural performance. Initially, series of physical prototypes are made to study the visual performance of the system and to develop a bonding method that allows for the even spread of the adhesive and the minimization of defects such as bubbles, air gaps, etc. The visual mock-ups give valuable input on the maximum tolerances allowed for architectural purposes and for achieving an even layer of the adhesive – the corresponding experiments are presented in chapter 5.4.2. Following, several series of full-scale prototypes are made and are experimentally tested in compression, 4-point bending, hard-body impact and thermal shock in order to derive the mechanical properties and evaluate the safety of the developed adhesively bonded glass block assembly.

5.4 Materials

In this section the choice of adhesive and glass type as well as the manufacturing process of the glass blocks are discussed and analysed.

5.4.1 Selection of Adhesive

The architectural prerequisite was to obtain a completely transparent and at the same time structurally feasible solution. To meet this requirement, a combination of solid glass blocks and colourless adhesive was chosen for the construction of the glass masonry wall. The mechanical properties of the adhesive are equally critical to the ones of the glass bricks for the developed system; it is their interaction as one structural unit that determines the structural capacity and properties of

the assembly. The most favourable structural performance is obtained when the adhesive and glass bricks fully cooperate and the masonry wall behaves as a single rigid unit under loading, resulting in a homogeneous load distribution. More specifically the adhesive should:

- be completely transparent and colourless and not discolour when exposed to sunlight
- present good short and long term compressive behaviour
- establish high bond strength with glass
- result in a monolithic masonry wall
- provide a rigid structure
- present good resistance to weathering and good aging behaviour
- allow for fast, easy and safe construction
- have no emissions of noxious or poisonous chemicals during processing and curing

An adhesive that meets all the above demands is *DELO Photobond (DP) 4468*, a colourless, one-component, UV-curing acrylate, designed for high force transduction in glass/glass and glass/metal bonds (Delo Industrial Adhesives 2014). Adhesives of the *Delo Photobond* family have already been applied for the bonding of all-glass structures, e.g. in the frames of the glass shell of the *Leibniz Institute for Solid State and Materials Research* (Delo Industrial Adhesives 2011; Weller et al. 2012; Weller et al. 2010b, a).

TABLE 5.1 Indicative properties of *Delo Photobond 4468* according to (Delo Industrial Adhesives 2014)

Property	Unit	Delo 4468
Viscosity	mPas (at 23 °C)	7000
Density	g/cm ³	1.0
Young's modulus	N/mm ²	250
Glass-glass compression shear strength	N/mm ²	22
Tensile strength	N/mm ²	14
Elongation at tear	%	200
Glass transition temperature	°C	74
Shrinkage	Vol%	9
Index of refraction	-	1.5
Water absorption	weight %	0.9
Creep resistance CTI	-	600M
Shore hardness A	-	83
Shore hardness D	-	45

The selected adhesive is optimized for high force transduction in glass-to-glass and glass-to-metal bonds and presents high shear stiffness, good short and long term compressive behaviour and long lifetime due to high humidity resistance (Delo Industrial Adhesives 2014). Visually, besides being colourless, it has a similar refractive index to glass and does not discolour when exposed to sunlight. Another important feature is its photo-catalytic curing, allowing for fast construction: The adhesive can be fully cured in a minimum of 40 seconds using 60 mW/cm² UVA intensity (Delo Industrial Adhesives 2014). After curing, it obtains its full structural capacity and becomes moisture- and water- resistant. The cured product is normally used in a temperature range of -40 °C to +120 °C. The properties of *DP 4468* adhesive are listed in Table 5.1.

5.4.2 Defining the optimum thickness range of the adhesive

There are no clear guidelines from the adhesive manufacturer on the recommended application thickness of *DELO Photobond 4468*. Moreover, there is not yet a generally approved theory concerning the effect of adhesive thickness in the strength of the bond. Although the classical elastic analyses predict that the strength increases with the adhesive thickness, experimental results show the opposite (da Silva et al. 2006). Research by (Grant et al. 2009), (da Silva et al. 2006), and (Crocombe 1989) suggest different reasons⁴⁰ why a thicker bond layer provides a decreased joint strength. Based on experimental work by (Riewoldt 2014), Fig. 5.5 exhibits how a comparatively thicker layer can negatively influence a rigid (i.e. epoxy or acrylate) adhesive's bond strength and subsequently the structural performance of the entire system. In practice, (Wurm 2007) mentions that acrylates present their highest strength in an application thickness between 0.1 mm and 0.5 mm, whereas (Puller, Sobek 2008) suggest an optimum thickness of 0.2 mm for a glass to metal bond with *DELO Photobond 4468*.

Prior and parallel to structural testing, several architectural mock-ups of the masonry wall were built to study the visual performance of the system and determine the maximum allowable thickness of the adhesive -and correspondingly the minimum acceptable size tolerances of the blocks- for aesthetic purposes. Initial research

⁴⁰ (Crocombe 1989) suggests that thicker single-lap joints have a lower strength considering the plasticity of the adhesive, whereas (da Silva et al. 2006) found that interface stresses are higher for thicker bondlines. (Grant et al. 2009) suggests that as the bondline thickness of a T joint increases, there is an increase in the bending stress since the bending moment increases, reducing the strength of the joint.

indicated that due to the medium viscosity of the selected adhesive (7000 mPa·s at 23°C, measured by *Brookfield* viscometer (Delo Industrial Adhesives 2014)), the vertical joints of the blocks cannot be homogeneously bonded: the adhesive would flow downwards before it could be cured. Therefore, it was determined that only the horizontal surfaces of the glass blocks would be bonded; the vertical ones are left dry, allowing as well for thermal expansion.

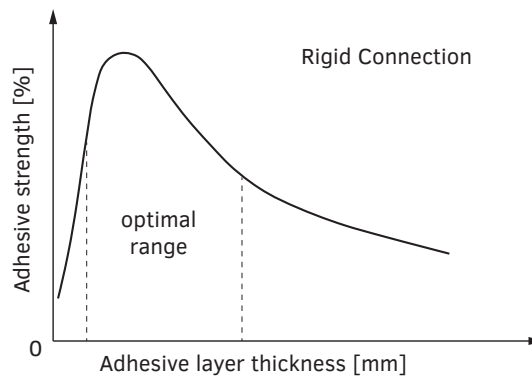


FIG. 5.5 Schematic illustration of the relation between a stiff adhesive's strength and thickness by (Riewoldt 2014; den Ouden 2009; Wurm 2007).

Next, 3 successive wall mock-ups (Fig. 5.7) were made comprising glass elements with a different tolerance range. Multiple trials suggested that a consistent, even adhesive distribution occurs when the adhesive is spread in an X pattern on the bonding surface – this allows any bubbles to be pushed out of the adhesive layer prior to its curing. The findings from the visual prototypes are summarized in Table 5.2. It can be derived that larger tolerances lead firstly to significant offsets in the height and width of the façade, secondly to open joints between adjacent blocks and thirdly, and most importantly, to an uneven spread of the adhesive (Fig. 5.6) that can greatly affect the structural performance of the wall. Besides compromising the visual result, inconsistent bonding introduces weaker structural zones. Especially voids against the glass substrate in stiff adhesives can cause major stress concentrations (O' Regan 2014). The wall prototypes pointed out that a homogeneous bond thicker than 0.3 mm cannot be obtained due to the adhesive's flow properties and medium viscosity. Based on the adhesive's optimum application thickness, it was determined that the glass blocks' top and bottom surfaces should be flat within 0.25 mm for guaranteeing an even adhesive layer of the highest strength. Any accumulated deviation larger than the required 0.2-0.3 mm thickness of the adhesive could lead to uneven and improper bonding.



FIG. 5.6 Common flaws occurring in the adhesive layer: air gaps, capillary action and dendritic patterns.

Based on the findings, a fourth mock-up was constructed with the desired tolerance on the blocks. In this mock-up, the construction of the buttress was also tested and an improved bonding method was employed: Customized *PURE*[®] (self-reinforced polypropylene) forms are employed for the distribution of the adhesive in an X pattern, controlling its amount, flow and spread. Once the adhesive is evenly spread, the brick is held in position and under constant (manual) pressure and is exposed to low intensity UV-light for 5 s. This pre-curing step was introduced for practical reasons: the partial curing stabilizes the glass brick to its final position while still allowing the wiping-off of any adhesive overflow. After cleaning, the adhesive is further cured by low and medium intensity UV-radiation, in the range of 20-60 mW/cm², for a period of 60 - 180 s, depending on brick size. The final result can be seen in Fig. 5.8.

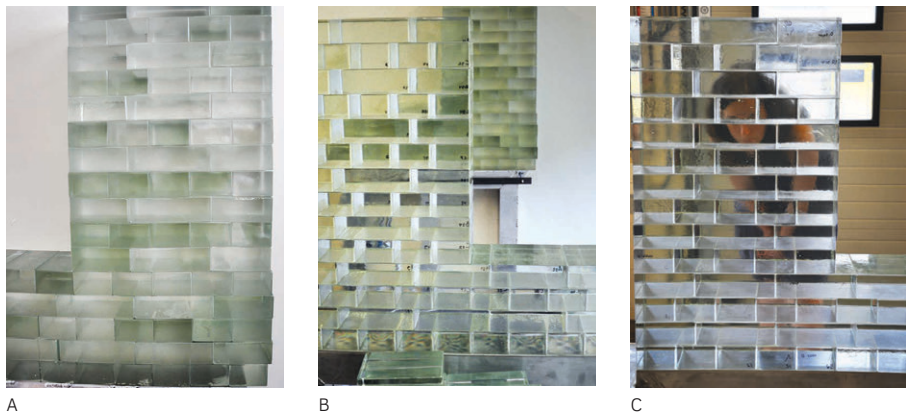


FIG. 5.7 Photographs of the three mock-ups. Mock-up A was made with higher tolerances. As a result there were significant offsets in both height and width, as well as open joints between blocks. Mock-up B was made with blocks of higher accuracy that prevented a substantial offset in height. Still, any unevenness up to ± 0.5 mm in flatness resulted to cavities and bubbles in the bond area. In mock-up C all blocks meet the ± 0.25 mm tolerance, resulting in an even spread of the adhesive and thus, in homogeneous bonding and satisfactory visual result without any cavities and bubbles of substantial dimensions.

TABLE 5.2 Observations from the architectural mock ups

Mock-up	Tolerances				remarks
	rectangularity [mm]	height [mm]	width [mm]	flatness [mm]	
A	±0.5	±0.5	±0.5	±0.5	<ul style="list-style-type: none"> - The inaccuracy in rectangularity leads to open joints of up to 5 mm. - Considerable offsets in both height and width of the prototype - Inconsistency in bonding surface
B	±0.25	±0.25	±0.25	±0.5	<ul style="list-style-type: none"> - No offset in height and width of the prototype - Inconsistency in bonding surface: bubbles, gaps, unsatisfactory optical result
C	±0.25	±0.25	±0.25	±0.25	<ul style="list-style-type: none"> - No offset in height and width of the prototype - Uniform distribution of the adhesive, satisfactory optical result.



FIG. 5.8 The final (4th) wall mock-up which includes the buttress's construction by interlocking glass blocks

5.4.3 Choice of glass

From the previous chapter it can be derived that the adhesive's low to medium viscosity and ideal bond thickness of a quarter of a millimetre combined with glass's elastic nature introduce exceptionally strict tolerances on the size of the individual glass elements. This accuracy, determined to be ± 0.25 mm in the height and flatness of the elements is essential for attaining an even, homogeneous spread of the adhesive, required not only for the most favourable structural capacity, but also for a visual result of maximized transparency. An inconsistent spread of the adhesive can result in visible gaps and bubbles. But most importantly, considering that the joints between adjacent blocks have virtually zero thickness, even a tolerance of 0.5 mm per block could result in a sizeable offset in the height or width of the entire construction.

Cast glass blocks with such strict tolerances in size and flatness have never been produced before. In projects where a metal substructure is employed, sealant joints considerably thicker can be accommodated, which in turn can compensate for substantially coarser tolerances. The sole comparable structure to the one examined here is the *Atocha Memorial*. However, in that case, the overall cylindrical shell geometry contributes greatly to the structure's rigidity, allowing for a tolerance range of ± 1 mm (Christoph, Knut 2008) in the size of the blocks, without compromising the structural capacity. This is 4 times more than the tolerance allowed in the presented adhesively-bonded system. The solid glass bricks, used in the *Atocha Memorial*, utilized borosilicate glass and precision press moulds for obtaining highly accurate units (Schober et al. 2007). Borosilicate glass was favoured over soda-lime glass owing to its comparably lower thermal expansion coefficient [$3.2\text{--}4 \times 10^{-6}/\text{K}$] over soda-lime glass [$9.1\text{--}9.5 \times 10^{-6}/\text{K}$] (Granta Design Limited 2015). This, in turn, results in considerably less natural shrinkage during cooling and accordingly to a cast element of higher dimensional accuracy. A high precision press mould further confines the cast element to the desired dimensions, by pressing the molten glass during the initial, rapid cooling stage. With this method the desired ± 1.0 mm (Goppert et al. 2008) size tolerance was achieved for the cast glass blocks without any machine processing.

Nonetheless, in the given case study, the 10 m x 12 m dimensions of the façade and its flat geometry necessitate an increased masonry strength and consequently require the optimum thickness of the adhesive. The required ± 0.25 mm tolerance would necessitate the mechanical post-processing of the blocks' horizontal (bonding) surfaces, even for borosilicate glass. Consequently, to avoid an unnecessary increase in manufacturing costs, soda-lime glass and open precision moulds were opted for the final fabrication of the glass blocks.

Soda-lime is the least expensive form of glass (Corning Museum of Glass 2011d) and requires a significantly lower working temperature than borosilicate. As a drawback, due to the higher thermal expansion coefficient of soda-lime a considerably longer annealing -and manufacturing- time of the components is needed. For example, the borosilicate glass blocks of 70 mm x 200 mm x 300 mm in dimensions and 8.4 kg weight (shown in Fig. 5.9), used in the *Atocha Memorial*, required a total annealing time of circa 20 h (Goppert et al. 2008). Whereas, the comparatively smaller soda-lime glass bricks of 65 mm x 210 mm x 210 mm in dimensions and 7.2 kg weight used in this project, required 36-38 h of annealing time respectively (Fig. 5.10). High precision open moulds were preferred over press moulds, since the use of the latter was considered an expensive and unnecessary solution in view of the inevitable post-processing. The final fabrication method of the glass blocks is described in detail in Section 6.2.1 of the following chapter. An overview of the technical specifications of the soda-lime glass used is given in Table 5.3.



FIG. 5.9 Left: the 300 x 200 x 70 mm borosilicate glass block of the *Atocha Memorial* made by press mould. Centre: a 210 x 105 x 65 mm soda-lime glass block of the *Crystal Houses* prior to post-processing. Right: a 210 x 105 x 65 mm soda-lime glass block of the *Crystal Houses* after post-processing.

TABLE 5.3 Technical specifications of the soda-lime cast glass blocks as provided by *Poesia*

Average compression resistance	397 N/mm ²
Thermal conductivity	0,974 ± 0,036 W (m K)
Linear Thermal dilatation coefficient	10.2 - 10.6 (10 ⁻⁶ °C ⁻¹)
Mohs hardness	3
Fire resistance	REI 60 by standard pose with cement mortar

To ensure that the higher expansion coefficient of soda-lime glass will not cause excessive thermal stresses on the façade, a simulation of the expected thermal loads in a yearly cycle was performed by an external company specializing in building physics. Based on the optical transmittance data provided by *TU Delft* for the solar gain (see Fig. 5.11), the orientation of the specific location, the height of the surrounding buildings and the assumption of a constant heating load in

winter and cooling load in summer from the indoors air-conditioning, heat and light transmittance of the wall were simulated. The results indicated acceptable thermal strains (less than 14.3×10^{-3}) for the soda-lime cast glass even under the most extreme weather conditions for Amsterdam.

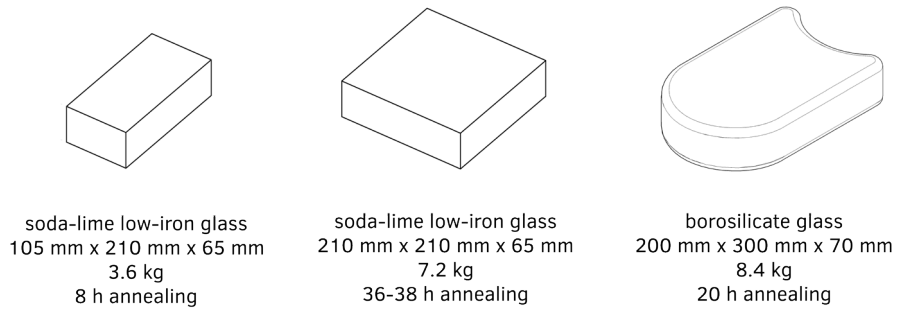


FIG. 5.10 Size and annealing time of the *Crystal Houses* blocks (left and centre) and of the *Atocha Memorial* block (right).

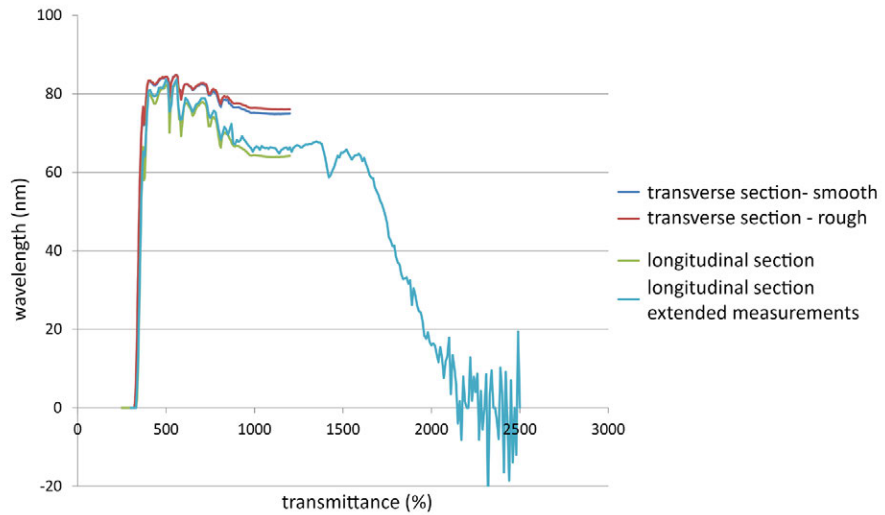


FIG. 5.11 Optical transmittance data of a standard *Poesia* brick by (Tijssen 2014).

5.5 Experimental

5.5.1 Test specimens

The novelty of the developed glass system came with a lack of standardized strength data and building guidelines on both solid glass blocks and chosen adhesive. Accordingly, in order to determine the structural behaviour of the glass-adhesive system and validate the proposed tolerance specifications of the bricks as well as the adhesive's application method, a wide range of structural experiments had to be carried out. In summary, the following experiments have been conducted over the course of 18 months:

- Compression of single blocks
- Compression of glass pillars out of adhesively bonded glass blocks
- 4-point bending tests on glass beams out of adhesively bonded glass blocks
- 4-point bending test of a glass architrave out of adhesively bonded glass blocks
- hard body impact and vandalism test of an adhesively bonded glass wall
- thermal shock of individual glass blocks

Fig. 5.12 provides an illustrated overview of the tests and the dimensions, composition and number of prototypes per test. All prototypes have been made with soda-lime solid glass blocks cast by *Poesia* company in Italy. The glass block assemblies are bonded together with *Delo Photobond 4468* (DP 4468), except if stated otherwise. Five different glass block sizes have been used in the prototypes – the different sizes are presented in Table 5.4. At the early stages of this research, prototypes have been made with standard *Poesia* bricks, namely N_s and N_L blocks. These blocks are included in the standard production of *Poesia* and had been readily-available for manufacturing prototypes for experimental work. These first prototypes and corresponding experiments have been valuable for validating the necessity of the required flatness tolerance of ± 0.25 mm of the blocks, essential for achieving the desired structural behaviour of the adhesively bonded solid glass block system. The custom-made blocks of ± 0.25 mm precision in size and flatness, namely S, M and L, had been manufactured several months later by *Poesia*, and after exploring multiple variables through the aid of visual prototypes, described in chapter 5.4.2. In addition, the final custom-made blocks (S, M and L) follow the general dimensions desired by *MVRDV Architects* so that the block modulus matches the one of the previous, 19th century elevation of the building.

For the ease of the reader, the extensive experimental research is not presented in chronological order, but instead, in the most reasonable order. Some initial experiments comprising different adhesives or block configurations have been excluded on purpose, as they were considered insufficient for deriving statistical data.

Test name	Specimen composition	Number of specimens
Compression test - individual blocks specimens	<p>S, M and L blocks (thickness 210 mm)</p>	3 A _L 3 A _M 3 A _S
Compression test - glass pillars specimens	<p>N_L blocks bonded with DP 4468 along the horizontal joints only N_S blocks bonded with DP 4468 along the horizontal joints only</p>	1 B _{NL1} 1 B _{NL2} 2 B _{NS}
4-point bending test - glass beam specimens	<p>S, M and L blocks bonded with DP 4468 along their horizontal joints and along the bottom-layer's vertical joints.</p>	4
4-point bending test architrave specimen	<p>customized tapered blocks bonded along the vertical joints with DP 4468. DP 4494 has been applied in few locations where the joint gaps were above 0.3 mm thick. The horizontal joints are left open.</p>	1
Impact & vandalism test - wall specimen	<p>N_L blocks bonded with DP 4468 along the horizontal joints only.</p>	1
Thermal shock specimens	<p>N_L blocks tested in thermal shocks by different types of water immersion after they are pre-heated for 4 hours to 60 °C and 80 °C degrees.</p>	60 °C: 80 °C: 2 F ₁ 2 F ₁ 2 F ₂ 2 F ₂ 2 F ₃ 2 F ₃ 2 F ₄ 2 F ₄

FIG. 5.12 Overview of tests and of the various dimensions, composition and number of specimens.

TABLE 5.4 Type of blocks used for the manufacturing of the prototypes

Brick type	Dimensions	Size Tolerances	Material
N _S	121 x 116 x 53 mm	± 0.5 mm	Soda-lime glass
N _L	246 x 116 x 53 mm		
S	105 x 105 x 65 mm	± 0.25 mm	Soda-lime, low-iron glass
M	157.5 x 105 x 65 mm		
L	210 x 105 x 65 mm		

5.5.2 Set-up of compression tests on single blocks

To investigate the compression strength of the glass blocks, three series of soda-lime blocks of the different custom-made sizes (S, M and L) have been tested in a displacement-controlled hydraulic compression machine of 3 MN maximum load capacity. In the first two series of tests, the blocks have been placed directly on the machine's metal surface; in the third series, two 18 mm thick plywood sheets have been inserted between each glass block and the steel surfaces of the testing machine (Fig. 5.13). For safety reasons, all specimens were wrapped in several layers of clear PET plastic foil and were placed in a safety steel cage with polycarbonate windows.

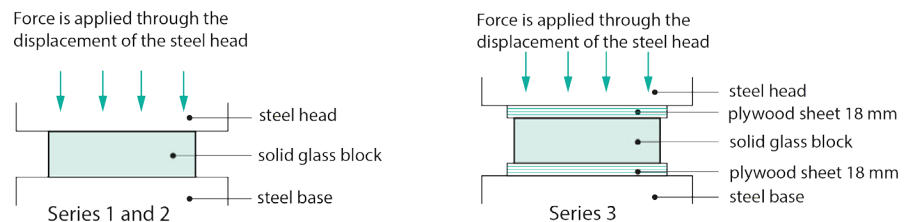


FIG. 5.13 Set-ups of the compression tests on single glass blocks.

5.5.3 Set-up of compression tests on glass pillars out of adhesively bonded glass blocks

4 glass pillars have been tested in a force-controlled hydraulic compression machine, to investigate the compression strength of the glass block-adhesive system. The columns have been constructed of standard N_L *Poesia* blocks (specimens B_{NL1} and

B_{NL2}) and N_s blocks (specimens B_{NS1-2}), adhesively bonded along their horizontal joints only. Three different configurations have been formed (Fig. 5.14), to study how the strength is affected. B_{NL1} and B_{NL2} columns were adhesively bonded across the largest faces of the N_L bricks. These faces present a convex plane of approximately 0.5 mm at the centre. Thus, the bonding layer is of a variable thickness: it is thinner at the edges and thicker in the middle of the brick. Specimens B_{NS1} and B_{NS2} use a different configuration and a different block size (N_s): the glass blocks are bonded across their shorter and much more even surfaces, resulting to a consistent adhesive layer thickness of approx. 0.2 – 0.3 mm.

Two 18 mm thick plywood sheets have been placed at the top and the bottom surface of each pillar to prevent direct contact between the glass elements and the steel surface of the machine. During the experiment, a transparent plastic box was placed around the column as a safety precaution.

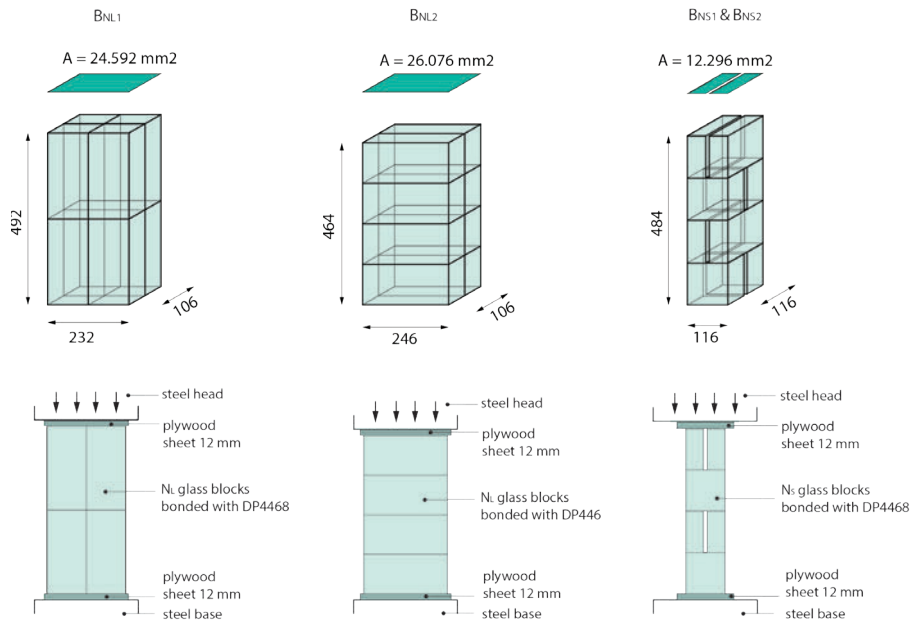


FIG. 5.14 Dimensions and experimental set-up of the glass pillars.

5.5.4 Set-up of 4-point bending tests on glass beams out of adhesively bonded glass blocks

To determine the flexural strength of the glass masonry wall, 4 glass beam prototypes were constructed and tested in-plane in 4-point bending until failure. Each specimen was made of 23 solid soda-lime glass bricks, bonded together into a beam configuration by *Delo Photobond 4468*. More in detail, each specimen consists of 3 arrays of glass blocks. The top and bottom arrays comprise each 2 M and 4 L glass blocks, while the middle array consists of 11 S blocks. The dimensions, configuration and experimental set-up of each specimen are illustrated in Fig. 5.16. In the proposed masonry system, the blocks are bonded only along their horizontal faces. Nevertheless, in order to represent more accurately the boundary conditions of the glass masonry wall in the specimens, the blocks forming the bottom array have also been bonded to each other along their vertical faces to achieve a continuous bottom zone. The glass blocks of the upper two arrays have been bonded only along their horizontal surfaces, leaving open vertical joints.

The specimens are tested in in-plane 4-point bending until failure in a *Zwick Z100* displacement-controlled universal testing machine, where the upper steel head moves downwards with a constant displacement rate of 2 mm/min. A specially fabricated steel frame is used for the bottom supports of the experimental set-up (see Fig. 5.15). None of the supports corresponded to a joint (see Fig. 5.16). Prior to testing, all specimens were wrapped in several layers of clear PET plastic foil as a safety precaution.

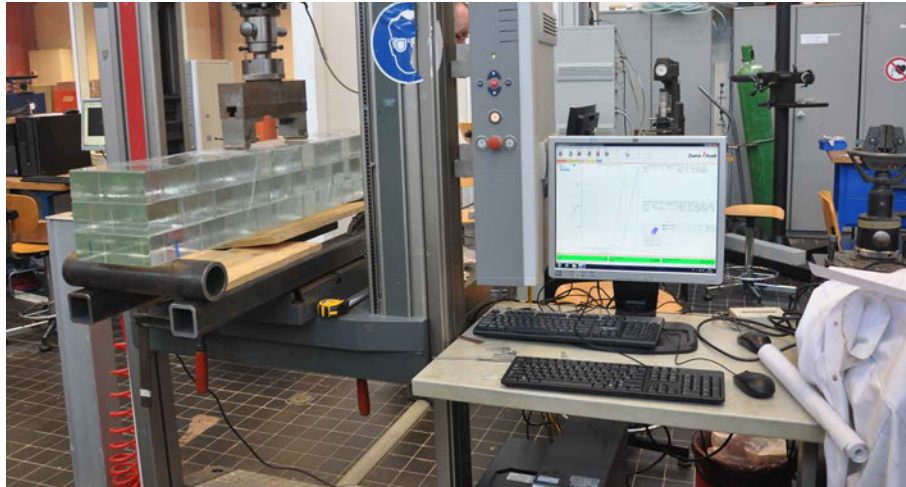


FIG. 5.15 Experimental set-up of the 4-point bending tests

The specimen was tested in in-plane 4-point bending until failure in a *Zwick Z100* displacement-controlled universal testing machine, with a speed of 2 mm/min. A specially fabricated steel frame was used for the bottom supports of the experimental set-up (see Fig. 5.18). The architrave was placed to the testing machine with the aid of a crane. The architrave was loosely supported by ropes from the crane during testing to prevent the falling of big pieces on the floor after failure.

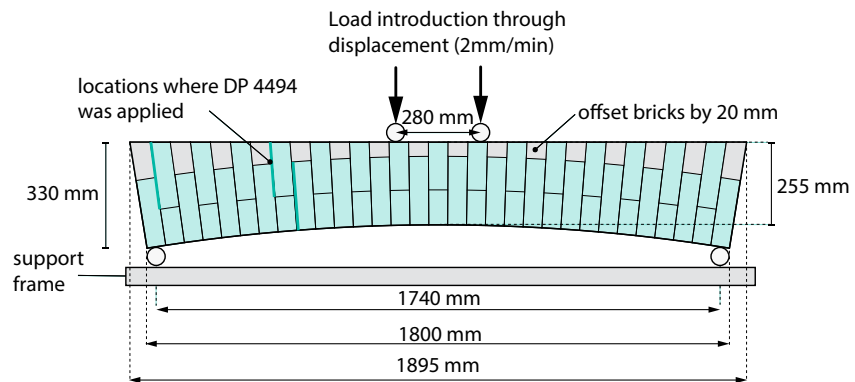


FIG. 5.17 Dimensions and experimental set-up of the glass architrave



FIG. 5.18 4-point bending set-up of the architrave

5.5.6 Impact and vandalism test set-up

The glass masonry facade could be potentially subject to impact from a variety of causes, such as the accidental impact from bicycles, skateboards, etc. or to the sustained attack with objects such as bottles, bricks, tools, etc. in the case of vandalism. Hence, a rigid body impact test and a vandalism test were performed on an experimental glass wall. The mock-up consisted of 22 N_L blocks, adhesively bonded to form a wall (see Fig. 5.19). The glass wall mock-up was mounted into a wooden frame, which was fixed to a rigid concrete wall to simulate the inertia conditions of the glass facade. The specimen was not pre-loaded in compression. Considering the total dimensions of the façade and based on an even dead-load distribution the expected pre-compression of the entire envelope is of less than 0.2 MPa at the lower rows of the façade. This amount of pre-stress in compression is virtually negligible for a glass structure.

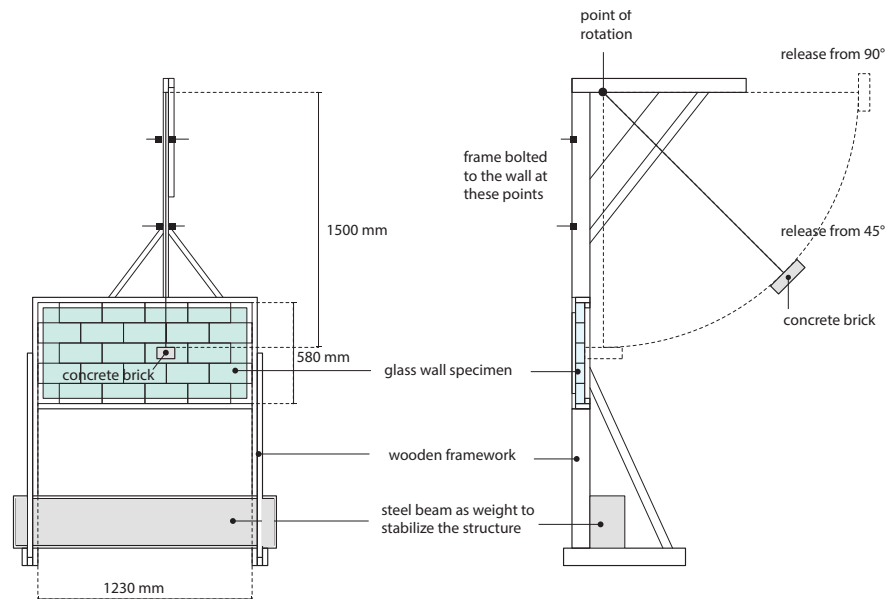


FIG. 5.19 Schematic illustration of the hard body test set-up.

Two different tests were conducted to the specimen:

- a hard body impact test by a solid concrete brick suspended from 45 and 90 degrees angle
- a vandalism test by a 4 Kg sledgehammer

In the hard body impact test, a concrete brick of 65 x 102.5 x 215 mm in dimensions and 3.4 kg in weight was placed in front of the facade, touching the target brick. At that position it was suspended with a hook from a 1.5 m long metal wire, hanging down from a wooden cantilever projecting above the mock-up (see Fig. 5.19 and Fig. 5.20). The concrete brick, attached to the wire, was then swung outwards by a 45 degrees angle and released from there. The test was repeated 2 times from a 45 degrees angle, then another 2 from 90 degrees angle.

Afterwards, a vandalism test was carried out on the same experimental wall using a 4 Kg sledgehammer wielded by the author.



FIG. 5.20 Set-up of the hard body impact and vandalism test

5.5.7 Set-up of thermal shock test on single blocks

On a warm, sunny day the glass blocks can heat up significantly. In the event of rain on the same day, the warmed glass blocks will come into contact with the colder rainwater and a limited thermal shock can occur. The shock intensity is related to the temperature difference between the material and the environment and the rate of heat flow from the glass. In this context, a hot-cold thermal shock is more harmful to glass than a cold-hot thermal shock, because it generates tensile stresses on the rapidly cooled surface. These stresses may be sufficient to activate pre-existing micro-cracks and lead to fracture. Hence, to evaluate the performance of the glass blocks under peak temperature fluctuations, specimens were heated for 4 h in a furnace with a constant temperature of 1) 80°C and 2) 60°C. Following, they were

cooled down by being immediately immersed into water of 20°C for approximately 10 min each. Specimens were:

- half-immersed into water (F_1)
- completely immersed into water (F_2)
- immersed only with one face into the water (F_3)
- splashed on one face (F_4)

Two samples were used per test per temperature. An illustration of the test set-ups is shown in Fig. 5.21.

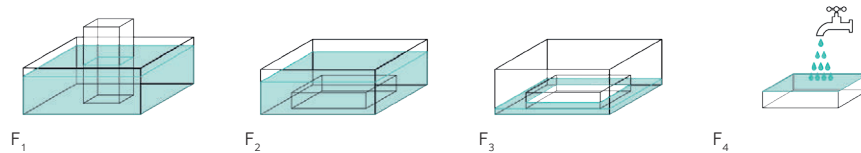


FIG. 5.21 Illustration of the four different thermal shock tests

5.6 Results and Discussion

5.6.1 Compressive tests on single blocks

Table 5.5 summarizes the results of the compressive tests on single blocks. The compressive tests were interrupted when the first cracks were (visibly) observed. In general, the crack patterns in all tested specimens demonstrate the absence of internal residual stresses in the glass blocks, indicating in turn a proper annealing cycle. In specific, no secondary crack branching – an effect of internal residual stress – was observed in any of the specimens, even under high compression loads.

The results of the two first specimens per compression series (A_s , A_M and A_L), where no intermediary was used between the glass blocks and the steel head of the testing

machine, presented obvious cracks in a nominal compressive stress between 20-30 MPa; this is significantly less than the compressive strength value of glass stated in literature⁴³. The reduced compressive stress is attributed to the high concentrated contact pressure between the stiff glass blocks and the stiffer steel plates of the compression machine (see Fig. 5.22). Any unevenness or micro-asperity in the contact surface of the two hard materials induces local peak tensile stresses, which, in a brittle material like glass, propagate local cracks⁴⁴. This stresses the importance of properly supporting the glass components along their whole surface and preventing any stress concentration in the supports.

TABLE 5.5 Results of glass blocks' compression tests

Specimen series	Dimensions [mm]	Specimen number	End conditions	Load at first observed crack [kN]	Nominal compressive stress at first observed crack [MPa]
A _S	210x105x65	1	Direct contact with steel	1690 [†]	76.6
		2	Direct contact with steel	500	22.7
		3	Wooden intermediary	2977	135
A _M	210x157.5x65	1	Direct contact with steel	999	30.2
		2	Direct contact with steel	870	26.3
		3	Wooden intermediary	>3000 [*]	>90.70
A _L	210x210x65	1	Direct contact with steel	1248	28.3
		2	Direct contact with steel	882	20
		3	Wooden intermediary	> 3000 [*]	>68

* Max. load capacity of the testing machine. No cracks were observed up to the max. load in these specimens.

† At this load multiple cracks were already observed at the specific specimen.

Accordingly, to ensure an even load distribution, in the third specimen of each series, an 18 mm thick plywood plate was used as intermediary on both the top and bottom surface of each glass block (see Fig.5.22). In this series, the smallest block (A_{S3}), presented its first crack at 2980 kN load, a load 5 times higher than the complete dead load of the *Crystal Houses* façade. The block specimens of larger dimensions (A_{M3} and A_{L3}) did not crack until the compressive machine reached its force limit of 3000 kN. This series of experiments emphasizes the importance of designing proper

⁴³ Even so, each of the tested S blocks could withstand a load higher than the 40t (392.4 kN) dead load of the designed façade prior to failure.

⁴⁴ For a more elaborate explanation on the influence of flaws on the strength of glass refer to Chapter 2.6.

connections that ensure an even load distribution to the glass masonry wall. Poor detailing or execution can result in high local stresses that significantly reduce the overall strength of the glass structure. Connections that provide a uniform load distribution will result in considerably higher failure loads.



FIG. 5.22 Compression tests of glass blocks. Top left: Test set-up for the first two series. Bottom left: Test set-up for the specimens of the third series with plywood as intermediary. Right: Typical initial crack pattern in specimen.

5.6.2 Compressive tests on columns out of adhesively-bonded glass blocks

Table 5.6 gives an overview of the results of the compression tests on the 4 glass columns. All specimens were tested until complete failure, thus, the values mentioned at Table 5.6 concern the ultimate failure stress of each column. Essentially, at the stated stress values, the specimens lost their integrity, as cracks propagated through the blocks causing the entire assembly to split or shutter (Fig.5.24). Forking (branching) of the cracks was denser and greater as the applied stress increased: specimens B_{NS1} and B_{NS2} essentially shuttered into pieces compared to specimens B_{NL1} and B_{NL2} .

TABLE 5.6 Results of the compression tests on the glass column specimens

Specimen	Dimensions [mm]	Observations	Failure load [kN]	Nominal compressive stress at failure [MPa]
BNL1	232x106x492	Bonding across the large surfaces	2090	85
BNL2	246x106x464	Inconsistent bond thickness, up to 0.5 mm thick in the middle	1296	49.7
BNS1	116x121x484	Bonding across the small surfaces	1597	113.8
BNS2	116x121x484	Consistent, approx. 0.2-0.3 mm, bond thickness	1484	105.7

A crucial observation on the failure behaviour of the specimens is that the cracks, initiated at one of the glass blocks, did not follow the adhesive joints between the bricks, as would be anticipated in a conventional masonry assembly, but propagated through the glass elements as if the assembly was one monolithic unit (see Fig.5.23). This indicates that in compressive stresses of the examined magnitude the applied adhesive has higher resistance to delamination than glass has to crack propagation.

Furthermore, the compression tests of the 4 glass columns revealed significant differences in the compressive strength of the different configurations. This can be attributed to:

- the creation of indirect local tensile stresses due to the oblong shape of the specimens
- the different configurations of the glass blocks
- improper bonding

Indeed, prototypes B_{NL1} and B_{NL2} that presented non-homogeneous bonding demonstrated down to half the strength than prototypes B_{NS1} and B_{NS2} . The latter specimens follow a different configuration and block size that allows for a constant and comparably thinner adhesive layer. Due to the stronger adhesive bonds formed, B_{NS1} and B_{NS2} columns showed a noticeably more monolithic behaviour and a higher compressive strength.

Although the number and size of the samples are limited for deriving quantitative results, they indicate that the compressive strength of the structure is greatly influenced by the quality of the bonding surfaces and thus, by the thickness of the adhesive layer.

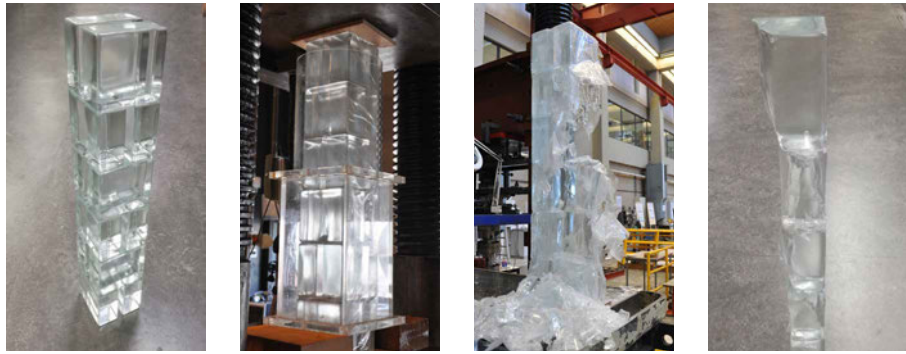


FIG. 5.23 Left: B_{NS} column prior to testing. Centre left: Initiation of crack. Centre right: Same specimen at complete failure. Right: Intact piece of the tested specimen after failure: the principal crack essentially propagated vertically, defying the adhesive joints.



FIG. 5.24 The glass column specimens after testing. Left two pictures: B_{NS} specimens. Right two: B_{NL} specimens

5.6.3 4-point bending tests on adhesively bonded beams

In accordance with the failure load and geometry of each specimen, the nominal flexural strength formula was used in order to derive the flexural strength:

$$\sigma = \frac{3F(L-L_i)}{2bd^2}$$

EQUATION 5.1

Symbol	Definition	Unit	Experimental set-up value
σ	flexural strength	MPa	-
F	load at the fracture point	N	-
L	length of the outer (bottom) support span	mm	1000
Li	length of the inner (top) support span	mm	300
b	width	mm	210
d	height	mm	195

The results of the experimental testing are summarized in Table 5.7 below:

TABLE 5.7 4-point bending tests results

Specimen	Failure Load [N]	Nominal Flexural strength [MPa]	Failure zone	Failure mode
C ₁	42800	5.63	One block offset from the middle	Vertical cut without branching, essentially splitting the beam in two halves
C ₂	36400	4.79	middle	
C ₃	38600	5.08	middle	
C ₄	53300	7.01	middle	

The results of the 4-point bending tests suggest an in-plane flexural strength at failure between 4.79-7.01 MPa, with most specimens failing at a flexural stress value closer to 5 MPa. Hence, a flexural strength of 5 MPa can be used as a conservative design value, given the fact that the flexural strength of glass itself is considerably higher. The lower values in fact occur because the beam specimens are only bonded horizontally, resulting to stress concentrations on the open vertical joints, which decrease the strength of the specimen. Nonetheless, in the actual façade construction, the glass blocks are confined by the boundaries of the structure and therefore the vertical joints of the wall are prevented from opening, hence, the strength is expected to be higher. No visible cracks were observed before the specimens reached the failure load.

The fracture pattern of the specimens clearly demonstrates the monolithic behaviour of the adhesively bonded glass block assembly and the absence of considerable internal residual stresses: All specimens failed with a straight, parallel to the loading direction cut, following one of the top and bottom open vertical joints. In specific, specimen C₁ broke in an offset of one block from the middle, while the rest of the specimens failed at their middle. In all cases, the glass block of the middle horizontal layer corresponding to the propagating vertical joint was split in half. No significant

delamination nor branching of the crack was observed at any of the specimens. The breaking pattern indicates that the adhesive's shear strength is sufficient to assure that the beam specimens behave in a monolithic way under failure.

The typical failure pattern of the specimens are seen in Fig. 5.25 and Fig. 5.26:

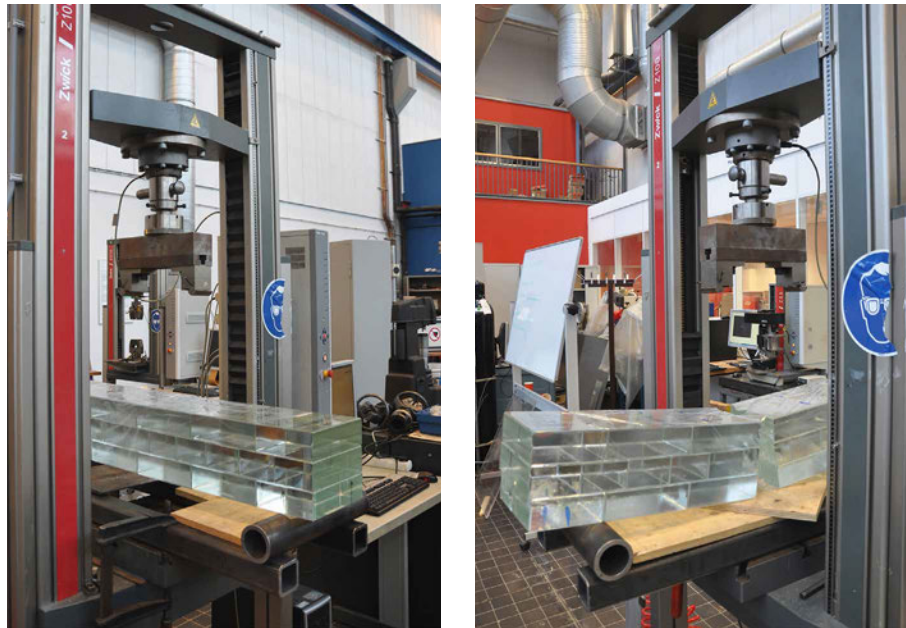


FIG. 5.25 Left: Experimental set-up. Right: Typical failure mode (Specimen C_3)

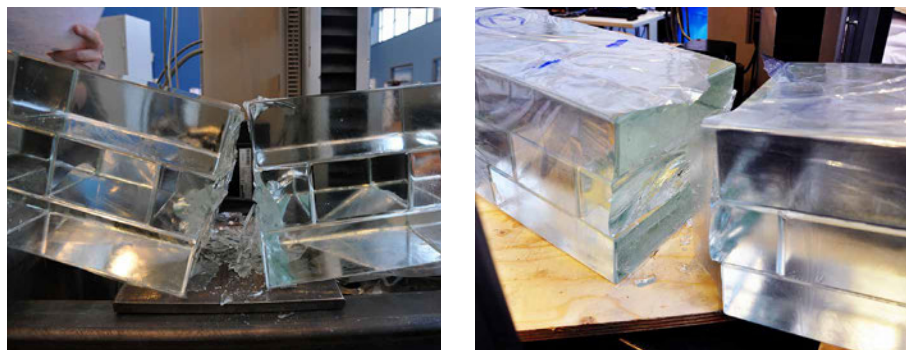


FIG. 5.26 Typical failure mode of specimens, a clear, vertical cut at the middle of the beam.

5.6.4 4-point bending test on adhesively bonded glass architrave

Table 5.8 provides an overview of the geometrical characteristics and failure mode of the tested architrave.

TABLE 5.8 Results of the 4-point bending test of the architrave

Specimen geometric characteristics	Failure Load [N]	Nominal Flexural strength [MPa]	Failure zone	Failure mode
L = 1740 Li = 280 b=210 d=255 [†] (average)	41600	6.7	Vertical joint where DP 4494 was applied.	Vertical cut without branching, essentially splitting the specimen in two halves

[†] The height of the specimen varies from 255-330 mm; however, the area where the height increased above 255 mm is constrained at a small zone close to the edges of the specimen. Thus, the height variation was neglected from the calculation under the assumption that the highest bending moments occur in the middle zone where the height is constantly 255 mm.

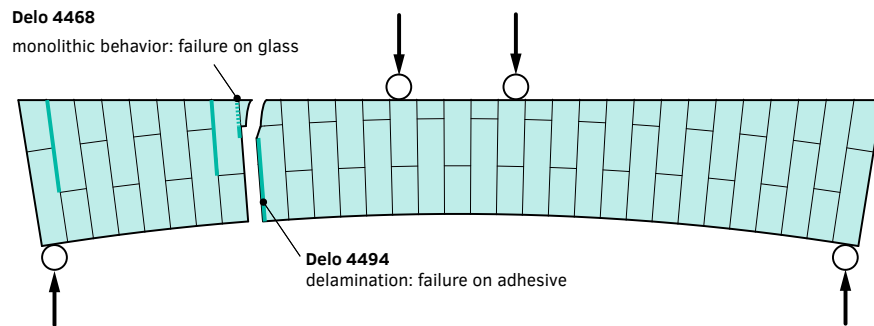


FIG. 5.27 Illustration of the breaking pattern of the tested specimen

The arch specimen failed at 41600 N, corresponding to an approximate nominal flexural strength of 6.7 MPa. At that load the specimen split by a clear cut in 2 uneven pieces, as illustrated in Fig. 5.27. Prior to the failure load, no cracks were observed. In particular, the specimen instead of breaking in the middle zone where bending moments are the highest, as was the case with the beam specimens tested in 4-point bending, split at the closest to the centre joint where DP 4494⁴⁵

⁴⁵ DP 4494 was applied due to a thicker joint that could not be sufficiently covered by DP 4468

was applied. In that location, the bottom block, which was bonded with *DP 4494*, delaminated, subsequently causing crack propagation. However, the crack path did not follow the upper seam, which was bonded with *DP 4468*, but instead, continued within the glass interface of the upper block as can be seen in Fig. 5.28. No visible delamination of the *DP 4468* adhesive was observed. Although this single experiment cannot be used for deriving quantitative data, it provided valuable input on the influence of different adhesives of the DP family on the failure behaviour and strength of the assembly. The experiment suggested that (1) a thicker joint and (2) the use of *DP 4494* can reduce or even alter the structural behaviour and capacity⁴⁶ of the assembly. Nonetheless, the tested architrave could withstand a substantial load, more than double⁴⁷ than the one anticipated by the structural engineers of the project.

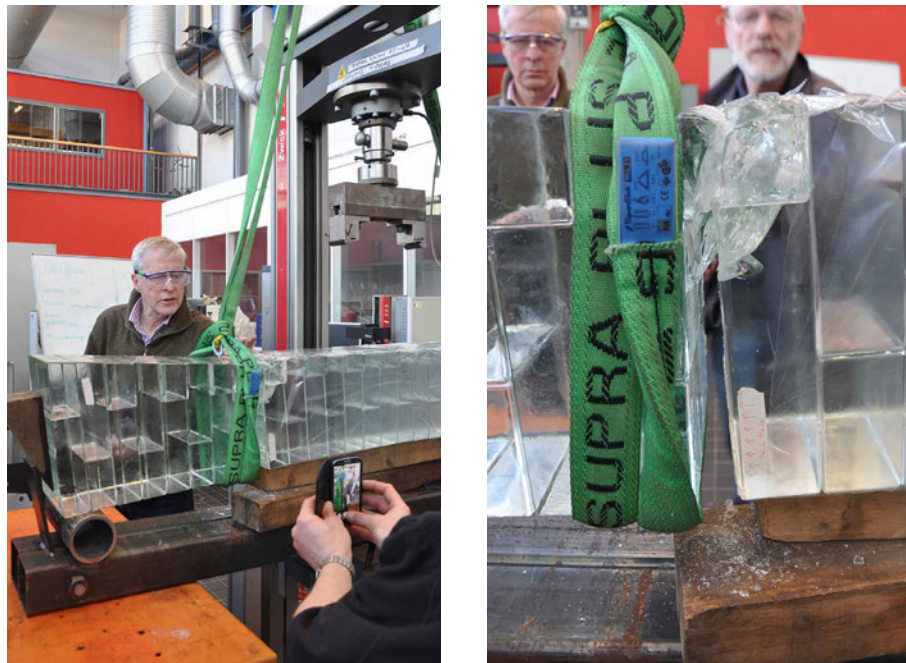


FIG. 5.28 The architrave specimen after failure.

⁴⁶ Although in literature *DP 4494* presents higher values in both tensile strength and Young's Modulus, it is an adhesive engineered principally for plastic bonding. It presents good adhesion to glass but with a comparatively decreased mechanical performance than the one stated in literature.

⁴⁷ According to the calculations by *ABT structural engineers*, the architrave specimen should be able to withstand 20 kN of load prior to failure.

5.6.5 Impact and vandalism test

Table 5.9 summarizes the findings from the hard-body impact and vandalism tests:

TABLE 5.9 Findings from the hard-body impact and vandalism test

Test	Test repetition	Observations
Hard-body impact test release from 45°	2	No damage on the glass specimen. Concrete suspended block chipped off at its corner
Hard-body impact test release from 90°	2	No damage on the glass specimen. Concrete suspended block chipped off at its corner
Vandalism test	2	Aimed block cracked mainly internally. No damage on the adjacent blocks. The same observations applied on the 2 nd test, which was performed on one of the blocks adjacent to the cracked one.

The glass wall prototype resisted successfully all 4 impact tests without presenting any visible cracks; the concrete brick used as impactor was severely damaged. Accordingly, it is expected that the facade can withstand the accidental impact of normal objects such as bikes, bottles, etc.

The vandalism test with a sledgehammer resulted to internal cracks to the aimed glass block. No damage or crack propagation occurred to any of its adjacent blocks. A second, adjacent block was then hit by the sledgehammer, and the same internal cracking pattern appeared (see Fig. 5.29). The results indicate that (1) a rapid impact force only causes local damage, which does not transfer to adjacent bricks and (2) the damaged blocks still maintain a smooth external surface – there is no risk of passers by being hurt by flying shards. It should be noted that an unavoidable by-product of the glass facade is that the glass blocks will already be in compression due to the self-weight of the structure. Nonetheless, the anticipated pre-compression of the blocks is not expected to significantly alter the results⁴⁸.

The vandalism test emphasized the significance of developing a replacement method in case a brick is damaged. Accordingly, a procedure of replacing a damaged brick was developed using the same specimen:

⁴⁸ Considering the total dimensions of the façade and based on an even dead-load distribution the expected pre-compression of the entire envelope is of less than 0.2 MPa at the lower rows of the façade. Even if the entire weight of the façade (approx. 40 tn) is imposed uniformly on one of the S blocks, it would not result to more than 19 MPa of pre-compression.

First the largest part of the mass of the damaged block is mechanically removed until only small shards attached to the adhesive are left. The adhesive is then locally heated above 120 °C with a hot air blower. This is the transition temperature where *DP 4468* starts to become viscoelastic and softer, allowing for easy mechanical removal of the last glass shards and of the adhesive layer itself, without damaging the adjacent blocks. A new glass block, machined down by 0.1 mm in dimensions to slide easily into the empty slot, can be then inserted (see Fig. 5.29, bottom right). Adhesive can then be injected into the surrounding seams, using a syringe.

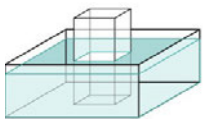
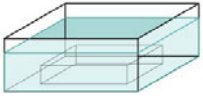
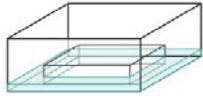


FIG. 5.29 Top: Result of the first vandalism test. Bottom left: Following, the vandalism test was repeated to an adjacent brick. Again, only the aimed block was damaged. Bottom right: The prototype after the replacement of one of the damaged blocks.

5.6.6 Thermal shock tests on individual blocks

The results of the thermal shock tests are summarized in Table 5.10.

TABLE 5.10 Results of thermal shock tests. Two samples were used per test per temperature.

T.	F ₁	F ₂	F ₃	F ₄
				
60 °C	Interior cracks only at the part that was in the water.	Completely cracked in the interior.	No cracks	No cracks
80 °C	Interior cracks only at the part that was in the water. The cracks are more severe than in 60 °C.	Completely cracked in the interior. The cracks are more severe than in 60 °C.	No cracks	No cracks

Specimens F₃ and F₄ are the closest simulation of the hot facade's resistance against summer rain; in the event of rain, only the external surface of the blocks will be exposed to rainwater. No cracks appeared in either case. However, all specimens from the F₁ and F₂ series that were half- or completely immersed into water after being heated to 60 °C or 80 °C presented considerable cracks in their interior due to the abrupt temperature change between their surface and the core. More specifically, both F₂ samples developed internal cracks throughout their volume, while in specimens of the F₁ series cracks were observed only in the part that was immersed in water (see Fig. 5.30). In that case, a clear, almost horizontal cut marks the waterline. In all samples of the F₁ and F₂ series, the cracks continued to grow significantly after they were removed from the water (Fig. 5.30).

The results suggest that the blocks can withstand the elements if applied in an external building wall such as the case study, where they will be susceptible to a rapid temperature change mainly on their external surface. Nonetheless, the blocks may be susceptible to damage in locations with extreme weather conditions. If the concept is to be used in a less moderate climate than Amsterdam, it is recommended to test for thermal shock using appropriate parameters and/or consider the use of borosilicate glass that has a significantly improved thermal shock resistance.



FIG. 5.30 Specimens of the F_1 and F_2 series tested in thermal shock from 80 °C to 20 °C. Left: Cracks in the specimens immediately after they were removed from the water. Right: Growth of the cracks in the same specimens after approx. one day.

5.7 Conclusions

An innovative, self-supporting glass masonry wall system, consisting of annealed soda-lime solid glass blocks bonded together by *Delo Photobond 4468*, a UV-curing, colourless adhesive has been developed for the *Crystal Houses* façade in Amsterdam.

The conducted experimental work proves the structural feasibility of the given case study: the structural system developed for the *Crystal Houses* façade allows for a glass wall of considerable dimensions that can carry its own weight without cracking or buckling. In fact, even one glass block can successfully carry the entire weight of the façade if properly supported. In particular, the experimental results indicate that the structure presents a monolithic behaviour against the anticipated load, offering compressive and flexural strength comparable to or better than the strength of typical B80 high performance concrete.

The flat geometry of the facade and its high slenderness ratio necessitate the reinforcement of the facade against lateral forces and buckling that may occur due to eccentricity in construction, or wind. This is done by the four 5.5 m tall buttresses on the inner side of the glass wall. In this way a completely transparent solution is achieved using the geometry of the facade, sparing the necessity of additional non-transparent steel elements.

Visual prototypes and structural experiments demonstrated that the glass components' dimensional tolerances should not exceed ± 0.25 mm deviation in size

and flatness. Visual prototypes with a larger deviation in the height and flatness of the glass blocks could not be homogeneously bonded, resulting in visible air gaps and dendritic patterns in the adhesive layer. Furthermore, inhomogeneous bonding can significantly reduce the structural performance of the assembly, as was proven by the compression tests on adhesively bonded glass columns and by the 4-point bending test of the architrave specimen. Among the column specimens tested in compression, the prototypes with improper bonding failed at considerably lower stress values than the specimens made of glass blocks of stricter dimensional and surface tolerances, ensuring a consistent and comparably thinner adhesive layer. The architrave testing further confirmed the importance of proper bonding and of the use of *DP 4468* as the bonding media: The architrave specimen failed in the closest to the centre location where another adhesive, *DP 4494*, was applied due to a considerably larger gap that could not be filled with *DP 4468*. The specimen delaminated where *DP 4494* was used, whereas on the upper layer, which was bonded with *DP 4494*, a crack was initiated within the glass.

The beam specimens tested in 4-point bending, which were made of blocks of the recommended ± 0.25 mm tolerance presented a consistent, monolithic failure of the assembly and indicated a flexural strength of the system of approx. 5 MPa. The failure mechanism of the glass-adhesive assembly is different than the one of conventional masonry works, where the cracks follow in principle the mortar joints.

Compression tests on single blocks emphasized the importance of a proper connection design: Glass blocks directly in contact with the steel surface of the testing machine failed at values between 20–30 MPa, whereas blocks that were tested with plywood as intermediary reached the load limit of the machine without failure; essentially, each block could withstand more than the entire load of the façade.

All the above emphasize the importance of strict tolerance specifications in the brick fabrication and the necessity of a homogeneous adhesive layer of the recommended thickness in order to ensure a consistent, predictable and optimum structural and visual performance.

The impact and vandalism tests demonstrate that the *Crystal Houses* façade can withstand accidental impacts of objects but may endure cracks in case of vandalism. This stresses the necessity of a replacement method in case of a damaged element. Accordingly, a replacement method by controlled heating of the adhesive has been developed and experimentally proved.

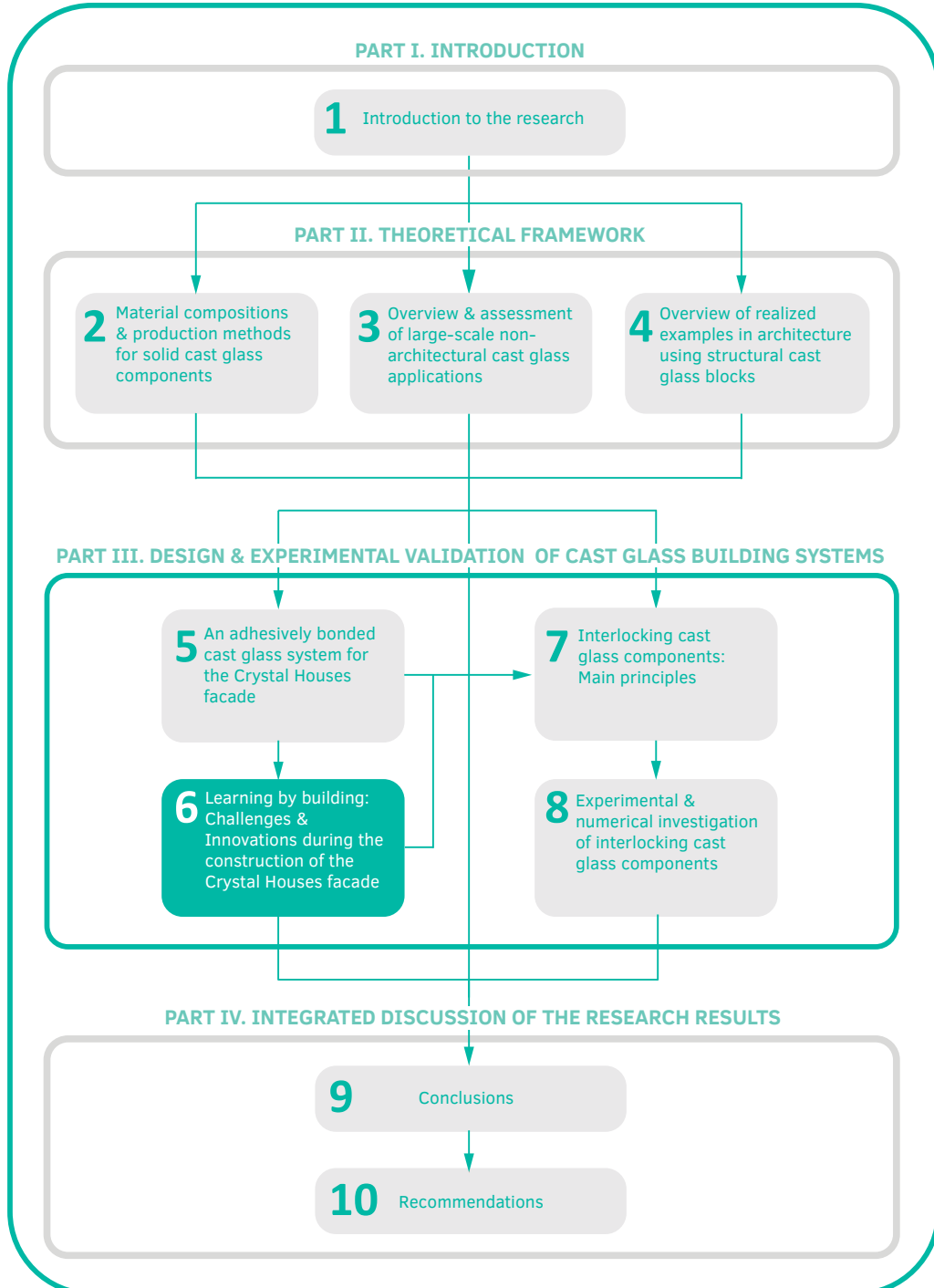
Given the high dimensional precision required for the cast units, soda-lime glass and open moulds were preferred to reduce the manufacturing costs, as the post-processing of the elements was considered inevitable. Even though in soda-lime glass the thermal stresses occurring are much higher than for borosilicate glass, the experiments prove that soda-lime glass blocks can withstand the anticipated rapid temperature changes when applied to an external wall in a temperate climate.

Overall, although the experiments and research presented were conducted for the specific case study, the principles and experimental data of the adhesively bonded solid glass block system can be used as an established guideline for further structural or self-supporting applications of the developed adhesively bonded system.





Exploring the third dimension of glass



Solid cast glass components and assemblies for structural applications

6 Learning by building – Challenges & Innovations during the construction of the Crystal Houses façade

Continuing from the experimental validation of the adhesively bonded system, this chapter presents the main challenges confronted and records the innovative solutions implemented during the consecutive construction steps of the adhesively-bonded cast glass façade⁴⁹. These include the manufacturing and quality control of the bricks, the set-up of the construction site, the levelling of the reference supporting beam, the bonding method used and the fabrication and installation of customized elements such as the architraves, window and door frames and the intermixing zone of glass with terracotta bricks. The experimental work on prototype elements, described in Chapter 5, resulted into the use of a colourless, UV-curing adhesive of the *Delo Photobond* family for bonding the solid glass blocks together. The tests indicated as well that the desired monolithic structural performance of the glass masonry system and a homogeneous visual result can only be achieved when the selected adhesive is applied in a 0.2-0.3 mm thick layer. In accordance, the bricks have to meet a strict dimensional tolerance of ± 0.25 mm. On the facade as a whole, this means that the overall size deviations will be limited to a few mm. The nearly zero thickness of the adhesive together with the request for unimpeded transparency introduced numerous engineering puzzles, addressed in this chapter. The fundamental difference between conventional brickwork and the developed glass masonry system is that a standard mortar layer compensates for the size deviations of the bricks, while the selected adhesive cannot. This manifests the level of complexity introduced by the manual bonding and the significance of constantly

⁴⁹ This chapter has been published as: Oikonomopoulou F., Britogianni T., Veer F., Nijse R. The construction of the *Crystal Houses* façade: Challenges and Innovations. *Glass Structures & Engineering*, 2017. (Oikonomopoulou et al. 2017a)

controlling the entire construction with high precision methods. Based on the conclusions of the research and the technical experience gained by the realization of the project, recommendations are made on the further improvement of the presented glass masonry system for future applications.

Credits

Supervision of the construction together with

- Telesilla Bristogianni,
Faculty of Civil Engineering & Geosciences, TU Delft

Technical support and assistance

- Kees Baardolf – *assistance in levelling the starting surface*,
Stevin II Laboratory, Faculty of Civil Engineering & Geosciences, TU Delft
- Kees van Beek – *assistance in developing the “laser-milk” system*,
DEMO, Faculty of Civil Engineering & Geosciences, TU Delft
- Ruud Hendrikx – *XRF Analysis*,
Department of Materials Science & Engineering, Faculty of Mechanical, Maritime & Materials Engineering

Research Supervisors

- Rob Nijssse,
Faculty of Civil Engineering & Geosciences, TU Delft
- Fred A. Veer,
Faculty of Architecture & the Built Environment, TU Delft

Architectural Design

- MVRDV

Co-Architect

- Gietermans & Van Dijk

Glass brick manufacturer

- Poesia

Adhesive Consultant

- Siko B.V. - Rob Janssen

Contractor

- Wessels Zeist, Richard van het Ende, Marco & Ronald van de Poppe

Numerical modelling

- ABT B.V. Consulting Engineers

6.1 Introduction

In the previous chapter the design and experimental validation of a novel adhesively-bonded glass block system, developed for the *Crystal Houses* façade in Amsterdam, was presented. The architectural concept of the façade is to achieve a completely transparent reproduction of the original brick façade of a former townhouse in Amsterdam. Based on the original design the resulting façade comprises more than 6500 solid glass bricks, reinterpreting the traditional brick pattern, and elaborate cast glass elements for the replication of the window and door frames. To achieve unhindered transparency, the 10 m x 12 m glass block façade has to be self-supporting. The experimental work described in Chapter 5 concluded that it was necessary to use *Delo Photobond 4468*, a clear, UV-curing adhesive of high stiffness as the bonding media. Experimental work on prototype elements indicated that the desired structural and visual performance of the glass masonry system are only guaranteed when the selected adhesive is applied in a 0.2 – 0.3 mm thick layer. To meet this requirement, the glass blocks should comply with a strict dimensional tolerance of ± 0.25 mm in both height and flatness. The nearly zero thickness of the adhesive together with the request for unimpeded transparency introduced numerous engineering challenges. These include the production of highly accurate glass bricks and the homogeneous application of the adhesive to achieve the construction of the entire façade with remarkably tight tolerances. This chapter presents the main challenges confronted during the construction of the novel façade and records the innovative solutions implemented, from the production and control of the glass units to the completion of the façade.

6.2 Manufacturing and quality control of the glass blocks

6.2.1 Manufacturing process of the glass bricks

The fabrication of approximately 7500⁵⁰ solid glass bricks in total, was assigned to the Italian company *Poesia* (<http://www.spaziopoesia.it>). Each brick is manually cast by pouring molten glass in high precision, open steel moulds with a removable bottom surface (Fig. 6.1). A low-iron glass recipe is used for high optical quality. The final chemical composition of the glass, as measured by a X-ray fluorescence (XRF) spectrometer, is shown in Table 6.1. To attain the desired smooth external texture the steel moulds are preheated to a constant temperature of approximately 650°C - 750°C. If the mould's temperature falls below this range, then the hot glass coming into contact with the metal surface freezes instantly, creating a rough, wavy surface. On the other hand, if the mould is heated to a higher temperature, the glass tends to adhere to the walls of the mould. A release coating on the mould surfaces further prevents the adhesion of the molten glass to the working surface and the development of micro-cracks.

After the glass has been poured into the mould, it is left at ambient temperature to rapidly cool until ~700°C. This rapid cooling through the critical crystallization zone is essential to obtain an amorphous structure and avoid the molecular arrangement of the melt in crystals, which would result in a cloudy glass of reduced transparency (Shelby 2005). During this initial cooling phase, the glass has still low viscosity that can allow any induced thermal stress to relax out to a negligible amount immediately (Shelby 2005). After the glass temperature has dropped to its softening point (~720°C⁵¹), the viscosity of the glass is sufficient for it to retain its shape and not deform under its own weight (Shand 1968). At ~700°C, the glass

⁵⁰ This figure reflects the final order for the construction of the façade and includes the production of spare blocks. The façade consists of approx. 6500 bricks.

⁵¹ The temperatures given here for the softening, annealing and strain points are indicative for soda-lime glass and are based on research by (Albert Napolitano, Earl G. Hawkins 1964). The values may differ according to the exact composition of the glass. The exact temperatures referring to the soda-lime recipe of the glass blocks have not been disclosed to the authors by *Poesia*.

element is removed from the mould by suction at the top surface, and moved into the annealing oven.

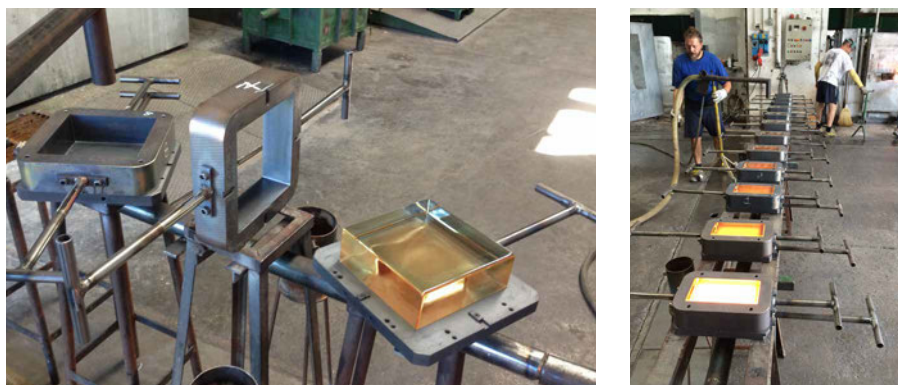


FIG. 6.1 Left: The high precision, open steel moulds. Right: Molten glass bricks during the rapid cooling phase from 1200°C to ~700°C degrees.

TABLE 6.1 Composition of the applied cast glass based on XRF chemical analysis

compound	wt%	absolute error (wt%)
SiO ₂	75.606	0.1
Na ₂ O	15.833	0.1
CaO	5.142	0.07
K ₂ O	1.836	0.04
Sb ₂ O ₃	0.821	0.03
CuO	0.402	0.02
Al ₂ O ₃	0.165	0.01
MgO	0.072	0.008
ZrO ₂	0.043	0.006
SO ₃	0.034	0.006
TiO ₂	0.02	0.004
Fe ₂ O ₃	0.01	0.003

There, a long and meticulously controlled annealing process eliminates any possible differential strain built up between casting and demoulding, as well as prevents the generation of internal residual stresses during further cooling. Upon this point, key reference temperatures are the annealing point (~545°C) and the strain point (~505°C) of soda-lime glass. The annealing point is defined as the temperature at which the viscosity of glass will allow any induced stress to relax out substantially

in just a few minutes (Shelby 2005). The strain point is the temperature where the same stress is reduced to acceptable values in four hours (Shand, Armistead 1958; Shand 1968). The cast glass should be maintained for adequate time at the annealing point to relieve any existing strains and then cooled at a rate sufficiently slow so that residual stresses will not reappear when the glass temperature has reached equilibrium (Shand, Armistead 1958). Effectively, below the strain point, stress cannot relax in time and is considered permanent (Watson 1999). When the temperature of the entire glass component has dropped below the strain point, the component can cool at a faster pace until ambient temperature, yet still sufficiently slow to prevent breakage due to thermal shock (Shand, Armistead 1958)⁵².

As already discussed in chapter 2.4 the heat transfer needed for accomplishing the desired temperature difference is influenced by multiple parameters that are challenging to accurately simulate for solid cast glass components. Instead, companies such as Poesia, use an empirical annealing schedule based on their experience and furnace facilities. In this case, the company concluded that each *Crystal Houses* brick with 65 mm x 105 mm x 210mm dimensions requires approximately 8 h of annealing, whereas bricks of double the volume (65 mm x 210 mm x 210 mm) require 36-38 h respectively to prevent the generation of perceptible permanent residual stresses. The 65 mm thickness of the components hindered -at that time- an accurate through-the-thickness stress measurement by a *Scattered Light Polaroscope* (SCALP) stress-meter using the current hardware/software. Instead a qualitative analysis of strain concentration was performed using a polarized white light source and a crossed polarized film that blocks the transmission of light. If glass is subjected to stress, it exhibits optical anisotropy. Glass without any stress will appear completely dark (Schott AG 2004). If the specimen presents besides black only grey-scale spectral composition, it has low residual stresses. When the colour spectrum appears the amount of stress is higher but cannot be quantified⁵³. This method was used by Poesia to control all produced bricks. Bricks such as the one on the left of Fig. 6.2, with a clear indication of internal stresses by a coloured spectrum, were discarded. Only bricks such as the one on the right of Fig. 6.2, with dark and white areas were used in the façade. The fracture pattern of tested specimens also suggested low residual stresses – there was no excessive fragmentation or branching observed in the components.

⁵² For a detailed explanation of the annealing process of cast glass objects refer to Chapter 2.4

⁵³ See chapter 2.4 for a more detailed explanation.

During the initial rapid cooling, natural, inevitable shrinkage occurs to the glass volume during the material's transition from liquid to solid state. The shrinkage causes dimensional differences between units, uneven surfaces especially on the top, open surface of the cast component owing to the additional gravity force (see Fig. 6.1 and Fig. 6.3).

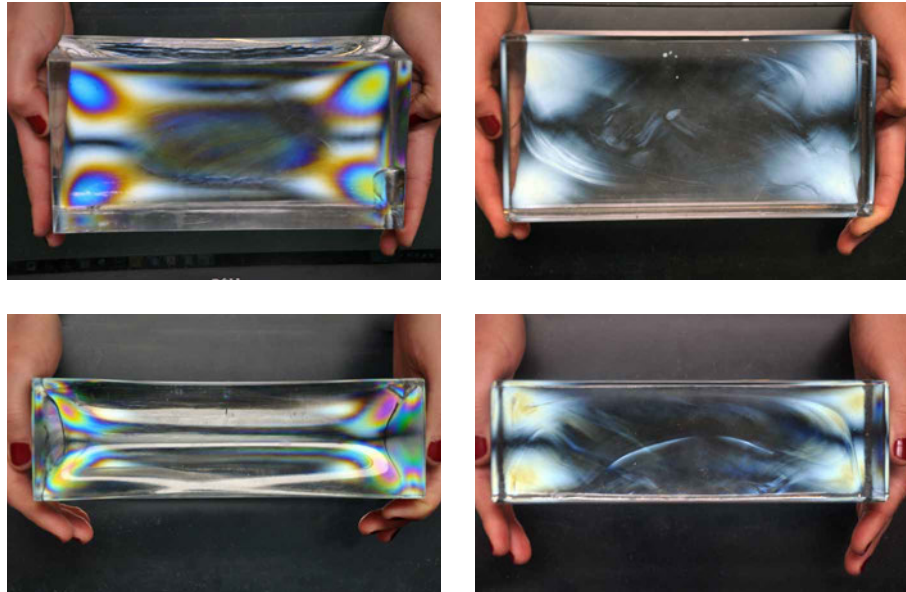


FIG. 6.2 Qualitative analysis of strain concentration by polarization test. Bricks such as the ones shown on the left image, with a clear indication of residual stresses, were discarded. Specimens such as the one on the right, with no visible considerable strain concentration, were employed in the façade.



FIG. 6.3 Glass bricks of 210 mm x 210 mm x 65 mm coming out of the annealing oven after circa 36-38 h. The natural shrinkage is visible on the top surface.

Different casting orientations were tested for minimizing the resulting shrinkage in the larger, bonding surfaces of the bricks. Fig. 6.4 demonstrates that even when molten glass is rapidly cooled in a vertical orientation, there is still visible shrinkage on the larger, bonding faces of the components.

Considering that regardless of orientation of the mould, the bricks' bonding surfaces required further processing, the horizontal position was favoured in terms of aesthetics, where the non-bonding sides are not visibly distorted. Thus, to achieve the desired ± 0.25 mm precision, the blocks are originally cast slightly higher. After the annealing process, a CNC machine mills the top layer of each block to remove the natural convex and obtain the precise height and flatness. Finally, both top and bottom faces of each block, i.e. the bonding surfaces, are polished to a smooth flat surface of the desired dimensional accuracy. The four vertical surfaces remain unprocessed as they do not influence the structural system. Mechanical testing on both CNC polished and unpolished bricks showed no deterioration of the mechanical properties of the former.



FIG. 6.4 Glass bricks rapidly cooled down to the annealing point in vertical orientation. The natural shrinkage is evident besides the top surface, also across the larger surfaces.

6.2.2 Quality control of the glass bricks

The processed glass bricks are then subjected to two separate dimensional controls to verify their conformity. Both controls were performed first at *Poesia* and then again at *TU Delft* for verification. The first control is accomplished by a cut-out metal plate jig that controls the total length and width of the bricks in 1.00 mm accuracy (Fig. 6.5). The second control employs a customized electromechanical measurement bench with five *Linear Variable Differential Transformer* (LVDT) sensors of 1 μm accuracy attached to an aluminium frame (Fig. 6.6). By taking point measurements close to the four edges and at the center of each unit, the sensors check if the bricks meet the required 0.25 mm tolerance in both height and flatness from the nominal height of 65.00 mm. It should be clarified that the range of acceptable height varies between 64.75 - 65.25 mm but within each particular brick the height deviation cannot exceed 0.25mm. Accordingly, through this measuring control, the acceptable bricks are sorted in two groups based on the point with the maximum height:

- Group A comprises bricks between 64.75 mm and 65.00 mm high
- Group B comprises bricks between 65.00 mm and 65.25 mm high respectively.

Only bricks of the same group were used per row of construction to maintain the 0.2-0.3 mm requirement for the adhesive thickness.

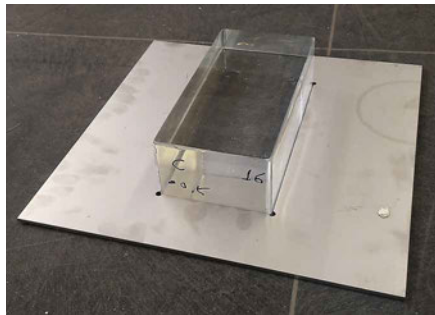


FIG. 6.5 The jig used in the first dimensional control.



FIG. 6.6 Set-up of the second control for checking the height and flatness of the components.

Besides the dimensional controls, a visual inspection of the bricks is performed. Flaws on the bricks' bonding surfaces, usually in the form of minute cracks or scratches, even less than 1 mm deep, commonly caused during the handling and transportation, can trigger the propagation of visible cracks after the adhesive's curing process. In specific, during curing the adhesive shrinks by max. 9% vol at

ambient temperature (Delo Industrial Adhesives 2014) because of polymerization triggered by UV-light (Delo Industrial Adhesives 2007), inducing a considerable amount of tension to the minute cracks that can start to propagate, eventually resulting in visible cracking⁵⁴ (see Fig. 6.7). Only the glass components that pass both the measuring and visual controls were used in the construction of the façade.

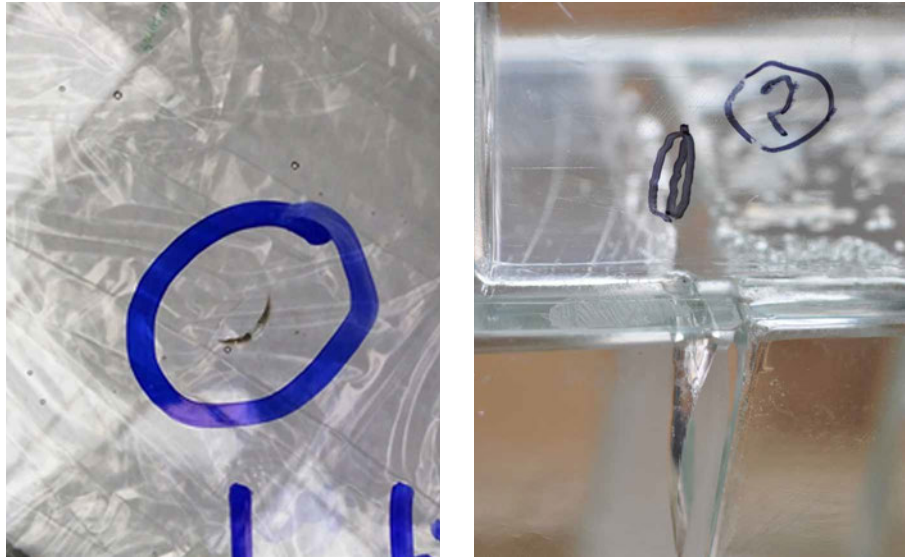


FIG. 6.7 Left: A minor crack on a brick's bonding surface. Right: The propagation of such a minor crack after the curing of the adhesive.

⁵⁴ According to the research and experimental work conducted by (Pratzsch 2015), a curing process of increased duration and decreased intensity, carried out in steps, allows for better settlement of UV-curing adhesives and results in less internal stresses. As described in chapter 6.3.3, the curing process followed in the façade's construction follows a two-step curing process. The duration of the curing and intensity have been chosen in consultancy with Siko B.V. Still, the resulting tensile stresses at the adhesive layer were sufficient to cause crack propagation from surface damage.

6.3 Construction of the glass brick wall

6.3.1 Construction site set-up

The upper conventional masonry façade of the top residential floor, based on a steel beam spanning its length, was completed 6 months prior to the construction of the glass elevation (Fig. 6.8). The level of complexity of the manual bonding process of the glass façade, called for a highly skilled building crew and a strictly controlled construction. A 12 h working schedule was established, five days per week. 7-9 highly skilled workers bonded and sealed an average of 80-100 glass blocks per day under the supervision of 2 quality control engineers and the construction site supervisor.



FIG. 6.8 The masonry wall was already constructed prior to the glass elevation.

The special characteristics of the adhesive required the construction of the façade inside a UV-filtering tent for protection against solar radiation, adverse weather conditions and dust. To ensure a controlled level of temperature and humidity, heating equipment was installed inside the tent so that the bricks and the adhesive

be maintained within workable temperatures during winter. During the summer, when the ambient temperature exceeded 30 °C the construction would temporarily stop. Due to limited space in the construction site, the glass blocks were stored in pallets in a separate warehouse and were gradually transported to the site upon demand.

A scaffolding with a mast climbing working platform was installed for the construction of the glass brick wall. Simultaneously, three mobile elevated working platforms were placed at the inner side of the wall for the construction of the buttresses. Bricks for one full row of construction were loaded and lifted each time on the mast climbing working platform, from where they were distributed for bonding. An elaborate network of horizontal aluminium guides was utilized to prevent any misalignment during the erection of the wall (Fig. 6.9). Customized vertical aluminium frames were temporarily installed as place holders of the wall openings.



FIG. 6.9 Left: the installed aluminium place holders of the opening. Right: The mast climbing working platform and one of the three mobile elevated platforms.

6.3.2 Levelling the starting bonding surface

The erection of the glass masonry wall started on top of a 0.60 m high by 0.20 m wide reinforced concrete plinth, essential for the protection of the lower part of the façade against hard body impact; it has been calculated to resist a vehicle collision travelling with a velocity of 50 km/h. To match the texture and colour of the glass wall, the vertical faces of the concrete base are coated with a laminate of a stainless steel sheet and annealed patterned glass, laminated together by *SentryGlas*[®] foil. A

30mm thick stainless steel plate fixed by bolts on top of the plinth forms the base for the glass masonry wall (Fig. 6.10).



FIG. 6.10 On the left the bolts used for levelling the stainless steel plate, seen on the right.

The prerequisite for extreme accuracy of the developed glass block system necessitates a reference building surface of corresponding flatness. Accordingly, the stainless steel plate had to be levelled to an accuracy of 0.25 mm for the entire 12 m length of the façade. Such high measuring accuracy called for the development of an innovative measuring and levelling system. Specifically, the bolts, set 275 mm apart (Fig. 6.10) allow for the levelling of the stainless steel plate in consecutive steps. By employing standard levelling equipment the plate was initially levelled to an accuracy of 3 mm over the 12 m length. Fig. 6.11 demonstrates the principle of the measuring system developed to further level the stainless steel plate to the desired precision: A continuous open metal conduit with both ends sealed, supported directly on the concrete surface, is filled with a non-transparent, reflective liquid. When still, a liquid will achieve absolute horizontal flatness, establishing the reference level for calibrating the plate. A laser scanner with a sensor of 1 μm precision, fixed on an aluminium frame with three legs is then moved over a set of consecutive points on the stainless steel plate, taking measurements in reference to the liquid's surface, mapping the plate along its entire length. The use of an opaque reflective liquid (e.g. full fat milk) is essential for ensuring that the laser beam will take all measurements exactly at the same reference level. After the entire surface of the plate is mapped, by tightening or releasing the nuts and counter nuts of the bolts the plate was successfully levelled with a maximum height deviation of 0.24 mm for the total 12 m length. The resulting gap between the concrete base and the plate was filled with non-shrinkage concrete and left to cure.

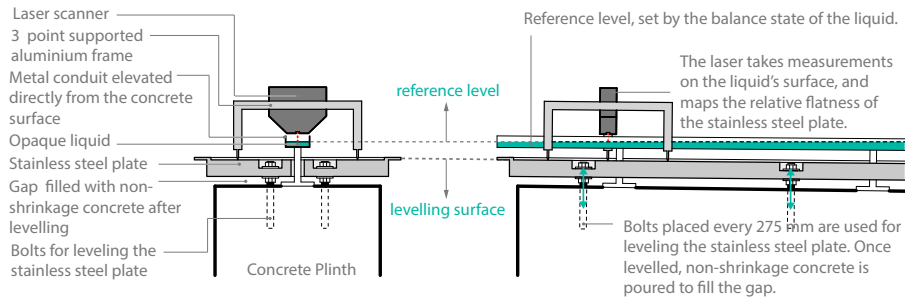


FIG. 6.11 Principle of the developed levelling system.

6.3.3 Bonding Process

The 0.2-0.3 mm optimum thickness of the adhesive layer demanded extreme precision in each construction layer. In traditional terracotta brickwork the mortar plays the dual role of bonding and compensating for tolerances in the size of the bricks. However, the selected adhesive's inability to compensate for any dimensional discrepancies in the construction can result to an accumulated offset of a few centimetres in the total height of the façade, even when the allowable tolerance per glass component is only ± 0.25 mm. To eliminate the development of fluctuations in the height of the construction, all the glass bricks of a new row are laid down prior to bonding. The thickness of the resulting horizontal joint between the laid bricks and the bonded ones below is then checked by a feeler gauge (Fig. 6.12). When the seam is larger than the suggested 0.25 mm, the corresponding brick is replaced with another one that accomplishes better contact in the specific location. The final selection of bricks is then numbered to guarantee their correct bonding sequence.

Previous structural and visual tests by (Oikonomopoulou et al. 2015b), described in Chapter 5, suggested the bonding of the complete contact surface between blocks. The uniform application of the adhesive besides ensuring a homogeneous load distribution is also essential for maximizing transparency. Indeed, the façade's visual result is deeply affected by any form of air gaps and bubbles in the adhesive layer, as well as from stains caused by the adhesive's overflow or capillary action. To eliminate such defects, a customized bonding procedure was applied.

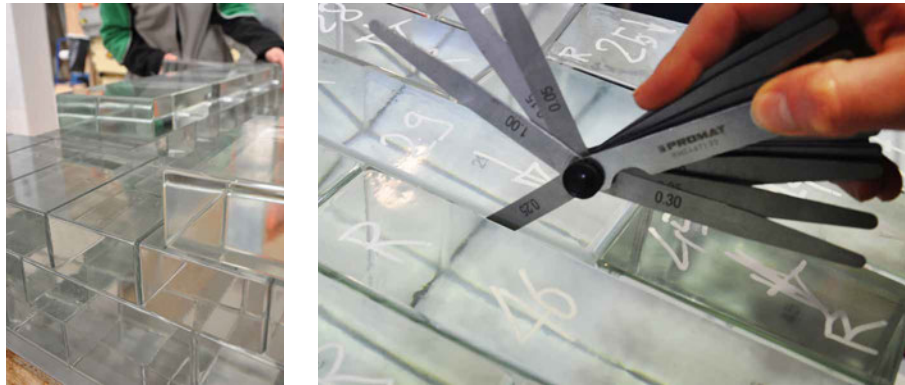


FIG. 6.12 Bricks of a new row laid down prior to bonding (left). Afterwards, a feeler gauge is used for checking the thickness of the resulting seam (right). The blade of the feeler gauge is sufficiently flexible and round not to induce any surface damage on glass.

Initially, the bricks are visually inspected on site for any defects, as explained in section 6.2.2. Then, the surfaces to be bonded are cleaned with 2-propanol. Specially designed self-reinforced polypropylene forms out of *PURE*[®] (DIT b.v. 2016) are placed for the distribution of the adhesive in an X pattern, controlling the flow, spread and amount of the adhesive (Fig. 6.13 and Fig. 6.14). To prevent any capillary effect along the vertical faces of the glass bricks, a special, UV beam light is used to locally harden the liquid adhesive in case it arises on the vertical seams.

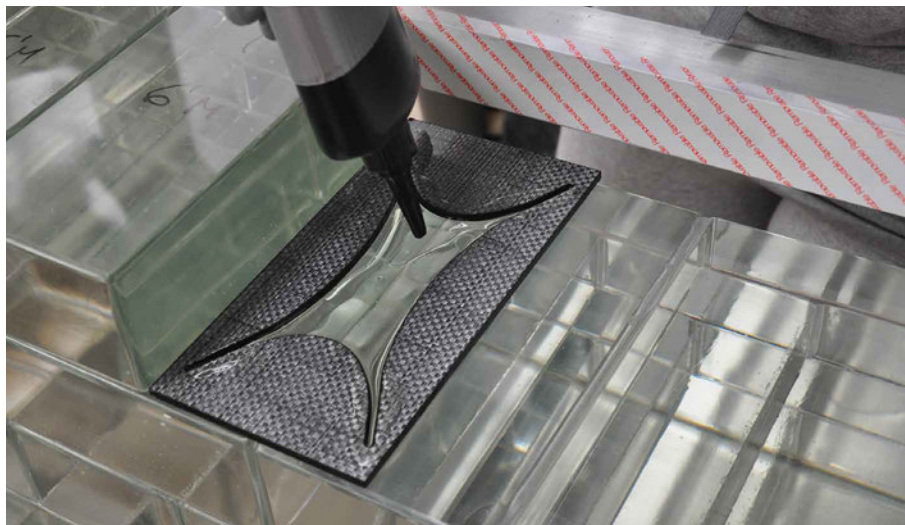


FIG. 6.13 *PURE*[®] mould used for the application of the adhesive on the final façade wall.



FIG. 6.14 Bonding steps from left to the right: 1. Application of the adhesive with the aid of the *PURE*® form. 2. Resulting X pattern. 3. Local hardening of the adhesive by a UV beam light for preventing capillary action. 4. UV-lamp used to cure the adhesive for 60—120 seconds.

Once the adhesive is evenly spread, it is initially exposed to low intensity UV-light for 5 s while the brick is kept in position and under pressure. This partial pre-curing step was introduced for practical reasons⁵⁵. It allows for the stabilization of the glass brick; at the same time the wiping-off of adhesive overflow can be easily made. After cleaning, the adhesive is further cured by low and medium intensity UV-radiation in the range of 20-60 mW/cm² and for a period of 60 - 180 s, according to brick size. Once a complete brick layer is bonded, all joints are sealed in order to guarantee the dust, water- and moisture- tightness of the façade. For the sealing, *Delo Photobond 4497* (Delo Industrial Adhesives 2016b), a more flexible and viscous, clear UV-curing *Delo Photobond* acrylate, specially designed for outdoor applications, is selected due to its good visual performance, compatibility with *Delo Photobond 4468* as well as for its easy and quick application (Fig. 6.15). This adhesive requires only 10 s of UV-curing to be completely cured.

⁵⁵ This pre-curing time was set experimentally. Testing of specimens cured in this way did not reveal any differences with specimens cured once off.



FIG. 6.15 Left: Sealing of the already bonded bricks. Right: the final, visual result achieved by the novel bonding method.

The first row of glass blocks was directly bonded onto the stainless steel base by *Delo Photobond 4468*. As previously mentioned, *Delo Photobond 4468* is recommended by the manufacturer for glass to metal bonding as well. Previous research on such a bond has been conducted by (Puller, Sobek 2008; Tasche 2007). The established rigid connection was considered imperative by the structural engineers in order to eliminate any horizontal movements of the free-standing façade. Any movements due to temperature strains in the structure are compensated by the flexible connections at the sides and top of the façade (see section 6.3.6).



FIG. 6.16 The top connection is completely masked by the ceramic strips.

Every 2 m of elevation, the levelling along the total length of the façade is recorded using a high accuracy total station survey equipment. Bricks with a 0.5 mm or 1.0 mm reduction in height were specially manufactured for the levelling of the wall in case of height deviations. Such bricks were required to level the wall segments when reaching the level of the architraves of the ground and first floor. At the top of the elevation, the glass wall is connected to a steel beam by a 22 mm thick structural modified silane (MS-) polymer bond. This flexible connection can accommodate displacements due to the different thermal expansion and stiffness between the

upper construction and the glass wall. A flexible waterproof tube filled the gap towards the interior of the wall, to further prevent water leakage. As ceramic strips cover the entire top row, the connection details are fully hidden (Fig. 6.16).

6.3.4 Construction and installation of the architraves

The architraves above the window and door openings of the original 19th century elevation are also reinterpreted into glass components by special tapered glass bricks bonded together by the same adhesive across their vertical surfaces. Due to the low viscosity of the *DP 4468* each architrave had to be pre-assembled into one single component in a custom made rotating steel fixture. The rotating fixture ensures the horizontal application of the adhesive, as well as the desired arch geometry, with a straight top line in accordance to the maximum 0.25 mm deviation rule. The finished components, preassembled in the *TU Delft Glass & Transparency Lab*, were then transported to the building site and installed one by one in situ with the aid of a jib fixture on the fork lift, as shown in Fig. 6.17.



FIG. 6.17 Left: The special rotating fixture for the preassembly of the architraves. Right: The installation of the bonded architraves on site.

6.3.5 Transition layer between standard and glass masonry

To obtain a smooth, gradual connection to the standard brickwork of the final, residential floor of the building, the initial intention of the architects was to realize a transition zone of intermixing glass and normal terracotta bricks towards the top of the façade. Nonetheless, the structural blend of the two materials presented various

practical implications, as can be seen in Fig. 6.18. Besides having different mechanical properties, the two types of bricks vary substantially in acceptable tolerances. Whereas in the glass bricks the required precision in height is ± 0.25 mm, for the terracotta bricks is at least ± 1.0 mm. Most importantly, the bonding between the two brick types necessitates the application of different adhesives, involving the risk of their intermixing. Lastly, the strongly alkaline character of most mortars used for the bonding of standard ceramic bricks attacks the glass surface and must be avoided. It should be mentioned that, as the upper conventional masonry façade was completed 6 months prior to the construction of the glass elevation and the mortar was fully cured, there was no hazard of alkaline reaction between the mortar and glass.



FIG. 6.18 Practical implications were encountered when combining terracotta and glass blocks.

Due to all the aforementioned reasons the option of combining terracotta and glass was rejected. The following solution was applied instead: Glass bricks, 40 mm shorter in width, clad with an 18 mm thick ceramic strip at each external side, replace the traditional bricks in the intermixing zone. The ceramic strips are bonded on the façade after all glass blocks have been bonded in place, preventing the occurrence of adhesive stains on their exterior surface. *Tec 7* (Novatech N.V. 2016), a brown coloured modified silane polymer is applied for bonding the strips to the glass units. With an application thickness of circa 3 mm the adhesive compensates for any difference in thermal strains between the two materials. Once all the ceramic strips have been bonded to the façade, the seams around the strips and the glass are sealed by *Zwaluw Joint Fix 310 ml lichtgrijs* (Den Braven 2017), an acrylic based mortar of similar texture and colour to the mortar used for building the wall above (Fig. 6.19). The selected mortar is less brittle than conventional mortar due to its acrylic content and features considerably less volume shrinkage (5%)(Den Braven 2017) after hardening

in comparison to standard mortar types, preventing thus its delamination from the glass blocks. The completed intermixing, gradient zone can be seen in Fig. 6.20.



FIG. 6.19 Left: Bonding of the ceramic strips to the shorter bricks. Right: The final visual result.



FIG. 6.20 End result of the intermixing, gradient zone.

6.3.6 Boundary connections of the façade

The façade forms a free standing wall firmly connected to the concrete plinth. To allow for displacements due to the different thermal expansion and stiffness between the glass wall and its boundaries, the façade is joined via flexible connections to the top metal beam, supporting the residential level above, and to the stainless steel

columns on the vertical sides. The top connection of the two structures is realized by a modified silane (MS-) polymer adhesive bond as described in Section 6.3.3.

Regarding the connection along the vertical sides, this varies between the right and left (as seen from the street) side of the wall at the ground floor, since the left side is self-supported by a buttress. On the right side at the ground floor, as well as on both sides at the first floor, the glass masonry wall is connected by a 10 mm thick layer of a clear silyl-terminated semi-elastic polymer to the stainless steel L-shaped columns to compensate for thermal displacements of the wall. Since for the curing of the specific MS-polymer adhesive the contact with atmospheric conditions is essential, the adhesive was applied gradually with a glue-kit dispenser using compressed air row by row, so that each glue layer can set until the next row of bricks is completed (Fig. 6.21). The bricks at the right side of the ground floor are each clad with two 1mm thick stainless steel strips at their adjacent to the L-shaped column sides, to mask the rough detailing of the welded stainless steel structural components (Fig. 6.21). The cladding is applied to the bricks prior their bonding to the façade. For such a connection, *DP 4497* is used, to ensure impact resistance.



FIG. 6.21 From left to right: Bonding of the steel plate to the corner brick. Positioning of the brick by a suction cup holder. Application of the semi-elastic polymer.

6.3.7 Installation and bonding of the cast glass window and door frames

The reproduction of the previous, historic elevation's wooden openings in cast glass was an extra challenge added to the engineering and construction of the *Crystal Houses* as it included the manufacturing and bonding of massive cast glass elements. The glass frames were cast by *Poesia* in open graphite moulds (Fig. 6.22), ground along their open surface to remove the material shrinkage layer and polished with a rotational band manually. As such pieces present larger tolerance problems, *DELO*

Photobond 4494 (Delo Industrial Adhesives 2016a) was chosen to bond the frame elements together due to its higher viscosity and application thickness that allow for easier tolerances, while maintaining a clear optical result. This adhesive has a comparatively lower mechanical resistance to *DP 4468*, yet sufficient for integrating the glass frames into the construction.

The window and door frames were placed after the completion of the glass wall. During the bonding process, aluminium place holders were used to secure temporarily the location of the openings. First each frame was assembled in place by *DP 4494*. Based on the UV-measurements per m² done by *Siko b.v.* the sill of each window frame, of 1145 mm x 143 mm footprint, required 4 minutes of total curing by two UV-lamps travelling back and forth along its length.

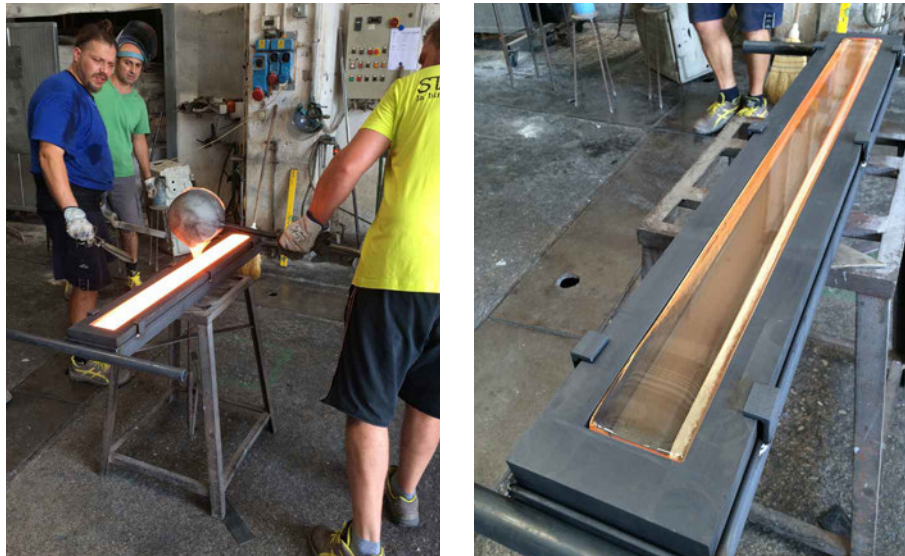


FIG. 6.22 The graphite moulds used for the fabrication of the frames.

Once the frame was in place, the side and top connection to the glass masonry wall was established. The thickness of this connection was designed to be 8 mm, to compensate for horizontal and vertical deviations in the glass masonry wall, and was achieved by the same clear silyl-terminated semi-elastic polymer used also at the top and side connections of the wall. To avoid the entrapment of air, the polymer was injected at both sides simultaneously from bottom to top (Fig. 6.23). After a few days, when the polymer had reached a satisfactory strength, the aluminium frames were removed. Then the cast glass mullions were bonded to the glass frames via the

same polymer applied in a 2mm thick layer. Finally, the glass panes were bonded to the mullions by a standard transparent silicone, completing the façade. The end result can be seen in Fig. 6.23.



FIG. 6.23 Left: The simultaneous application of the polymer from both sides. Centre and right: The final result of the bonded glass frames.

6.3.8 Maintenance

The proposed system is practically maintenance free. Glass block are durable building components and is generally not subject to weathering (Dietrich et al. 1995). In order to minimize the cleaning requirements of the facade, a spray of hydrophilic coating (e.g. Vindico (Vindico 2014)) can be externally applied to the wall as a soft coating, so that the rainwater will clean the facade. The coating needs to be re-applied every ten years. To avoid moisture and dust entering the joints of the glass blocks, they are sealed with a moisture- and water-resistant adhesive of the same UV-modified acrylate family, yet with a significantly higher viscosity. This adhesive is also resistant to glass detergents. Both adhesives are aging resistant and do not discolour when exposed to direct sunlight.

The façade was completed in May 2016 and has been since exposed to weathering. Neither discolouring of the *DP 4468* interlayer nor penetration of moisture has been observed up to the date of this dissertation.

6.4 Conclusions

A novel, completely transparent self-supporting glass masonry wall system has been developed and realized through pioneering research in the *Crystal Houses* façade (Fig. 6.24). With the exclusive use of solid cast glass elements bonded together by a clear, high stiffness, adhesive and with the aid of geometry for enhancing the lateral stability, the 10 m x 12 m façade combines the desired structural performance with pure transparency. Previous experimental work indicated *DP 4468*, a one-component, UV-curing acrylate for attaining both the desired monolithic structural performance and high transparency level. The experiments also demonstrated that the desired structural and visual performance is only guaranteed when the adhesive is applied in a uniform layer of a mere 0.2-0.3 mm thickness. This in turn leads to an allowable dimensional tolerance of a quarter of a millimetre in the height and flatness of the cast glass components. This demand of extreme dimensional precision introduced new challenges in the engineering of the façade from the manufacturing of the bricks to their bonding method, calling for pioneering solutions.

Due to the inevitable natural shrinkage of molten glass, such dimensional accuracy could only be attained by CNC-cutting and polishing of the bricks' horizontal faces to the desired height. Since the post-processing of the bonding surfaces was considered unavoidable, soda-lime glass and open, high precision moulds were preferred over borosilicate glass and precision press moulds to reduce the manufacturing cost. Special measuring equipment was developed for controlling the dimensional accuracy of the components.

Nonetheless, even blocks of such high dimensional accuracy can still lead to a significant offset in the façade's total height. Considering that the maximum allowable deviation per layer of construction is ± 0.25 mm, this mere fact manifests the level of complexity deriving from the manual bonding and the significance of constantly controlling the entire construction with high precision methods.

A completely transparent façade is moreover linked with the inability to hide any possible flaws in the construction. The development of a novel bonding method for the homogeneous and flawless application of the adhesive resulted in imperceptible connections in the constructed façade.



FIG. 6.24 The completed *Crystal Houses* façade. Source: MVRDV Architects / Image copyright: Daria Scagliola and Stin Brakkee.



6.5 Recommendations

Overall, the innovative glass masonry system developed for the *Crystal Houses* façade illustrates the great potential of adhesively bonded cast glass blocks as an answer to the quest of structural transparency and can form the basis for novel architecture applications. The system can be further engineered in order to simplify and accelerate its application, minimize the interlinked challenges and decrease the cost.

Most of the engineering puzzles elaborated in this paper can be solved with the use of a thicker transparent adhesive of equal structural performance that in turn can allow for larger tolerances. The fundamental difference between a conventional brickwork and the developed glass masonry system is that a standard mortar layer compensates for deviations in the size of the bricks, while the selected adhesive cannot; this leads to a meticulous and strictly controlled building process.

In this direction, different envelope geometries can enhance the rigidity of the structure, allowing for thicker, more elastic adhesives and correspondingly for larger tolerances in the brick units. A good example on this direction is the *Atocha Memorial*, where the elliptical, almost cylindrical, shape of the adhesively-bonded structure allowed for a less rigid adhesive of 2 mm thickness (Goppert et al. 2008).

In another direction, the development of a casting method of glass units of higher accuracy without the need of post-processing would significantly facilitate the entire production and building process, enhance the structural and architectural result and reduce the corresponding manufacturing costs.

Likewise, the choice of glass recipe plays a crucial role in the total annealing time and in the scale of resulting natural shrinkage. Although a faster and more accurate casting process can be achieved with borosilicate glass instead of soda-lime, the total manufacturing cost and dimensional precision prerequisites should be considered prior to the glass recipe choice.

Another important aspect to be addressed is the permanent nature of an adhesively bonded glass structure. As described in Chapter 5, *DP 4468* has no known solvent besides heat, rendering the structure irreversible. In turn, this means that the blocks cannot be retrieved intact at the end-of-life of the building, nor can they be easily recycled due to adhesive contamination. Taking into account the global drive

towards circularity, it is crucial to further investigate the development of solid glass block systems that can be reversible, and thus, reusable and recyclable.

Lastly, glass casting can provide the designer with a great freedom in the shapes and sizes of the building component. Owing to the architectural concept of the *Crystal Houses* façade, it was determined that the glass block unit should follow the geometry of the original masonry bricks. Nonetheless, the rectangular geometry of the blocks is not compatible with casting as a manufacturing process – as discussed in chapter 2.4 sharp edges result to uneven cooling rate and concentration of residual stresses. In view of that the choice of shapes that follow more organic, curvy shapes is highly recommended for future applications.



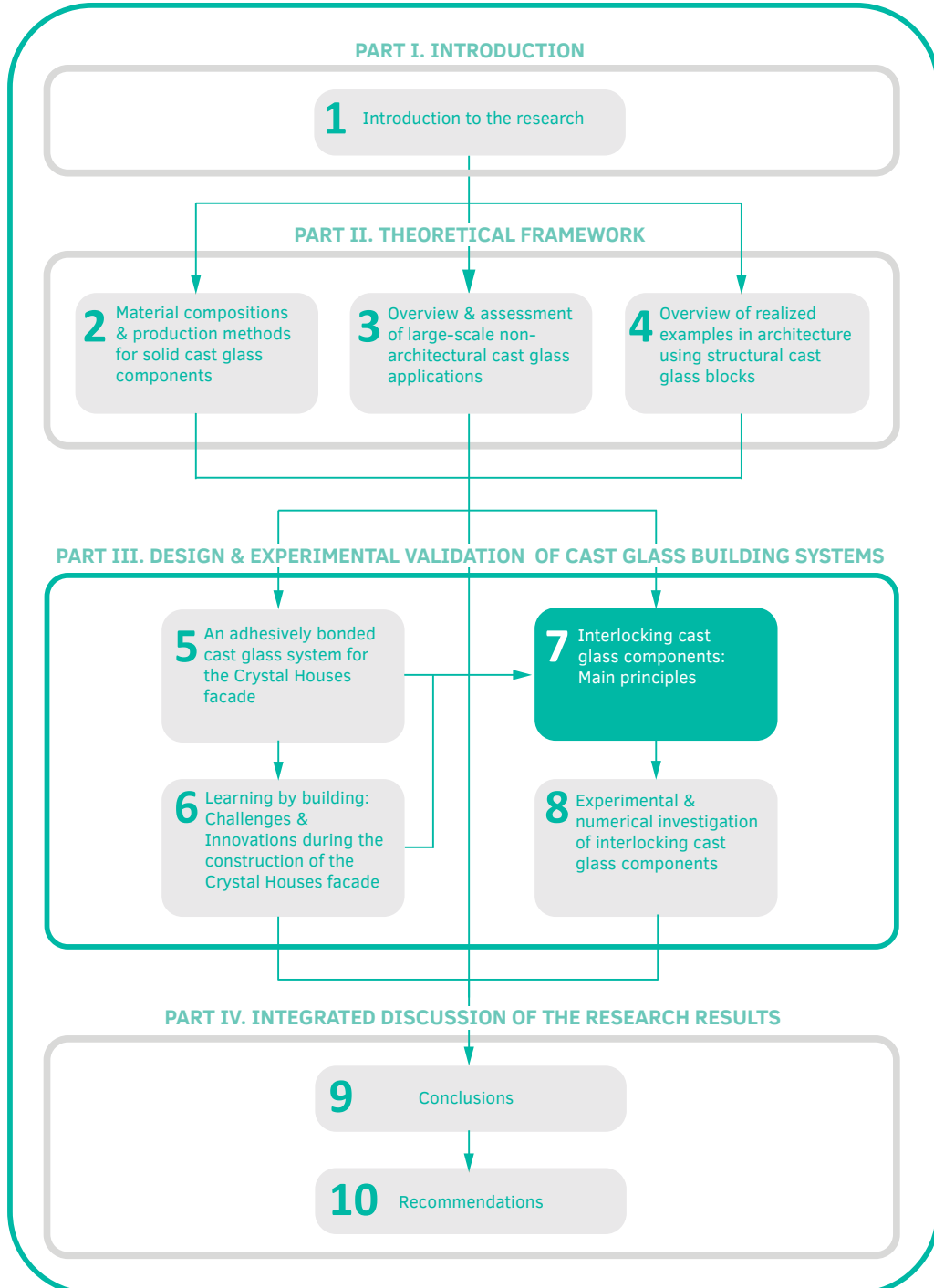
Interlocking cast glass prototypes made of recycled art glass at the *Glass & Transparency Lab* of TU Delft.

Interlock [verb]

(of two or more things) Engage with each other by overlapping or by the fitting together of projections and recesses.

Definition by the Oxford English Dictionary

Exploring the third dimension of glass



Solid cast glass components and assemblies for structural applications

7 Interlocking cast glass components: Main principles

In this chapter⁵⁶ a novel, reversible all-glass system consisting of dry-assembly, interlocking cast glass components is introduced that can tackle the irreversibility, strict tolerances and meticulous construction process of the adhesively bonded system presented in Chapters 5 and 6. Thanks to the interlocking geometry, the proposed system can attain the desired stiffness with the aid of minimal, if any, metal framing. The integrity and structural stability of the assembly is provided by the shape and the arrangement of the blocks themselves. The use of adhesives is obviated in the system by employing a dry, colourless interlayer as an intermediate medium between the glass components. The deformation of the interlayer can compensate for surface asperities and dimensional tolerances, allowing for an even stress distribution. Moreover, the dry-assembly enables the structure to be dis- and reassembled, which is critical for a circular economy in the built environment. Accordingly, this chapter lists the key considerations and establishes the design criteria for the development of interlocking cast glass structures. Based on the established criteria, various component geometries, forms and interlocking mechanisms are developed. The interlocking forms are kiln cast in 1:2 scale and are comparatively assessed in terms of mechanical interlocking capacity, mass distribution, residual stress generation and ease of fabrication. In parallel, a literature research is conducted on different materials for the dry, transparent interlayer, concluding that interlayers of the polyurethane family (PU and TPU) present the highest potential for a building application. From the developed designs, osteomorphic blocks are selected as the most promising concept to be further investigated.

⁵⁶ This chapter has been partially published as: Oikonomopoulou F., Bristogianni T., Barou L., Veer F., Nijse R. Interlocking cast glass components. Exploring a demountable, dry-assembly structural cast glass system. HERON 63 (1/2), 2018.

Credits

Research Initiators

- Telesilla Bristogianni,
Faculty of Civil Engineering & Geosciences, TU Delft
- Faidra Oikonomopoulou,
Faculty of Architecture & The Built Environment, TU Delft

Contribution to the interlocking designs

- Telesilla Bristogianni,
Faculty of Civil Engineering & Geosciences, TU Delft
- Lida Barou,
Faculty of Civil Engineering & Geosciences, TU Delft
- Giulia Frigo,
Politecnico di Milano
- Erwin Jacobs,
Faculty of Civil Engineering & Geosciences, TU Delft

Assistance in prototype manufacturing

- Telesilla Bristogianni,
Faculty of Civil Engineering & Geosciences, TU Delft
- Tommaso Venturini,
Faculty of Civil Engineering & Geosciences, TU Delft
- Jiyong Lee,
School of Art & Design, Southern Illinois University (SIU)
- Katherine Rutecki,
School of Art & Design, Southern Illinois University (SIU)

Research on recycling of glass waste in collaboration with

- Telesilla Bristogianni,
Faculty of Civil Engineering & Geosciences, TU Delft

Manufacturing Facilities

- Stevin II Laboratory,
Faculty of Civil Engineering & Geosciences, TU Delft
- Kiln working studio & Cold Working studio
School of Art & Design, Southern Illinois University (SIU)

The research work presented in this chapter has been partly funded by a 4TU.bouw Lighthouse grant for the project Re³ Glass

7.1 Introduction

The development of an adhesively-bonded glass block system, presented in the previous two chapters, highlighted the potential of cast glass for attaining all-glass structures. The real application of the developed system at the *Crystal Houses* façade further proved its feasibility but also revealed its inherent engineering challenges. These were strongly linked to the extreme dimensional accuracy required for achieving an adhesively-bonded transparent structure of satisfactory visual and structural performance. Furthermore, the permanent bonding of the blocks by the adhesive resulted in an irreversible structure that cannot be easily recycled. Taking the above aspects into account, in this chapter a new system out of dry-stacked interlocking cast glass components is introduced that avoids the use of adhesives and allows for a reversible structure: the components can be retrieved intact to be either reused or recycled. The proposed system attains the desired stiffness and stability mainly through its interlocking geometry and its boundary conditions. A flexible dry-interlayer is used to compensate for dimensional discrepancies and surface micro-asperities, allowing for a homogeneous load distribution between the components and an easy assembly and disassembly process. Concerning the casting manufacturing process and the annealing principles of solid cast glass components, geometries that follow more organic and curved shapes are proposed. The definition and principles of interlocking structures in architecture are presented in section 7.3. Thereafter, section 7.4 discusses the establishment of design criteria for such a system based on both the interlocking principles and glass casting as a manufacturing process. Based on these criteria, in section 7.5 the development and prototype manufacturing of different interlocking designs is presented. Section 7.6 presents a literature research on different interlayer materials. Finally section 7.7 discusses the circular use of glass and conclusions are withdrawn in section 7.8.

7.2 Methodology

Cast glass interlocking components have been little explored in the past, without, so far, a consistent establishment of design criteria. Hence, initially a series of design criteria are established in respect to the principles of interlocking, the casting process and the properties of glass. Based on these criteria, different component

geometries are developed. Prototypes of the proposed designs are kiln-cast in 1:2 scale and are qualitatively assessed in terms of mechanical interlocking capacity, mass distribution, generation of residual stresses and ease of fabrication. In parallel, literature research is conducted on different materials for the dry, transparent interlayer. Based on the above, the most promising interlocking shapes and colourless interlayer material are selected for further investigation.

7.3 Definition and mechanical principles of interlocking structures in architecture

7.3.1 Definition

An interlocking (mortar-free) system consists of -often identical- components whose geometrical shape and mutual arrangement provide the kinematic constraint and therefore stability of the structure in one or two directions, typically the one normal to the assembly plane and its transverse. The whole assembly is stabilized by compressive forces; at times, even the self-weight of the construction is sufficient for this purpose (e.g. Inca walls). In such mortar-free systems, the only factors that hold the components in place are weight and friction (Dyskin et al. 2012). Interlocking can be achieved by providing the building blocks with locking “keys” – a well-known example is the *LEGO*® brick. Such keys can, however, become stress concentrators – especially for cast glass units- that may compromise the overall strength of the structure. A relatively new approach for interlocking structures is the one of topological interlocking, introduced by (Dyskin et al. 2001). In this concept, the blocks follow a geometry of concave and convex surfaces allowing them to establish self-locking whilst remaining free of stress concentrations. The distinctive feature of topological interlocking is that, not only in-plane, but also out-of-plane movement of a block is prevented by its neighbours, without the need of connectors or binders (Djumas et al. 2016), i.e. the form of the blocks provides an inherently stable assembly. Fig. 7.1 illustrates the main mechanical principle of interlocking and topological interlocking systems.

The concept of dry-stacked, interlocking, compressive structures is not new in architecture. Ancient Greeks had developed ingenious dry-stacked, self-aligned

systems in the marble column drums of the classic temples. An example of this practice can be found in the columns of the Parthenon, where the marble column drums are self-aligned with wooden pins that lock into recesses carved into both bases of each drum (Korres 2000). Incan dry stone walls (Fig. 7.2) made by irregularly shaped interlocking stone polygons allowed for stable, self-aligned, mortar-free structures with high seismic resistance. Roman arches and Japanese wood joinery are other established examples of interlocking engineering.

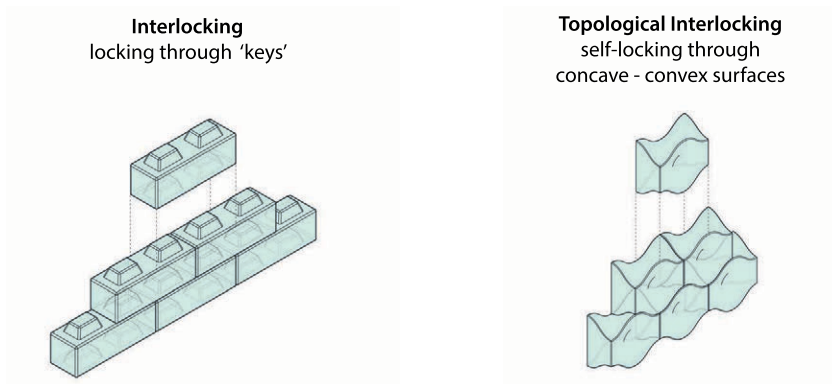


FIG. 7.1 Principle of interlocking and topological interlocking systems



FIG. 7.2 Interlocking wall made by the Incas at Ollantaytambo, Peru.

Owing to their segmented nature, interlocking structures offer several engineering advantages, especially for brittle materials like glass, such as high resistance to crack propagation and improved fractured toughness, tolerance to local failures, redundancy and reversibility. These benefits as well as the main mechanical principles of interlocking systems are briefly presented in the following sections.

7.3.2 **Enhanced resistance of the assembly against crack propagation**

The fragmented nature of interlocking, dry-assembled systems can lead to an enhanced redundancy against crack propagation. As the blocks are not bonded to each other, boundaries between them are a natural barrier to prevent crack propagation. Hence, in contrast to a monolithic structure, failure of individual blocks does not lead to overall failure. Cracks are thus confined within a block's mass and do not spread among adjacent elements, increasing the effective fracture toughness.

Enhanced stability is also achieved by the ability of the units to undergo small relative displacements within the structure. Such displacements provide the segmented assembly with a degree of flexibility – *a desirable property that effectively transforms rigid and brittle materials to compliant and ductile ones* (Dyskin et al. 2019). This is particularly important in seismic zones as the interlocking structures are able to dissipate the vibrational energy (Estrin et al. 2011). Compared to a mortar masonry wall, which would act monolithically against loading, a dry interlock wall allows for the resettlement of the building blocks, transforming part of the seismic load to kinetic and frictional energy.

7.3.3 **Improved mechanical properties due to inverse scale effect**

Based on the inverse scale effect, which states that the strength of a solid –especially of a brittle one like glass– is reduced as its size increases, a segmented solid may possess mechanical properties superior to those of a monolithic body (Ashby, Brechet 2003). In other words, the chances that each component in the assembly has a critical weakness or flaw are less compared to a component of the size of the total assembly. The idea is that, even if one block has a critical flaw that causes it to crack, the cracks do not propagate into the rest of the structure since no rigid connections such as adhesives are used. The failed block stays in place due to the interlocking geometry and the overall structure does not lose its integrity;

due to its built-in redundancy it can continue to be loadbearing. This is particularly interesting for a glass structure: owing to the segmented nature of an interlocking assembly, the dimensioning and engineering of such a structure based on the possible occurrence of critical flaws can be avoided, leading to a comparably more slender solution.

7.3.4 Redundancy - tolerance to missing components

Interlocking structures can present an inherent level of redundancy. Experimental testing by (Molotnikov et al. 2007) and numerical simulations by (Estrin et al. 2004) have demonstrated that in given interlocking geometries, a planar assembly maintains its integrity even after the random removal of elements: Even if several of the units fail, the rest are kept in place by the kinematic constraint from the adjoining blocks⁵⁷, allowing the assembly to maintain its integrity. Experimental work by (Dyskin et al. 2003; Khor et al. 2002; Khor et al. 2004; Dyskin et al. 2005; Dyskin et al. 2008) at topologically interlocking assemblies demonstrated that failure of the interlocking assembly is localized: only a small group of elements failed and the assembly could maintain its structural integrity. In contrast, in a monolithic variant, the crack would propagate to the entire surface impairing its structural integrity.

7.3.5 Out-of-plane behaviour

The out-of-plane deformation of plate-like topologically interlocking assemblies, made of either tetrahedral or osteomorphic blocks of brittle materials has been experimentally investigated by *Dyskin* and his research group (Dyskin et al. 2003; Khor et al. 2002; Khor et al. 2004; Dyskin et al. 2005; Dyskin et al. 2008) by applying indentation to the centre of the plate, held and constrained at the periphery. The results suggest that such a system presents a lower bending stiffness compared to a monolithic variant. This is due to the freedom of the blocks to rotate under bending, continually decreasing the contact area in the course of loading. The only moment counteracting this phenomenon comes from the constraint force imposed by the peripheral structure. The tested assemblies also presented a noticeably lower bearing capacity. On the other hand, the interlocking assemblies could sustain

⁵⁷ This principle is relevant to the specifics of the block shape and the pattern of assembly and is not valid for all interlocking geometries. E.g. in a roman arch, if the key component fails, the arch will collapse.

considerably higher deflections before failure, compared to a monolithic variant of the same thickness. This allows an assembly made of brittle components to behave as a pseudo-ductile structure: visible deformation can provide a warning mechanism prior to failure, thus increasing the safety of the structure.

7.3.6 Buildability and Reversibility

An interlocking system can provide a multifunctional, easily assembled and disassembled (reversible) structure, provided that a removable sealing can be applied to protect the structure from weathering. The self-aligning nature of such structures allows blocks to fit into each other without adjustment, increasing the construction productivity and the resulting quality of the assembly. Reversibility is one of the pivotal aspects for applying an interlocking system to cast glass structures. According to research made by (Eurostat 2014), glass waste is currently the second largest waste material in the European Union, even though it can be endlessly reused and recycled – provided that it is kept free of contaminants, including adhesives or coatings. A dry-assembly, reversible interlocking system promotes the dismantling of the assembly and the reusability of the components since they can be retrieved intact. Moreover, the absence of an adhesive bonding and thus, of contamination, further facilitates the recycling of the components.

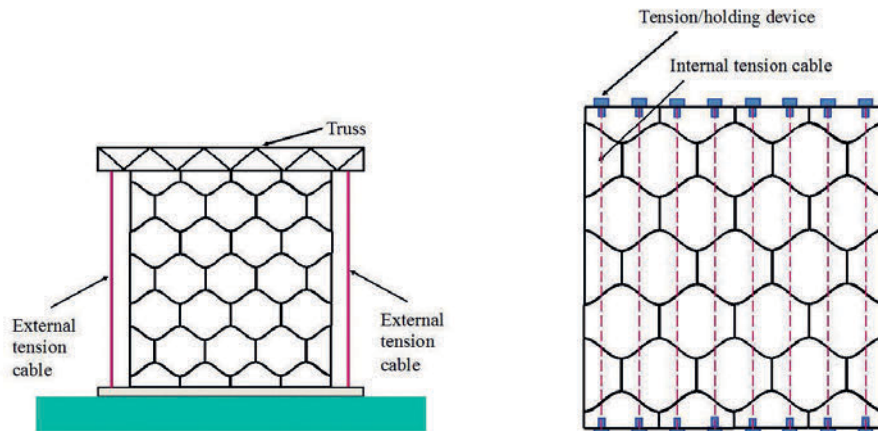


FIG. 7.3 Proposed type of peripheral constraint by (Dyskin et al. 2019). Left: lateral constraint imposed by a specially built frame. Right: constraint produced by internal tensioned cables

7.3.7 Global constraint

(Dyskin et al. 2019) states that a global constraint is essential to maintain the integrity of the overall structure. One solution is the installation of a frame which also allows the tuning of the bending stiffness of the structure by applying a controlled pre-compression through the frame. A more elegant solution is the installation of tensioning cables threaded through the assembly (Estrin et al. 2009; Zareiyan, Khoshnevis 2017) (see fig. 7.3). By varying the magnitude of the compressive pre-load imposed on the structure through the cables its bending rigidity can be controlled in a broad range, from that of a stiff plate to that of a rollable compliant matt.

7.3.8 Use of soft interlayer as intermediary

The mechanical properties of interlocking assemblies out of brittle materials (such as glass) can be further improved if the interlocking components are interleaved with a soft, rubber-like polymer (Estrin et al. 2015). (Dyskin et al. 2001) suggests that a soft interlayer or binder between the interlocking elements can improve ductility and enhance the fracture toughness of the resulting assembly via energy absorption. A soft interlayer can prevent crack propagation due to local peak stresses generated from micro-asperities at the surface of adjacent elements. It can also stop propagating cracks induced e.g. by impact and prevent them for spreading into the adjacent blocks, increasing the local strength of the assembly and its impact resistance.

7.4 Establishment of design criteria

So far, interlocking systems out of cast glass components have been little explored, principally within the academic world. A realized application of the system does not yet exist. In 2015, on the initiative of the *Glass & Transparency* group and with major involvement of the author, several interlocking systems made of cast glass were explored. As an example (Akerboom 2016) has proposed a design for an interlocking cast glass column, whereas (Barou et al. 2016; Frigo 2017; Jacobs 2017), have developed alternative interlocking glass block systems that restrain both planar

directions for the transparent and reversible restoration of historic monuments (Fig. 7.4). (Aurik 2017; Snijder et al. 2016) have studied the concept of a dry-assembled arched glass masonry bridge where an interlocking mechanism is achieved along the longitudinal direction.

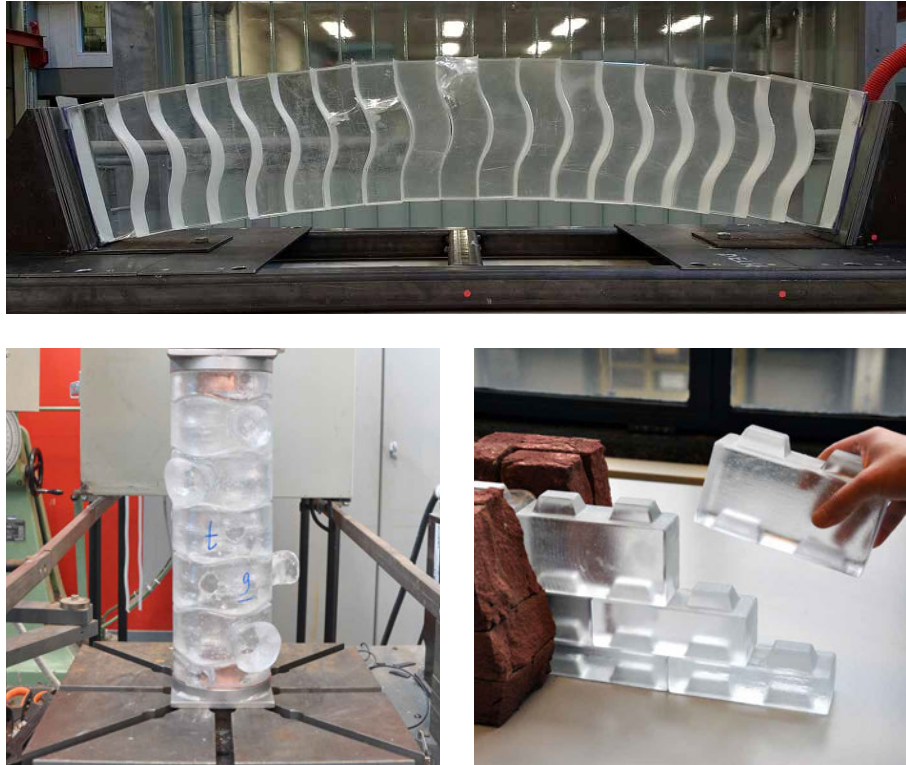


FIG. 7.4 Interlocking glass block systems currently explored. Top: Tested prototype of the glass arch bridge by (Snijder et al. 2016). Bottom left: Glass column by (Akerboom 2016). Bottom right: Interlocking glass wall system developed by Oikonomopoulou, Bristogianni and Barou for the *3TU.bouw* project *Restorative Glass*, presented in (Oikonomopoulou et al. 2017a).

To this end, a thorough establishment of design criteria for interlocking cast glass structures in respect to the casting process and the nature of the material has yet to be made. Dry-stack masonry systems already exist in various materials, such as wood and stone. Given that such systems have been developed considering different manufacturing and material properties it would not be sensible to adapt the existing interlocking geometries to glass. For that reason, a series of design criteria are established for the cast glass components taking into account the principles of

existing interlocking systems but adapted to fit the characteristics and peculiarities of cast glass as a construction material. These requirements are thus divided into criteria for the establishment of interlocking and criteria imposed by glass as a material and by casting as a manufacturing process.

7.4.1 **Design criteria related to interlocking principles**

Based on the principles of interlocking, the designed units should fulfil the following criteria (Fig. 7.5):

Movement confinement in both longitudinal and transverse direction

To enhance the monolithic behaviour of the assembly and ensure the desired stiffness of the structure against lateral forces, the interlocking system should confine both planar direction movements. In the case of compressive structures, i.e. the ones discussed in this paper, restraint in the third axial (z) direction can be achieved by the self-weight of the construction in combination with an external constraining frame.

Optimizing shear capacity

Interlocks following smooth convex curvatures, such as in topological interlocking, are preferred as they allow for a relatively even distribution of the shear forces occurring at the interface area. Due to the unforgiving nature of glass, traditional connectors or keys that are of a considerably smaller cross-sectional area compared to the gross cross-sectional area should be avoided as they result in concentrated stresses that can lead to premature failure.

Self-alignment

The interlocking mechanism should promote the self-alignment of the units, allowing for a relatively easy and fast construction of high quality. According to (Dyskin et al. 2003), convex contact areas exhibit good self-adjusting properties and also lead to reduced stress concentrations.

Multi-functionality

Towards multi-functionality, a unit geometry that permits multiple configurations of stacking is preferred.

7.4.2 Design criteria related to glass casting

Limited volume

The meticulous and excessively time-consuming annealing process of cast glass can jeopardize the marketability of the components and render them financially unaffordable (Oikonomopoulou et al. 2015a). The mass of the glass component is the most critical aspect. The larger the component, the exponentially longer the annealing time. Hence, for this research, solid cast glass elements are designed within a 10 kg mass limitation and roughly corresponding to the size range of standard masonry units.

Rounded shape and equal mass distribution

A rounded shape and an equal mass distribution are key aspects for the prevention of concentrated residual stresses during annealing. Curved, convex geometries are favoured over sharp, pointy edges where internal residual stresses can occur due to inhomogeneous shrinkage⁵⁸. To this end, an equal cross-sectional area throughout the unit, allows it to gradually cool down uniformly, further preventing the generation of residual stresses. Subsequently, projections such as small connectors or notches should be avoided.

Limited number of different units

A repetitive component geometry is preferred towards facilitating the production and assembly of the structure and limiting the associated manufacturing costs. Specifically, assembly becomes easier as each unit can take any place in the

⁵⁸ Edges cool faster due to exposure in cooling from multiple sides. In comparison, the core cools relatively slower, creating residual stresses at the edges due to this differential shrinkage. In this context, ellipsoid shapes are favourable as they allow for homogeneous cooling and correspondingly to an even shrinkage rate.

structure, instead of predefined locations as is the case with systems featuring multiple geometries, such as the Incan walls. Moreover, a single geometry results in a decreased number of moulds and a standardized production process. Given the above, a single geometry is favoured but configurations with a limited number of different components could also be cost-effective.

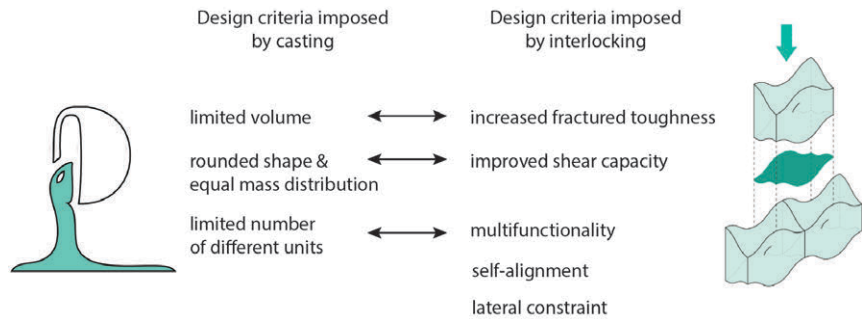


FIG. 7.5 Overview of the established design criteria. The double arrows indicate the alignment between the two different sets of criteria, due to casting and due to interlocking

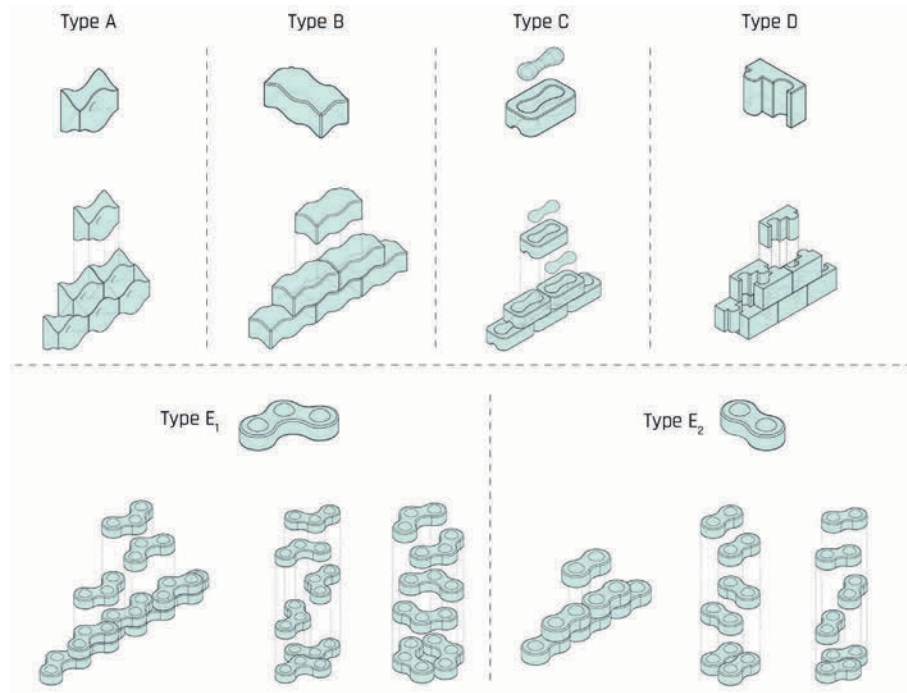


FIG. 7.6 Developed interlocking designs

7.5 Interlocking designs and prototypes

Based on the above criteria, several alternative interlocking designs are developed to explore the potential of different interlocking mechanisms. The designs and block types can be seen in Fig. 7.6. Glass prototypes in 1:2 scale are manually produced using the kiln-cast method to comparatively assess the different designs in terms of mechanical interlocking capacity, mass distribution, generation of residual stresses and ease of fabrication. The manufactured prototypes can be seen in Fig. 7.10 – Fig. 7.13.

7.5.1 Prototype manufacturing

For the production of the components, disposable investment moulds are produced employing the *lost-wax technique*. A step-by-step process of the *lost-wax technique* can be seen in Fig. 7.7. In brief, the shape to be cast in glass is 3D-printed and a silicone mould is produced around it. Aim of this step is to use the silicone mould to obtain multiple wax models of the desired shape. Then, an investment casting slurry is poured around the wax model, in order to construct the heat-resistant mould for the glass casting. The investment casting slurry used is *Crystalcast M248* – a powder mixture of Cristobalite, Quartz and Gypsum with a stated maximum service temperature of 900°C (SRS, 2003). After the mould is hardened, the wax is removed by steaming, and the mould is thoroughly cleaned and dried before being used for casting. Terracotta flowerpots, placed above the moulds, are employed for feeding the molten glass (see Fig. 7.8 and Fig. 7.9). After the kiln-casting is complete, the moulds are immersed into water to facilitate their removal.

To address the issue of recyclability⁵⁹, various different waste glass families are used for the production of this series of visual prototypes. These include lead crystal, several soda-lime types (mouth-blown, machine-blown, float) and alkali-barium silicate. The opaque or coloured prototypes presented in the following chapter are the result of these recycling experimentations.

⁵⁹ Using waste glass for the production of safe structural cast glass components is out of the scope of this work, yet a crucial topic of research for the author. The results of this ongoing research are published by (Bristogianni et al. 2018a).



FIG. 7.7 Step-by-step process of the lost wax technique employed for the casting of the prototypes.

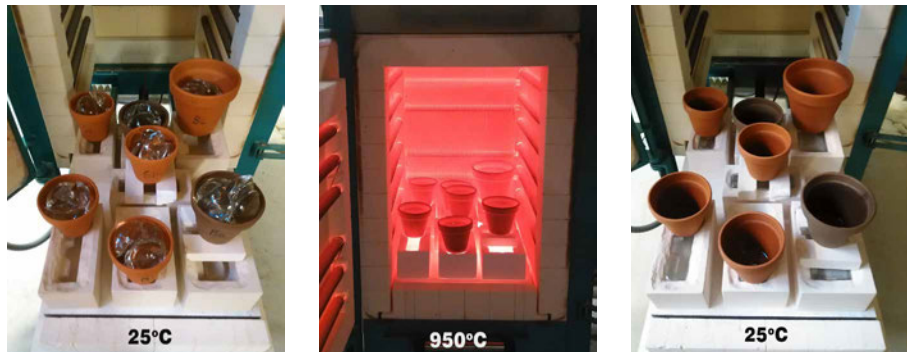


FIG. 7.8 Kiln-casting method employed at the lab for the casting of prototypes.

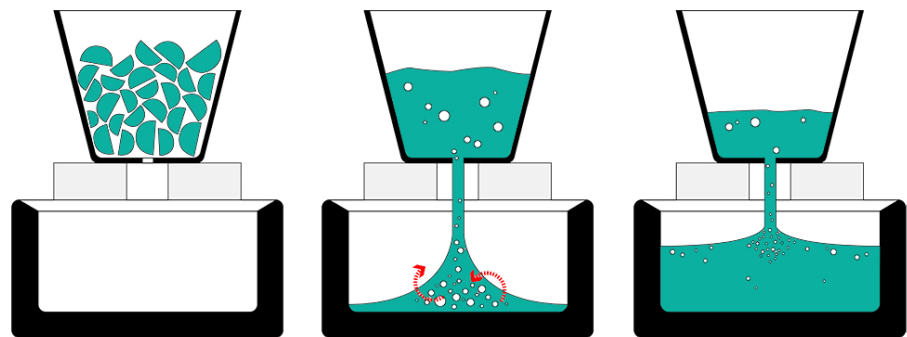


FIG. 7.9 Illustration of the kiln-casting method employed to manufacture the glass interlocking prototypes.

Types A & B: Osteomorphic (topologically interlocking) blocks

Type A and B blocks (Fig. 7.10) follow an osteomorphic geometry as defined by (Dyskin et al. 2003). These shapes have been engineered with non-planar concavo-convex surfaces. The convex parts of the surface of one element match the concave parts of the other and vice versa. In this way, relative movements in both planar directions are impeded, provided that the assembly is constrained at the periphery. A benefit of the osteomorphic shapes is, given that the contact surfaces are sufficiently smooth, the generation of mild stress concentrations compared to the ones produced by conventional interlocking connectors or keys (Dyskin et al. 2003). In the developed designs, the symmetry of the interlocking unit in the x and y axis allows the use of the same component parallel or perpendicular to the one placed below. Thus, corners at right angles can be easily obtained with the same block unit. The assembly of the structure can be easily realised by stacking the blocks on top of each other. Only the blocks on the periphery need to be separately constrained.



FIG. 7.10 Osteomorphic blocks. Left: Type A. Right: Type B

Type C: Two-component interlock

In this system interlocking is achieved through matching male and female components. This design provides more freedom in terms of material use and visual aesthetics. For example, components of one group can be made of glass while the ones of the other can be made of another material, e.g. metal, plastic or coloured glass as shown in Fig. 7.11. Materials can also be selected to match the stress distribution of the system; it is anticipated that stresses will not be evenly distributed in both components due to the difference in geometry. Annealing is considered to

be homogeneous for the bone-shaped component because of its relatively even mass distribution and ellipsoid ends. The block-shaped component requires a precise annealing cycle to prevent internal residual stresses due to its relatively inhomogeneous cross-section (solid in the middle, with cavities at the edges). This design does not allow for the creation of corners in the structure with the same elements, due to the block's non-symmetrical interlock in the transverse direction, calling for the design of additional elements. A peripheral constraint is to stabilize the structure.



FIG. 7.11 Type C Prototype. The bone-shaped components are made of recycled coloured glass.

Type D: Puzzle brick

This design follows a different interlocking mechanism than the ones previously described: here, the components slide vertically to each other. In particular, the components are positioned halfway in height and width in relation to their adjusting components (Fig. 7.12). In this fashion, continuous joint lines -weak zones susceptible to stress concentrations- are prevented. Compared to the aforementioned interlocking mechanisms, this system restricts the self-alignment of the bricks in both planar directions and thus, decreases its damping properties. In addition, the relatively complex shape of this unit may result in internal residual stresses during the annealing of the cast element, as well as local stress concentrations during loading. As with type C, due to the unit's asymmetrical interlocking mechanism, corners employing the same component cannot be achieved in the structure.



FIG. 7.12 Type D prototype made of clear glass, recycled float glass (teal) and recycled Cathode Ray Tube (CRT) screen (black).

Type E: Rotational brick

The almost semi-spherical key of this geometry provides further flexibility in the form of the overall assembly compared to the previous solutions. As an example, the same module can be used to make either planar or cylindrical structures. The two different block types (E1 and E2) can also be combined together to create one structure (Fig. 7.13). The curved geometry of these block types can guarantee a satisfactory homogeneous annealing. However, the considerable projections of the semi-spherical connections may result in local shear stress concentrations during loading.



FIG. 7.13 Prototype using E1 and E2 glass blocks from clear glass and recycled mouth-blown coloured glass.

7.5.3 Assessment and selection of interlocking topology

A comparative assessment of the five interlocking designs can be seen in Table 7.1.

TABLE 7.1 Comparative assessment of the different interlocking block types based on the established design criteria

Block type	A	B	C	D	E
					
Interlocking mechanism	smooth curves	smooth curves	male and female blocks	sliding blocks – intense curves	semi-sphere keys for vertical stacking – ability to rotate
Shear capacity	high	high	moderate	moderate	moderate to high
Self-alignment	high	high	high	low	high
Multifunctionality	high	high	moderate	moderate	high
Equal mass distribution/homogeneous annealing	effective	effective	risk of internal residual stresses	risk of internal residual stresses	effective
Lim. number of dif. units/Ease of assembly	high	high	moderate	moderate	high

Out of the established designs the osteomorphic blocks (types A, B) are considered to be the most promising elements for further development due to their multi-functionality, ease of assembly and ability to prevent peak stress concentrations, both during the manufacturing process and during loading. The smooth curves and even mass distribution of the components allow for their homogeneous annealing preventing the generation of internal residual stresses. The smooth concave-convex interlocking mechanism of the elements ensures its high shear capacity as well. Even though stress concentrations may occur in the concave parts of the surfaces upon loading, these are likely to be small compared to the simultaneous stress concentrations in the small keys or connectors (Dyskin et al. 2003). The system also has high damping properties: restricted movements of the blocks relative to each other are still possible, allowing for self-alignment and dissipation of energy in case of seismic loading. Moreover, the inherent redundancy of an assembly made by this type of blocks has been proved before by (Dyskin et al. 2003). Such a system is highly tolerant to local failures; it has been demonstrated that after the collapse of random blocks the structure can resist by percolation of damage until nearly 25% of block failure. Lastly, in terms of multi-functionality, the symmetry of the developed osteomorphic blocks in both planar directions enables their assembly in

configurations with 90° rotations, allowing, for example, the construction of columns and wall corners (Fig. 7.14 and Fig. 7.15). Half-blocks are necessary to finish the edge of the structure.

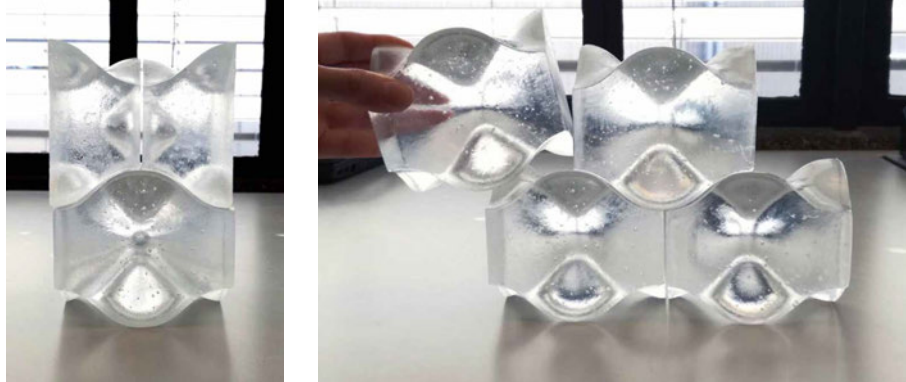


FIG. 7.14 Possible structural geometries using osteomorphic blocks (Type A).



FIG. 7.15 Prototype with osteomorphic blocks made using various types of waste glass, exhibited at the Dutch Design Week 2018

7.6 Properties of dry-interlayer

Due to the inability of glass to deform plastically, any unevenness at the contact surface of the components will result in high local tensile stresses, even when the interlocking glass structure is loaded in compression. The brittle nature of glass can respond to such peak stresses with crack initiation and propagation, compromising the overall strength of the interlocking assembly. This has been well demonstrated by the results of axial compressive tests performed on soda-lime cast glass blocks by (Oikonomopoulou et al. 2015b) described in section 5.6.1. Solid cast components tested in compression presented obvious cracks in a nominal compressive stress between 20 – 30 MPa, when the glass came in direct contact with the steel surfaces of the testing machine. In comparison, specimens where a softer intermediary was used, presented a considerably higher nominal compressive strength, of at least 135 MPa.

Accordingly, a resilient (dry) interlayer between the glass blocks is essential for their structural application. The interlayer can accommodate surface asperities by deformation – escaping thus the need for post-processing of the glass units- and can evenly redistribute the stresses on the contact area. Indeed, (Dyskin et al. 2001) and (Estrin et al. 2015) confirm that the mechanical properties of interlocking assemblies out of brittle components can be improved if the interlocking components are interleaved with soft, rubber-like polymers: a soft interlayer between the interlocking elements improves the ductility and the fracture toughness of the assembly via energy absorption. A soft interlayer not only prevents crack propagation due to local peak stresses generated from micro-asperities at the surface of adjacent elements; but it can also stop further spreading of cracks into adjacent blocks (e.g. by impact), increasing the local strength of the assembly and its overall impact resistance.

For a contact application such as the one examined, the hardness⁶⁰ of the interlayer is considered the most significant parameter for choosing the material. To allow for an even load distribution, it is crucial that the interlayer material is neither too flexible nor too stiff. The hardness of the interlayer material should be high enough to avoid penetration, yet sufficiently low so that the material can adapt to the micro-asperities of the glass surface. For common polymer and rubber materials the hardness is expressed through the Shore hardness scale, which essentially measures

⁶⁰ Unlike the Young's Modulus, hardness shows size dependence in materials with near surface hardness being different from bulk hardness.

the resistance of a material to indentation. The Shore A scale measures a wide range of materials, from very soft and flexible to semi-rigid ones without almost any flexibility. The Shore D scale refers to very hard rubbers, semi-rigid and rigid plastics. Fig. 7.16 provides an illustration of the two shore hardness scales, indicating as well the shore scale of common applications and the existing overlap between the two scales.

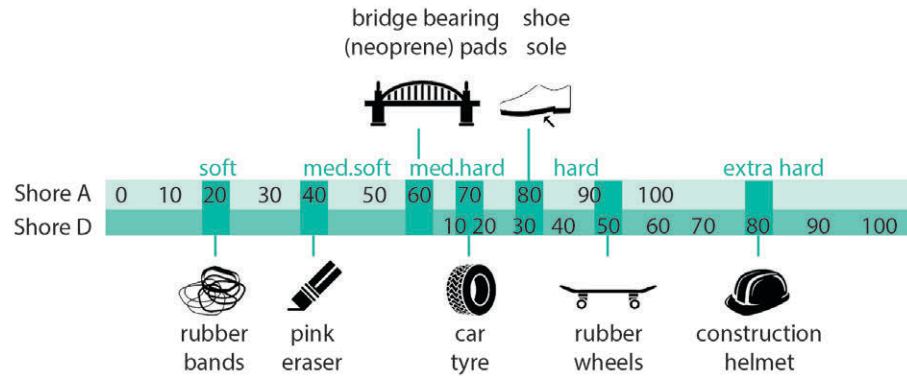


FIG. 7.16 Diagram of the shore hardness scales, including an indication of the shore hardness of common objects

Based on the common applications presented in Fig. 7.16 an interlayer material with a shore hardness between 60A – 80A (30D) was selected for further experimentation for the discussed application. Interlayers softer than 60A were not chosen in this study due to the risk of easy perforation, nor interlayers with a shore hardness higher than 80A, as their higher stiffness would not easily allow for an even spread of the stresses by deformation and would not provide sufficient friction.

Another important factor is that the interlayer will be subject to constant compressive loads. Hence, it should be able to resist significant compressive stresses without significant creep. As a first estimation, the surfaces of the interlayer and glass should be in full contact before reaching an average compressive stress of 20 MPa, in order to prevent the early failure of the assembly, as suggested by the experimental work by (Oikonomopoulou et al. 2015b).

Finally, the material should be able to be shaped into the particular interlocking shapes of the glass blocks with an accurate and consistent thickness. In this direction, the interlayer's thickness plays a crucial role in the overall performance as well. A thickness of min. 3 mm is proposed to accommodate dimensional tolerances. In general, the interlayer material should be as thin as possible, as thicker interlayers

compromise the stiffness of the assembly. Moreover, thicker than necessary interlayers can induce eccentricity to the assembly due to external lateral forces that can skew the interlayer horizontally.

Adding to these properties, the following requirements are considered for the selection of the interlayer:

- Shore hardness between 60A to 80A.
- Compressive strength ≥ 20 MPa
- Good creep resistance and controlled deformation under static long-term compressive load
- Ability to be pre-formed in a consistent thickness (t_{int}) in the desired shapes
- $3 \text{ mm} \leq t_{int} \leq 6 \text{ mm}$
- Transparency and durability to UV-lighting
- Water resistant
- Service temperature between $-20 \text{ }^\circ\text{C}$ and $+50 \text{ }^\circ\text{C}$
- Slow-burning/self-extinguishing/non-flammable

According to *CES Edupack 2015* program (Granta Design Limited 2015) the following thermoplastic and elastomer polymers fulfil the above-mentioned criteria:

- PEBA – Polyether block amide
- PU - Polyurethane (rubber/cast)
- PVC – Polyvinyl Chloride (soft)
- TPU – Thermoplastic polyurethane

TABLE 7.2 Mean properties of the selected material families that fulfil the interlayer requirements by CES2015

Material	PEBA	PVC	PU	TPU
Design Compressive Strength [MPa]	41	25-30	48	61
Poisson's ratio	0.48	0.47	0.48	0.49
Yield Strength [MPa]	>34	>20	>50	>50
Transparency	clear	clear	clear	clear
UV-resistance	fair	fair	fair	fair
Flammability	Slow burning	Slow burning	Slow burning	Slow burning

These materials can be processed to the desired shape either by injection moulding or extrusion. The mean properties of the chosen material families can be seen in

Table 7.2. From these, PU, PVC and TPU have already been applied in the building industry and are considered the most promising candidates. Experimental work by (Aurik et al. 2018) on a vertical assembly of dry-stacked rectangular cast glass blocks with Polyvinyl chloride (PVC), Polyurethane 70 Shore A (PU70) and Polyurethane 90 Shore A (PU90) interlayers as intermediary, each tested in 1,2,3 and 4 mm thick variants, has indicated that:

- The thicker interlayer variants (3-4 mm) allow for a more homogeneous spread and an increased stiffness. Essentially the interlayer becomes stiffer as the contact area increases.
- Under compression, the PVC interlayers achieve a more homogeneous contact area compared to the PU ones, due to high lateral deformation of the material. PU interlayers behave as more stiff materials and do not spread so evenly upon pressure and thus are considered more sensitive to failure due to surface imperfections than PVC. PU90, which is the stiffest material, does not achieve full contact with the glass surface. The thicker variants of PU70 present an almost complete contact area under pressure.
- The Young's Modulus of PVC is strongly time-dependent and creep occurs under static loads. PVC interlayers of 3 and 4 mm thickness were flowing out of the edge during compression. On the contrary, the PU interlayer variants remain relatively stable over time.
- After removing the load, the residual deformation of the PVC interlayer remains considerable, whereas PU interlayers recover relatively quick.

TABLE 7.3 Material properties used by (Aurik et al. 2018)

Property	Unit	PVC	PU70	PU90
Shore-hardness	Shore A	80 (± 5)	70 (± 5)	90 (± 5)
Tensile resistance	N/mm ²	16	≥ 40	≥ 45
Elongation at break	%	340	≥ 550	≥ 575

Although in the specific tests, PVC achieves a more homogeneous and consistent contact area than PU, it is considered unsuitable for this research due to its creep under pressure, resulting to a constantly decreasing Young's Modulus (Aurik et al. 2018). Moreover, based on Table 7.2, PVC presents a marginally acceptable design compressive strength and a relatively low yield strength.

As a compromise, for this research it is concluded that a PU interlayer is most fitting. Despite the fact that the tested PU specimens showed a comparatively non-homogeneous load distribution, they exhibited satisfactory creep-resistance and stable stiffness.

According to the experimental work by (Aurik et al. 2018) and the established design criteria, a thickness of 3 mm seems to be an optimum, for allowing for a consistent contact area while absorbing surface irregularities. It should be noted that this minimum acceptable interlayer thickness is preferred over thicker variants that can further compromise the stiffness of the interlocking assembly.

Lastly, PU interlayers with a shore hardness between 60A - 80A are considered to be the best candidates, as stiffer interlayers fail to achieve complete contact under pressure even with flat glass surfaces as follows from (Aurik et al. 2018).



FIG. 7.17 Cast PU interlayer following the osteomorphic geometry of the cast blocks.

7.7 Potential for a circular use of glass and recycling of glass waste

7.7.1 Reversibility of the structure and reuse of the components

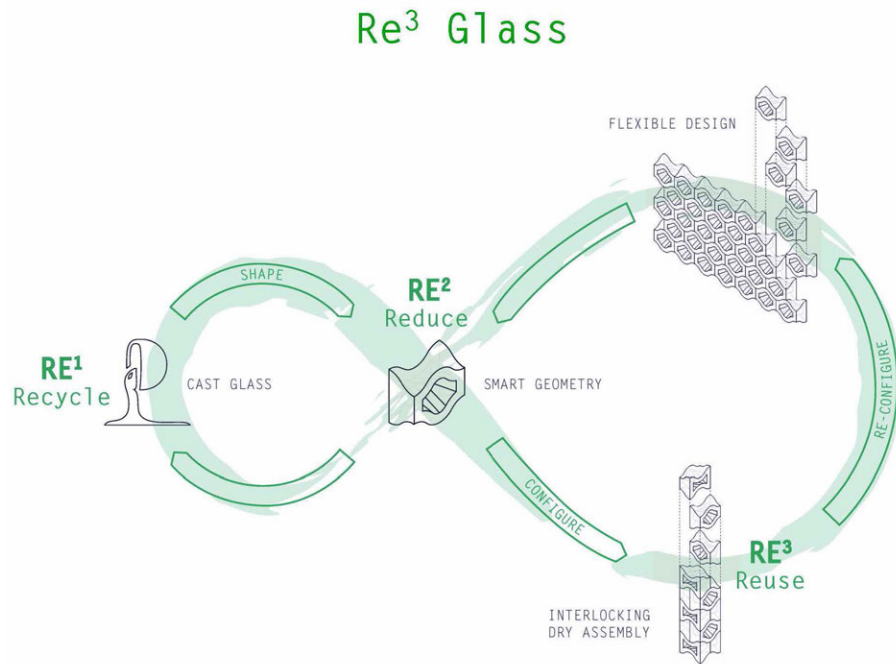


FIG. 7.18 Principle of circular use of glass in dry-assembled interlocking structures by the *Re³ Glass* project.

As already mentioned, the reversibility of interlocking cast glass structures presents major advantages in the reuse and (eventual) recyclability of glass components. This attribute in combination with the use of waste glass as raw material allows for the design of a circular glass building system, as this was co-developed, and co-initiated

by the author of this dissertation, for the *Re³ Glass* project⁶¹ (Fig. 7.18). The *Re³ Glass* strategy focuses on the recycling of discarded glass into cast interlocking structural components such as the ones discussed in this chapter. Owing to their interlocking geometry, the components allow for the easy assembly and eventual disassembly of the glass structure. Accordingly, the reuse of the components in other architectural or interior applications is facilitated. Eventually, the components, if not reused, can be recycled⁶² as they are not contaminated by adhesives or coatings. It should be noted here that to attain a weather- and dust- proof structure, the sealing of the external joints of the interlocking assembly is considered necessary. This can be achieved by a silicone sealant that can be easily removed (with the aid of a scraper or through heating) at the end of life of the specific building application, so that the cast glass units can be retrieved intact.

7.7.2 Recycling of discarded (waste) glass

Concerning the recycling of discarded (waste) glass, the choice of casting as a manufacturing technique is of key importance for enabling the closed-loop recycling of glass that would normally get down-cycled or discarded either due to contamination or due to their difference in composition (recipe mismatching).

In theory, glass can be endlessly recycled, without losing its quality. There are several advantages involved in glass recycling that make cullet (waste glass crushed into small segments) attractive for the glass industry: Recycling of glass can reduce the amount of accumulated waste in the landfills, as well as the extraction of raw materials needed for forming glass such as sand, sodium carbonate and quicklime. More than that, the mass of already formulated glass (and cullet) is 20% lower than the corresponding batch materials. Most importantly, cullet (crushed glass) presents a lower melting energy requirement (thus, less temperature) than the constituent raw materials, since the endothermic chemical reactions linked with glass formation have already been completed. Accordingly, by using cullet in the batch, the energy

⁶¹ This project has been co-initiated by the author of this dissertation and has received a 4TU.bouw 2017 grant. Further information on the project can be found at: <https://www.tudelft.nl/bk/over-faculteit/afdelingen/architectural-engineering-and-technology/organisatie/leerstoele/structural-design/glass-transparency-research-group/research-topics/re3-glass/>

⁶² Actually the biggest challenge in this case is anticipated to be the crushing of the cast components into cullet. According to personal communication with *Vlakglas*, the current recycling infrastructure allows for the crushing of glass up to 30 mm in thickness without damaging the crushing blade.

consumption of the (re)melting process can be substantially reduced. In specific, with every 10% of cullet added to a batch of melting glass, the furnace energy consumption is reduced by 2.5 – 3% (Nilsson et al. 2007). In addition to the above, the use of cullet increases the life of the furnace by up to 30% due to decreased melting temperatures and a less corrosive batch (Worrell et al. 2008).

However, despite the common notion that glass is 100% recyclable, numerous of the everyday discarded glass objects – excluding food and beverage containers – are at present neither reused nor recycled, mainly due to a lack of recycling infrastructure/ scheme for glass recipes other than soda-lime glass. Effectively, until now, closed-loop glass recycling is only achieved by the soda-lime container glass recycling industry. In specific, up to date, the prevailing glass type recycled concerns bottles and containers by the packaging industry, with an average recycling percentage of 73- 74% within the EU (FEVE European Container Glass Federation 2016). In the Netherlands this percentage is 80%. Out of that, 68% is used for new container glass products (Verening Nederlandse Glasfabrikanten 2012).

According to (Vlkglas Recycling Nederland 2017), the Netherlands is currently the leading country in the recycling of float glass coming from the building industry, with an achieved recycling percentage between 80-90%. However, most of the collected float glass is down-cycled into bottles by the packaging industry or processed into insulation products⁶³. Only a small percentage (9%) meets the strict quality criteria and can be recycled as cullet directly by the float glass industry.

Other types/compositions of glass such as ceramic glass (e.g. kitchen glass, glass disks of the microwaves, etc.), borosilicate glass (light bulbs, ovenware, laboratory ware, etc.), lead glass, aluminosilicate (e.g. mobile phone screens) and coated float glass are not currently integrated in any glass recycling scheme. This can be attributed to the comparably limited amount of the above glass

63 In particular, from the collected flat glass waste, approximately 80% is recycled and another 10% is directly considered top quality cullet - e.g. from the single glazing of extra clear glass from greenhouses. The remaining 10% is demolition waste. The disposed float glass can contain pieces of metal (e.g. insulating glass units are not separated from the metal spacer) which are removed during the crushing and selection process. The larger aluminium frames should be removed in advanced, mainly due to logistics reasons. From the (80%) recycled float glass:

- 59% is recycled by the packaging industry (i.e. in bottles). The packaging industry favours cullet made of float glass waste as it reduces the amount of lead in packaging glass.
- 29% is recycled into insulation products, such as glass wool.
- 9% is recycled again to float. Ultimate aim is to recycle a higher percentage of float glass back to float.

Lamination is not hindering the recycling of float glass as the Netherlands has facilities that can brush the foil away or/and separate it through centrifugal force.

types, the lack of relevant recycling infrastructure (e.g. collecting points and recycling plants specialized in glasses other than soda-lime) but also to coatings, adhesives, recipe incompatibility, other contaminants or a required labour intensive demounting process.

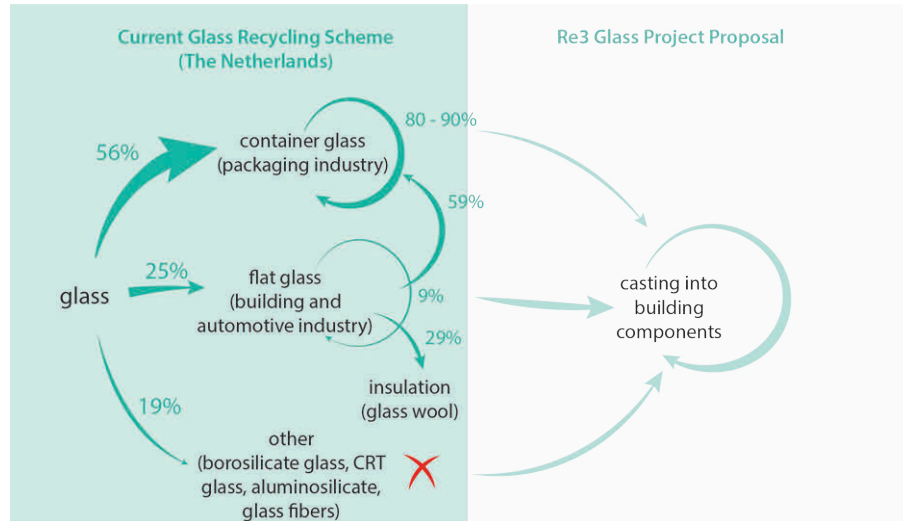


FIG. 7.19 Rough illustration of the current glass recycling scheme in the Netherlands and the Re³ Glass proposal.

In this direction, casting is a promising manufacturing method for the re- and up-cycling of the different glass recipes, due to the inherent flexibility of this production method (see Fig. 7.19). As a tangible example, a change in the raw material batch at the continuous float line results in the discard (and loss) of up to 7 days of production so that the material composition in the continuous ribbon has been successfully altered⁶⁴. On the contrary, casting can be considered a more flexible process that allows for a simple switch between different glass recipes without any loss of production. Although in float lines each manufacturing line is largely based on a specific recipe and annealing scheme, in casting different glass recipes can be melt in the same furnace and formed by the same moulds, by simply altering the annealing scheme without causing contamination of the kiln. Even small-scaled glass casting studios can easily experiment with different glass recipes. Moreover, such components due to their substantial cross-section, are expected to tolerate a

⁶⁴ This information is based on personal communication with the float production line of AGC in Belgium.

higher percentage of inclusions than float or container products, without necessarily compromising their mechanical or aesthetical properties.

This potential has already been demonstrated by the successful recycling by kiln-casting and the experimental testing of numerous specimens made out of waste glass of various recipes by the *Glass & Transparency Group* of TU Delft. In specific, experimental work by (Scholtens 2019) demonstrated that recycled borosilicate glass (glass rods, tubes, ovenware and laboratory-ware) presents comparable Young's Modulus and flexural strength to standard borosilicate glass. Moreover, research work by (Anagni 2019) has demonstrated the feasibility of mixing incompatible glass recipes with the aim to obtain safe structural components. In specific, combinations of soda-lime, borosilicate and lead crystal glass were examined (two different glass recipes per mixture), in different cullet sizes (fine powder to coarse cullet), ratios (30%-70%, 50%-50%) and at different temperatures (970°C, 1120°C, 1200°C). The prepared cullet would be thoroughly mixed prior to casting. The samples were annealed at two annealing points, corresponding to the two glasses composing the mixture. None of the glass combinations cracked during annealing and cooling. Cast glass samples made by fine cullet with a composition of 50% lead and 50% (float) soda-lime waste glass and kiln-cast at 1120°C were found the most promising in terms of mechanical properties.

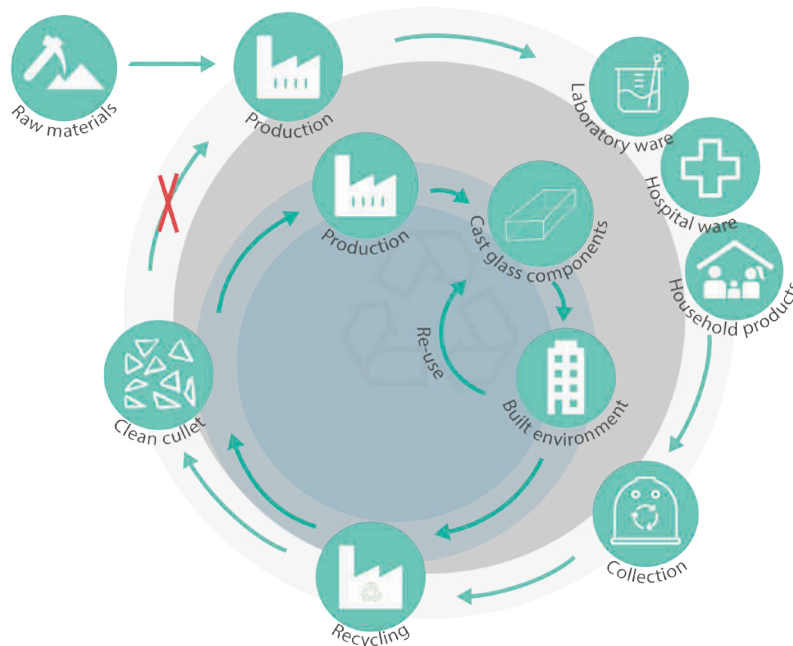


FIG. 7.20 Proposal for a borosilicate recycling scheme by (Scholtens 2019).

Furthermore, (Bristogianni et al. 2018b) argues that cast glass components can tolerate a higher content of flaws in their meso-structure in comparison to thin glass objects (windows, food containers) due to their substantial mass and the fact that flaws in the meso-structure are less prone to cause failure (see Chapter 2.6). In this direction, experimental work at the *TU Delft Glass & Transparency Lab* by (Yu 2019) has demonstrated that recycling of float glass with soft and hard coatings to cast glass building components can be a viable solution: the resulting cast components present a slightly reduced Young's Modulus but still sufficient to be used as structural elements. More implications can arise however in the recasting of float glass with metallic or ceramic frit coatings (Bristogianni et al. 2019) These coatings, due to their content of high-temperature melting compounds, introduce miniscule flaws in the glass network that deteriorate the mechanical properties of the glass specimens. Although the components can be used structurally, a lower strength and Young's Modulus should be expected.

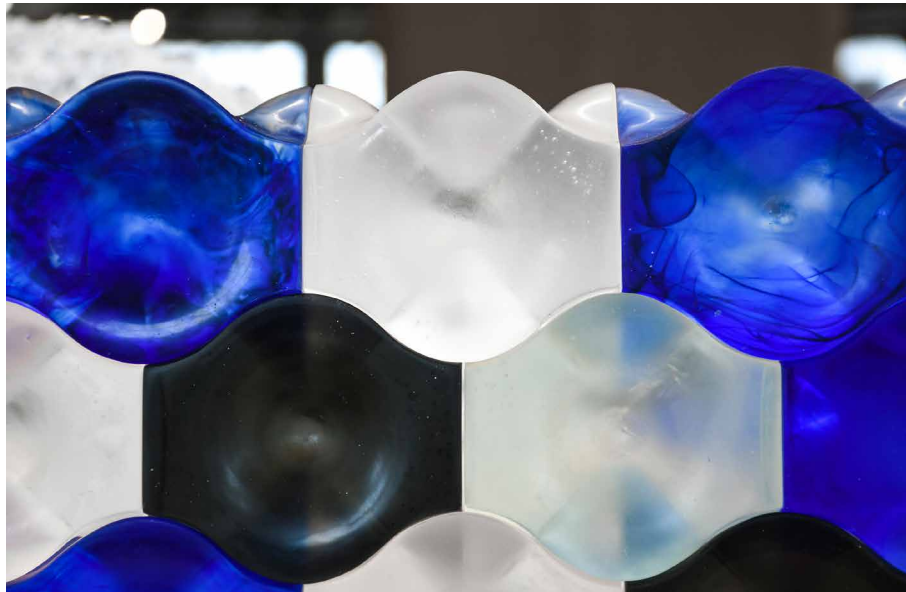


FIG. 7.21 Prototypes of the Type A osteomorphic topology made of recycled artware glass (blue), CRT screens (black), float glass (light blue) and optical lenses (clear) within the context of the Re³ Glass project.

In summary, the experimentation with various different glass recipes from commercial glass waste with the aim of producing safe cast glass structural components can lead to a broad palette of glass products. The possibilities are not only numerous in terms of aesthetic variety, but also in terms of physical and

mechanical properties. Within the context of Re³ Glass project several physical prototypes of the investigated geometries were co-produced by the author of this dissertation employing various sources of waste glass, such as glass artware, CRT screens, float glass, mirrors and laboratory-ware. These prototypes, some of them shown in Fig. 7.21 and Fig. 7.22, demonstrate the potential of such a solution. Several steps have already been taken by the TU Delft Glass & Transparency Lab for the validation of the mechanical properties and for mapping the involved challenges of such cast glass components.

Although, the in-depth analysis of the mechanical and physical properties of cast glass elements made of waste glass remain out of the scope of this research, all aforementioned examples indicate the promising prospects of this solution; at the same time they highlight that the closed-loop recycling of such types of glass remains still a largely unexplored field.



FIG. 7.22 Prototypes of the Type C topology made from the re-melting of different types of glass waste within the context of the Re³ Glass project.

7.8 Conclusions

A new design concept for load-bearing cast glass structures has been introduced in this chapter. Owing to its segmented and reversible nature, the proposed system out of dry-assembled interlocking cast glass components offers several engineering advantages compared to its progenies such as an improved toughness resistance and an increased deformation (and thus a warning mechanism) prior to failure. The dry-assembly and fragmentation of the structure diminishes the overall influence of critical flaws in the individual components and offers resistance to crack propagation, which in turn results in localized failure. Thus, it can be derived that an interlocking cast glass assembly has an inherent safety mechanism, crucial for a material like glass whose failure behaviour is still not fully predictable and comes without warning.

A significant advantage of this system is its buildability: The self-aligning nature of interlocking components can speed up considerably the construction process and enhances the seismic resistance of the construction. Geometries that allow for various stacking arrangements are preferred for their multifunctionality. Repetition in block type is further desired to reduce the manufacturing costs and ease the assembly process.

Reversibility is considered one of the major benefits of the presented concept, especially at present, when recyclability and circularity in the building sector are becoming essential. In the proposed system, the glass elements can be retrieved intact and reused without having to be re-melted which comes with added carbon and energy footprint. Eventually, they can be recycled as they are contaminant-free.

To further improve the toughness and impact resistance of the structure, a soft, dry-interlayer is considered essential. Such an interlayer can further enhance the buildability of the system by accommodating dimensional tolerances on the size of the individual components – thus sparing the necessity of post-processing of the individual units- and ensure a more even stress distribution, achieving by deformation a full-contact between the elements. The initial literature review suggests that interlayers of the polyurethane family (PU and TPU) are the most promising candidates for real life applications.

In respect to the principles of interlocking and glass casting several design criteria are established for designing interlocking assemblies out of cast glass components. These result in components of limited volume, equal mass distribution, rounded shapes and to a limited number of different units. Based on the established design

criteria, various designs and interlocking mechanisms were developed and physical prototypes of each design were kiln cast in 1:2 scale. The assessment of the prototypes by the established criteria suggests that blocks following osteomorphic interlocks are the most promising solution for cast glass components: they present an equal mass distribution, homogeneous annealing, multi-functionality, high shear capacity and good damping properties.



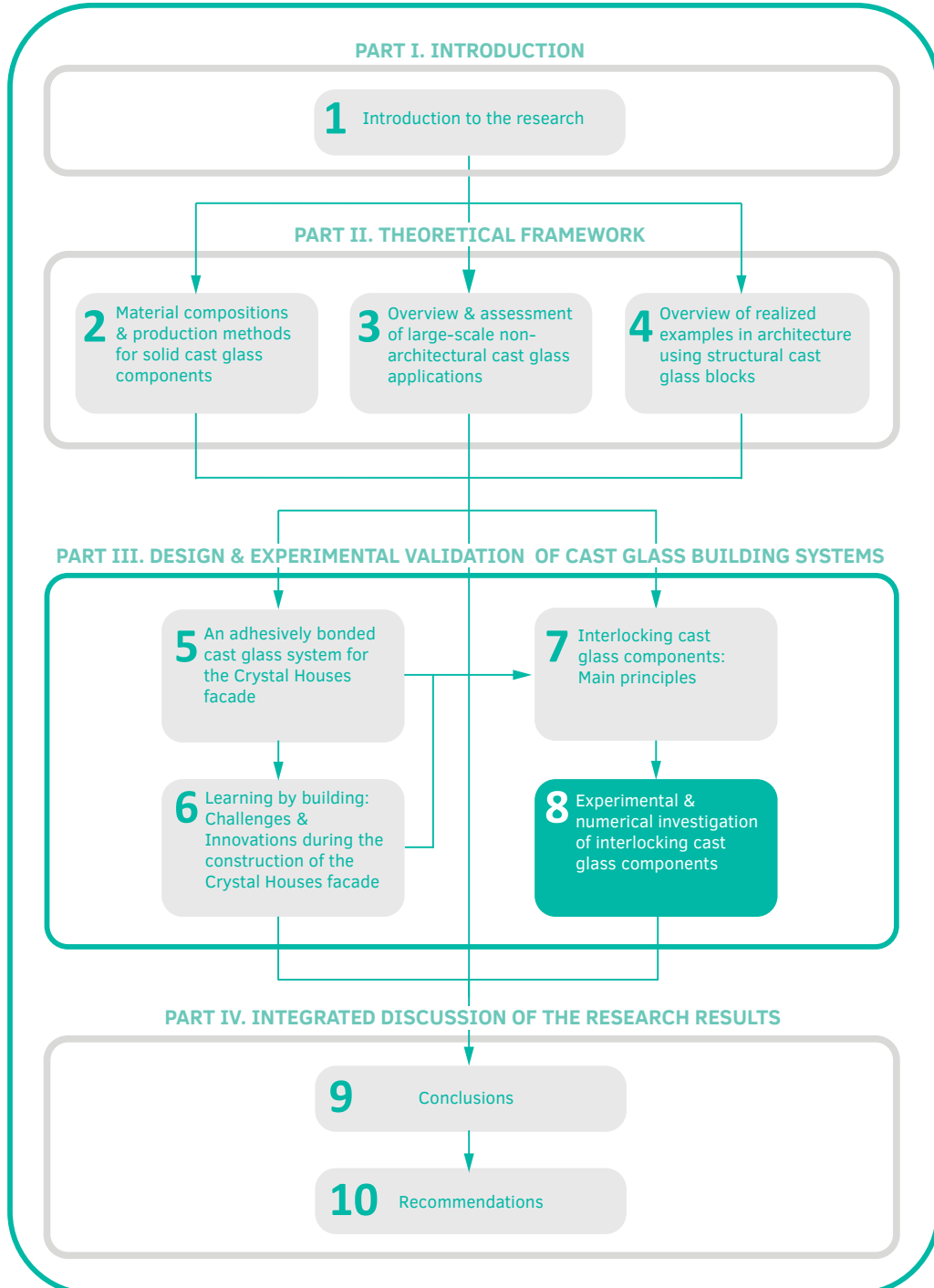
FIG. 7.23 Prototypes of the E typology made from the mixing of different colours of recycled art (lead) glass.



A dry PU interlayer between two osteomorphic cast glass blocks



Exploring the third dimension of glass



Solid cast glass components and assemblies for structural applications

8 Experimental and numerical investigation of an interlocking system out of osteomorphic cast glass components

The previous chapter concluded that blocks following an osteomorphic geometry are the most promising in respect to the principles of interlocking and glass casting. Moreover, interlayers of the polyurethane (PU) family are considered the most suitable for a building application, without compromising the transparency of the resulting structure. Based on these findings, this chapter aims at investigating the structural behaviour of an interlocking assembly employing osteomorphic blocks and PU as an interlayer. Initially, experimental research is conducted in different PU interlayers available in the market, aiming on finding one that fulfils the established design criteria and mechanical properties, as discussed in chapter 7.6. Different readily available two-component PU interlayers, with a Shore Hardness ranging between 60A – 80A, are cast to follow the osteomorphic interlocking geometry and are tested under static compressive load between two half osteomorphic kiln-cast glass blocks in series of 3 specimens and in 2 different thicknesses (3mm and 6mm). The results suggest that the tearing strength of the interlayer is as important as its Shore Hardness; whereas the geometry of the interlocking form can further influence the overall resistance of the assembly against tearing. They also highlight that insufficient contact (mismatch) of the interlayer with the glass blocks, due to dimensional deviations, can lead to the eventual failure of the assembly even under static load due to peak stresses that are further increased by the lateral stresses occurring due to the creep of the interlayer. From the examined interlayers, PU with a shore hardness between 70A – 80A, are considered as the most suitable for the further experimental validation of the assembly. Following, to investigate the influence of the interlocking mechanism to the structural behaviour of the proposed

system, series of assemblies of osteomorphic blocks with different amplitudes, namely 10, 15 and 20 mm, interweaved with 6 mm thick 70A PU interlayers are tested in out-of-plane shear. The results indicate that blocks with higher amplitudes are stiffer and fail at higher loads and less total deformation. But they are also more prone to dimensional tolerances and eccentricity of the construction. This indicates that a geometry with multiple interlocking mechanisms may be more favourable for the self-alignment of such an assembly. Moreover, all specimens presented visible deformation prior to failure. The pseudo-ductile performance of the assembly and its ability to prevent crack propagation are key-aspects for engineering a safe glass structure. It should be noted that the kiln-cast laboratory fabrication of the examined glass blocks and the use of disposable moulds has resulted in significantly lower dimensional accuracy compared to blocks that would be industrially fabricated using high precision moulds and hot-pouring. These significant dimensional deviations have negatively influenced the behaviour of the assemblies, and therefore, the derived data should be considered only qualitative – it is expected that industrially made blocks will present a considerably improved interlocking behaviour.

Thus, to further explore the influence of the most crucial geometrical aspects of the interlocking mechanism, namely the height and amplitude of the glass components, to the overall structural performance under shear a numerical model⁶⁵ is made. In accordance with the output of the experimental validation, here an osteomorphic block with multiple locks is tested, considering a 4 mm thick 70A PU interlayer. The results of the numerical model indicate that bricks of reduced height are more susceptible to failure by bending, whereas with taller brick variants shear lock failure is more critical. It is also confirmed that an increased amplitude of the interlock can be beneficial as it leads to an increased shear capacity and lower uplifting effects. It is also shown that specimens with increased height reach the failure stress limit with considerably smaller deformations, thus, requiring a higher manufacturing precision.

⁶⁵ The numerical model presented in this chapter is part of the MSc Thesis: Jacobs, E.A.M., Structural consolidation of historic monuments by interlocking cast glass components. TU Delft, 2017.(Jacobs 2017)

Credits

Research partly conducted in collaboration with

- Telesilla Bristogianni – *experimental testing*,
Faculty of Civil Engineering & Geosciences, TU Delft
- Erwin Jacobs – *development and validation of numerical model*,
Faculty of Civil Engineering & Geosciences, TU Delft

Technical support and assistance in prototype manufacturing

- Kees Baardolf,
Stevin II Laboratory, Faculty of Civil Engineering & Geosciences, TU Delft
- Tommaso Venturini,
Faculty of Civil Engineering & Geosciences, TU Delft
- Rong Yu,
Faculty of Civil Engineering & Geosciences, TU Delft

Manufacturing Facilities

- Stevin II Laboratory,
Faculty of Civil Engineering & Geosciences, TU Delft

Research Supervisors

- Rob Nijssse,
Faculty of Civil Engineering & Geosciences, TU Delft
- Fred A. Veer,
Faculty of Architecture & the Built Environment, TU Delft

The research work presented in this chapter has been partly funded by a 4TU.bouw Lighthouse grant for the project Re³ Glass

8.1 Introduction

In the previous chapter a novel structural system employing interlocking cast glass blocks was presented. The proposed system offers several engineering advantages such as an inherent redundancy and resistance to crack propagation, as well as reversibility. To achieve a circular system and at the same time obtain a homogeneous stress distribution the use of a dry, and preferably transparent, interlayer is proposed as an intermediary between the glass units. A preliminary research on different interlocking geometries and interlayer materials, presented in Chapter 7, pointed out that blocks following an osteomorphic geometry and interlayers made of polyurethane (PU or TPU) are the most promising for further development and validation of the system. Following the aforementioned findings, this chapter investigates by both experimental testing and numerical simulation the structural behaviour of an interlocking, dry-assembly made of osteomorphic cast glass blocks and PU as a dry interlayer.

8.2 Methodology

Initially different interlayers are cast in the desired form and are then placed between 2 half osteomorphic glass blocks to be tested under a static compressive load. Based on the experimental data, the most promising interlayer is selected for further investigating the influence of the interlocking geometry to the structural behaviour of the whole assembly. Accordingly, out-of-plane shear tests are performed in 3 series of assemblies, each made of 3 Type A blocks (as presented in the previous chapter) interleaved with the chosen interlayer. The blocks of each series have a different amplitude, namely 10, 15 and 20 mm. The set-ups and results of the experimental work are discussed in section 8.3. In respect to the findings of the experiments, a numerical FEM model of an osteomorphic assembly using a type B osteomorphic block is made to reconfirm the influence of the amplitude to the structural behaviour of the blocks, as well as to investigate the influence of the block's height to it. The aim of the numerical model is not to provide absolute design values, but to provide insights into the effects of all individual parameters in the overall performance. The numerical investigation is described in section 8.4. General conclusions and further recommendations are drawn in section 8.5 and 8.6 respectively.

8.3 Experimental

In brief, two different series of experiments using osteomorphic glass blocks and PU interlayers were carried out in order to investigate the mechanical behaviour of the proposed dry-assembled cast glass system:

- a compressive testing under static load of PU interlayers of different Shore Hardness and thickness.
- out-of-plane shear tests on assemblies of 3 glass blocks with different amplitudes

More specifically, initially, several series of compressive testing are carried out for PU interlayers of different Shore Hardness, between 60A – 80A and of different thickness, namely 3 and 6 mm. The interlayers, which are cast in the desired form, are placed between two half osteomorphic blocks, each measuring approx. 75 mm x 37.5 mm x 37.5 mm and tested under compression. The experiments and the relevant findings are discussed in sections 8.3.2 and 8.3.3 respectively. Based on the output of the first testing, the most promising interlayer is chosen to perform the out-of-plane shear tests on assemblies of various amplitudes, namely 10 mm, 15 mm and 20 mm. These are presented in section 8.3.4. All the prototypes have been produced in the Glass & Transparency Lab, by kiln-casting soda-lime osteomorphic glass blocks in two different scales and by manually casting two-component PU interlayers.

8.3.1 Materials

Glass blocks

The osteomorphic blocks, each measuring approximately 75 mm x 75 mm x 37.5 mm (full brick) or 75 mm x 37.5 mm x 37.5 mm (half brick), were kiln-cast at the *TU Delft Glass & Transparency Lab*. The moulds were made by the lost-wax technique. In specific, a 3D- printed full scale model of each interlocking design was used to create a silicone mould out of *Mould Max 30*. With this silicone mould, multiple wax models of the design were produced. *Crystalcast M248* investment material, in a powder to water volume ratio of 3:1, was poured around the wax models. Full brick moulds were made single, whereas half brick moulds were combined in pairs. The moulds were left to cure for an hour prior to steaming the wax out of the mould. *Schott B270*

modified soda-lime glass (main oxides as identified by the *XRF analysis* conducted at TU Delft: 71.8% SiO₂, 10.1% Na₂O, 6.3% K₂O, 5.2% CaO, 2.2% ZnO) was chosen for the production of the glass components. The amount of glass corresponding to each mould was introduced in the form of fragmented glass lenses (Ø75 mm) in terracotta flowerpots that were positioned above the moulds supported by 20 mm thick ceramic fiber strips (see Fig. 8.2). The glass blocks were kiln-cast at 970°C for 10 h and annealed between 540°C – 510°C, using a *ROHDE ELS 200 S Kiln* with 5-sided heating. The complete kiln-casting and annealing schedule can be seen in Fig. 8.1.

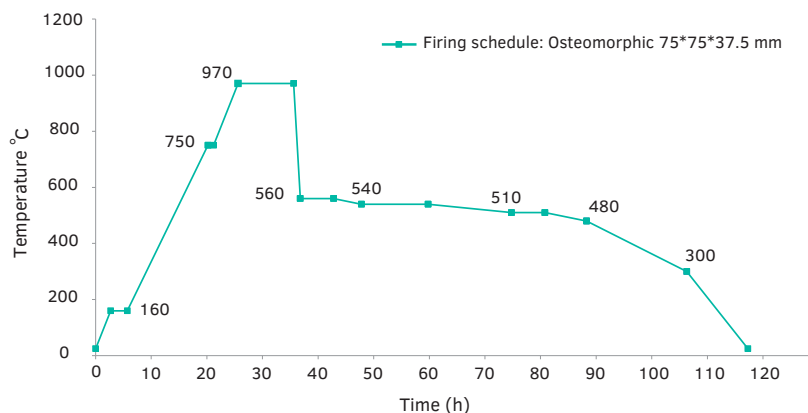


FIG. 8.1 Firing schedule followed for the kiln-casting and annealing of the osteomorphic blocks.



FIG. 8.2 From left to right: Arrangement of the glass-containing flowerpots above the crystal cast moulds and set-up of the kiln; View of the kiln at 970°C; Kiln-cast osteomorphic blocks prior to mould removal.

Afterwards, the face (top of the mould) from where the glass was poured was cut to size – to remove any excessive glass. The prototypes were then ground and polished

by a *Provetro* flat grinder machine. Specifically, the bottom face and the cut face of the blocks were ground and polished using diamond discs in a consecutive order of coarse to fine: 60, 120, 200 and 400 grit. A *Dremel* rotary tool with interchangeable diamond pads, similarly covering a range of 60 to 400 grit scale, was used to round the edges of the interlocking mechanism and eliminate possible imperfections at the interlocking wavy surface. There was no other post-processing on the other four faces of the blocks, including the interlocking surface. Due to the manual fabrication (and cutting of the one side), the bricks presented considerable size deviations (estimated to be $\pm 3\text{mm}$); the largest observed deviation was at the apex of the interlocking geometry.

Interlayer

Based on the criteria established in Chapter 7.6, readily available PU interlayers with a Shore Hardness between 60A - 80A were sought that could be cast in the desired shape. PU interlayers can be formed also by other techniques to the desired shape, such as vacuum forming or thermoforming, yet, two-component polymer casting was favoured as it guarantees an accurate, constant thickness throughout the interlayer's section. Table 8.1 gives an overview of the selected PU interlayer materials for the experimental validation of the system. Due to logistic reasons (availability of materials in the Netherlands as resins, etc.) most of the selected interlayers do not meet the transparency criteria. Even so, at this research stage the crucial factor to examine is to establish the most favourable Shore Hardness of the interlayer and thus, non-transparent interlayers were also considered when no alternative was readily available.

TABLE 8.1 Properties of a selection of cast PU interlayers available in the market as provided by the manufacturer

Material	Shore Hardness	Break El.	Tensile Strength	Die C tear strength	Colour
	-	%	MPa	N/mm	-
PMC 746	60A	650	4.8	17.5	translucent amber
PMC 770	70A	750	5.2	35.1	translucent amber
Permacol 5450	75A/25D	unk	unk	unk	clear transparent
Task 16	80A/30D	233	15	34.5	light yellow

A two-part 3D-printed mould out of polylactic acid (PLA) was used for casting each PU resin to a constant 3 mm thick interlayer matching the osteomorphic geometry of the blocks (Fig. 8.3 and Fig. 8.4). Each specimen was manually poured into the mould and was left to cure for 24 h prior to removal. To prevent accidental direct contact of glass-to-glass at the edges, the cast interlayers are cast extending in all four sides.

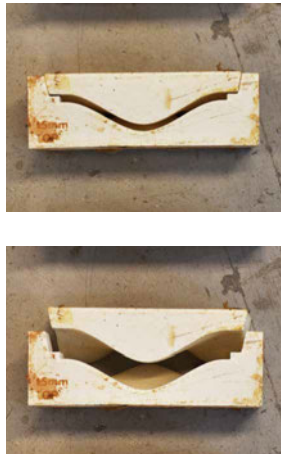


FIG. 8.3 Two-part 3D-printed mould out of PLA for casting the interlayers.



FIG. 8.4 Prototype of a 3 mm thick, cast PU interlayer.

8.3.2 Interlayer testing under compressive static load

8.3.2.1 Method

Fig. 8.5 shows the typical set-up of the experiment. Each interlayer was placed between two half osteomorphic glass blocks with 15 mm amplitude and tested in compression in a *Zwick Z100* universal testing machine at a rate of 250 N/s up to a given load, which was determined to be 40 kN⁶⁶. The use of cast glass blocks of the desired form was chosen to derive results that are representative of the system and shed light in the collaboration of the interlayer with complex surface geometries in glass. Each interlayer material was tested in a series of three specimens in order to derive statistical data. The specimens have been named according to their shore hardness and interlayer thickness as shown in Fig. 8.6.

⁶⁶ Due to human error, for some specimens a load of 40 kN was directly applied, without a gradually increasing load rate. Such specimens are represented by a linear slope until the set 40kN load at the F-u diagrams. Nonetheless, it is anticipated that this error does not alter the results of the creep performance of the interlayer under the given constant load.

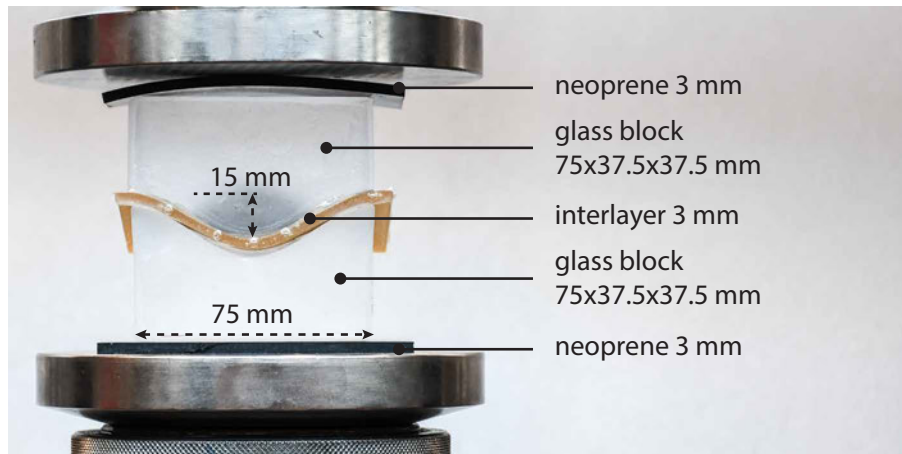


FIG. 8.5 Experimental set-up

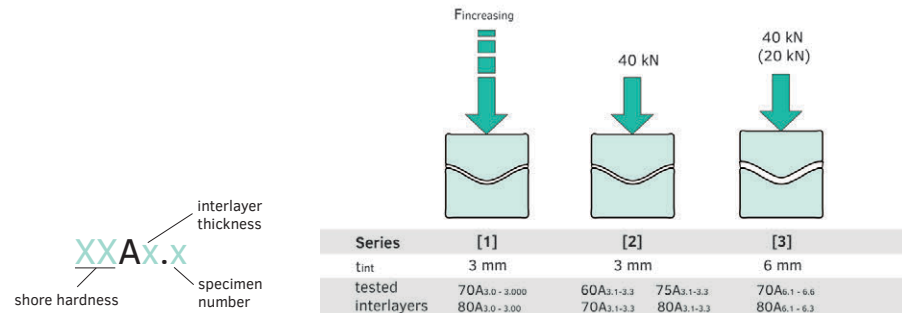


FIG. 8.6 Labelling principle of the specimens

FIG. 8.7 Schematic illustration and overview of the three series of experiments under compressive load on interlayers.

To prevent the failure of the system due to localized peak stresses occurring from the direct contact of glass with steel, 3 mm thick neoprene or 10 mm thick wood plates were placed between the steel plates of the machine and the glass assembly. The aim of this series of experiments is the evaluation of the interlayers' resistance under the given constant load; thus, the deformation under creep is regarded as the main output. Due to the influence of several external factors, such as the initial settling of the machine, the dimensional tolerances of the kiln-cast blocks, the initial deformation of the neoprene or wood intermediates and possibly the self-realigning (sliding) of the blocks in relation to each other upon initial loading, the early displacement of the assembly until the specimens reach the set static load is not considered as it is not representative of the interlayer's performance regarding creeping. To provide a comparison and evaluate the interlayer's contribution to the structural performance of the interlocking system, an assembly of two glass

blocks without interlayer in between is also tested in compression. In essence, three different series of compression tests are performed (Fig. 8.7):

Initially, a few specimens (namely $70A_{3,0} - 70A_{3,000}$ and $80A_{3,0} - 80A_{3,00}$) with 3 mm thick PU interlayers are tested in compression under higher loads in order to estimate the max. force that should be applied [Series 1]. Based on the results, it was determined to apply a max. load of 40kN to the next two series, corresponding to approx. 14.2MPa nominal compressive stress on the glass surface⁶⁷. Upon reaching the load of 40kN, the force is maintained constant for another 900s (15 min) in order to measure the deformation of the interlayer under creep. Accordingly, two series of specimens, first with PU interlayers of 3 mm thickness and then with PU interlayers of 6 mm thickness are tested [Series 2 and Series 3 respectively (see Fig. 8.8)].

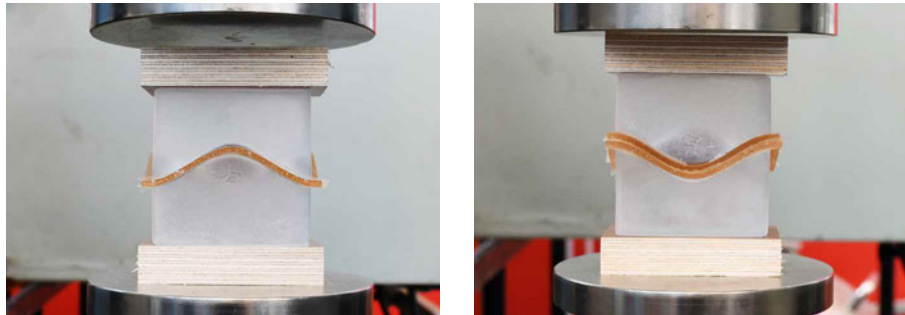


FIG. 8.8 Prototype with 70A interlayer of 3 mm thickness (left) and of 6 mm thickness (right).

8.3.2.2 Results

Table 8.2 summarizes the main results of the 3 series of experiments. The data have been processed so that only the deformation under creep (u_{creep}) is provided. Due to all the aforementioned reasons, the total displacement of the specimens in the (u-t) unprocessed graphs provided in this section is considerably higher than the 3 mm thickness of the interlayer. To compensate for the influence of the external factors all graphs are also presented showing only the deformation under creep mode. Thus, these graphs show the deformation over the last 900s of the tests. A minor effect by

⁶⁷ This compressive stress is already more than 70 times higher than the one imposed to the bottom array of glass blocks of the *Crystal Houses* façade due to the own weight of the construction (see chapter 5.6.5).

the deformation of the neoprene intermedium or/and of relevant sliding of the blocks is anticipated to still occur; however, these could not be isolated and quantified.

TABLE 8.2 Main results of the compression tests on PU interlayers.

Test Series	Specimen	t_{int}	F_{maxset}	$F_{fail.}$	T_{creep}	u_{creep}	intermediate	Failure mode
		mm	kN	kN	s	mm		
[1] Load Calibration	70A _{3.0}	3	-	72.5	-	-	neoprene	(a), (i)
	70A _{3.00}	3	-	57.8	-	-	neoprene	
	70A _{3.000}	3	-	63.5	-	-	neoprene	
	80A _{3.0}	3	60	60	66	0.6	neoprene	(a), (ii)
	80A _{3.00}	3	50	50	426	7.5	neoprene	
[2] 3mm thick interlayers	80A _{3.1}	3	40	-	900	0.9	neoprene	(c), (iv)
	80A _{3.2}	3	40	-	900	1.5	wood	
	75A _{3.1}	3	40	25.4 [†]	-	-	neoprene	(b), (i)
	75A _{3.2}	3	40	15.9 [†]	-	-	neoprene	
	75A _{3.3}	3	40	15.9 [†]	-	-	neoprene	
	70A _{3.1}	3	40	-	900	1.3	wood	(c), (iii)
	70A _{3.2}	3	40	-	900	1.1	wood	
	70A _{3.3}	3	40	-	900	1.8	wood	(c), (iv)
	60A _{3.1}	3	40	40	121	0.5	neoprene	(b), (ii)
	60A _{3.2}	3	40	40	58	0.8	neoprene	
	60A _{3.3}	3	40	-	900	0.7	neoprene	(c), (iii)
G _{glass}	0	40	4	-	-	neoprene	(i)	
[3] 6mm thick interlayers	70A _{6.1}	6-	20	-	900	0.9	neoprene	(c), (iii)
	70A _{6.2}	6-	20	-	900	1.0	neoprene	
	70A _{6.3}	6-	20	-	900	1.0	neoprene	
	70A _{6.4}	6-	40	-	900	1.0	neoprene	(c), (iii)
	70A _{6.5}	6-	40	-	2700	1.0	neoprene	(d), (iii)
	70A _{6.6}	6-	40	-	900	1.4	wood	(c),(iii)
	80A _{6.1}	6-	40	-	900	1.3	wood	(c), (iv)
	80A _{6.2}	6-	40	-	900	1.3	wood	
	80A _{6.3}	6-	40	-	900	1.5	wood	

(a) Failure of the glass blocks at their shortest section. No tearing of the interlayer observed.

(b) Perforation of the interlayer leading to glass to glass contact.

(c) assembly successfully withstood the max. set load for the scheduled 900 sec.

(d) assembly successfully withstood the max. set load for the scheduled 2700 sec.

(i) failure at increasing load

(ii) failure under creep mode

(iii) no failure – interlayer presented plastic deformation

(iv) no failure – interlayer presented no or negligible plastic deformation

[†] Test stopped when visible tearing of the interlayer was observed.

- applied as 2 x 3 mm

8.3.2.3 Series [1]: Load Calibration

Initially, different max. loads were set for the interlayers in order to determine the max. load for testing the specimens under creep. In specific, specimens interleaved with *PMC 770* (70A) and *Task 16* (80A) 3mm thick interlayers were tested on increasing load until failure. Specimens of the 70A series failed under an increasing load ranging between 56 – 72 kN. Accordingly, a max. load was set first to 60 kN and then to 50 kN. Although specimens of the 80A series successfully reached the max. set loads of 60 kN and 50 kN they failed shortly after due to creeping of the interlayer. In all cases failure occurred at the glass; no tearing of the interlayer was observed.

More specifically, all tested specimens failed with a consistent Y breaking pattern at the middle of their concave (shorter) section. The tip of the crack always originated at the apex of the concave section, as shown in Fig. 8.9. The peak stresses are assumed to have been caused by the insufficient (partial) contact of the interlayer at that area due to the increased manufacturing tolerances of the kiln-cast components. The shear stresses occurring in-plane at the interlayer due to its increasing deformation further contributed to failure (Fig. 8.10); this was especially evident in the case of the 80A specimens which failed under static load.

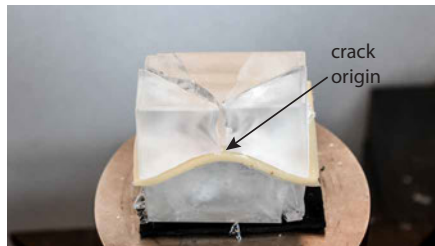


FIG. 8.9 Typical Y breaking pattern originating at the shortest section of the block (specimen 80A₁)

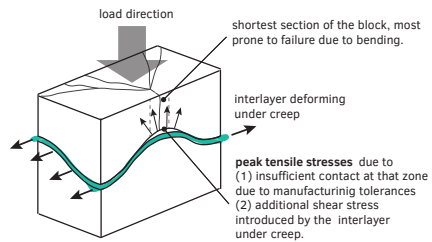


FIG. 8.10 Possible explanation of the cause of failure of the specimens interleaved with *PMC770* (70A) and *Task 16* (80A).

8.3.2.4 Series [2]: Compression testing of 3 mm thick interlayers

Based on the input from the first series of testing, it was determined to set the max. load to 40kN; upon reaching this force, it was set as a constant load and the specimen was maintained under it for 900s in order to evaluate the performance

of the interlayer under creep. Accordingly, 3mm thick interlayers of all 4 different selected PU materials (with a shore hardness ranging between 60A – 80A) were tested. The main results are summarized in Table 8.3.

TABLE 8.3 Main results of the compression tests on 3 mm thick PU interlayers (Series 2).

Specimen	t_{int}	F_{maxset}	F_{fall}	T_{creep}	u_{creep}	intermediate	Failure mode
	mm	kN	kN	s	mm		
80A _{3,1}	3	40	-	900	0.9	neoprene	(c), (iv)
80A _{3,2}	3	40	-	900	1.5	wood	
75A _{3,1}	3	40	25.4 [†]	-	-	neoprene	(b), (i)
75A _{3,2}	3	40	15.9 [†]	-	-	neoprene	
75A _{3,3}	3	40	15.9 [†]	-	-	neoprene	
70A _{3,1}	3	40	-	900	1.3	wood	(c), (iii)
70A _{3,2}	3	40	-	900	1.1	wood	
70A _{3,3}	3	40	-	900	1.8	wood	(c), (iv)
60A _{3,1}	3	40	40	121	0.5	neoprene	(b), (ii)
60A _{3,2}	3	40	40	58	0.8	neoprene	
60A _{3,3}	3	40	-	900	0.7	neoprene	(c), (iii)
G _{glass}	0	40	4	-	-	neoprene	(i)

(b) Perforation of the interlayer leading to glass to glass contact.

(c) assembly successfully withstood the max. set load for the scheduled 900 sec.

(i) failure at increasing load

(ii) failure under creep mode

(iii) no failure – interlayer presented plastic deformation

(iv) no failure – interlayer presented no or negligible plastic deformation

[†] Test stopped when visible tearing of the interlayer was observed.

- applied as 2 x 3 mm

The results clearly demonstrate that interlayers with a comparably lower tear resistance, namely *Permacol 5450* (75A) and *PMC 746* (60A) are improper for the examined application. In particular, the assemblies interleaved with *Permacol 5450* (75A) and *PMC 746* (60A) failed due to the early tearing of the interlayer which lead to glass-to-glass contact. The testing of the 75A specimens (*Permacol 5450*) was aborted once visible perforation of the interlayer was noticed under considerably lower loads than the max. set 40 kN. The interlayer was always first torn at the sharpest edges of the interlocking blocks as can be seen in Fig. 8.11.

Specimens from the 60A series reached the max. set 40kN load; nevertheless, two of the three specimens (60A_{3,1} and 60A_{3,2}) failed soon after they entered the creep mode, due to the perforation of the interlayer, as shown in Fig. 8.12. Specimen

60A_{3.3} successfully withstood the constant 40kN force for 900s and reached an almost stable deformation under the given constant load. Nonetheless, upon the removal of the load, it was observed that the interlayer had presented evident plastic deformation: at the contact surface the interlayer had been plastically deformed to less than half of its initial thickness and had been locally perforated at the edges of the assembly, as shown in Fig. 8.13.



FIG. 8.11 75A specimen after the test was aborted due to visible tearing of the interlayer.



FIG. 8.12 Typical glass failure originating at the edge of the assembly caused by the perforation/tearing of the interlayer (specimen 60A₁)

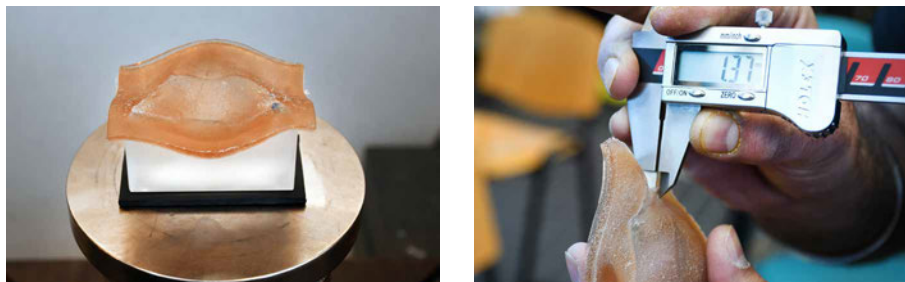


FIG. 8.13 Specimen 60A₃ after the completion of the test. There is evident plastic deformation.

In comparison, specimens interleaved with 70A and 80A interlayers successfully withstood the 40 kN load for 900s. Specimens $80A_{3,1}$, $80A_{3,2}$ and $70A_{3,3}$ did not present any visible plastic deformation after the testing (see Fig. 8.14). Specimens $70A_{3,1}$ and $70A_{3,2}$ presented limited plastic deformation at the contact area of the interlayer with the glass blocks.



FIG. 8.14 One of the 80A interlayer specimens during (right) and after (left) testing. No visible plastic deformation was observed.

Nonetheless, the deformation of both 70A and 80A interlayer materials remained time-dependant for the duration of the creep testing, as indicated by the deformation in time curve $[u - t]$ of the specimens, shown in Fig. 8.15. Without reaching a stable deformation (which would be expressed as a horizontal line in the $[u-t]$ diagram) it is difficult to predict if the tested interlayers would successfully sustain the given load for a longer period.

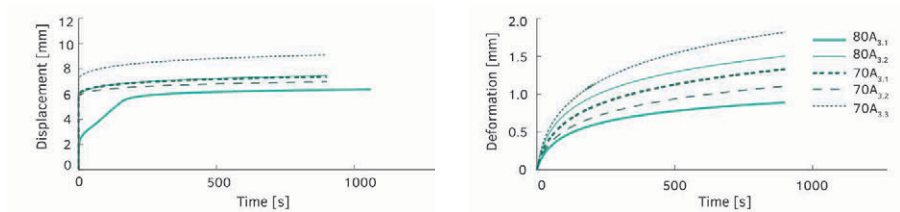


FIG. 8.15 Displacement in time graph of $70A_{3,x}$ and $80A_{3,x}$ specimens (left) and processed so that only the deformation in time under the static 40 kN load is shown (right)

Finally, in comparison to the specimens with interlayer in-between, the G_{glass} specimen, in which there was direct glass to glass contact, failed at a considerably lower load of just 4kN, at the sharpest edge of the assembly (Fig. 8.16), similar to the specimens that failed due to tearing of the interlayer. The failure load of the

G_{glass} specimen -which is 10 times less than the 40kN load that the 70A and 80A specimens could resist- highlights the importance of a soft-interlayer for enhancing the structural performance of the assembly. It should be noted that the failure load of this specimen corresponds to a nominal compressive stress of approx. 1.4 MPa – a value considerably less than the failure stress value of the rectangular solid glass blocks tested without an interlayer in Chapter 5.6.1. This difference in strength can be partially attributed to the kiln-cast fabrication and manual post-processing of the osteomorphic blocks compared to the hot-poured and CNC polished solid glass blocks of the *Crystal Houses* façade. The interlocking geometry has a significant influence on the resistance of the blocks against localized stresses as well: compared to the flat geometry of the *Crystal Houses* blocks, the complicated geometry of the contact surface of the blocks is more prone to the generation of peak tensile stresses.



FIG. 8.16 Failure mode of glass specimen without the use of an interlayer.

Overall, it was concluded from these experimental series that the examined 60A and 75A interlayer materials are not appropriate for the selected structural application due to their low tear strength. Both 70A and 80A interlayer materials are considered promising candidates. From the 1st series it was observed that due to the manual casting and post-processing of the glass blocks, dimensional deviations higher than 3 mm occur at the interlocking surface – particularly at the apex of the interlocking mechanism – which cannot be fully compensated by a 3 mm thick interlayer. This in turn, leads to stress concentrations at the points where there is insufficient contact

between glass and interlayer, which leads eventually to failure, even during static load due to the shear stresses caused by the creeping of the interlayer. This was manifested by the failure mode of the specimens tested in Series [1] and has as well been indicated by the experimental work of (Aurik et al. 2018). Hence, to further validate the mechanical behaviour of the assembly, a third series of experiments was carried out, similar to the last one but employing interlayers of 6 mm thickness.

8.3.2.5 Series [3]: Compression testing of 6 mm thick interlayers

After evaluating the previous two series of testing, it was determined to further test interlayer variants of 6 mm thickness under a constant 40kN load for 900s in order to evaluate if thicker interlayers perform better under creep mode⁶⁸. This series of experiments was carried out only on 70A and 80A interlayer specimens, which demonstrated satisfactory tear and creep resistance in the previous series of experiments. Due to time restrictions it was determined to apply the 6 mm interlayer as two layers of 3 mm⁶⁹. The two 3mm thick interlayers were simply placed on top of each other and positioned in between the two glass blocks (Fig. 8.21 and Fig. 8.22). A series of 70A specimens was also tested under creep with a set constant load of 20 kN, which results to a nominal compressive stress (approx. 7 MPa) that is closer to the one anticipated in a real application. In all the specimens 3mm neoprene or 10mm thick hard wood plates were used as intermediary between the steel head of the machine and the glass blocks.

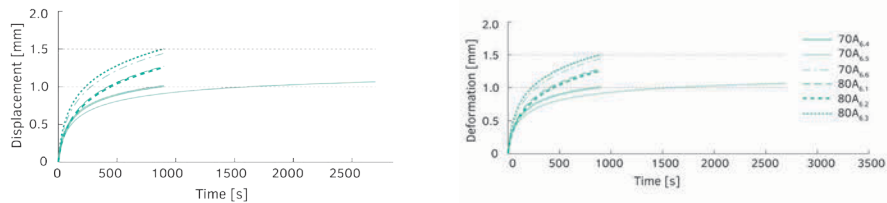


FIG. 8.17 Displacement in time ($u - t$) graph for the 70A and 80A 6 mm thick specimens tested to 40kN load for 900 s (left) and processed so that the deformation in time is shown only during the static 40 kN load (right).

⁶⁸ In some of the specimens the 40kN load was accidentally imposed instantly, without a constant increasing rate of 250 kN/s. This results in a completely straight initial line at the [F-u] diagrams (as there was a 0 N force and then instantly a 40 kN force) and to a vertical initial line at the [u - t] graph.

⁶⁹ Due to time restraints that did not allow for the manufacturing of a second 3D-printed mould for the casting of the interlayers, it was determined to use 2 times 3 mm thick interlayers to estimate the performance of a 6mm thick variant.

The corresponding deformation in time [u-t] graph, both unprocessed and processed so that the initial displacement due to external factors is compensated, can be seen in Fig. 8.17. The main results are summarized in Table 8.4.

TABLE 8.4 Main results of the compression tests on 6 mm thick PU interlayers (Series 3).

Specimen	t_{int}	F_{maxset}	F_{fall}	T_{creep}	u_{creep}	intermediate	Failure mode
	mm	kN	kN	s	mm		
70A _{6,1}	6	20	-	900	0.9	neoprene	(c), (iii)
70A _{6,2}	6	20	-	900	1.0	neoprene	
70A _{6,3}	6	20	-	900	1.0	neoprene	
70A _{6,4}	6	40	-	900	1.0	neoprene	(c), (iii)
70A _{6,5}	6	40	-	2700	1.0	neoprene	(d), (iii)
70A _{6,6}	6	40	-	900	1.4	wood	(c),(iii)
80A _{6,1}	6	40	-	900	1.3	wood	(c), (iv)
80A _{6,2}	6	40	-	900	1.3	wood	
80A _{6,3}	6	40	-	900	1.5	wood	

(c) assembly successfully withstood the max. set load for the scheduled 900 sec.

(d) assembly successfully withstood the max. set load for the scheduled 2700 sec.

(iii) no failure – interlayer presented plastic deformation

(iv) no failure – interlayer presented no or negligible plastic deformation

- applied as 2 x 3 mm

All specimens successfully withstood the set 40 kN (or 20 kN) load for 900s. In particular, none of the 80A specimens had “plastic” deformation after the removal of the load. In comparison, the 70A specimens clearly had visible plastic deformation at the contact area of the interlayer with the glass blocks (see Fig. 8.23).

Overall, the 70A specimens showed less deformation (1.0 – 1.4 mm) during the creep mode than the 80A variants (1.3 – 1.5). The 80A specimens showed similar creep resistance in both 3 and 6 mm thickness and a rather broad range of deformation under creep in both cases as can be seen in Fig. 8.18.

The 6 mm thick 70A interlayers had a relatively stiffer and more consistent behaviour under creep compared to the 3 mm variant: all 3 specimens (70A_{6,4} – 70A_{6,6}) showed between 1.0-1.4 mm total deformation under creep compared to 1.1-1.8 mm of the 70A_{3,1} – 70A_{3,3} specimens (see Table 8.2 and Fig. 8.19). In particular, specimen 70A_{6,5}, which was subject to a 40kN constant load for 2700s, showed the closest approximation to a horizontal slope at the (u-t) diagram shown in Fig. 8.19; in the last 1450 s of the test the interlayer deformed by 0.1 mm. It is unclear if this deformation can be attributed to the interlayer material or the neoprene used as intermediate between the glass blocks and the steel machine, or both. The 70A

specimens tested in compression under a constant load of 20kN ($70A_{6.1} - 70A_{6.3}$) presented a nearly consistent deformation under the creep test duration, equal to 0.9 – 1.0 mm (Fig. 8.20), comparable to the deformation of similar specimens tested under double the load.

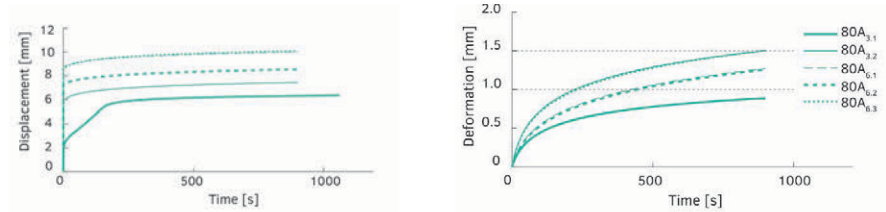


FIG. 8.18 Displacement in time ($u - t$) graph for the 80A interlayer specimens of 3 mm and 6 mm thickness tested under 40 kN load for 900s (left) and processed graph so that the deformation in time is shown only during the set 40kN constant load (right).

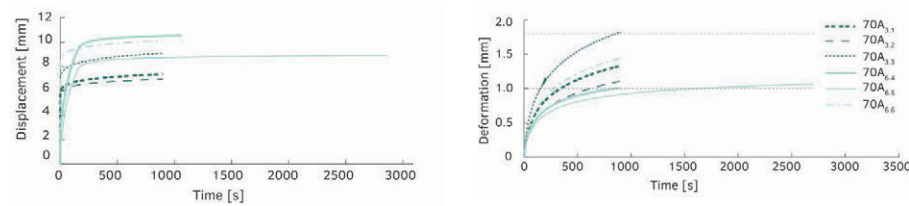


FIG. 8.19 Displacement in time ($u - t$) graph of 70A interlayer specimens of 3 mm and 6 mm thickness tested under a static 40 kN load for 900 s (left) and processed graph so that the deformation in time is shown only during the static 40 kN load (right).

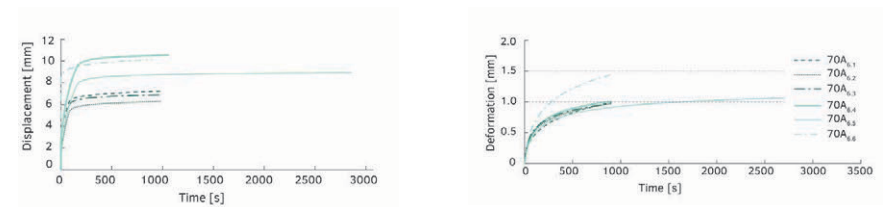


FIG. 8.20 Displacement in time ($u-t$) graph for 70A interlayer specimens, 6 mm thick tested under 20 kN ($70A_{6.1} - 70A_{6.3}$) and 40 kN ($70A_{6.4} - 70A_{6.6}$) load for 900s (left) and processed graph so that the deformation in time is shown only during the set constant loads (right).

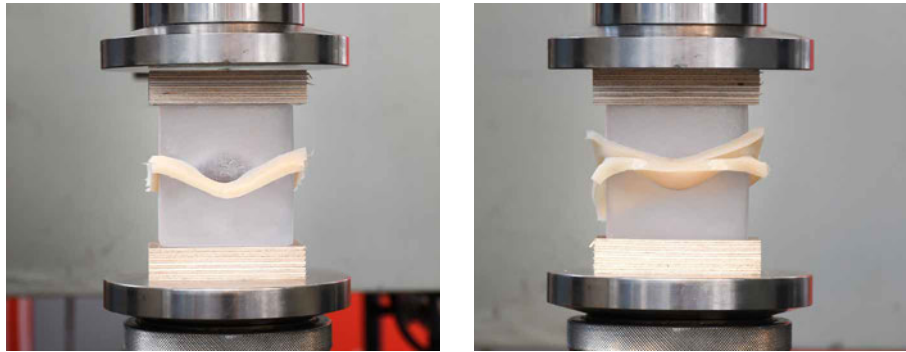


FIG. 8.21 A 6 mm thick 70A specimen before (left) and during (right) resting under 40 kN constant load

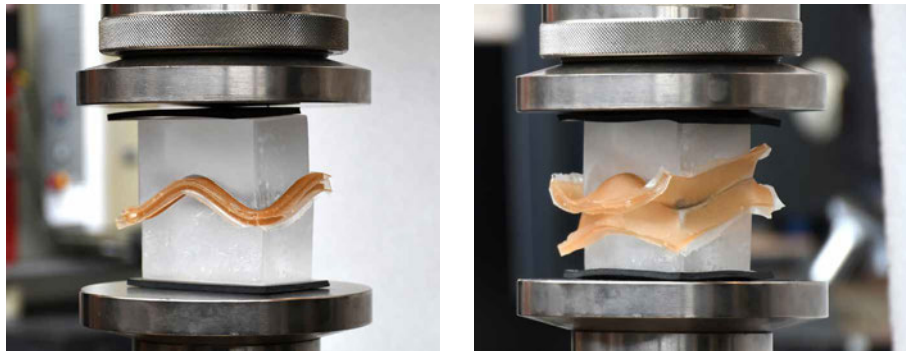


FIG. 8.22 A 6 mm thick 70A specimen, before (left) and during (right) testing under 40 kN constant load.



FIG. 8.23 Visible plastic deformation of 70A specimen directly after the completion of the test.

8.3.3 Conclusions on Interlayer material

Three different series of specimens out of kiln-cast glass interlocking blocks interleaved with different cast PU interlayers were tested under compression as follows:

- 1 3 mm thick interlayers were tested until failure by a constantly increasing compressive load
- 2 3 mm thick interlayers were tested in compression up to a max. set load of 40 kN; upon reaching that value the load was maintained constant for 900 s.
- 3 6 mm thick interlayers were tested in compression up to a max. set load of 40 kN; upon reaching that value the load maintained constant for 900 s.

Table 8.5 summarizes the main findings of each series. Overall, it can be derived that the creep and tear resistance of the interlayer are of crucial importance to the structural performance of the interlocking assembly.

TABLE 8.5 Summary of the main results of the interlayer testing.

Series	Interlayer applied	t_{int} mm	No of Specimens	$F_{max.set}$ kN	Creep mode s	Failure mode/ observations
1	70A	3	3	-	-	(a ₁)
	80A		2			
2	60A	3	3	40	900	(a ₂)
	70A		3			(b ₁)
	75A		3			(a ₂)
	80A		2			(b ₂)
3	70A	6	6	20 / 40	900 (2700)	(b ₁)
	80A		3	40	900	(b ₂)

(a₁) Failure due to insufficient contact of the interlayer at the concave-convex interlocking area of the blocks, combined with the shear stresses occurring at the interlocking surface due to the increasing deformation of the interlayer under constant or increasing load.

(a₂) Failure due to penetration of the interlayer leading to glass-to-glass contact

(b₁) No failure – visible plastic deformation

(b₂) No failure – no observable plastic deformation

In the first series [1] all specimens failed under increasing or constant (≥ 50 kN) load due to insufficient contact of the interlayer at the concave-convex interlocking area of the blocks, combined with the shear stresses occurring at the interlocking surface due to the increasing deformation of the interlayer. Although in several of the specimens the assembly reached the maximum set load without cracking, the

continuous deformation of the interlayer under static load thereafter introduced further tensile stresses that eventually lead to failure of the glass elements. Accordingly, it was determined to set the max. load to 40 kN for the next 2 series. In addition, the aforementioned failure mode of the specimens indicated that due to the manual fabrication and post-processing of the kiln-cast blocks an interlayer thicker than 3 mm might be essential for preventing the generation of localized peak stresses due to the insufficient surface contact between the glass and the interlayer.

In the second series [2] of experiments, it was derived that interlayers with a lower tear resistance, namely *Permacol 5450 (75A)* and *PMC 746 (60A)* are unsuitable for the examined structural application due to the penetration of the interlayer, which leads to the eventual glass-to-glass contact and thus to failure at lower stress values. On the contrary, all 70A (*PMC 770*) and 80A (*Task 16*) specimens were able to successfully withstand the set 40kN constant load for 900s. Nonetheless, none of the interlayer specimens stabilized within the 900 s interval at the given load and interlayer thickness: in all cases, the deformation in time (u-t) graph of the specimen indicated that the interlayers were creeping through the duration of the test. If the test had been programmed for a longer duration, failure would have possibly occurred similar to the one described for the first series due to the increased dimensional tolerances of the blocks in combination with the increasing shear stresses imposed within the interlayer due to creep. Thus, it was determined to further validate these two more promising materials in a larger thickness, of 6 mm, under the same constant load of 40 kN for 900s. It was also determined to test one of the series to a constant 20 kN load, which corresponds to a nominal compressive stress that is in closer proximity to the one anticipated in an actual construction.

Indeed, the results of the third series [3] showed that the thicker variants behave stiffer under compression. This is particularly the case for the 70A_{6,x} specimens, which deformed less in creep than the 3 mm variants (70A_{3,x}). The 70A_{6,5} specimen, which was the only one tested under creep for 2700s, presented an almost stable deformation after approx. 1300s. This suggests that the examined interlayer could possibly reach equilibrium if tested for longer duration and present the desired time-independent deformation. This, however, is yet to be experimentally confirmed.

Although the 70A specimens presented apparent plastic deformation, whereas the 80A did not, the former presented a comparatively more horizontal slope in the deformation in time (u-t) curve and better creep resistance than the latter. Thus, *PMC 770 (70A)* of 6 mm thickness was determined to be used in the out-of-plane shear experiments, described in the following section. It is considered that the 80A interlayer is an equally promising candidate for further investigation.

From the interlayer testing several more important outcomes were withdrawn regarding the geometry of the interlocking glass units:

The experiments demonstrated that an insufficient fillet radius at the edges of the interlocking mechanism can lead to local perforation of interlayers with lower tear resistance and in turn to the early failure of the assembly due to glass-to-glass contact. Thus, smoother changes in curvature along the interlocking surfaces are preferred.

Another conclusion regarding the interlocking geometry derived from the tests is that the greater the amplitude of the interlocking system, the more sensitive the assembly is to manufacturing intolerances and thus to the introduction of peak tensile stresses because of insufficient contact (mismatch) and collaboration between the interlayer and the glass units. This can be improved either by introducing a thicker interlayer (4-6 mm), which however would further compromise the stiffness of the assembly, or by a smoother interlocking mechanism.

8.3.4 **Shear tests on osteomorphic blocks with different amplitude height**

8.3.4.1 **Method**

Aim of this experiment is a comparative evaluation of the mechanical performance of blocks of various amplitudes and to investigate the effect of the geometry of the interlocking mechanism to the structural behaviour of the assembly. The block's amplitude height is defined as the distance between the planes of the highest and lowest points of the interlocking mechanism. Accordingly, assemblies out of osteomorphic blocks with different amplitudes, namely 10 mm, 15 mm and 20 mm, were tested in out-of-plane shear, in series of 3 specimens each (see Fig. 8.24). An illustration and a photograph of the experimental set-up can be found in Fig. 8.25 and Fig. 8.26 respectively.

Based on the output of the experimental testing on the interlayer material it was determined to apply 6 mm thick 70A interlayers in between the blocks of each assembly to ensure the full contact of the interlayer and the blocks and the even spread of stresses. Accordingly, each assembly consists of 3 blocks - two halves and one full block in the middle - which are interleaved with 6 mm thick 70A interlayers

in between. A steel frame stabilizes and supports the assembly. The frame is pre-compressed by two steel threaded rods in a plane vertical to the applied load. The pre-compression of the rods is applied by a mechanical torque wrench set in a consistent, low pre-stress, value. The set-up is flipped by 90 degrees when the pre-compression is applied in order to facilitate the self-alignment of the blocks; after pre-compressing the assembly, it is flipped back to a horizontal position. Soft 3 mm thick neoprene interlayers are placed as intermediary between the glass blocks and the steel plates. A soft aluminium rectangular bar, 20 mm wide is placed under the steel bar that applies the deformation force to the assembly. The aluminium bar allows the accurate measurement of the deformation of the middle glass block, without introducing concentrated stresses to the glass surface. All the tests are carried out in a Zwick Z100 displacement-controlled universal testing machine at a loading rate of 5 mm/min.

It should be noted that due to the manual fabrication of the blocks, some of the specimens would self-align in a shifted position compared to each other. Due to the resulting eccentricity, the load was not applied in an absolutely vertical direction.

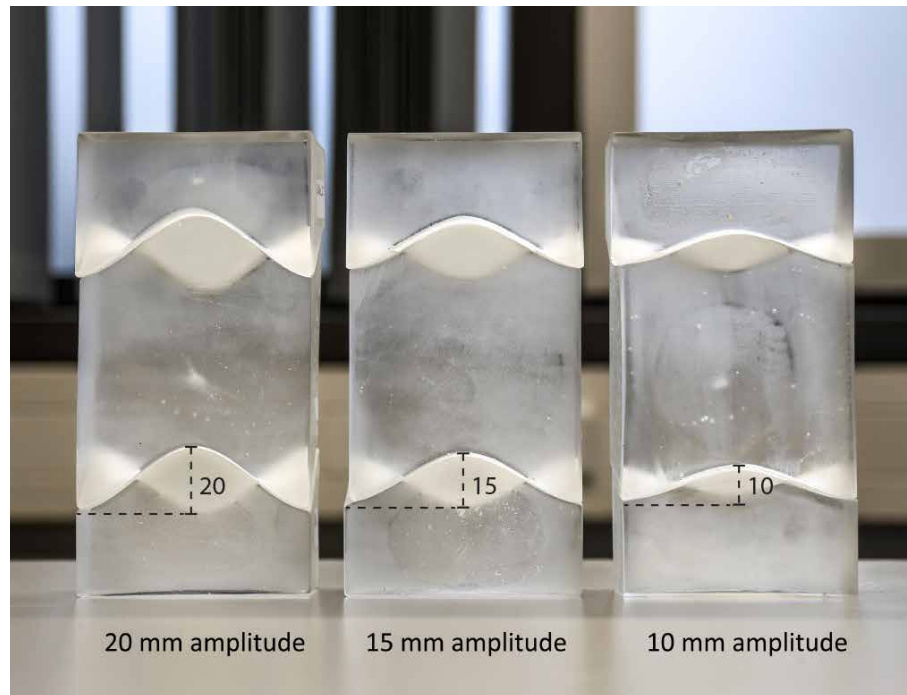


FIG. 8.24 Assemblies (without the use of an interlayer) of blocks with the different examined amplitudes.

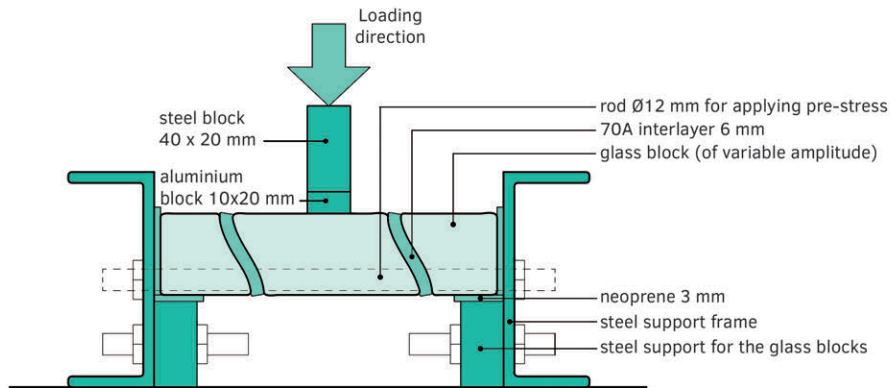


FIG. 8.25 Illustration of the experimental set-up.

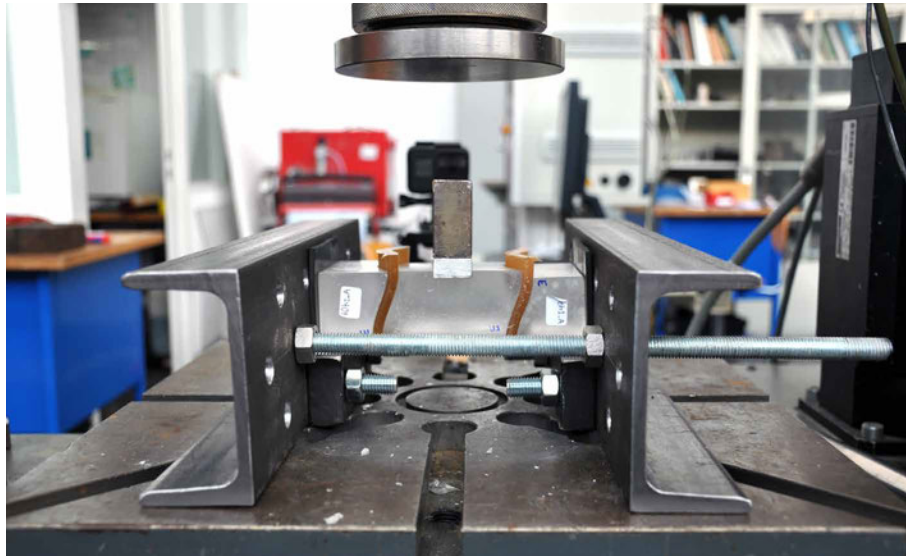


FIG. 8.26 Experimental set-up

8.3.4.2 Results

Table 8.6 summarizes the main results. The Standard Force vs displacement (F-u) graph of all specimens can be seen in Fig. 8.27. The tests were stopped when there was evident cracking of the blocks which resulted in a significant loss of load-carrying capacity.

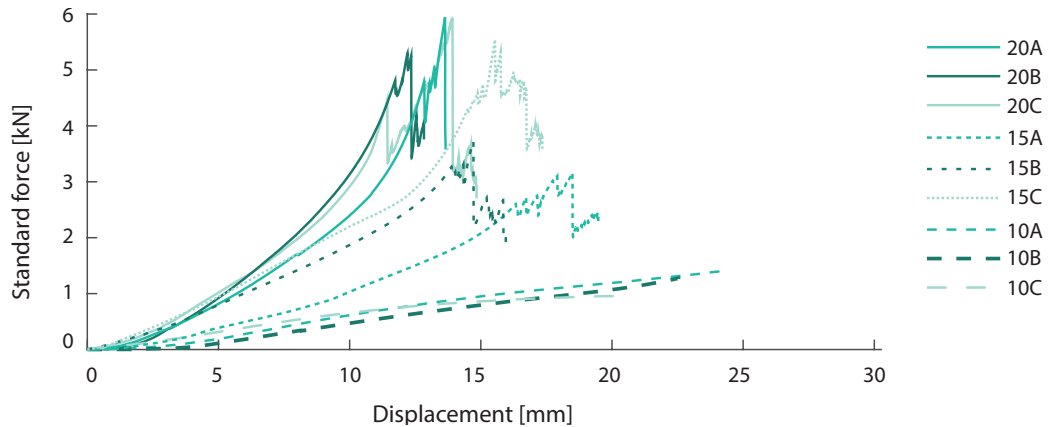


FIG. 8.27 Displacement - Standard Force diagram for all specimens

TABLE 8.6 Summary of the main results

Series	Specimen	F_{crack} [N]	U_{crack} [mm]	Cracked blocks H: side block M: middle block	Remarks
10	A	1410	24.1	-	(i), (ii)
	B	1280	22.5	-	(i), (ii)
	C	967	20.5	-	(i), (ii), *
15	A	3170	19.5	M	(ii), (a), *
	B	3740	15.9	M	(ii), (a)
	C	5553	17.3	H, M	(ii), (a), *
20	A	5950	13.6	H, M	(ii), (a), (b), *
	B	5310	12.8	M	(ii), (a)
	C	5930	14.8	H, M	(ii), (a), (b), *

(i) test aborted when the total deformation (incl. initial deformation of the settling of the machine) was 25 mm. No damage occurring at the blocks, nor plastic deformation of the interlayer.

(ii) visible shifting of the middle block downwards with increasing load

(a) crack initiated close to the change of interlocking curvature of the middle block

(b) crack initiated close to the change of interlocking curvature of the half block

* load was applied in a slightly inclined direction due to the initial misalignment of the assembly

The following main conclusions were drawn from these experimental series:

- All specimens showed visible deflection, expressed as the shifting of the middle block downwards, prior to failure. This is because the blocks are in principle free to rotate. The resistance to the bending moment is provided by the peripheral constraint force, which in the experimental set-up is considerably low. This in turn results to a limited load-bearing capacity of the system prior to failure. Yet, the low bending stiffness

of the assembly can also be seen as a warning mechanism that allows for increased safety in a structure, due to its pseudo-ductile behaviour prior to failure.

- As expected, the specimens had localized failure and thus, an effectively increased damage tolerance compared to a monolithic variant: cracks do not spread from one element to another in the specimens. In the cases where two blocks would crack, this would happen non-simultaneously and occurs at different locations (see Fig. 8.31 and Fig. 8.32).
- Blocks with a higher interlocking amplitude are in principle more favourable as they present a higher shear capacity and stiffness and fail at less deformation (see Fig. 8.28).
- Internal flaws (within the meso-structure of the blocks) or defects at locations that are not anticipated to be subject to peak stresses do not seem to compromise the overall performance of the assembly. Actually all specimens failed at the same locations; either at the edges or close to the middle of the interlocking mechanism.
- After removal of the load, all specimens tended to resettle towards their original configuration; yet the assemblies remained visibly misaligned (Fig. 8.29, Fig. 8.30, Fig. 8.31).
- Higher pre-stress values and the use of thinner interlayers are essential for obtaining a stiffer assembly/system.
- The relatively low dimensional accuracy of the kiln-cast components has influenced the structural performance of the specimens. Yet, due to the magnified effect of such deviations, they also revealed that the examined geometry is prone to eccentricity during assembly caused by the sliding of the components relevant to each other. The resulting eccentricity is higher as the amplitude increases.

In general, the specimens of each series presented relatively consistent failure values and stiffness curves, as can be seen in Table 8.6 and in the F-u diagram of Fig. 8.27. Overall, it can be inferred that the higher the amplitude, the stiffer the behaviour of the assembly is, failing at higher loads and at less deformation. More specifically, specimens with 20mm amplitude failed at approx. 5 times the load and at almost half the deformation compared to specimens with half the amplitude (10mm) (see Fig. 8.28). From the graph of Fig. 8.27 it can also be observed that the stiffness of the specimens with 15mm amplitude is closer to the one of the 20mm variant than the 10mm one.

In all three series, the middle block was evidently shifted downwards, prior to cracking (see Fig. 8.28). This high deformation is attributed primarily to the low pre-stress value applied (the threaded rods were loosely fastened) and secondly to the relatively thick interlayer of 6mm, essential for accommodating the dimensional discrepancies of the manually fabricated glass blocks. The dimensional deviations, combined with the necessity for a relatively thick interlayer, have also resulted in many cases into an initial eccentricity of the assembly during installation in the test rig. The relatively low forces at failure can also be attributed to the low bending stiffness of the specimens.

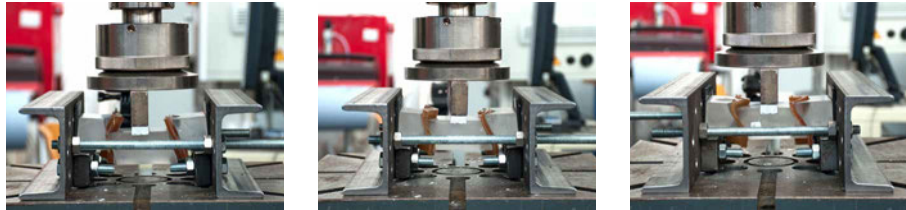


FIG. 8.28 Maximum deformation prior to failure of assemblies with blocks of 10 mm (left), 15 mm (center) and 20 mm (right) amplitude. The tests with blocks of 10 mm amplitude were aborted once the assembly reached an apparent deformation of 25 mm.



FIG. 8.29 Assembly of block with 10 mm amplitude before (left), during (centre) and after testing (right). It can be seen that upon load removal the assembly is self-realigned towards its original configuration.

More specifically, the testing of the 10mm amplitude series was aborted when the total deformation (including the initial settling of the testing machine) reached 25mm. There were no cracks observed at any of the specimens, yet the middle block in all cases had slid almost entirely out of the assembly (Fig. 8.29). In this case, the insufficient pre-compression applied at the external frame and the accumulated thickness of all the interlayers (two 6 mm PU sheets and two 3 mm neoprene sheets) could allow the slide-out of the middle block of just 10 mm amplitude. When the load was removed the assembly self-realigned towards its initial configuration. Due to time restrictions the assembly had to be removed a few minutes after testing and

thus it was not checked if the specimen would eventually resettle fully to its original position. The other two assemblies behaved similarly, with the 20mm amplitude series presenting the highest shear capacity.

In all specimens of the series of 15mm and 20mm amplitude, failure occurred at the interlocking surface, in particular, either close to the middle of the side interlock, where there is a change in interlocking curvature⁷⁰ (see Fig. 8.30, Fig. 8.31 and Fig. 8.32) or at the edges of the blocks. In specific, after the middle block has shifted downwards, the assembly becomes stiffer. This appears at the F-u diagram in Fig. 8.27 as a change to a steeper inclination of the specimens prior to failure. The stiffening can be attributed to an increased contact area after the resettling of the individual components. Upon stiffening, high peak stresses are generated at the upper part of the middle block. As a result, all specimens consistently failed at the middle block. Owing to the fragmented nature of the system, there was no crack propagation to the adjacent blocks. When one of the support (half) blocks also failed, the crack in the latter would again initiate from one of the locations where the curvature changes at the interlocking surface. This could be either in close proximity to the point of origin of the initial crack of the middle block or to a completely different location (e.g. on the other interlocking side of the block) (see Fig. 8.32). There was no plastic deformation observed at any of the interlayers. In some cases, due to the energy released by the crack, the interlayer would be locally sliced from the glass fragments after failure had occurred.

An important observation derived from the experimental set-up itself, is that the examined interlocking geometry is prone to eccentricity during assembly due to the limited number of interlocking shear keys. The higher the amplitude the more the resulting eccentricity due to manufacturing dimensional tolerances, as blocks tend to slide away from each other. Thus, although the highest amplitudes are preferable for shear resistance and reduced global deformations, they are also the most prone to induce eccentricity to the assembly. An interlocking mechanism of average amplitude, i.e. in this case 15 mm, is in this case considered the best compromise between shear capacity and accuracy in construction. In addition, the design of an interlocking mechanism with multiple locks, such as the Type B osteomorphic block presented in sections 7.5.2 and 7.5.3 is suggested as a more favourable form: the multiple interlocking locks of this geometry enhance the self-aligning capacity of the components, and to this extent, of the resulting structure as well.

⁷⁰ This location is different to the one anticipated by the numerical model described in chapter 8.3 as the latter has been made to simulate in-plane shear stresses.

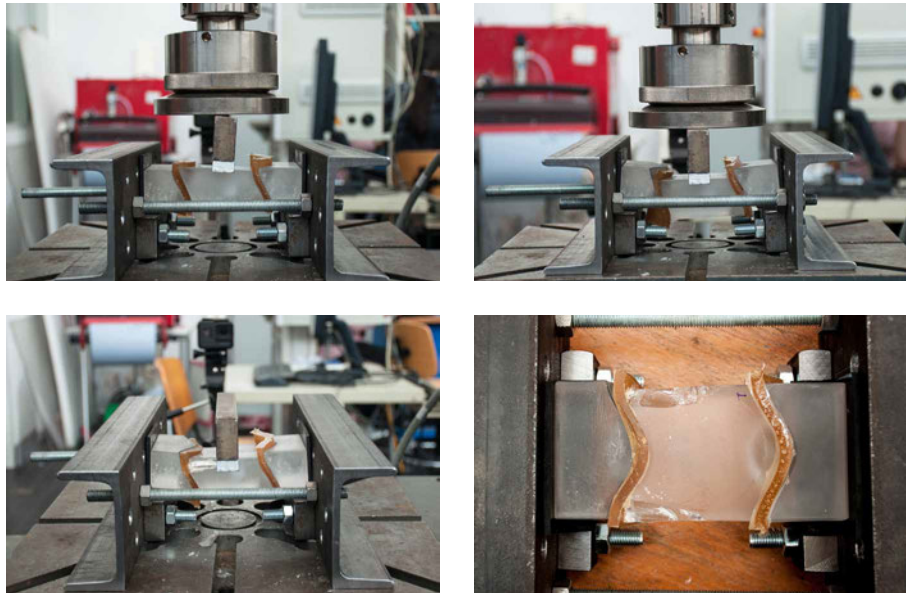


FIG. 8.30 Specimen out of blocks with 15 mm amplitude before testing (top left); at max. deformation (top right); and after failure (bottom left and right).

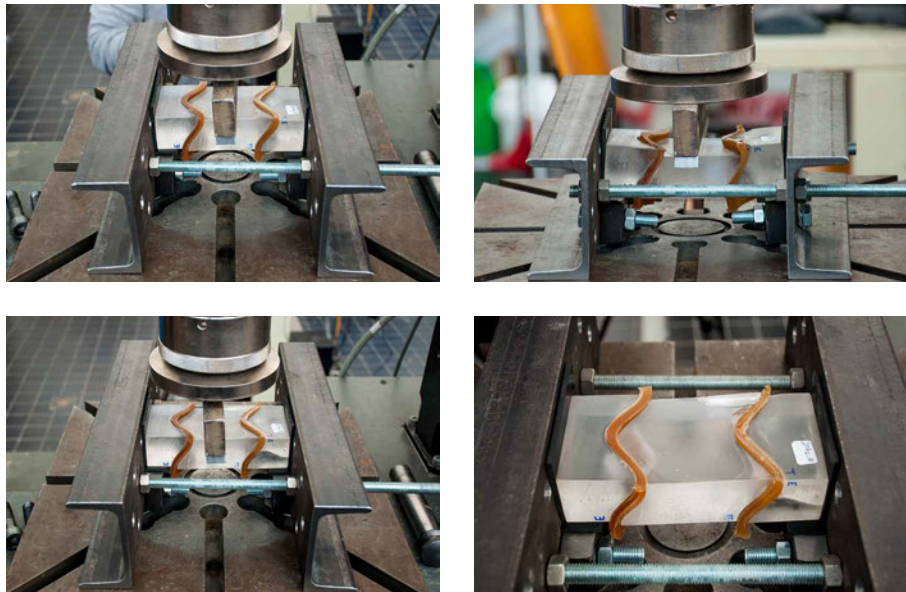


FIG. 8.31 Specimen out of blocks with 20 mm amplitude before testing (top left); at max. deformation (top right); and after failure (bottom left and right)

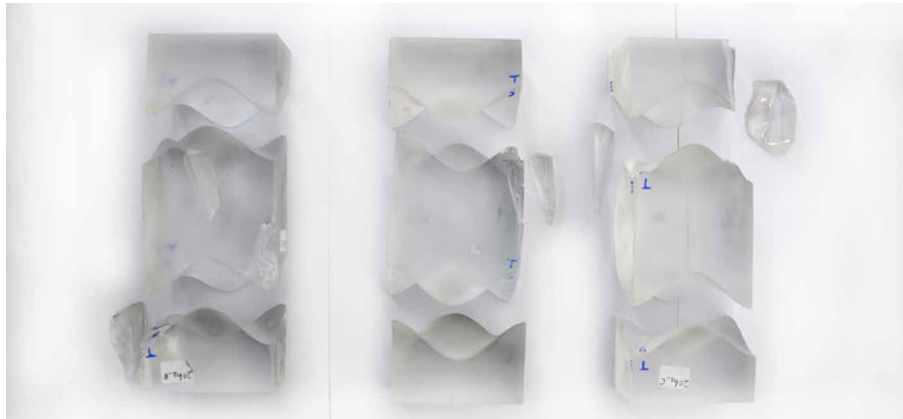


FIG. 8.32 Specimens out of blocks with 20 mm amplitude after testing. It is evident that the crack in adjacent blocks are not continuous.

8.4 Numerical investigation of the interlocking geometry of the osteomorphic blocks

8.4.1 Model set-up

The experiments indicated that higher amplitudes are more favourable in terms of shear capacity, yet they are as well more prone to eccentricity caused by dimensional deviations. A solution to this is the design of an interlocking unit with multiple shear keys, which enhance its self-alignment capacity, such as Type B block described in section 7.5.2. Moreover, the experiments suggested that for the manufactured kiln-cast specimens a thicker than 3 mm interlayer is necessary to accommodate the dimensional discrepancies. The thicker the interlayer, the more compromised becomes the stiffness of the entire assembly. In case that industrially manufactured glass blocks are used, it is anticipated that interlayers between 3-4mm thickness should suffice for accommodating the dimensional discrepancies of the individual blocks but also of the entire construction.

Accordingly for the numerical model, developed by (Jacobs 2017), an osteomorphic block with multiple locks, similar to Type B⁷¹ form (discussed in Chapter 7, see Fig. 7.10) is used. The reference brick dimensions are 300x150x150 mm. The geometry of this block is generated by multiplying type A block –used in the previous experiments– four times and scaling it up by a factor of 2 (see Fig. 8.33). A 4 mm 70A PU interlayer is simulated as the intermediate between the blocks.

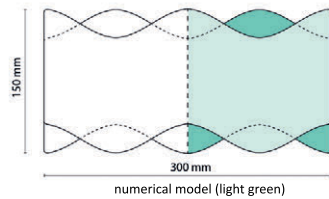


FIG. 8.33 Numerical model (Type B block) vs experimentally tested block (Type A).

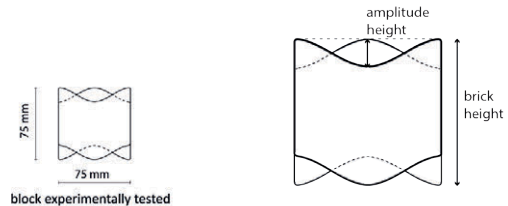


FIG. 8.34 Definition of block height and amplitude height.

Aim of the model is to further assess the influence of the most crucial geometrical aspects of the interlocking mechanism, namely the amplitude and the brick height, to its structural performance.

The amplitude height of each block is defined as the distance between the planes of the highest and lowest points of the interlocking mechanism, as shown in Fig. 8.34. The studied range concerning the block height is from 40mm to 150mm and the amplitude height is from 5mm to 20mm. A detailed description of the model set-up can be found in (Jacobs 2017). The geometry of the block is generated through the Grasshopper plug-in for Rhinoceros. This plug-in allows for automatic generation of new geometries by changing certain input parameters. The model variations⁷² are then exported as a solid, using a STEP-file and imported into DIANA FEA, a finite element software.

⁷¹ A more detailed study regarding the presented numerical model can be found in (Jacobs 2017). The numerical model has been developed for type B block but corresponds to both types, since Type B block is generated by multiplying Type A. It is expected that compared to type B, type A blocks will present a slight decrease in load capacity due to extra eccentricity in loading.

⁷² Form deviations due to fabrication tolerances in the size of the unit were not considered in the final model.

Due to the fact that glass is a brittle material with a stated compressive strength approximately ten times its tensile strength, its failure behaviour cannot be described by a single-property criteria such as Von Mises stresses, which do not distinguish the value between compression and tension strength and implies a ductile behaviour. Thus, the variation models are evaluated applying the Christensen's failure criterion, which essentially converts the principal stresses and its material properties into a failure envelope definition, including a limitation for the tensile capacity of brittle materials (Christensen 2013). The criterion is given in equation 8.1:

$$\left(\frac{1}{T} - \frac{1}{C}\right) (\sigma_1 + \sigma_2 + \sigma_3) + \frac{1}{2TC} [(\sigma_1 - \sigma_2)^2 + (\sigma_2 - \sigma_3)^2 + (\sigma_3 - \sigma_1)^2] \leq 1$$

EQUATION 8.1

In which, $\sigma_1, \sigma_2, \sigma_3$ are the principal stresses, T is the tensile strength and C is the compressive strength.

The criterion includes extra conditions for brittle materials, which occur when $T/C \leq 1/2$. These conditions are given in equation 8.2.

$$\begin{aligned} \sigma_1 &\leq T \\ \sigma_2 &\leq T \\ \sigma_3 &\leq T \end{aligned}$$

EQUATION 8.2

According to (Christensen 2013) glass presents a ratio between tensile and compressive strength of approx. $T/C = 1/8$. Hence, the criterion can be used to predict at which point of the geometry tensile surface stresses become critical and can lead to failure by activating flaws. Accordingly, by loading the interlocking brickwork in shear, the generated contour plots show directly how tensile peak stresses are spread on the contact surface (Fig. 8.35). Essentially, these contour plots can be used to indicate:

- 1 where flaws in the geometry would be most influential (tensile opening of cracks)
- 2 how stress concentrations spread across the contact surface
- 3 the stress gradient at sections in the geometry

By evaluating both the contour plots and the shear lock capacity multiple geometry variations can be evaluated on their applicability as cast glass interlocking

components. The numerical model showed that any compressive load puts the geometry in a compressive state and hence yields higher shear capacities compared to when no compressive force is applied. Hence all variants were tested without any compressive load; instead the shear-load-inducing bricks were constrained in the global z-direction.

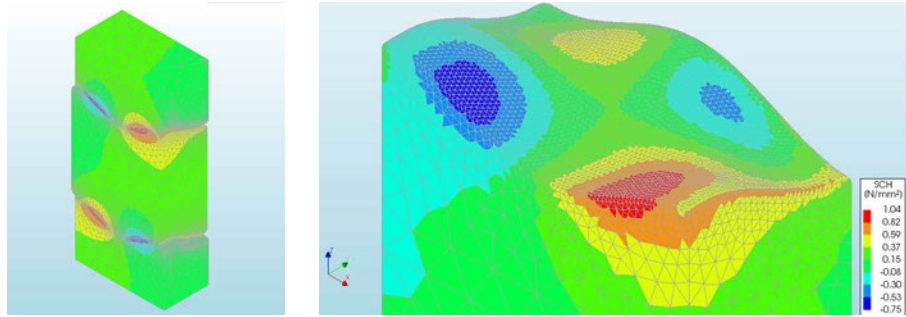


FIG. 8.35 Left: Numerical set up and results for Christensen's failure criterion value of one (SCH=1) of the tested variants. Right: Christensen's output (SCH=1) of middle brick (amplitude 10 mm). Shear capacity at failure is approximately 155 kN. Source:(Jacobs 2017).

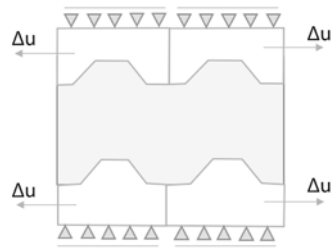


FIG. 8.36 (left) 2D Full scale principle of the model. Source:(Jacobs 2017).

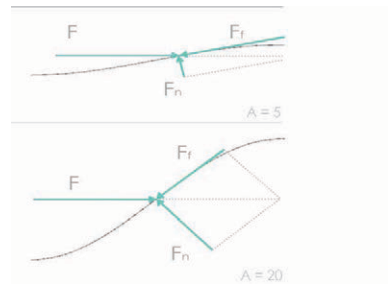


FIG. 8.37 (right) Uplifting principle for interlocking blocks with $A=5$ mm and $A=20$ mm. The shear force is depicted as a concentrated force (F) halfway the amplitude. Dead weight and weight of upper structure are not accounted for. The force is conveyed in an uplifting force (Ff) by traction tangent to the steepness at that point and in a force (Fn) by compression normal to the geometry. Source:(Jacobs 2017).

Geometry set-up

Considering the symmetry of the Type B brick design the whole model can be reduced to a quarter of its original size. This leads to fewer elements and a more efficient calculation time. Thus, to simulate a shear test, one quarter of a Type B

brick (equivalent to a full type A brick) is held between two one-eighth Type B bricks (equivalent to two halves type A bricks); in-between the glass elements two 4 mm thick PU interlayers are placed (Jacobs 2017). Fig. 8.36 shows a full-scale principle of the DIANA model in 2D.

Material settings

The input properties can be found in Tables 8.7 and 8.8 as established by (Jacobs 2017). As discussed in chapter 7.6, in general the Shore durometer scale is used to define the hardness and resistance to indentation of elastomer (and plastic) materials such as the applied PU interlayer. In theory the hardness of a polymer in a given thickness can be converted to a Young's Modulus value when in compression, as described by (Kunz, Studer 2006). Based on their experimental work on 6mm thick interlayers, the following formula for calculating the Young's Modulus of 6mm thick PU in compression is derived:

$$E_{PU;c\ 6mm} = \frac{1-\nu^2}{2RC_3} * \frac{c_1+c_2*Sh_A}{100-Sh_A} * (2.6 - 0.02 Sh_A) \quad [MPa] \quad \text{EQUATION 8.3}$$

In which $E_{PU;c\ 6mm}$ is the Young's Modulus of a 6mm thick PU in compression [MPa], ν is the Poisson's ratio, Sh_A is the Shore A hardness. R , C_1 , C_2 and C_3 are constants derived from the experimental set-up by (Kunz, Studer 2006) and have the following values:

$R = 0.395$ mm, $C_1 = 0.549$ N, $C_2 = 0.07516$ N and $C_3 = 0.025$ mm. Minor effects of friction and deviation from the ideal Poisson's value ($\nu = 0.50$) can be considered negligible. However, this formula was only validated for 6 mm polymer interlayers; there is no factor in the equation that concerns the thickness of the interlayer and no tests were performed in polymers of smaller thicknesses.

TABLE 8.7 Input properties of glass and polyurethane interlayer

Material	Glass	Polyurethane
Density	2.5*10 ⁻⁹ t/mm ³	1.1*10 ⁻⁹ t/mm ³
Poisson's ratio	0.22	0.48
Young's Modulus	70000 N/mm ²	50 N/mm ²
Tensile Strength	45 N/mm ²	-
Compressive Strength*	360 N/mm ²	-

* For the tensile strength (T) of glass the characteristic strength of annealed float glass is used. Christensen states that $T/C = 1/8$ for glass, thus, its compressive strength (C) is set to 360 MPa. In reality the compressive strength of glass can be significantly higher, but to satisfy the Christensen criterion the earlier mentioned value is applied in the model. As the leading fracture mechanism in glass occurs only due to tensile peak stresses it is not necessary to excessively review the influence of compressive stresses on the geometry.

TABLE 8.8 Input properties of interface elements

Parameter	Value	Unit
Cohesion c	0.001	N/mm ²
Normal stiffness modulus z	70 *10 ⁶	N/mm ³
Shear stiffness modulus x	7 *10 ⁶	N/mm ³
Shear stiffness modulus y	7 *10 ⁶	N/mm ³
Tensile strength gap criterion f_t	0.0005	N/mm ²
Friction angle ϕ	1.1	rad
Dilatancy angle	0	rad
Interface opening model	Gapping model	-

Thus, for the numerical model, the values for Poisson's ratio and Young's modulus used are calibrated using the experimental results of (Aurik et al. 2018) for PU70 interlayers of 1, 2, 3 and 4 mm thickness tested in compression. Hence the applied values are only valid for a PU with a hardness of 70A. A detailed explanation of the calibration method can be found in (Jacobs 2017). To calibrate the Young's modulus of PU to a realistic value, part of the test set up discussed in (Aurik 2017) is modelled in DIANA FEA by (Jacobs 2017). A fine mesh with element size of 2 mm is applied on the PU interlayer, and to limit calculation time and file size the mesh size is gradually increased to 20 mm. A compressive distributed load of 10.88 MPa is applied on the top glass face to conform the test setup discussed in (Aurik 2017). The Young's modulus is then varied until a deformation of 0.13 mm is found, corresponding to the result of the laboratory test. The results suggested a value of $E=50$ MPa with a Poisson's ratio equal to $\nu=0.48$ (Jacobs 2017).

Support conditions

A scheme of the support conditions can be seen in Fig. 8.38. The main object of the model is to calculate the shear capacity of the interlocking geometry. The most critical brick is expected to be at the top of the construction, where the least vertical loading is applied. Thus, one desired result of the model is to define the force necessary to prevent uplifting. Fig. 8.37 shows the principle of uplifting in the studied geometry.

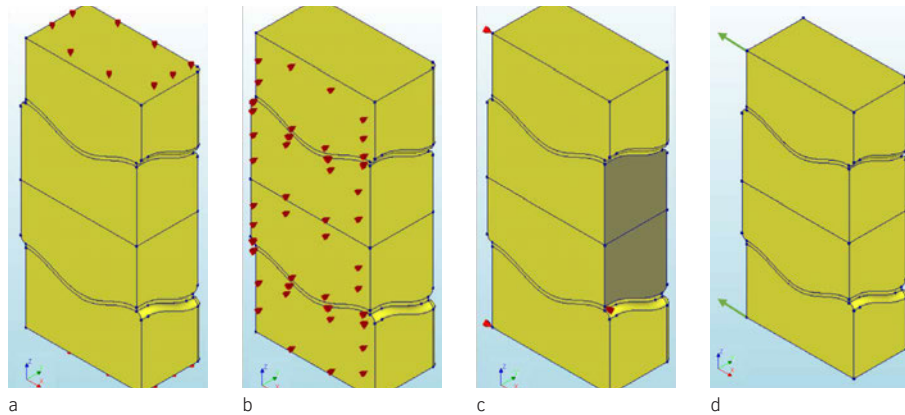


FIG. 8.38 Support conditions in a) Z-direction, b) Y-direction and c) X-direction. d) Tied vertices loaded with a prescribed deformation load. Source: (Jacobs 2017)

To evaluate the uplifting behaviour, the upper and bottom plane of the assembly are restraint in the Z direction. Due to the shear loading it is expected that parts of the geometry will tend to move upward, creating reaction forces across the planes. To simulate the symmetric geometry of the type B block, supports are added in the Y-direction. The sliced face is thus restrained in the Y-direction. In the X-direction, a similar support is needed for the middle block. One vertex is supported here which is tied to shaded faces. In this way, any deformation set in any node of these faces will have the same deformation as the master node. All reaction forces are summed into this master node, which enables easy access to the desired value of the characteristic shear strength of the geometry. Two more supports are added in the X-direction for the top and bottom bricks, to accommodate the prescribed deformation loads that introduce the desired shear loading of the assembly. Again the nodes are tied to the future mesh nodes on the corresponding surface, gaining supports and the same prescribed deformation (Jacobs 2017).

Loading conditions

As previously mentioned, a prescribed deformation is applied to the top and bottom blocks. Owing to the sliding support on top and bottom, these geometries are free to move, with only the interlocking geometry as obstacle. The applied load is conveyed through the PU interlayer to the middle block, which will in turn display the resulting stress concentrations according to Christensen's failure criterion. The load is applied on the supported vertexes, which due to the tying will copy the same deformation to any of the nodes on the tied surface. A prescribed deformation of $\Delta u = -0.1$ mm is applied to both vertexes (Fig. 8.38d) (Jacobs 2017).

Parameter ranges tested

A selection of models with different amplitude and height variants are generated and tested in DIANA. The initial model is set with an amplitude of 10 mm and a height of 150 mm. The tested amplitudes are in a range from 5 mm to 20 mm. The parameter variations for the height are between 40 mm and 150 mm. Higher bricks than 150 mm are considered impractical in terms of installation and fabrication, as the initial brick design is already approx. 17 kg in weight (Jacobs 2017).

8.4.2 Results

Fig. 8.39 gives an overview of the influence of different amplitude and brick height variants on the shear capacity.

Fig. 8.40 demonstrates that a higher amplitude would increase the shear capacity due to a larger contact area for the stresses to be distributed, while reducing the relative uplifting tendency. This is in line with the findings of the shear experiments described in section 8.3.4. A higher amplitude would also increase the chances of a shear-key failure, which is considered beneficial as it provides a warning failure mechanism. As can be depicted from the contour plots in Fig. 8.41, the tensile and compression areas grow in horizontal direction in the shear keys. This increases the probability of a shear key failure instead of a splitting brick failure. A negative effect of an increase in amplitude is that a higher precision of the brick geometry is required, as the failure limit is reached at a smaller deformation (Fig. 8.39). A

deviation from the perfect geometry⁷³ would hence lead to earlier failure for brittle materials (as also discussed by (Dyskin et al. 2003) compared to lower amplitude variations. An excessively small amplitude however would result in uplifting to become a crucial factor, needing a heavier top constraint and relying more on friction than on the interlocking geometry (Jacobs 2017). This was evident as well by the shear experiments: the osteomorphic blocks with the smallest amplitude (10 mm) would essentially slide out in a set-up of low pre-compression. The choice for a higher amplitude is therefore considered a trade-off between a higher shear capacity and a reduction in uplifting behaviour on the one hand, and geometry manufacturing precision on the other hand.

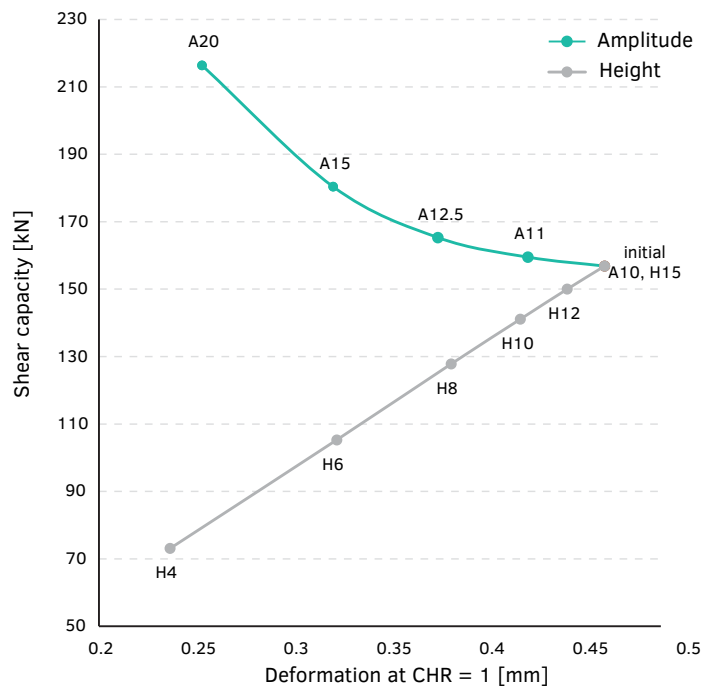


FIG. 8.39 Shear capacity and deformation at failure of the different variants. Source: (Jacobs 2017)

⁷³ As a reference, in current adhesively-bonded cast glass applications, cast glass blocks are made with fabrication tolerances ranging between ± 0.25 mm (Oikonomopoulou et al. 2015b) to ± 1.00 mm (Goppert et al. 2008).

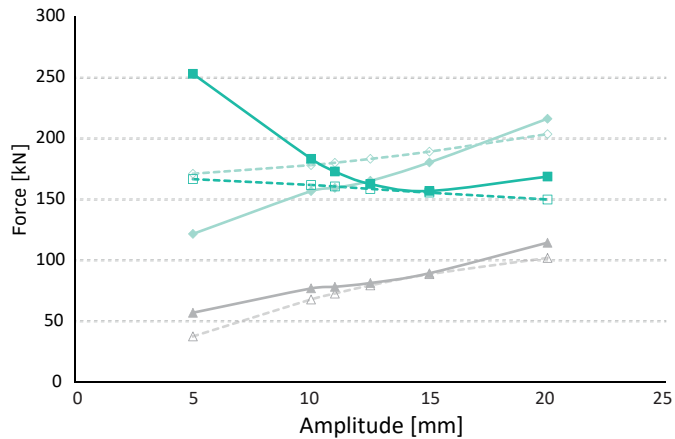


FIG. 8.40 Influence of amplitude on shear capacity, uplifting force (parallel to interlock curvature) and reaction forces. The prediction lines are based on hand calculations described in (Jacobs 2017).

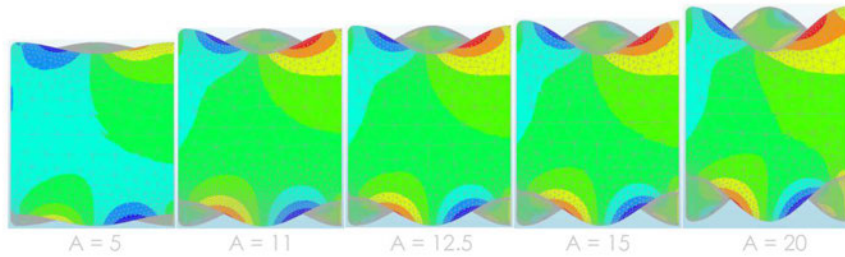


FIG. 8.41 Contour plots at failure load for various amplitude variations, demonstrating the stress redistribution of the given geometries. For the failure loads of each amplitude variation refer to Fig. 8.39. Source: (Jacobs 2017)

Fig. 8.42 exhibits the influence of the height of the brick on the failure mode of the glass brick. The graph suggests that failure through bending is critical in lower brick heights (in this case less than 80 mm in height) as they are subject to higher stresses due to eccentric loads. Higher variants are more resistant to this, leading to shear key failure. These failure mechanisms are expected to occur in the most flaw-prone area, as derived from the Christensen's failure criterion. Thus, the upper boundaries were determined from a simplified hand calculation, described in (Jacobs 2017), using the characteristic strength of glass. It is expected that the real value is to a certain degree lower, as the combination of the principal stresses in the

Christensen's criterion lead to failure before this characteristic value is reached. Thus, Fig. 8.42 incorporates the results from the finite element analysis versus the simplified hand calculations. Regarding geometry tolerances, higher bricks are also advantageous, as the failure load occurs at a larger deformation. This means a larger geometry deviation is allowable when producing higher bricks compared to shorter bricks. Therefore, a higher brick is beneficial for brick design, as load capacity is increased, tolerances can be slightly higher and there is an increased probability for the preferred failure mechanism: an interlock chipping off would leave the remainder of the component intact, maintaining thus to a certain extent the structural integrity of the unit.

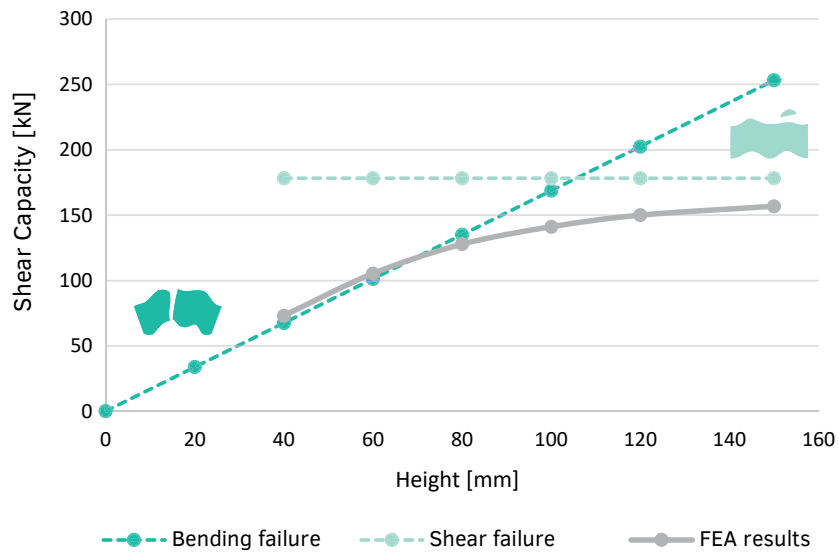


FIG. 8.42 The effect of the height on the shear capacity of the brick plotted together with the expectations from hand calculations. Source: (Jacobs 2017).

8.5 Conclusions

In this chapter, the experimental and numerical investigation of a dry-assembly system out of interlocking solid cast glass blocks has been presented in order to investigate the influence of various parameters in the overall performance of the system. The main parameters that are investigated are the amplitude and height of the interlocking blocks and the thickness and Shore Hardness of the interlayer.

8.5.1 Conclusions from the interlayer testing under static load

As discussed in Chapter 7, the use of a dry interlayer is essential for evenly distributing the stresses between the blocks and preventing direct contact between the glass elements. Thus, a selection of interlayers with a Shore Hardness between 60A – 80A and a thickness of 3 or 6 mm were tested under static creep at a 40kN compressive load for 900 s, corresponding to a nominal compressive stress of approx. 14.2 MPa. It should be noted that the applied load is considered very strict – in a real application a considerably less nominal compressive stress is anticipated.

Each interlayer was cast in the desired shape, matching the interlocking geometry of the blocks and tested between two half osteomorphic cast glass blocks. The results highlighted that the tear strength of the interlayer is equally important to its Shore Hardness. Interlayers with a relatively low tear strength will fail due to the tearing of the interlayer, leading to the direct contact of the glass blocks which in turn results in concentrated stresses and local failure. It was also concluded that harder interlayers, e.g. with a Shore Hardness between 70A and 80A are the most promising candidates for the realization of the examined system; they can withstand the anticipated compressive static loads with little or no plastic deformation. Nonetheless, experiments on higher loads suggested that the lateral deformation of the interlayer due to creep in combination with high manufacturing tolerances can lead to the eventual failure of the glass blocks due to peak stresses. Further research is thus necessary in order to find a transparent interlayer that presents a time-independent behaviour under static compressive load. The testing under static load of glass block assemblies with different interlayers indicated that 6mm interlayers behave stiffer than the 3 mm variant for the given interlocking geometry and manufacturing tolerances. The increased stiffness can be attributed to the increased contact achieved by the thicker interlayer. Nonetheless, it should be noted that although the interlayer itself becomes stiffer when thicker, the stiffness of the overall assembly

is actually compromised (and the risk for buckling is thus increased), as discussed in Chapter 7. Thus, an interlayer of the minimum required thickness for full contact between the blocks is recommended. In our case, due to the manual fabrication and post-processing of the blocks, it was determined to proceed with 6 mm thick interlayers for the further experimental investigation of the system in out-of-plane shear. In a real application though, where the high manufacturing accuracy of the blocks is presumed, interlayers 3 mm thick should suffice for accommodating the dimensional discrepancies, providing a higher overall stiffness. Lastly, this series of tests highlighted that the geometry of the interlocking system is equally as, or even more critical to the interlayer used. As the experiments demonstrated sharp changes of curvature, such as the ones at the edges of the interlocking system, can lead to the local perforation of (some of) the interlayers and in turn to the early failure of the assembly due to glass-to-glass contact. Thus, smoother curvature changes along the interlocking surfaces are preferred.

Another conclusion regarding the interlocking geometry derived from this series of tests is that the more pronounced the amplitude of the interlocking system, the more prone is the assembly to manufacturing intolerances and thus to the introduction of concentrated tensile stresses because of insufficient contact (mismatch) and collaboration between the interlayer and the glass units. This can be improved either by introducing a thicker interlayer, which however would further compromise the stiffness of the assembly, or by a smoother interlocking mechanism with reduced wave amplitude.

8.5.2 **Conclusions from the out-of-plane shear testing of assemblies with various amplitudes**

In this series, assemblies of 3 osteomorphic blocks, with various amplitudes, namely 10, 15 and 20 mm were tested in series of 3 specimens each under increasing load in out-of-plane shear. Overall, the results indicated that assemblies out of blocks with higher amplitudes in their interlocking mechanisms behave stiffer and withstand higher loads. They also present less visible deformation, expressed as the shifting of the loaded middle block downwards, prior to failure. The findings are in line with the conclusions derived by the numerical model described in chapter 8.4.

All specimens - with the exception of the specimens with 10 mm amplitude that reached the max. set deformation without cracking - failed initially at the middle glass block. The latter, prior to cracking, shifted visibly downwards; as the assembly is free to rotate under bending. The only resistance to the bending moment is

provided by the peripheral constraining force, which in this case was considerably low. This in turn results to a limited load-bearing capacity of the system prior to failure. In particular, the middle block consistently got fractured at the point where the interlocking curvature was changing from concave to convex. There was no crack propagation occurring at any of the assemblies – cracks at the adjacent blocks occurred non-simultaneously and at different locations, validating the assumption that the assembly presents an increased fracture toughness. None of the specimens collapsed upon failure; the fragmented blocks were still able to carry the load.

Moreover, upon release of the load the individual blocks showed a tendency to self-align towards their initial configuration. Due to time restrictions, the amount of recovery after the load removal was not investigated in detail. Although compared to a monolithic variant the assembly is less stiff and is anticipated to fail at considerably lower stress, its increased structural safety and damage tolerance can allow the engineering of structures with a considerably lower safety factor. Firstly, the failure of the described system is localized and does not lead to global failure. Secondly, despite the lower bending stiffness of the proposed system compared to the one of a monolithic variant, the high deflection at failure allows the assembly, made of brittle components, to behave as a pseudo-ductile, as discussed in Chapter 7. This behaviour provides a warning mechanism prior to failure that increases the safety of a relevant structure.

The consistent locations of the cracks in all specimens also suggest that defects in the meso-structure (inner volume) of the blocks or in locations where peak stresses are not anticipated are not expected to be critical in the overall structural performance of an interlocking assembly. This, however, should be further investigated.

Lastly, this series of specimens highlighted that the overall stiffness of the assembly can be compromised by multiple factors that should all be considered in a real construction. These include the dimensional tolerances of the individual blocks, as well as of the entire construction. These tolerances are in turn reflected to the thickness of the employed interlayer. In principle, the thinner the interlayer, the stiffer the assembly, provided that there is complete contact achieved. As explained previously, the geometry of the interlocking mechanism further influences the stiffness. Interlocking mechanisms of higher amplitudes are in principle yielding a more stiff structure. Yet, as the experiments indicated, they are also more prone to failure due to dimensional deviations, due to the generation of peak stresses at areas of insufficient contact. Moreover, higher amplitudes are more prone to induce eccentricity in construction during assembly. An alternative solution to prevent this,

would be the design of a component with multiple interlocking mechanisms and thus, improved self-aligning capacity, such as the Type B block presented in Chapter 7.

Lastly, the amount of pre-stress employed plays a crucial role in stiffening the assembly. Higher pre-stressing can further stiffen the structure and prevent the misalignment of the blocks by the anticipated lateral loads. Yet, this presumption needs to be further investigated and validated. An additional challenge of the described dry-assembly, interlocking system anticipated in a real construction concerns the assembly, proper alignment and controlled pre-compression of such a system upon installation.

8.5.3 Conclusions from the numerical modelling

The numerical model provided valuable input regarding the influence of the geometrical parameters of the interlocking geometry in the overall structural performance in shear. In specific, it was shown that a decrease in the height of the blocks lowers their shear capacity and alters the system's failure mechanism: a lower brick is more susceptible to bending failure, whereas for higher brick variants the shear lock failure is proven to be more critical. Both failure mechanisms are nevertheless still possible, even for higher bricks, as peak tensile stresses occur at the middle of the block. The latter was confirmed as well by the first series of compressive tests on different interlayers. A flaw in that area could lead to crack propagation normal to this region. It was also demonstrated that an increased amplitude of the interlock is beneficial as it leads to an enhanced shear capacity and decreased uplifting effects, as was also suggested by the out-of-plane shear experiments. Increased amplitudes also require a higher precision in manufacturing as the components can reach the failure stress limit at considerably lower deformation.

8.6 Recommendations

Overall, a novel dry-assembly system employing interlocking solid glass blocks was introduced in the last two chapters. The numerical and experimental investigation of the proposed system offered valuable insights into the mutual influence of various

parameters on the mechanical performance; yet, it also showed that there is still a lot of room for exploration. Accordingly, in this section some possible directions for future research are briefly discussed.

Firstly, although the general principles of the osteomorphic interlocking geometry have already been experimentally investigated, the performance of the system will be further improved if smoother curvature changes are incorporated at the blocks, particularly at their edges. Smoother curvature changes reduce the risk of perforating the interlayer and together, the risk of localized stresses in these locations. Yet, smoother curvatures can also result in an interlock of lower amplitude, of reduced shear capacity and decreased uplifting resistance.

The experiments in out-of-plane shear clearly demonstrate that an assembly of the given geometry allows for significant deformation under loading. This is partially attributed to the manufacturing tolerances of the kiln-cast components that necessitated the use of thicker (6 mm) interlayers. The re-investigation of the system with components produced by hot-pouring in high accuracy steel moulds is strongly recommended. It is expected that cast glass units that are industrially manufactured will present a considerably higher degree of dimensional accuracy which in turn would not necessitate an interlayer thicker than 2-4 mm. The use of borosilicate glass can further contribute in achieving high accuracy components due to its reduced thermal expansion coefficient (and thus shrinkage during annealing)⁷⁴.

It was also shown that components with increased amplitudes in the examined osteomorphic interlocking mechanism, although able to sustain considerably higher loads, are more prone to eccentricity during assembly. To minimize the occurrence of eccentricity in a construction, the design of an interlocking geometry with more locks is recommended, such as Type B block presented in chapter 7.5.2 and used in the numerical investigation of the system. Such a geometry can present improved self-alignment properties and extra redundancy in case of failure of individual locks of the interlocking mechanism.

Further research is also necessary in order to find a transparent interlayer that presents a time-independent behaviour under long-term static load. The use of a multi-layer interlayer – with a stiffer core and softer external layers - but also the use of soft aluminium as an interlayer are recommended for future research. The most suitable thickness of the interlayer should be determined using interlocking blocks

⁷⁴ Based on the work of (Goppert et al. 2008), it is anticipated that industrially manufactured glass blocks can present a dimensional accuracy of ± 1.0 mm without any post-processing.

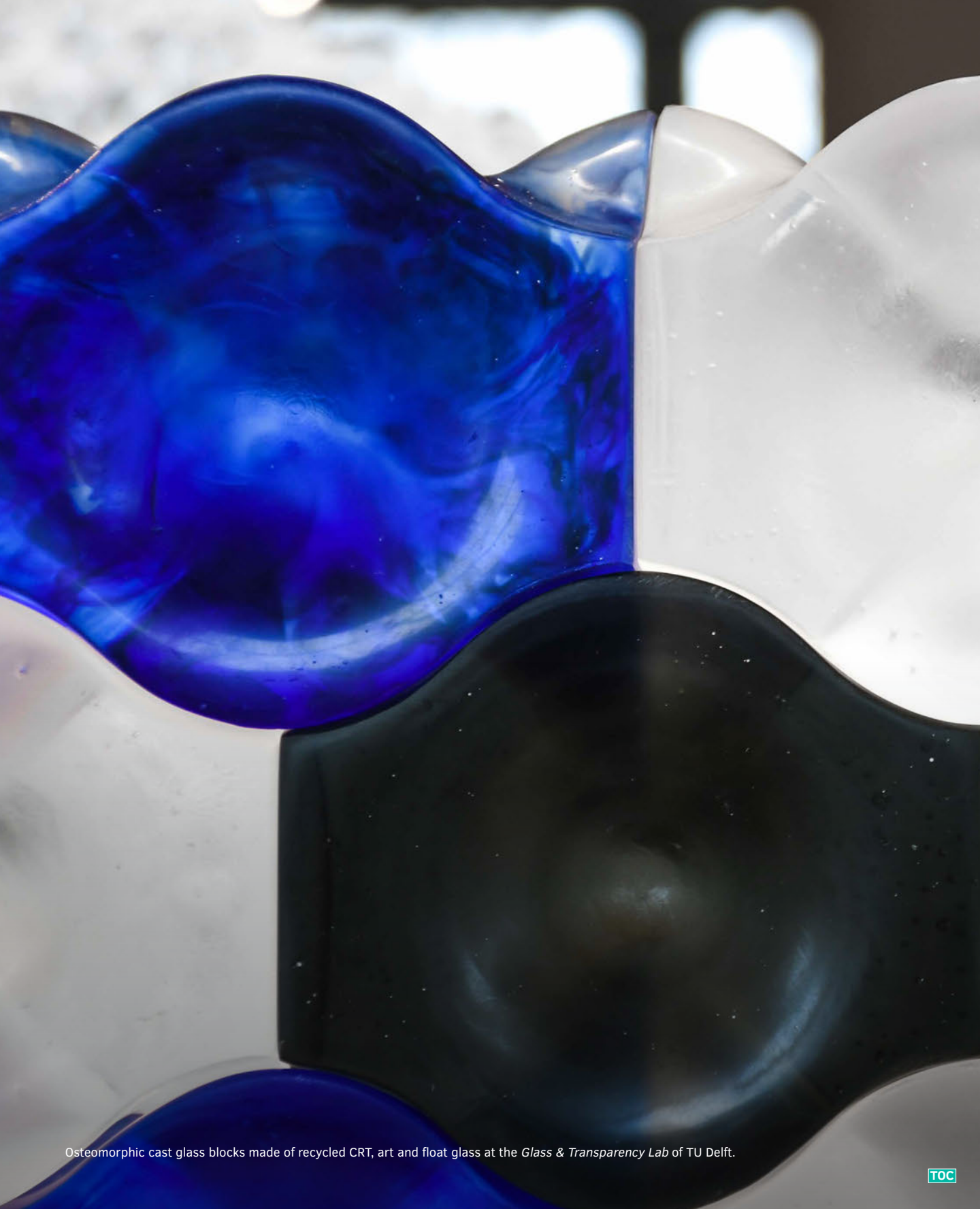
industrially manufactured with a higher dimensional precision. For assemblies out of interlocking blocks, the degree of self-realigning back to the initial configuration upon load release should also be documented in detail.

Due to time and financial constraints, the effect of pre-stress was not investigated in this work. The engineering of a constraining frame with a controlled pre-stressing mechanism that can further stiffen the assembly is essential for the real application of the presented system in the built environment. In this direction, future research should focus on evaluating the stiffness of the assembly based on different amounts of pre-stress. Work by (Dyskin et al. 2003) focusing on a concentrated load test on a plate-like assembly out of similar (yet smaller in scale) osteomorphic blocks made by brittle *PolyLite 61-209* resin has already indicated that the deformation behaviour and stiffness of such an assembly is strongly pressure dependant.

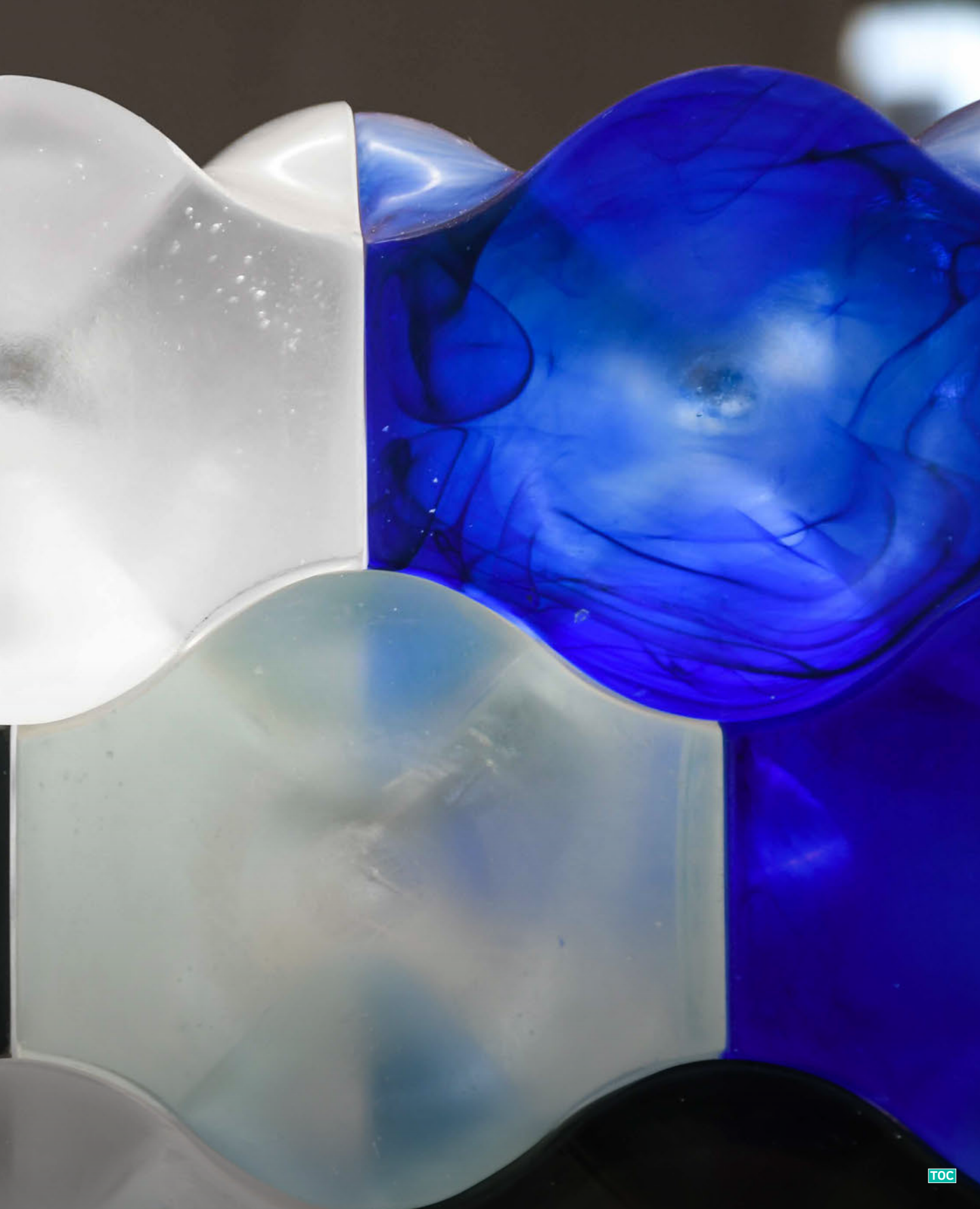
Moreover, an assembly method that ensures the proper alignment of the components prior, during and after the necessary pre-compression should be developed.

A detailed study on the sealing of the system against weathering and its performance under thermal fluctuations are also recommended.

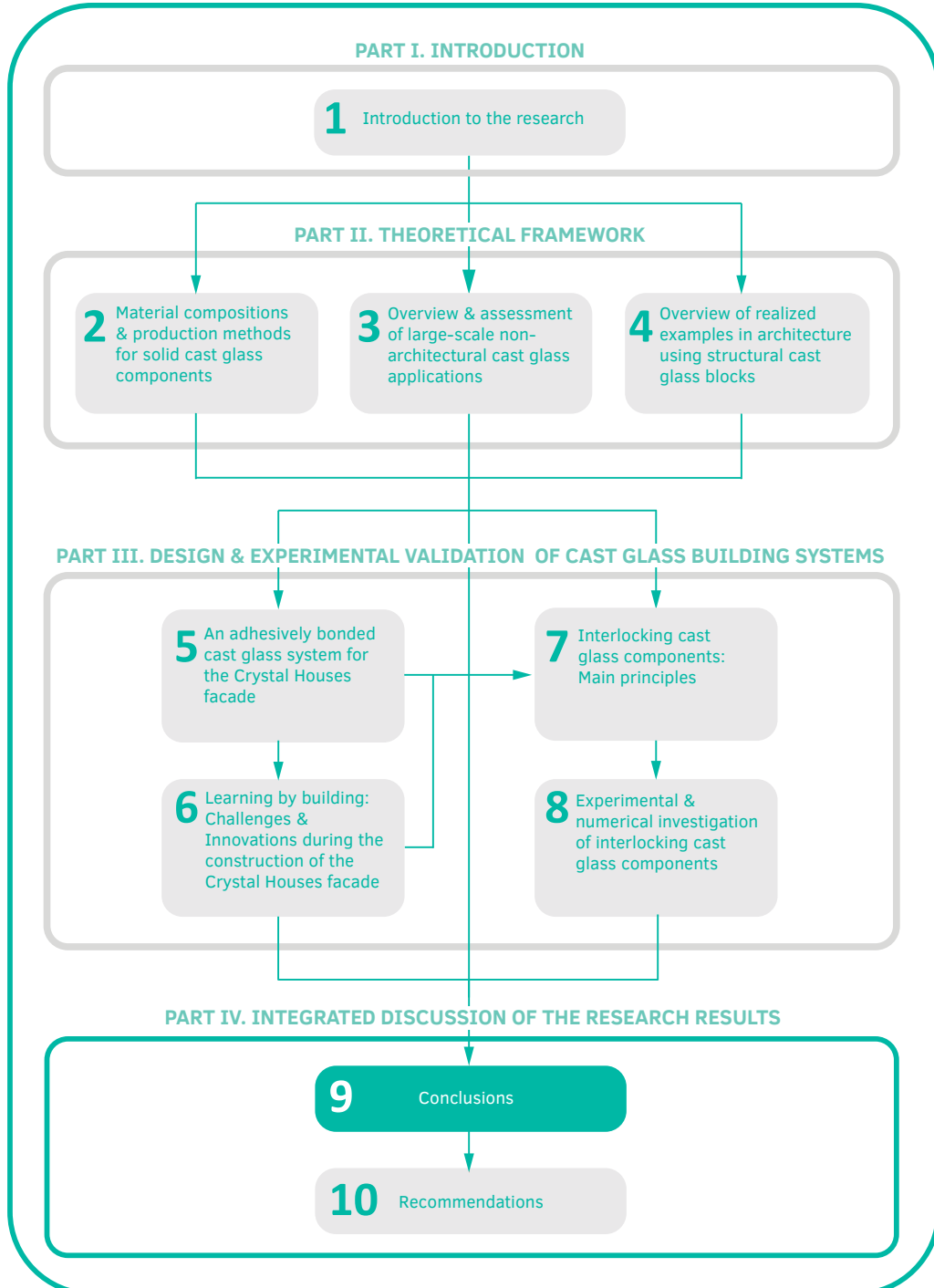
Lastly, a valuable experiment that could further quantify the properties of the proposed interlocking system is the comparison of the performance of an interlocking plate-like assembly under concentrated load to the ones of a monolithic glass plate of equivalent thickness and of a similar assembly that is adhesively bonded.



Osteomorphic cast glass blocks made of recycled CRT, art and float glass at the *Glass & Transparency Lab* of TU Delft.



Exploring the third dimension of glass



Solid cast glass components and assemblies for structural applications

9 Conclusions

This dissertation aims to explore the possibilities and constraints of employing cast glass for structural, self-supporting applications in architecture. This chapter summarizes and discusses the main outcomes of the dissertation. Initially, responses to the sub-research questions are given, presenting their particular findings. Based on the latter, a comprehensive answer to the main research question driving the research project is given. Recommendations for further developments in the field are given in Chapter 10.

9.1 Introduction

The prime aim of this research was to investigate and unveil the potential and limitations of using cast glass for structural components. Casting as an alternative manufacturing and fabrication method for structural glass components allows us to escape the 2-dimensionality of float glass; instead we can perceive and design with glass used as a 3-dimensional material. Given the, so far, limited exploration of cast glass in structural applications, an in-depth research of cast glass applications developed in other fields, such as astronomy and art, was essential for understanding the potential and limitations of this manufacturing method. Following, the structural potential of cast glass was demonstrated in this work through the research and development of two distinct structural systems for self-supporting envelopes: adhesively bonded and interlocking. The validation of the proposed systems was conducted mainly through experimental work. This chapter presents the main findings of this work. These are given as responses to the sub-questions first, which summarize the main findings per chapter. These partial outcomes lead to a comprehensive response to the main research question, featured directly after.

9.2 Answers to the sub-questions

1 What are the main practical implications and limitations of employing casting for structural glass elements? (Chapter 2)

In theory, there is no limit in the size of a glass component that can be produced by casting. In practice though, to achieve a financially feasible solution, several factors constrain the size of cast glass components to a few kg in weight. The most decisive factor is the required annealing time, explained in detail in Chapter 2. The annealing time is directly influenced by the thermal expansion coefficient -and thus by the chemical composition and type- of glass, the thickness and geometry of the component and the amount of residual stresses allowed. Indirectly, annealing is influenced by several more parameters related to the geometry of the component but also to the physics of the furnace set-up involved. In brief, the thicker and larger the component, the exponentially longer the annealing time required. Real examples of this effect are the blanks of the giant telescope mirrors, presented in Chapter 3: weighing several tons each, they require from months to years of annealing to prevent the generation of residual stresses. Such a prolonged annealing time may be acceptable for astronomical research, yet it would render a cast glass component financially unjustifiable for architectural and structural applications. A limited mass to a few kg further facilitates practical aspects such as the transportation, handling and buildability of a structure in architecture.

Another restraining factor in the use of cast glass elements for structural applications is the, so far, limited, if any, standardized reference data on the strength of solid cast glass components. In contrast to float glass, there is no standard yet regarding the strength of solid cast glass components. Given that the casting manufacturing process is still not fully standardized/automatized the surface quality is anticipated to be lower than that of float glass. Moreover, due to the lack of customized quality control equipment, it is difficult to determine the amount and size of randomly distributed critical flaws within the cast components. Towards this direction, the inverse scale effect in brittle materials implies that the larger the component, the higher the probability of critical flaws within it, which in turn can result in a decrease in the probabilistic strength. Often, small air bubbles and inclusions, visible by the naked eye, exist in cast glass components. Such defects are unacceptable by the control standards of the float industry. However, given the fact that the most influential flaws are the ones at the surface of the component and considering that the surface area to volume ratio for cast glass is much smaller

compared to float glass (it is the inner volume that is considerably larger and thus, the defects in the meso-structure), it is anticipated that cast glass has a comparable -yet to some extent reduced- strength compared to standardized float glass. This has so far not been systematically investigated and confirmed. Besides the lack of standardized strength data, there is not yet an accurate through-the-thickness residual stress measurement method for cast glass. Most of the times, the residual stress is qualitatively evaluated through cross polarization.

Accordingly, the experimental validation of structural systems out of cast glass components is considered necessary in order to derive statistical engineering data and ensure their safe structural application.

2 In what ways can different glass recipes, geometry and fabrication methods affect the manufacturing process and thus the feasibility and marketability of the resulting component, as suggested by relevant pre-existing applications in other fields? (Chapters 2 & 3)

This question sought to investigate the influence of the leading contributing parameters to the feasibility of the resulting cast glass component: the type (composition) of glass used, the desired geometry and the fabrication method. These parameters, analysed in Chapter 2 and highlighted through relevant applications in Chapter 3, should be considered from the design stage in order to make feasible, cost-efficient cast glass components.

Chapter 2 discusses how the alternative glass recipes present, besides distinct mechanical properties, considerable differences in their melting and working temperatures and thermal expansion coefficient. Accordingly, glass compositions with a low thermal expansion coefficient require substantially less annealing time, as they are able to sustain greater temperature deviations between the warmest and the coolest part of the component during cooling; moreover, they result in less shrinkage of the cast element. Under this assumption, we would ideally use 96% silica glass for cast glass structural elements, a glass that presents a thermal expansion coefficient approximately ten times less than that of soda-lime glass. However, the glass recipes with the lowest thermal expansion coefficient, such as 96% silica and fused silica glass, require as well the highest working temperatures, which render them challenging to fabricate – even at those high temperatures they are essentially too viscous to be worked with. The high working temperature increases substantially the manufacturing cost as well. For the above reasons, soda-lime and borosilicate glass are considered the most feasible solutions, for cast glass applications in architecture. They are the least expensive options, have comparatively low melting temperatures

and satisfactory mechanical properties. Of the two, borosilicate glass features a more attractive thermal expansion coefficient but comes at a higher cost due to the prerequisite of a higher working temperature. Nonetheless, the considerably shorter annealing time required and the attained high manufacturing accuracy can ultimately render borosilicate glass a competitive solution in terms of overall cost: the manufacturing process can be considerably faster and post-processing can be avoided. Overall, the choice between soda-lime and borosilicate glass should be made taking into account the complete requirements for the component and the case-study, such as dimensional accuracy, climate, fire-resistance, etc.

The overall geometry of the component plays a key-role in defining the annealing time involved. An optimization of the ratio between the mass and stiffness of the component can greatly reduce the required annealing time and consequently the manufacturing cost of the element. Again, this has been well distributed in the fabrication of the giant telescope mirror blanks, analysed in Chapter 3. By creating a honey-comb structure with cavities and slender glass walls, the blank of the Giant Magellan telescope mirror of 16 t weight and 8.4 m in diameter required only 3 months of annealing; that is 4 times less than the annealing time of a solid blank of almost $\frac{1}{4}$ the diameter and total weight. Such smart geometry could as well be implemented in cast components for architectural, load-bearing purposes. For example, compared to solid ones, glass blocks following the honeycomb principle would be sufficiently rigid, but faster to produce and lightweight, facilitating transportation and handling. To further reduce the annealing time an even mass distribution and a relatively constant thickness of the element is essential. The thickest part of the component governs the annealing schedule. A homogeneous mass distribution and rounded shapes and/or edges are also preferred for preventing the generation of internal residual stresses as they ensure even cooling of the component.

The fabrication method can further reduce the required post-processing, decreasing the manufacturing costs and production time as well. In general, hot pouring is used for the mass fabrication of cast glass components. The choice of mould is relevant to the amount of identical elements produced and the desired accuracy. For mass production, steel or graphite high accuracy moulds are the best choice. Press steel moulds generally achieve a higher degree of accuracy than open moulds and are preferable if no post-processing is necessary. When post-processing is required, open, high-precision steel moulds are the most cost-effective option. For unique, more elaborate or variable components elements, disposable moulds should be chosen due to their low manufacturing cost, even though they require much more time for preparation and necessitate post-processing. A promising new technology in this direction is the fabrication of 3D-printed high-accuracy sand moulds.

3 Which are the current structural systems employed for creating self-supporting structures out of cast glass components? Which are the main advantages and drawbacks of each system? What is the buildability of these systems and which design principles do the glass components follow? (Chapter 4)

In general, the structural use of cast glass in architecture is still in an early stage of development. The custom-made and, to a certain extent, manual fabrication of the cast units together with the lack of a standardized construction method and strength data has currently confined cast glass to just a few load-bearing applications in architecture. Prior to the research conducted for this dissertation, only a few built structures existed, following two structural systems: either a supportive metal substructure was used or a stiff, colourless adhesive for bonding the cast units together was applied. A supportive steel structure is the prevailing solution, offering a relatively easy, fast and possibly reversible, construction. Furthermore, by directing the tensile forces to the metal structure, glass can be mainly loaded in compression, where it exhibits its highest strength. The main disadvantage of this solution is that it compromises the overall level of transparency. Prior to this dissertation, an adhesively bonded glass block system had only been used in the construction of the *Atocha Memorial*, where the cylindrical geometry of the structure contributed significantly in the overall stiffness of the structure. Owing to the colourless nature of the adhesive, such a solution attains a high degree of transparency, yet it results in an irreversible, non-recyclable and challenging construction requiring meticulous and intensive, high accuracy labour.

The few realized projects employ components made by primary casting (hot pouring) and high precision steel moulds, either open or press ones. All projects employed a singular block geometry of less than 10 kg in weight. The limited mass of the units also facilitates the transportation, installation and handling processes. Moreover, a repetitive component geometry is essential for simplifying the production and assembly and for minimizing the manufacturing costs, on account of a limited number of high-precision steel moulds and a standardized production process.

Regarding the overall shape, little exploration has been made in the realized projects on the forms that can be achieved by cast glass. Mainly a simple rectangular form has been favoured, replicating the standard masonry brick modulus. The only exemption is the block modulus of the *Atocha Memorial* that follows a shape with a concave and a convex shape to allow for the generation of the entire cylindrical structure by a singular unit.

Either borosilicate or soda-lime glass are employed, depending on the project's location and the required dimensional accuracy. A characteristic example is again the *Atocha Memorial*, where with the use of press moulds and borosilicate glass, a ± 1.00 mm accuracy was achieved at the manufactured blocks, without the need of any post-processing. In terms of maintenance, systems employing solid cast blocks are fairly maintenance-free, provided that, during construction, there is proper cleaning and then sealing of the joints between the glass blocks.

4 What is the structural potential and which are the main factors that influence the structural performance of an adhesively bonded cast glass system? (Chapter 5)

This question was answered through the research, development and experimental validation of the adhesively bonded system applied on the *Crystal Houses* façade, discussed in Chapter 5. It was experimentally proven that the strength of the adhesively bonded cast block assembly is highly dependent on the adhesive's thickness, therefore on the dimensional accuracy of the components and on proper connections. The overall geometry of the structure also plays a key role, as it can further contribute to the stiffness of the structure and thus, allow for the use of a less rigid (and thicker) adhesive.

The literature review discussed in Chapters 2 and 3 indicated several principles and design criteria for the geometry of the cast glass components; however, the specific case study was an externally assigned project, where the size and shape of the blocks was predetermined by the architects. Hence, there was no exploration of the shaping potential of cast glass in this case study.

The flat geometry of the façade necessitated the use of a stiffer, thinner adhesive compared to the one employed in the *Atocha Memorial*. A UV-curing clear acrylate was chosen for bonding the blocks together due to its colourless nature, high compressive strength and fast curing that facilitates construction. To further reinforce the stiffness of the self-supporting façade, a continuous glass wall with buttresses was proposed, creating a rigid 3-dimensional envelope.

It was experimentally proven that the use of the selected UV-curing, stiff acrylate, allows the assembly to behave monolithically against the anticipated loading and to present a compressive and flexural strength comparable to or better than the strength of typical B80 high performance concrete. Yet, the monolithic structural behaviour is only achieved if the adhesive is evenly distributed in a thickness that corresponds to the optimum bond strength. Visual and structural prototypes

demonstrated that when using the specific adhesive, a thicker bond layer results in a decreased bond strength and an inhomogeneous application. It was determined that for the given adhesive, the optimum bond thickness lies between 0.2 and 0.3 mm, indicating that the glass components should meet dimensional tolerances that do not exceed ± 0.25 mm in both size and flatness. Given this high level of required accuracy, post-processing of the horizontal (bonding) surfaces of the system was necessary. For that reason, for the fabrication of the blocks, soda-lime glass and open high precision moulds were preferred to decrease the manufacturing costs. Even though in soda-lime glass the thermal stresses occurring are much higher than those for borosilicate glass, the experimental work proved that soda-lime glass blocks can withstand the anticipated rapid temperature changes when applied to an external wall in a temperate climate.

Proper connection design is also essential for ensuring the desired structural performance in a cast glass block system. If properly supported, one solid glass block can carry the entire load of the façade without cracking. If, however, the blocks come to direct contact with each other or with another hard material, micro-asperities induce stress concentration at the surface of the components which can trigger crack initiation and propagation at comparatively low compressive loads.

5 Which are the main engineering challenges involved in an adhesively bonded cast glass system for structural applications? (Chapter 6)

The engineering challenges of an adhesively bonded cast glass system were discussed in detail in Chapter 6 through the real application of the developed system at the *Crystal Houses façade*. It was demonstrated that most of the engineering problems involved are generated by the relatively low thickness of rigid adhesives, combined with the architectural prerequisite of high visual performance. The fundamental difference between the developed adhesive system and a conventional mortar system is that a mortar layer can compensate for the intolerances in size of the bricks, while a rigid adhesive cannot; this leads to a meticulous and strictly controlled building process. Strict tolerances are essential not only per layer of construction but for the entire structure.

Moreover, in contrast to conventional masonry, in an adhesively bonded glass system, any flaws in the bonding layer are entirely visible. To attain imperceptible connections in the structure, the development of a bonding method for the homogeneous and flawless application of the adhesive is necessary.

An inherent challenge of an adhesively bonded cast glass system is the irreversible nature of the involved stiff adhesive that leads to a permanent, non-circular structure. Although local repairs using controlled heat are possible, overall the blocks cannot be retrieved intact at the end-of-life of the building, nor can they be easily recycled due to adhesive contamination. Taking into account the global drive towards increased circularity and reuse of building materials, this is a crucial aspect to address and improve in future applications of this system.

6 Which are the main engineering advantages, principles and design criteria for creating a dry-assembly, interlocking cast glass structure? (Chapter 7)

This question sought to define the engineering concept of a novel structural system out of interlocking cast glass blocks and establish the design criteria for shaping the components. This new structural system was triggered by the drawbacks of the developed adhesively bonded system, as a promising solution that circumvents all the inherent challenges of the latter. Owing to its segmented nature and dry-assembly, the proposed system offers several engineering advantages such as an improved toughness resistance, a visible deformation prior to failure, localized failure and a reversible construction that allows for easily retrievable and thus, reusable and recyclable components. Even though it is anticipated that such a system will present a reduced stiffness compared to an adhesively bonded cast glass structure, it provides a structure of enhanced safety. In specific, the fragmentation of the structure is expected to diminish the influence of individual critical flaws for the structure as a whole. The nature of the interlocking system confines any local failure to the cracked unit – cracks do not propagate to the rest of the structure, as would be the case in the monolithic variant. This in turn offers the possibility to dimension the assembly without considering the possible occurrence of critical flaws in the glass; hence, a reduced safety factor can be applied in the glass construction. Ironically, the safety of the structure is further supported by the low bending stiffness of such an assembly: The anticipated visible deformation and the pseudo-ductile behaviour of such a system upon excessive loading can provide a warning mechanism prior to failure.

Another benefit of an interlocking system is its relatively easy buildability due to the self-aligning nature of the components. To further simplify the assembly process -and reduce the manufacturing costs- components following a multifunctional geometry are recommended. To attain reversibility a soft, preferably transparent, dry-interlayer is proposed as an intermediary between the individual components. The interlayer, in addition to ensuring an even stress distribution by accommodating

by deformation the surface-asperities of the blocks, can also compensate for the size tolerances of the individual components in its thickness. To stabilize and restrain the overall structure a constraint frame is necessary, which can be engineered for minimal visual intrusion.

Taking into consideration both the physical principles of interlocking and glass casting, several design criteria are established for defining the geometry of the cast glass components: Components of limited volume are proposed to reduce the annealing time, facilitate the handling and construction and increase the fracture toughness of the system. Geometries following rounded shapes or/and edges, smooth interlocking mechanisms, an even mass distribution and consistent thickness are preferred for preventing the generation of uncontrolled residual stresses and improve the shear capacity of the system. Units following a multifunctional geometry that allows for multiple different configurations keep the manufacturing costs lower and can speed up the construction.

7 What is the potential of an interlocking system out of cast glass blocks for structural applications in architecture and which are the main factors that influence its structural performance? (Chapter 8)

The experimental and numerical investigation of an interlocking system out of osteomorphic glass blocks was presented in detail in Chapter 8. Although further validation of the system is necessary for applying it in a real construction, the findings of this chapter manifest that an interlocking system is a feasible solution for cast glass structures that can tackle all the downsides of the existing systems utilizing cast glass blocks. It allows for a reversible, almost fully-transparent system of enhanced safety, firstly due to its fragmented nature that allows for localized failure and secondly, due to its pseudo-ductile behaviour that provides visible warnings prior to failure.

As indicated by the numerical and experimental research, the structural potential of such a system is influenced by multiple, interlinked factors. These include the geometry and dimensional accuracy of the glass blocks and especially of the interlocking mechanism, the choice of interlayer material and its thickness and the amount of pre-stress applied.

In specific, it was proven numerically that a decrease in the height of the block lowers its shear capacity and alters the system's failure mechanism: a lower brick is more susceptible to cracking by bending, whereas for higher brick variants the shear lock failure is proven to be more critical. It was also shown that an increased

amplitude height of the interlocking mechanism leads to increased shear capacity, decreased uplifting effects and failure at considerably smaller deformation. These latter findings were confirmed experimentally by out-of-plane shear tests in assemblies of kiln-cast blocks of different amplitudes. As a disadvantage, higher amplitudes were proven to be more prone to critical dimensional deviations that can lead to peak stresses due to insufficient contact between the components and the interlayer, but also to induced eccentricity during the assembly of the system. The steeper curvature of the higher amplitudes, combined with the dimensional tolerances, can lead to the sliding of one component in relation to the others and thus, to an initial misalignment of the assembly. A solution to this is the design of an interlocking mechanism with multiple locks, enhancing the self-aligning capacity of the unit.

The dimensional tolerances of the interlocking mechanism of the glass blocks also play a key-role in the choice of interlayer material and its thickness and to this extent, to the overall performance and stiffness of the assembly. As the experiments indicated, interlayers with lower tear strength tend to fail at the spots of the interlocking geometry where there is a steep curvature change. More importantly, poor manufacturing tolerances of the glass blocks and particularly in their interlocking geometry necessitate the application of thicker interlayers. If the interlayer cannot accommodate the dimensional tolerances, failure can eventually occur due to the partial contact of the glass blocks and the interlayer that leads to concentrated stresses. In principle, the thicker the interlayer the stiffer it is, yet impairing the overall stiffness of the assembly and making it more prone to buckling. On the other hand, thinner interlayers ensure a better stiffness of the assembly but if they are too thin, they may result to unequal material distribution and thus bare a higher risk of local failure. The Shore Hardness of the interlayer is also crucial for the overall stiffness. In this direction, the conducted experiments suggested that interlayers with a Shore Hardness in the range of 70A – 80A are a good candidate for real applications.

The amount of pre-stress applied to constrain such a system plays an essential role to the overall stiffness of the construction as well. Due to time and financial limitations the effect of pre-stressing was not examined in this work. Yet, the results of the out-of-plane shear tests on assemblies of osteomorphic blocks indicated a low strength due to the low bending stiffness of the assembly, which can be attributed to several factors, such as the dimensional tolerances of the kiln-cast blocks, (therefore requiring) the use of a 6 mm thick interlayer and the low pre-stress applied at the constraining steel frame. It is anticipated that higher amounts of pre-stress can increase the stiffness of the system, yet this is to be validated.

It was also demonstrated that the complicated geometry of the interlocking blocks results in the generation of peak localized stresses at considerably lower nominal compressive stress values compared to blocks of flat geometry. This, in combination with the reduced stiffness of the assembly due to the relatively soft interlayer, lead to the conclusion that an interlocking assembly would present a lower strength compared to an adhesively bonded system made out of rectangular cast glass blocks. Yet, as the experiments indicated, the visible deflection and pseudo-ductile behaviour of the interlocking assembly in combination with localized failure and resistance to crack propagation lead to a structure with increased safety, providing visible warning mechanisms and a redundancy prior to failure.

Moreover, upon failure, the assemblies would still have a significant residual strength and upon load removal they would self-realign towards their original configuration. The extent of the ability of the system to self-realign was not investigated in detail and should be further validated in the future. The experiments also showed that internal flaws (within the meso-structure of the blocks) or defects at locations that are not anticipated to be subject to peak stresses, do not seem to influence the overall performance of the assembly.

Several more aspects need to be further studied and engineered in order to realize this system in the built environment, yet the results so far strongly support the feasibility of this novel type of construction utilizing solid cast components.

9.3 Main research question

What is the potential of using cast glass elements as structural components for the generation of self-supporting envelopes without the need of opaque reinforcement elements?

The driving force of the research project was to investigate the potential of cast glass components in architectural, structural applications. Prior to this research, little and rather sporadic exploration had been made in the use of casting as a manufacturing method for structural glass components in architecture. At present, there are only a few realized examples of self-supporting structures made of solid

cast glass elements. The, so far, limited demand has in turn led to the absence of a standardized manufacturing process, to a lack of consistent engineering data and building guidelines, and to a general unawareness of the potential of cast glass in structural applications in architecture.

A short, simplified answer to the main research question is that cast glass has a great potential for structural applications due to its ability to form 3-dimensional glass structures that are shaped to eliminate the risk of buckling due to slender proportions. The monolithic nature and substantial cross-section of cast glass components combined with the inherent compressive strength of glass allow us to escape the design limitations imposed by the, essentially, 2-dimensional nature of float glass. To demonstrate this potential, this work focused on the development and experimental validation of two distinct structural/building systems for self-supporting envelopes employing almost solely cast glass elements. These proved that to take full advantage of cast glass structural components certain requirements should be met, linked to the manufacturing process but also the means of assembly of the individual cast glass elements. These requirements have been discussed thoroughly by forming the answers in the sub-questions, each of which focuses on a specific aspect of the main research problem.

An inherent advantage of casting is that it provides great freedom in the size and shape of the resulting component; although there are practical limitations in the geometry largely due to the meticulous and lengthy annealing procedure involved. These limitations are explained in the answers of sub-questions 1 and 2. Accordingly, in architectural applications solid cast glass components have been currently commercialized up to the size range and modulus of standard masonry bricks. Such elements can be used as repetitive components to form self-supporting, 3-dimensional all-glass structures of undisturbed transparency.

Cast glass exhibits a great shaping potential, allowing us to create forms beyond the standardized brick modulus. Although the shaping potential of cast glass could not be fully explored in this work, design criteria in respect to casting were established and accordingly interlocking forms following curved shapes were developed. The first results of the study on the shapes and geometry of cast glass components have been presented in Chapter 7, demonstrating that casting as a manufacturing method and glass as a material *can* and *should* be made following different forms than the ones adopted for other building materials that have been produced by different methods.

To achieve load-bearing cast glass structures, it is essential to use an intermediate material between the individual glass elements. This intermedium influences the stiffness of the structure; equally importantly, it ensures even load distribution over

the glass components and prevents early failure due to peak stresses on surface micro-asperities triggered by glass-to-glass contact. To maximize transparency this intermedium should be colourless; moreover, any secondary supportive substructure should be minimized. Accordingly, the main contribution of this research work is the development of two distinct systems for self-supporting envelopes of maximized transparency: an adhesively bonded glass block system, using a colourless adhesive as an intermedium and an interlocking cast glass block system, employing a colourless dry interlayer. Although, in this work, both systems have been developed for self-supporting envelopes, they can, in principle, be applied on other compressive members as well, such as columns or arches as demonstrated in the cited case studies.

More specifically, the selected rigid UV-curing adhesive allows the adhesively bonded system to ensure a relatively monolithic behaviour under the anticipated forces and a high transparency level. Nonetheless, the resulting structure is irreversible and requires a meticulous and intensive construction of extremely high dimensional accuracy (Chapters 5 and 6). Essentially, in order to ensure a rigid connection, an adhesive of virtually zero thickness is necessary, which cannot accommodate any dimensional tolerances in the size and shape of the individual blocks but also of the entire construction. This in turn results in multiple engineering challenges during the construction of such a system.

In comparison, the developed interlocking system presents a relatively reduced ultimate load-carrying capacity and presents more distortion in terms of transparency; yet it is a reversible, easily assembled system that offers inherent safety due to its fragmented nature and visible deformation prior to failure (Chapters 7 and 8). Several factors influence the stiffness and structural behaviour of such a system, such as the geometry of the blocks and of the interlocking mechanism, the choice of interlayer, the amount of pre-stress applied. Dimensional tolerances of the building blocks are also critical in this case as thicker interlayers lead to a reduction in the overall stiffness of the assembly.

The findings on both systems have been positively received by the international architectural and engineering community. Specifically, the presented adhesively-bonded cast block system was realized at the *Crystal Houses façade*, which received numerous awards by the structural engineering society, including the *Outstanding Innovation Award* by the *Society of Façade Engineers* in 2016. Still, the *Crystal Houses façade* is merely a first real-scale prototype of the developed adhesively bonded system. The actual construction of the façade provided invaluable feedback on the engineering challenges and practicalities involved in such a system, giving room for new suggestions. This triggered the development of the 2nd presented

system with interlocking glass blocks. Due to time and financial limitations, this second system was developed in less detail and to an earlier stage compared to the adhesively bonded one. Although future work is necessary to apply this system in the built environment, the results so far demonstrate its feasibility. The interlocking cast glass block system, utilizing recycled cast glass components, although not yet applied in practice, has been exhibited in *The Venice Design 2018* and *Dutch Design Week 2018* and was nominated for the *New Material Award 2018*. An important spin-off discovery from the interlocking system is the potential of using waste glass for creating circular structural cast glass components. This was briefly discussed in Chapter 7.6, - the extensive research on this topic remains out of the scope of this thesis.

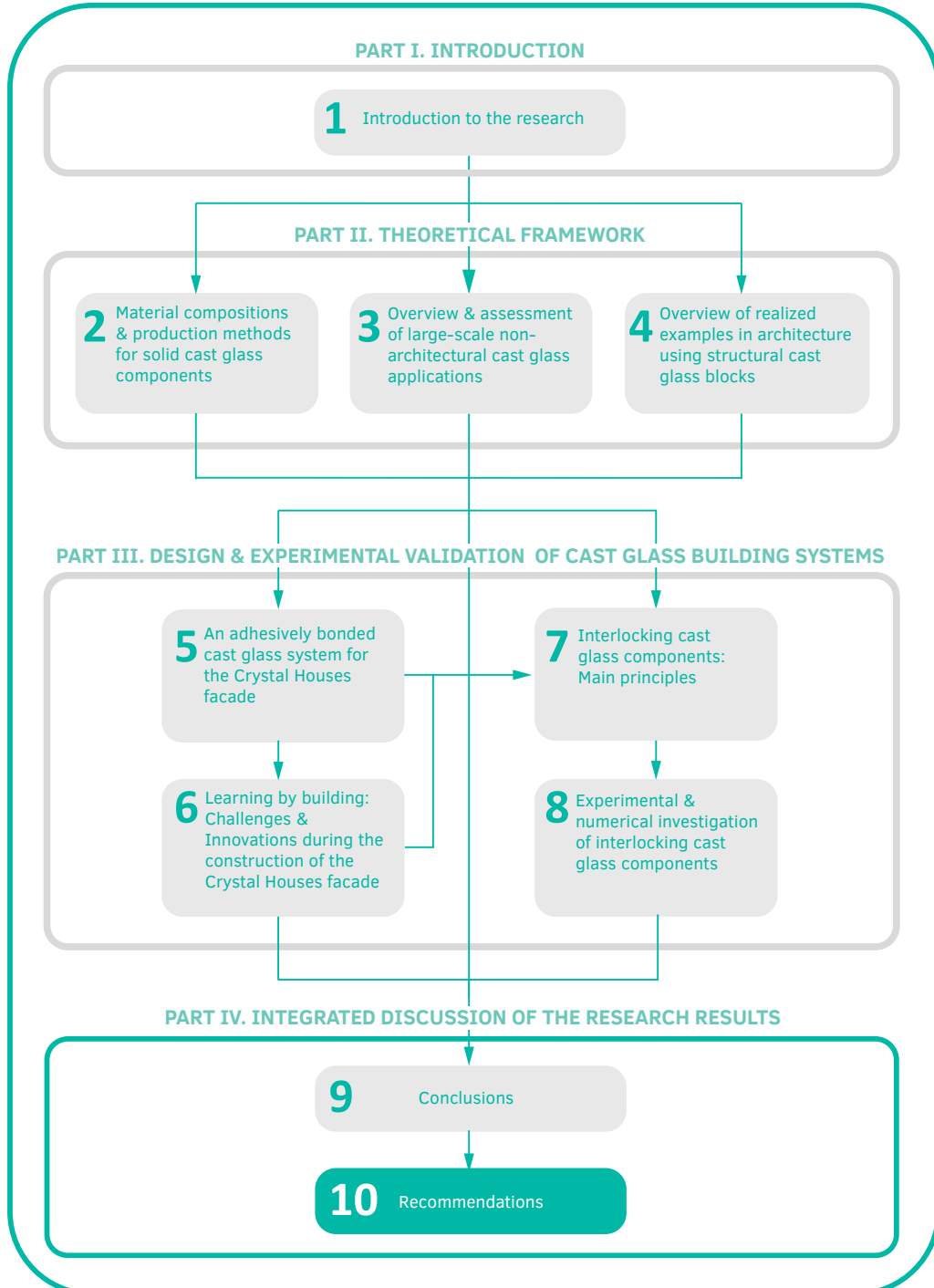
Even though cast glass has, so far, been rarely applied in structural applications, the development of new building systems and their experimental validation presented in this work provide a strong basis for further developments and applications in a range of compressive structures. At present, the most considerable drawbacks hindering the marketability of cast glass components are (a) the economic barriers imposed by their customized production and application and (b) the lack of standardized strength data and building guidelines. Thus, even if cast glass elements have proved to be suitable structural components, several economic aspects and logistics need to be tackled and performance issues need to be further explored in order to make cast glass a competitive manufacturing method compared to float production for structural components. The support of the building industry for turning cast glass into a competitive manufacturing method and the support of the architectural community for an increased demand are essential for further applying cast glass components in structures and achieving a standardized production method that can greatly reduce the manufacturing cost and improve the quality of cast glass components.



Prototype of a topologically optimized cast glass node for a grid shell application by (Damen 2019)



Exploring the third dimension of glass



Solid cast glass components and assemblies for structural applications

10 Recommendations

10.1 Introduction

Based on the main findings of this research, this chapter discusses the limitations of the applied research and provides recommendations for the further investigation of cast glass for structural members and systems.

10.2 Limitations of the research

Aim of this research was to manifest the potential and limitations of using cast glass for structural applications in architecture. This was achieved by developing two distinct structural systems for self-supporting envelopes made of cast glass components without the need of a secondary supportive structure. While these systems have been well received by the scientific, engineering and architectural communities, certain limitations of the presented work need to be discussed in order to define the validity of the systems in a wider sense and allow for their further applicability. These limitations are briefly discussed below; recommendations on their further development are given in section 10.3.

Firstly, the validation of both systems was experimentally conducted. As already mentioned, the described adhesively bonded glass block system has been developed in collaboration with, and support by, the industry. Accordingly, all experiments for this system used industrially manufactured glass blocks of high dimensional accuracy and surface quality. The provided results can be used as design guidelines for future applications. The second, interlocking system was developed within research context and had significantly less funding for the preparation of prototypes and the conduction of experiments. In this case, all prototypes were made by kiln-

cast glass blocks at the *Glass & Transparency Lab* of TU Delft and were manually post-processed. These blocks presented considerably lower dimensional accuracy and surface quality compared to the ones produced by the industry. These aspects had a significant influence on the experimental results, providing compromised values compared to prototypes made by industrially produced blocks. Thus, in this case, the experiments provided a qualitative guideline on different variables that influence the system but should not be used as strength values. The revalidation of this system with high-accuracy industrially made blocks is necessary before its real application in the built environment.

Secondly, the in-depth numerical modelling of the presented systems remained out of the scope of this study but could further contribute in refining their mechanical behaviour and properties. This in turn can lead to reduced safety factors and hence, to more slender and elegant solutions. The use of more slender and lightweight cast glass blocks also decreases annealing time, reduces the need for raw materials and decreases manufacturing costs.

Thirdly, this dissertation focused on the structural behaviour of cast glass assemblies. The strength of individual cast glass elements and the effect of flaws on their strength was only briefly discussed. In this direction, a study on the strength of cast glass and the establishment of standardized strength data would greatly facilitate the widespread application of cast glass in constructions.

Moreover, the thermal performance of systems out of cast glass components has not been addressed in this thesis. In principle, the monolithic nature of cast glass results in a high U-value and relatively poor thermal insulation properties. This is perhaps the biggest drawback in using cast glass in architectural envelopes, especially nowadays, where energy-efficient buildings are becoming more and more essential. The development of integrated solutions for cast glass envelopes with improved thermal performance would make cast glass considerably more appealing to the engineering and architectural community.

In addition, economic aspects related to the potential cost of the developed systems could not be directly assessed, due to the lack of disclosed cost data in any of the few realized projects, including the *Crystal Houses* façade. The, so far, limited demand of cast glass applications has led to the absence of a standardized manufacturing process and hence, to increased manufacturing costs. A thorough study on the establishment and the cost-effectiveness of a standardized cast glass production for structural components is essential for spreading cast glass elements into the market.

Finally, although the shaping potential of cast glass was largely discussed throughout this dissertation, it was only explored through the development of interlocking glass units. The geometry of the blocks used at the adhesively bonded system, developed for the *Crystal Houses* façade, was already defined and could not be altered. The shaping potential of cast glass can be further explored and lead to cost- and structurally-effective solutions, if design criteria in respect to the casting method, such as the ones discussed in Chapter 7, are incorporated from the initial design stages.

10.3 Recommendations for further research

Cast glass components for structural applications are still at an early stage of development and have been little explored. This thesis showcases the structural potential of cast glass by focusing on the development of building systems for self-supporting envelopes. The following recommendations do not only refer to the further improvement of the developed glass systems but aim on providing a wide overview of the aspects of cast glass that can and should be explored in the future.

10.3.1 Recommendations on the adhesively bonded glass system

The innovative glass masonry system developed for the *Crystal Houses* façade illustrates the great potential of adhesively bonded cast glass bricks as an answer to the quest of structural transparency. The pioneering research conducted can be used to evolve variable designs for architectural projects where maximum transparency is desired. Different types of clear adhesive can be applied according to the specific structural demands and possibly allow for larger tolerances in the fabrication process of the bricks. The greatest engineering challenges and practical implications of this system are intervened with the nature of the adhesive involved and the irreversibility of the structure. Further research is strongly recommended towards finding a thicker, clear adhesive that can accommodate the dimensional tolerances of the individual components in its layer while ensuring the desired structural performance. A promising solution would be the development of a foil that allows for in-situ lamination of the components by controllable heating. Such an adhesive technology would facilitate the construction and guarantee the desired visual result as well. Towards circularity, research on finding an adhesive that can be eventually dissolved and preferably reused is highly recommended.

10.3.2 Recommendations on the interlocking cast glass system

Further research is necessary for applying the proposed interlocking cast glass system in reality. Contrary to the presented adhesively bonded system, due to time and financial limitations, the investigation of this novel cast glass system has been made utilizing kiln-cast glass blocks that were made using disposable moulds at the *Glass & Transparency Lab*. The produced components were of significantly reduced dimensional accuracy and had a low surface quality. In turn, these aspects had a significant influence on the overall performance of the tested specimens. In order to derive accurate strength data it is essential that the proposed interlocking system is re-investigated and re-validated using industrially produced components of high accuracy and fine surface quality.

The current research focused on existing, readily available, PU interlayers for the validation of the proposed interlocking cast glass system. The chosen interlayer served its purpose of proving the feasibility of the system but is by no means the optimum choice – its creep resistance needs to be further examined. It is therefore recommended to investigate in more detail the effect of different interlayer materials, of various thicknesses and under longer creep duration, on the structural performance of the assembly. A promising solution would be the engineering of a composite (sandwich) interlayer as proposed by (Frigo 2017) with softer external layers, which can adapt to surface imperfections and displacements occurring under axial load and an inner layer that would be stiffer and more resistant. The possibility of using soft aluminium as an interlayer could also be investigated.

Complementary to this study, further research should focus on the engineering of the necessary peripheral constraint structure, offering compression in the direction perpendicular to the shear key surface, and on evaluating the effect of different pre-stress rates in the stiffness of an interlocking assembly. Attention should be given to the interface between the peripheral structure and the interlocking assembly and to the effect of different values of pre-compression on the assembly. It is anticipated that the pre-compression of the assembly can largely increase its out-of-plane loadbearing capacity. In addition, a detailed study has to be conducted regarding the assembly mode of the system in order to ensure its proper alignment and installation prior and during the necessary pre-compressing. Finally, considering a circular approach, a holistic proposal for the buildability of the interlocking system should be made, including the sealing and the un-sealing of the system during its eventual disassembly.

10.3.3 Possible other applications

The conducted research proved the potential of using cast glass for self-supporting structures that can evade the 2-dimensionality of float glass and the inherent structural challenges of it. Yet, self-supporting envelopes is only one of the possible structural applications of cast glass. Both developed systems can be adapted to create compressive structural members such as full-glass columns, arches and domes. Cast glass columns are of particular interest, as they are a promising solution for transparent structural members, capable of transferring the compressive loads in a building while allowing for light and space continuity. Research on adhesively bonded and interlocking cast glass columns, by (Felekou 2016; Akerboom 2016), in their MSc graduation thesis supervised by the author of this dissertation, have yielded promising results.

Another attractive and fascinating new field of application, especially for the interlocking cast glass system is its application for the structural restoration of historic monuments. The author of this thesis has been co-awarded as co-initiator a *3TU.bouw 2016* grant to further develop this idea. The concept is to use cast glass elements to rebuild the missing parts of monuments, from masonry walls to columns and decorative elements, as shown in (Barou 2016). This is in principle possible with advancements in glass casting technology, allowing for a vast possibility of shapes to be produced in glass. Hence, a fully transparent addition can be realized providing an answer to the ongoing debate of the materialization of restoration schemes. A glass restoration can demonstrate the monument both in the original and damaged condition at the same time, will not detract from its traditional setting and the balance of its compositions, and will preserve its original aesthetic and historic value. Moreover, it can provide a structural reinforcement for the monument due to the mechanical properties of glass. The principles of this new concept can be found at (Barou et al. 2018).

10.3.4 Investigating the strength of cast glass

Cast glass is still in an infant stage of development regarding structural applications in the built environment. As discussed in Chapter 9, the strength of cast glass structural components is a relatively unexplored field – there are yet no guidelines nor standardized strength data for such elements. As a consequence of this, the existing applications rely either to extensive experimental validation or to a secondary substructure that ensures the structural integrity of the assembly. Hence, there is need for further research on the mechanical properties of cast glass

and in particular on the influence of critical flaws. Particularly interesting is the investigation of the influence of the flaws occurring in the meso-structure of the solid glass, such as cord and inclusions to the total mechanical behaviour of the cast components. A consistent recording of the strength of cast glass components and a standardized production process can further reduce the material factors involved resulting to more slender and cost-effective cast glass solutions. For applications on the built-environment fire safety should as well be addressed and investigated. Proposals can include the glass type involved as well as the development of elegant, discreet safety mechanisms in case of fire.

10.3.5 Circular cast glass components out of glass waste

Glass casting is a promising manufacturing method for reintroducing discarded glass that is currently not recycled in the supply chain. Furthermore, by employing a dry-assembled, interlocking system such as the one discussed in Chapter 7 and Chapter 8, a fully reversible, circular building system can be achieved. The author of this dissertation has been co-awarded a *4TU.bouw 2017* grant and has been co-nominated for the *New Material Award 2018* for this idea and its first findings. Glasses of other recipes than soda-lime – such as mobile phone screens, crystal-ware, ovenware, laboratory-ware, light tubes, old TV screens, art glass- although pure and recyclable, end up as waste due to the lack of a recycling facility specialized in these glasses. Recycling them together with soda-lime is not possible by the industry as that would alter the end-recipe and also result in a different melting temperature. However, employing discarded glass of other recipes in cast components can be a way to reintroduce it to the supply chain. This alternative manufacturing method allows the use of customized recipes and their remelting without the aforementioned infrastructure implications. In that sense, everyday glass waste can be recycled into cast glass components. Through this initiative, *Pyrex*[®] trays and artware, even mobile phone and computer screens, are redirected from the landfill to the design and architecture sector, helping to tackle the scarcity of raw material resources. The first experiments at the *Glass & Transparency lab* of TU Delft with different glasses and cooling techniques have resulted in a wide range of clear, coloured, translucent and opaque/marbled circular glass elements. The first findings on the recycling by kiln-casting can be found at (Bristogianni et al. 2018b). In the future, extensive and systematic research is necessary for defining the mechanical properties of these new type of components.

10.3.6 **Development of cost-effective fabrication methods**

The real revolution in cast glass structures will come when a cost-effective production technique will be developed. The high costs that have restricted the application of cast glass components in just a few structural applications, are a result of the production time, mould-making and post-processing needed. The type of mould and glass used have also a great impact on the accuracy of the resulting component.

First of all, there is need for further research on the mould technology for cast glass elements. So far, the cost of high precision steel moulds has limited the number of different components to just a few in a structure. Research should focus on alternative mould fabrication technologies, such as adjustable steel moulds that can generate components of different sizes by the same mould. For customized or individually made components a promising solution is the development of 3D printed sand moulds, similar to the ones that have been recently used for metal casting. Research and experimental work by (Bhatia 2019) under the supervision of the author on the use of 3D-printed sand moulds for glass casting has already yielded promising results, suggesting the potential of this fabrication method for customized solid glass components.

Post-processing is a significant factor on the overall manufacturing costs and should be avoided; both manufacturing and construction of cast glass blocks for architectural envelopes require a high accuracy level. Spin-casting and press-moulds are two ways to achieve a higher precision.

The real breakthrough in cast glass structures would be the development of a low-expansion glass recipe with low working temperatures and production cost that would eliminate the size constraints and post-processing of soda-lime and borosilicate glass, allow for faster cooling and, in turn, for a faster and more economical production.

10.3.7 **Optimizing the geometry of the components with respect to the properties of glass**

So far, there has been little exploration on the shaping potential of cast glass. The structural cast glass components of the realized architectural projects mimic shapes derived from masonry structures – same as many of the marble decoration details in Greek temples are the descendants of the older wooden connections.

Yet, glass as a material has different properties and manufacturing process that in turn call for different forms. Osteomorphic blocks such as the ones presented in Chapter 7 and Chapter 8 are closer to this principle. Research on the optimization of the form of cast glass components can result in a more cost- and time-efficient production; i.e. honeycomb blocks can be lightweight yet stiff enough to create architectural structures similar to the ones realized. The glass mass can be optimized to match design loads whilst keeping the mass homogeneous for even cooling. A good example is the topologically optimized cast glass grid-shell node developed by (Damen 2019) for his MSc thesis under the supervision of the author of this dissertation. The resulting node is reduced by approx. 70% in mass compared to the original solid variant. Such reduction in mass is essential for reducing the requested annealing time which is currently one of the biggest drawbacks of cast glass components; a reduced annealing time can in turn, render cast glass components a financially competitive solution.

10.3.8 **Improving the thermal performance of cast glass structures**

The development of integrated systems that can improve the thermal performance of cast glass structures is highly encouraged. One of the biggest drawbacks of the current systems is the unsatisfactory thermal performance due to the monolithic nature of the glass and the absence of a cavity. Possible solutions to be investigated include the development of structural cast units with embedded cavities that do not compromise to a great extent the mechanical properties and transparency of the components. Components can be also developed to compensate for the energy loss; for example solid cast glass elements with an embedded lens system can be studied to concentrate and store solar power. It should be noted, however, that the high accuracy of the involved lenses and the perplexed geometry of the components may result in high manufacturing costs. An alternative approach is the study of integrated systems utilizing both cast glass elements and float glass for the creation of curtain walls and double-skin facades of improved thermal performance.



The two developed systems utilizing solid cast glass components.
In this page: *Adhesively bonded solid glass blocks.* Next page: *Dry assembled, interlocking cast glass components.*



Appendix

Annealing guideline for thick slabs by Bullseye glass.

TABLE 10.1 Indicative properties of *Delo Photobond* adhesives developed for glass bonding as provided by the manufacturer. Mechanical properties are given for a 0.1 mm thick adhesive layer.

Property	Unit	4468	4494	4497	4302	GB310	GB345	GB368
Application area B=bonding, S= sealing, C = coating		B	B	B/S/C	B	B	B	B
Colour cured product		clear	Clear	milky	clear	clear	clear	clear
Viscosity (at 23 °C)	mPas	7000	20000	30000	100	100	1500	5700
Young's modulus	N/mm ²	250	400	84	260	1600	1200	900
Compression shear strength (glass/glass)	N/mm ²	22	28	19	31	34	29	23
Tensile strength	N/mm ²	14	20	11	16	33	26	20
Elongation at tear	%	200	160	200	90	4	40	17
Glass transition T	°C	74	120	52	111	120	77	102
Shrinkage	Vol%	9	9	9	10	10	7	7
Index of refraction	-	1.5	1.5	1.5	1.5	1.5	1.5	1.5
Water absorption	weight %	0.9	1.3	0.9	1.4	0.4	0.9	0.5
Creep resistance CTI	-	600M	-	600 M	600 M	-	-	-
Shore hardness D	-	45	62	40	45	77	70	67
Special features of product	-	Glass-glass Glass-metal Tension equalizing USP XXIII Glass VI approval	Plastic adhesive Good adhesion to glass and metal Very fast curing and tough-hard	Multi-purpose adhesive Dry surface	Glass adhesive Capillary Tough adhesive layer Equalizes tensions well	Glass adhesive Capillary High-strength	Glass-to-metal connections	Glass adhesive Glass-to-plastic connections Dry surface

References

- AGC: Linea Azzurra. <https://www.agc-yourglass.com/gb/en/products/planibel-clear/linea-azzurra> (2019). Accessed 23rd of September 2019
- Akerboom, R.: Glass Columns, exploring the potential of free standing glass columns assembled from stacked cast elements. TU Delft (2016)
- Albert Napolitano, Earl G. Hawkins: Viscosity of a Standard Soda-Lime-Silica Glass. *Journal of Research of the National Bureau of Standards - A. Physics and Chemistry* **68A**(5), 439-448 (1964)
- Albus, J., Robanus, S.: Glass in Architecture - New Developments. In: *Detail - Glass Construction*, vol. 2. pp. 168-170. Institut für internationale Architektur-Dokumentation, Germany, (2015)
- Anagni, G.M.: Recycled glass mixture as cast glass components for structural applications towards sustainability. Politecnico di Milano + TU Delft (2019)
- Angel, J.R.P.: 8 m Borosilicate Honeycomb Mirrors. In: *ESO Conference on Very Large Telescopes and their Instrumentation*, Garching, Germany 1988. European Southern Observatory
- Ashby, M.F., Brechet, Y.J.M.: Designing hybrid materials. *Acta Materialia* **51**, 5801-5821 (2003)
- Ashby, M.F., Jones, D.R.H.: *Engineering Materials 2. An introduction to Microstructures, Processing and Design*, 3 ed. Elsevier, UK (2006)
- ASTM: ASTM C 1036-06. In: *Standard Specification for Flat Glass*. p. 8. ASTM International, USA, (2008)
- Aurik, M.: *Structural Aspects of an Arched Glass Masonry Bridge*. Delft University of Technology (2017)
- Aurik, M., Snijder, A., Noteboom, C., Nijse, R., Louter, C.: Experimental analysis on the glass-interlayer system in glass masonry arches. *Glass Structures & Engineering* **3**(2), 335-353 (2018). doi:10.1007/s40940-018-0068-7
- Barou, L., Bristogianni, T., Oikonomopoulou, F.: *Transparent Restoration*. TU Delft (2016)
- Barou, L., Oikonomopoulou, F., Bristogianni, T., Veer, F.A., Nijse, R.: A new remedial tool for the consolidation of historic structures. *HERON* **63** (1/2), 159-198 (2018)
- Bartuška, M.: *Glass Defects*. Práh, (2008)
- Bhatia, I.: *Shaping transparent sand in sand: fabricating geometrically optimized glass column using sand moulds*. MSc, TU Delft (2019)
- Bourhuis, E.: *Glass: Mechanics and Technology*. Wiley (2014)
- Bray, C.: *Dictionary of Glass. Materials and Techniques*, 2nd ed. A&C Black Limited, London (2001)
- Bricknell, D.: *Float: Pilkington's Glass Revolution*. Carnegie Publishing, (2010)
- Bristogianni, T., Oikonomopoulou, F., Justino de Lima, C., Veer, F.A., Nijse, R.: Cast Glass Components out of Recycled Glass: Potential and limitations of upgrading waste to load-bearing structures. In: Belis, J., Louter, C., Bos, F. (eds.) *Challenging Glass 6 International Conference on the Architectural and Structural Applications of Glass*, Delft 2018a
- Bristogianni, T., Oikonomopoulou, F., Justino de Lima, C., Veer, F.A., Nijse, R.: Structural cast glass components manufactured from waste glass: Diverting everyday discarded glass from the landfill to the building industry. *HERON* **63** (1/2), 57-102 (2018b)
- Bristogianni, T., Oikonomopoulou, F., Veer, F.A., Nijse, R.: The effect of manufacturing flaws in the meso-structure of cast glass on the structural performance. In: Zingoni, A. (ed.) *Seventh International Conference on Structural Engineering, Mechanics and Computation (SEMC)*, Cape Town 2019. Taylor & Francis
- Bristogianni, T., Oikonomopoulou, F., Veer, F.A., Snijder, A., Nijse, R.: Production and Testing of Kiln-cast Glass Components for an Interlocking, Dry-assembled Transparent Bridge. In: Vitkala, J. (ed.) *Glass Performance Days*, Finland 2017, pp. 101-106. *Glass Performance Days*
- Christensen, R.M.: *Theory of materials failure*. Oxford University Press, UK (2013)
- Christoph, P., Knut, G.: Innovative Glass Joints - The 11 March Memorial in Madrid. In: Bas, F., Louter, C., Veer, F. (eds.) *Challenging Glass: Conference on Architectural and Structural Applications of Glass*, Delft, the Netherlands 2008, p. 113/668. IOS Press, The Netherlands

- Corning: Nuclear Glass Blocks. <https://www.corning.com/worldwide/en/products/advanced-optics/product-materials/specialty-glass-and-glass-ceramics/radiation-shielding-glass/nuclear-glass-blocks.html> (2018). Accessed 05/02 2018
- Corning Museum of Glass: Glass and the Space Orbiter. <https://www.cmog.org/article/glass-and-space-orbiter> (2011a). Accessed 26-01 2018
- Corning Museum of Glass: The Glass Giant. <http://www.cmog.org/article/glass-giant> (2011b). 2016
- Corning Museum of Glass: The Mystery Slab of Beth She'Arim. (2011c). Accessed 27/10/2016 2016
- Corning Museum of Glass: Types of Glass. <http://www.cmog.org/article/types-glass> (2011d).
- Crocombe, A.D.: Global yielding as a failure criterion for bonded joints. *International Journal of Adhesion and Adhesives* **9**(3), 145-153 (1989)
- Cummings, K.: *Techniques of Kiln-formed Glass*, 2nd ed. A&C Black Publishers Limited, London (2001)
- Cummings, K.: *A History of Glassforming*. University of Pennsylvania Press, USA (2002)
- da Silva, L.F.M., Rodrigues, T.N.S.S., Figueiredo, M.A.V., de Moura, M.F.S.F., Chousal, J.A.G.: Effect of Adhesive Type and Thickness on the Lap Shear Strength. *The Journal of Adhesion* **82**(11), 1091-1115 (2006)
- Damen, W.: *Structural Glass Gridshell Nodes: designing structural cast glass gridshell nodes using parametric design and topology optimization*. MSc, TU Delft (2019)
- Delo Industrial Adhesives: *Bond it: Reference book on bonding technology*, 2nd ed. Delo Industrial Adhesives, Munich (2007)
- Delo Industrial Adhesives: *Glass Bonding: Requirements, Product Range and Design Examples*. In. Delo Industrial Adhesives, Munich, (2011)
- Delo Industrial Adhesives: *Technical Information: Delo-Photobond 4468*. In. Delo Industrial Adhesives, Windach, (2014)
- Delo Industrial Adhesives: *Delo Photobond 4494 Technische Information*. In. Delo Industrial Adhesives, Windach, (2016a)
- Delo Industrial Adhesives: *Delo Photobond 4497 Technische Information*. In. Delo Industrial Adhesives, Windach, (2016b)
- Den Braven: *Zwaluw Joint Fix Technische datasheet*. In: Den Braven (ed.). Oosterhout, (2017)
- den Ouden, G.: *Lastechnologie*. VSSD, Delft (2009)
- Dietrich, N., Jerry, S., Bruce, K.: Glass Block. In: Thomas, J. (ed.) *Twentieth-century building materials : history and conservation*. pp. 163-167. McGraw-Hill, New York (1995)
- DIT b.v.: *Pure - Technical Data Sheet*. In: DIT b.v. (ed.). Dinxperlo, (2016)
- Djumas, L., Molotnikov, A., Simon, G.P., Estrin, Y.: Enhanced Mechanical Performance of Bio-Inspired Hybrid Structures Utilising Topological Interlocking Geometry. *Scientific Reports* **6** (2016)
- Domus: *Pae White: Qwalala*. https://www.domusweb.it/en/news/2017/05/19/pae_white_qwalala.html (2017). Accessed 20th of September 2019
- Dyskin, A.V., Estrin, Y., Kanel-Belov, A.J., Pasternak, E.: A new concept in design of materials and structures: Assemblies of interlocked tetrahedron-shaped elements. *Scripta Materialia* **44**, 2689-2694 (2001)
- Dyskin, A.V., Estrin, Y., Pasternak, E.: *Topological Interlocking Materials. Architected Materials in Engineering and Nature*. Springer, Australia (2019)
- Dyskin, A.V., Estrin, Y., Pasternak, E., Khor, H.C., Kanel-Belov, A.J.: Fracture Resistant Structures Based on Topological Interlocking with Non-planar Contacts. *Advances Engineering Materials* **5**(3), 116-119 (2003). doi:10.1002/adem.200390016
- Dyskin, A.V., Pasternak, E., Estrin, Y.: Mortarless structures based on topological interlocking. *Frontiers of Structural and Civil Engineering* **6**(2), 188-197 (2012). doi:10.1007/s11709-012-0156-8
- Dyskin, A.V., Pasternak, E., Khor, H.C., Estrin, Y., Kanel-Belov, A.J.: Mortar-free construction based on topological interlocking. *Developments in Mechanics of Structures and Materials*. 665-670 (2005)
- Dyskin, A.V., Yong, D., Pasternak, E., Estrin, Y.: Stresses in topologically interlocking structures: two scale approach. In: Denier, J., Finn, M.D. and Mattner T., Eds (ed.) *ICTAM 2008, XXII International Congress of Theoretical and Applied Mechanics*, Adelaide, Australia 2008
- Estrin, Y., Dyskin, A.V., Pasternak, E.: Topological interlocking as a material design concept. *Materials Science and Engineering C*(31), 1189-1194 (2011)
- Estrin, Y., Dyskin, A.V., Pasternak, E., Schaare, S.: Topological interlocking in design of structures and materials. *Architected Multifunctional Materials* (2009)
- Estrin, Y., Dyskin, A.V., Pasternak, E., Schaare, S., Stanchits, S., Kanel-Belov, A.J.: Negative stiffness of a layer with topologically interlocked elements. *Scripta Materialia* **50**, 291-294 (2004)

- Estrin, Y., Molotnikov, A., Simon, G.P., Kaloshkin, S., Senatov, F., Maksimkin, A.: Flexible ceramics with self-stiffening capability. In: European Symposium on Intelligent Materials 2015, Kiel, Germany 2015 Eurostat: Waste Statistics in Europe. http://ec.europa.eu/eurostat/statisticsexplained/index.php/Packaging_waste_statistics (2014). Accessed 22 October 2017
- ExOne: Sand Mould Casting Applications. <https://www.exone.com/en-US/case-studies/Sand-Mold-Casting-Applications> (2019). Accessed 21st of September 2019
- Felekou, E.: Glass Tower in high-rise buildings. MSc, TU Delft (2016)
- FEVE European Container Glass Federation: Container glass collection for recycling rates in Europe. In: Brussels, (2016)
- Fink, A.: Ein Beitrag zum Einsatz von Floatglas als dauerhaft tragender Konstruktionswerkstoff. PhD, Technische Universität Darmstadt (2000)
- Flygt, E.: Utveckling av 3D-Printade sandformar for glasgjutning. In: GLAS. vol. 4-2018, p. 3. Stockholm, (2018)
- Frigo, G.: Restoration of partially collapsed historic wall using interlocking cast-glass components: the case of san michele castle in cagliari. Politecnico di Milano (2017)
- Goppert, K., Paech, C., Arbos, F., Teixidor, C.: Innovative Glass Joints - The 11 March Memorial in Madrid. In: Louter, C., Bos, F., Veer, F. (eds.) Challenging Glass: Conference on Architectural and Structural Applications of Glass, Delft, The Netherlands 2008, pp. 111-118. IOS Press
- Grant, L.D.R., Adams, R.D., da Silva, L.F.M.: Experimental and numerical analysis of single-lap joints for the automotive industry. *International Journal of Adhesion and Adhesives* **29**(4), 405-413 (2009)
- Granta Design Limited: CES EduPack 2015. In: Granta Design Limited, Cambridge, (2015)
- Griffith, A.A.: The phenomena of rupture and flow in solids. *Philosophical Transactions, Series A* **221**, 163-198 (1921)
- Haldimann, M., Luible, A., Overend, M.: Structural Use of Glass. In: *Structural Engineering Documents* 10. IABSE-AIPC-IVBH, Zurich, Switzerland, (2008)
- Hannah, B.H.: Jaume Plensa: Crown Fountain as Carnavalesque. Umi Dissertation Publishing, USA (2009)
- Hiroshi, N.: Residence in Hiroshima. *DETAIL: Transluscent and Transparent* **2** (2013)
- International Organization for Standardization: ISO 21690:2006 (en). In: *Glass in building — Glass blocks — Specification and test methods*. ISO, (2006)
- Jacobs, E.A.M.: Structural consolidation of historic monuments by interlocking cast glass components. Delft University of Technology (2017)
- James Carpenter Design Associates Inc: Projects. <http://www.jcdainc.com/projects> (2018). Accessed 20th March 2018
- Job, T., Ramaswamy, A.: Material Properties of Steel Fiber-Reinforced Concrete. *Journal of Materials in Civil Engineering* **19**, 385-392 (2007)
- Kergaravat, J.F.: Personal communication regarding the production method of Nuclear Glass Blocks at the Corning Facilities in Fontainebleau. In: Fontainebleau, (2017)
- Khor, H.C., Dyskin, A.V., Estrin, Y., Pasternak, E.: Mechanisms of fracturing in structures built from topologically interlocked blocks. *Structural Integrity and Fracture, SIF* 2004, 189-194 (2004)
- Khor, H.C., Dyskin, A.V., Pasternak, E., Estrin, Y., Kanel-Belov, A.J.: *Structural Integrity and Fracture*. (2002)
- Klein, J.: Additive manufacturing of optically transparent glass. MIT (2015)
- Korres, M.: From Pentelicon to the Parthenon: The Ancient Quarries and the Story of a Half-Worked Column Capital of the First Marble Parthenon. Oxford University Press, UK (2000)
- Kroller-Muller Museum: Roni Horn: Opposites of white. <http://krollermuller.nl/en/roni-horn-opposites-of-white> (2007). 2016
- Kunz, J., Studer, M.: Determining the Modulus of Elasticity in Compression via the Shore A Hardness. *Kunststoffe International* **6** (2006)
- Louter, C.: Fragile yet Ductile. PhD, TU Delft (2011)
- Lyons, A.R.: *Materials for Architects & Builders*, 4 ed. Elsevier, USA (2010)
- Martlew, D.: Chapter 5: Viscosity of Molten Glasses. *Properties of Glass-Forming Melts*. CRC Press Taylor & Francis Group, USA (2005)
- McKenzie, H.W., Hand, R.J.: *Basic Optical Stress Measurement in Glass*. Society of Glass Technology, Sheffield (2011)
- MIT Media Lab: GLASS II. <http://matter.media.mit.edu/environments/details/glass-ii#prettyPhoto> (2018). Accessed 23rd July 2018

- Molnár, G., Molnár, L.M., Bojtár, I.: Preparing a comprehensive analysis of the mechanical classification of structural glass. *Materials Engineering* **18**, 71-81 (2012)
- Molotnikov, A., Estrin, Y., Dyskin, A.V., Pasternak, E., Kanel-Belov, A.J.: Percolation mechanism of failure of a planar assembly of interlocked osteomorphic elements. *Engineering Fracture Mechanics* **74**, 1222-1232 (2007)
- Murray, S.: *Translucent building skins : material innovations in modern and contemporary architecture*. Routledge, London (2013)
- MVRDV Architects: *Crystal Houses*. <https://www.mvrdv.nl/en/projects/crystal-houses> (2016). Accessed 21/02/2017 2017
- Niehe, P.: Sand printing makes complex casted structural parts affordable. <https://www.arup.com/news-and-events/news/sand-printing-makes-complex-casted-structural-parts-affordable> (2017). Accessed 19/02 2018
- Nijssen, R.: *Glass in Structures: Elements, Concepts, Designs*. Birkhauser, Germany (2003)
- Nilsson, L., Persson, P.O., Rydén, L., Darozhka, S., Zaliauskiene, A.: *Cleaner Production: Technologies and Tools for Resource Efficient Production*. Baltic University Press, Uppsala (2007)
- Novatech N.V.: Tec7 Technical Data sheet. In: Novatech N.V. (ed.). Olen, (2016)
- O' Callaghan, J., Marcin, M.: Thinking Big with Structural Glass. In: Vitkala, J. (ed.) *Glass Performance Days, Tampere 2009*, pp. 59-63. Glaston Finland Oy
- O' Regan, C.: *Structural Use of glass in buildings second ed.* The Institution of Structural Engineers, London (2014)
- Ohara: *Bubble & Inclusion*. <https://www.oharacorp.com/o6.html> (2019). Accessed 20th of September 2019
- Oikonomopoulou, F., Bristogianni, T., Barou, L., Jacobs, E.A.M., Frigo, G., Veer, F.A., Nijssen, R.: A novel, demountable structural glass system out of dry-assembly, interlocking cast glass components. In: Louter, C., Belis, J., Bos, F. (eds.) *Challenging Glass 6 : Conferece on Architectural and Structural Applications of Glass, The Netherlands 2018a*
- Oikonomopoulou, F., Bristogianni, T., Barou, L., Veer, F.A., Nijssen, R.: Interlocking cast glass components. Exploring a demountable, dry-assembly structural glass system. *HERON* **63 (1/2)**, 103-138 (2018b)
- Oikonomopoulou, F., Bristogianni, T., Barou, L., Veer, F.A., Nijssen, R.: The potential of cast glass in structural applications. Lessons learned from large-scale castings and state-of-the-art load-bearing cast glass in architecture. *Journal of Building Engineering* **20**, 213-234 (2018c)
- Oikonomopoulou, F., Bristogianni, T., Nijssen, R., Veer, F.A.: Innovative structural applications of adhesively bonded solid glass blocks. In: Vitkala, J. (ed.) *Glass Performance Days, Tampere 2015a*, pp. 256-261. *Glass Performance Days*
- Oikonomopoulou, F., Bristogianni, T., Veer, F.A., Nijssen, R.: The construction of the Crystal Houses façade: challenges and innovations. *Glass Structures & Engineering*, 1-22 (2017a). doi:10.1007/s40940-017-0039-4
- Oikonomopoulou, F., Van den Broek, E.A.M., Bristogianni, T., Veer, F.A., Nijssen, R.: Design and expeirmental testing of the bundled glass column. *Glass Structures & Engineering* (2017b). doi:DOI 10.1007/s40940-017-0041-x
- Oikonomopoulou, F., Veer, F.A., Nijssen, R., Baardolf, K.: A completely transparent, adhesively bonded soda-lime glass block masonry system. *Journal of Facade Design and Engineering* **2(3-4)**, 201-222 (2015b). doi:10.3233/fde-150021
- Overend, M., De Gaetano, S., Haldimann, M.: Diagnostic Interpretation of Glass Failure. *Structural Engineering International* **2**, 151-158 (2007)
- Oxbow Books: *Glass of the Roman World*. Oxbow Books, Oxford & Philadelphia (2015)
- Palomar Observatory: The 200-inch (5.1-meter) Hale Telescope. <http://www.astro.caltech.edu/palomar/about/telescopes/hale.html> (2018). Accessed 1st February 2018
- Patterson, M.: *Structural Glass Facades and Enclosures*. John Wiley & Sons, USA (2011)
- Pfaender, H.G.: *SCHOTT Guide to Glass*. Springer Science & Business Media, (2012)
- Prautzsch, V.: *Development of transparently bonded glass frame corners and investigation of the structural behavior*. PhD, TU Dresden (2015)
- Puller, K., Sobek, W.: Glass-Steel Connections Using Acrylate Adhesives. In: Bos, F., Louter, C., Veer, F. (eds.) *Challenging Glass, Delft 2008*, pp. 273-278. IOS Press, Amsterdam (2008)
- Riewoldt: Riewoldt - adhesion - cutting - die cutting/Knowledge center. <http://www.riewoldt.de/en/knowledge-center/fundamentals-of-adhesive-technology/> (2014).

- Roeder, E.: Extrusion of Glass. *Journal of Non-Crystalline Solids* **5**(5), 377-388 (1971). doi:10.1016/0022-3093(71)90039-1
- Saint Gobain: Physical Properties. <http://uk.saint-gobain-glass.com/appcommportalchilddetails/713/442/711/378> (2016). 2016
- Sarkisian, M.: *Designing Tall Buildings: Structure as Architecture*. Routledge, New York (2012)
- Schittich, C., Staib, G., Balkow, D., Schuler, M., Sobek, W.: *Glass Construction Manual 2nd revised and expanded edition* ed. Birkhäuser, Basel (2007)
- Schober, H., Schneider, J., Justiz, S., Gugeler, J., Paech, C., Balz, M.: Innovations with glass, steel and cables. In: *Glass Performance Days*, Tampere, Finland 2007, pp. 198-201
- Scholtens, E.: Recycling borosilicate glass for application in an interlocking cast glass component facade system applied in Casa de Musica. MSc, TU Delft (2019)
- SCHOTT Advanced Optics: New Bubble Grades for Optical Glasses. In: AG, S. (ed.). p. 2. Germany, (2013)
- Schott AG: Technical Information: Stress in optical glass. In: SCHOTT (ed.) *Advanced Optics*. Schott AG, Mainz, (2004)
- SCHOTT AG: SCHOTT Tubing: glass tubes, rods and profiles. <http://www.schott.com/tubing/english/index.html?appid=ph> (2017). 2017
- Shand, E.B.: *Engineering Glass, Modern Materials*, vol. 6. Academic Press, New York (1968)
- Shand, E.B., Armistead, W.H.: *Glass Engineering Handbook*. McGraw-Hill Book Company, New York (1958)
- Shelby, J.E.: *Introduction to Glass Science and Technology: Edition 2*. (2005)
- Shribak, M.: Polychromatic polarization microscope: bringing colors to a colorless world. *Scientific Reports* **5**, 17340 (2015). doi:10.1038/srep17340
- SMOOTH-ON: Durometer Shore Hardness Scale. <https://www.smooth-on.com/page/durometer-shore-hardness-scale/> (2019). Accessed 22nd September 2019
- Snijder, A., Louter, C., van der Linden, L., Nijse, R.: The glass swing: a vector active structure. In: Zingoni, A. (ed.) *Advances in Engineering Materials, Structures and Systems: Innovations, Mechanics and Applications*, Cape Town 2019, pp. 633-634. Taylor & Francis
- Snijder, A., Nijse, R., Louter, C.: Building and Testing Lenticular Truss Bridge with Glass-Bundle Diagonals and Cast Glass Connections In: Louter, C., Belis, J., Bos, F. (eds.) *Challenging Glass 6 Conference on Architectural and Structural Applications of Glass*, Delft 2018
- Snijder, A., Smits, J., Bristogianni, T., Nijse, R.: Design and Engineering of a Dry Assembled Glass Block Pedestrian Bridge. In: Belis, J., Louter, C., Bos, F. (eds.) *Challenging Glass 5*, Ghent, Belgium 2016. Ghent University
- Tasche, S.: *Light curing adhesives in glass construction*. PhD, TU Dresden (2007)
- The Architectural Review: Optical Glass House, Hiroshima, Japan. <https://www.architectural-review.com/today/optical-glass-house-hiroshima-japan/8638709.article> (2012). 2018
- The Corning Museum of Glass: *The Corning Museum of Glass A Guide to the Collections*. Corning, New York (2001)
- Thwaites, A.: *Mould making for glass*. *Glass Handbooks*. A&C Black, UK (2011)
- Tijssen, M.: transmissie glazen baksteen. In: DIMES. TU Delft, Delft, (2014)
- Vereniging Nederlandse Glasfabrikanten: *Routekaart 2030 Nederlandse glasindustrie*. In: *Vereniging Nederlandse Glasfabrikanten*, The Netherlands, (2012)
- Vindico: Vindico <http://www.vindico.info/> (2014). Accessed 15/11 2014
- Vitalis, D., Veer, F.A., Oikonomopoulou, F.: Design and experimental testing of all glass sandwich panels. An experimental and numerical study for the glass floors of the Acropolis museum. In: Louter, C., Belis, J., Bos, F. (eds.) *Challenging Glass 6 Conference on Architectural and Structural Applications of Glass*, Delft 2018
- Vlakglas Recycling Nederland: *Jaarverslag 2017*. In: *Vlakglas Recycling Nederland*, The Netherlands, (2017)
- Watson, D.M.: *Practical Annealing* In: 11th Biennial Ausglass Conference, Wagga Wagga 1999. Mc Kinnon (1999)
- Weller, B., Döbbel, F., Nicklisch, F., Prautzsch, V., Rücker, S.: All Glass Enclosure with Transparently Bonded Glass Frames. In: Bos, F., Louter, C., Veer, F.A. (eds.) *Challenging Glass 2*, Delft 2010a, pp. 207-216. TU Delft Open
- Weller, B., Döbbel, F., Nicklisch, F., Prautzsch, V., Rücker, S.: Geklebte Ganzglaskonstruktion für das Leibniz-Institut für Festkörper und Werkstofforschung in Dresden. *Stahlbau Spezial "Konstruktiver Glasbau"*, 34-40 (2010b)

- Weller, B., Nicklisch, F., Prautzsch, V., Vogt, I.: Outline of Testing and Evaluation Program Used in Selection of Adhesives for Transparent Adhesive Joints in Glass Load-Bearing Structures. *Journal of ASTM International* **9**(4), 1-17 (2012). doi:10.1520/JAI104088
- Weller, B., Reich, S., Ebert, J.: Principles and Geometry of Modular Steel-Glass Space Structures. In: Bos, F., Louter, C., Veer, F.A. (eds.) *Challenging Glass*, Delft 2008, pp. 145-154. IOS Press
- Wiel Architects: WAA Academy of Art & Architecture. http://www.wielaretsarchitects.com/en/projects/academy_of_art_amp_architecture/ (2014). Accessed 20/08 2014
- Wörner, J.D., Schneider, J., Fink, A.: *Glasbau: Grundlagen, Berechnung, Konstruktion*. Springer, Berlin (2001)
- Worrell, E., Galitsky, C., Masanet, E., Graus, W.H.J.: Energy Efficiency Improvement and Cost Saving Opportunities for the Glass Industry. An ENERGY STAR Guide for Energy and Plant Managers. In: Ernest Orlando Lawrence Berkeley National Laboratory, California, (2008)
- Wurm, J.: *Glass Structures: Design and Construction of Self-supporting Skins*. Birkhauser, Germany (2007)
- Yu, R.: The applicability evaluation of recycled-glass beam made of waste float glass. TU Delft (2019)
- Zareyan, B., Khoshnevis, B.: Effects of interlocking on interlayer adhesion and strength of structures in 3D printing of concrete. *Automation in Construction* **83**, 212-221 (2017)
- Zirker, J.B.: *An Acre of Glass: A History and Forecast of the Telescope*. The Johns Hopkins University Press Baltimore (2005)

List of Tables

- 2.1 Approximate chemical compositions and typical applications of the different glass types as derived from (Shand, Armistead 1958). 53
- 2.2 Approximate properties of the different glass types of Table 2.1 based on (Shand, Armistead 1958)*. Mean Melting Point at 10 Pa.s as stated by (Martlew 2005). 54
- 2.3 Overview of existing glass fabrication methods for building components and their current size limitations. 66
- 2.4 Typical annealing scheme for commercial soda-lime glass based on Fig. 2.20, adapted from (Shand, Armistead 1958). 72
- 2.5 Characteristics of prevailing mould types for glass casting 75
- 2.6 Properties of standardized soda-lime and borosilicate glass according to EN572-1:2004 80
- 2.7 Strength values of standardized float/cast soda-lime and borosilicate glass by CES Edupack Program (Granta Design Limited 2015). 84
- 3.1 Dimensions and characteristics of some of the largest cast glass components made. Data for the telescope mirrors as provided by (Angel 1988; Zirker 2005). 100
- 4.1 Overview of the characteristics of realized self-supporting envelopes using solid cast glass components. 109
- 4.2 Design principles of the different structural systems employing cast glass components 128
- 5.1 Indicative properties of *Delo Photobond 4468* according to (Delo Industrial Adhesives 2014) 141
- 5.2 Observations from the architectural mock ups 145
- 5.3 Technical specifications of the soda-lime cast glass blocks as provided by *Poesia* 147
- 5.4 Type of blocks used for the manufacturing of the prototypes 151
- 5.5 Results of glass blocks' compression tests 159
- 5.6 Results of the compression tests on the glass column specimens 161
- 5.7 4-point bending tests results 163
- 5.8 Results of the 4-point bending test of the architrave 165
- 5.9 Findings from the hard-body impact and vandalism test 167
- 5.10 Results of thermal shock tests. Two samples were used per test per temperature. 169
- 6.1 Composition of the applied cast glass based on XRF chemical analysis 182
- 7.1 Comparative assessment of the different interlocking block types based on the established design criteria 227
- 7.2 Mean properties of the selected material families that fulfil the interlayer requirements by CES2015 231
- 7.3 Material properties used by (Aurik et al. 2018) 232
- 8.1 Properties of a selection of cast PU interlayers available in the market as provided by the manufacturer 253
- 8.2 Main results of the compression tests on PU interlayers. 257

- 8.3 Main results of the compression tests on 3 mm thick PU interlayers (Series 2). 259
- 8.4 Main results of the compression tests on 6 mm thick PU interlayers (Series 3). 264
- 8.5 Summary of the main results of the interlayer testing. 267
- 8.6 Summary of the main results 272
- 8.7 Input properties of glass and polyurethane interlayer 282
- 8.8 Input properties of interface elements 282
- 10.1 Indicative properties of *Delo Photobond* adhesives developed for glass bonding as provided by the manufacturer. Mechanical properties are given for a 0.1 mm thick adhesive layer. 326

List of Figures

- 1.1 The *Apple Store* in New York by *EOC Engineers* 35
- 1.2 The Crystal Houses façade in Amsterdam by *MVRDV Architects*, made of adhesively bonded glass blocks. Source: *Daria Scagliola and Stijn Brakke*. 36
- 1.3 Illustration of *Giuseppe Terragni* and *Pietro Lingeri*'s unrealized design for the *Danterium* (1938). Can we cast such solid, transparent glass columns? Source: *archeyes.com* 38
- 1.4 Glass casting (hot-pouring) 38
- 1.5 Solid glass sculptures by artist *Roni Horn*. 39
- 1.6 Methodology diagram of the thesis. 43
- 1.7 Research strategy scheme / dissertation outline 47
- 2.1 Schematic illustration of the float production process by (Louter 2011) based on (Wörner et al. 2001). 56
- 2.2 Float glass ribbon within the tin bath. Source: <https://www.skyre-inc.com/applications/hydrogen-recycling/> 57
- 2.3 Glass structure out of standard float panels up to 6 m in length by *EOC Engineers* in Philadelphia, USA. 57
- 2.4 The *Apple Store* in Chicago by *EOC Engineers*. Panels are 3 m wide and up to 10 m in height. Source: *EOC Engineers*. 58
- 2.5 Principle of the Danner process. 59
- 2.6 Extruded hollow tubes used at the facade of the *Johnson Building* in USA. 60
- 2.7 Left: 1.5 m long bundled glass columns at *TU Delft Glass Lab*. Top right: Extrusion profiles made by *SCHOTT AG*. Bottom right: A bundled glass column made of adhesively bonded extruded profiles developed by (Oikonomopoulou et al. 2017b). 60
- 2.8 The *glass truss bridge* at the *TU Delft campus* made of extruded glass profiles as described in (Snijder et al. 2018). 61
- 2.9 The glass swing developed by (Snijder et al. 2019) from *TU Delft*, in collaboration with *Arup*, *SCHOTT AG* and *RAMLAB* for the *GlassTec 2018* exhibition. 61
- 2.10 The glass sandwich floor developed by the *TU Delft Glass & Transparency Lab*, in collaboration with *Arup* and *SCHOTT AG* exhibited at *GlassTec 2018*. 62
- 2.11 Rendered cross-section of the Kiln Cartridge by (Klein 2015). 1. crucible 2. heating elements 3. nozzle 4. thermocouple 5. removable feed access 6. stepper motor 7. printer frame 8. print annealer 9. ceramic print plate 10. z-driven train 11. ceramic viewing window 12. insulating skirt. 63
- 2.12 Glass 3D-printing nozzle. Source: Steven Keating. 63
- 2.13 3m tall glass prototypes out of 3D-printed segments. Source: *Paula Aguilera, Jonathan Williams* and *The Mediated Matter Group*. 64
- 2.14 An array of 3D-printed glass components prepared in a 3x5x3 array ordered for assembly. Source: *The Mediated Matter Group*. 64
- 2.15 The cast glass blank of the Hale Telescope. Image credits: Collection of the *Rakow Library, The Corning Museum of Glass*. 67

- 2.16 Left: Primary casting method (hot-forming). Right: Secondary casting method (kiln-casting). 68
- 2.17 Left: Schematic representation of the volume's dependence on temperature for a glass and a crystalline material. During the cooling process from a liquid to a solid, glasses do not convert to a crystalline state. Right: Typical curve for viscosity as a function of temperature for a soda-lime-silica melt (NIST Standard No. 710). Defined viscosity points are indicated on the figure. Source: (Shelby 2005). 70
- 2.18 Approximate viscosity versus temperature curves plot for the most characteristic glass families described in tables 2.1 and 2.2 based on (Shand,Armistead 1958). 71
- 2.19 Schematic representation of the annealing temperature as a function of time for glasses of different volume by (Schott AG 2004). 71
- 2.20 Typical annealing scheme for commercial soda-lime glasses. 72
- 2.21 Qualitative analysis of strain concentration by polarization test. Bricks such as the ones shown on the right have a clear indication of residual stresses. Elements with grey-scale spectral composition, such as the one on the left, have low residual stresses. 73
- 2.22 Illustration of the most common mould types. 74
- 2.23 Disposable mould out of plaster and silica sand. 76
- 2.24 High precision open steel moulds used for the manufacturing of the glass blocks for the *Crystal Houses* façade. 77
- 2.25 Adjustable graphite mould at *John Lewis Glass Studio* for the components of the *Ice Falls* project by *James Carpenter*. 77
- 2.26 Cast steel node, designed by Arup, made in 3D-printed sand mould. Source: Arup/ Davidfotografie. 78
- 2.27 3D-printed sand moulds produced by *ExOne* and the resulting cast glass components for a topologically optimized cast glass grid-shell node by (Damen 2019) (left and top right) and for a structurally optimized cast glass column by (Bhatia 2019) (bottom right). 78
- 2.28 Schematic representation of the structure of soda-lime silica glass based on (Louter 2011).
Left: 3D schematic representation of a tetrahedral module built from one silicon and 4 oxygen atoms.
Right: 2D schematic representation of the irregular network of soda-lime silica glass. 79
- 2.29 Main glass flaw regional categories. Source: (Molnár et al. 2012) 82
- 2.30 Inclusion flaws in glass. From left to right: Bubbles, stones and cord. Source: (Molnár et al. 2012) and own image (right). 83
- 2.31 Early piece of float glass from the *Pilkington* archive demonstrating large bubbles across the entire ribbon prior to the introduction of a fully standardized/automated process and a strict automated control of flaws and inclusions. Over the last decades, float glass has seen great developments in both infrastructure and control technology. Yet, for cast glass these aspects still remain at an earlier stage of development. Source: (Bricknell 2010) 85
- 3.1 The 5 m glass mirror blank of the *Mt. Palomar* telescope. Source: Collection of the Rakow Research Library, The Corning Museum of Glass (number: 1000093965). 93
- 3.2 Fused-silica prototype of the *Hubble* blank at the *Corning Museum of Glass*. 95
- 3.3 Disposable mould for the blanks of the *Giant Magellan Telescope* built within the bottom part of the rotating kiln at the *Steward Observatory* in Arizona. 96
- 3.4 Right: Lead glass block. Left: Radiation shield made of multiple lead blocks. Source: *Corning Fontainebleau*. 97

- 3.5 Solid glass sculptures by artist *Roni Horn* 98
- 3.6 A human-scale cast glass piece by artist *Karen le Monte* at the *Corning Museum of Glass* 98
- 3.7 The 1.4 t cast component of the *Denis Altar*. Source: *Thierry Dannoux, Corning* 99
- 3.8 Evolution of the cast mirror blanks in size and annealing times (Zirker 2005) due to smart geometry and improved manufacturing process. 101
- 3.9 Segment of the *Giant Magellan's* blank at the *Steward Observatory, Arizona*. 101
- 3.10 The 5 m glass mirror blank of the *Mt. Palomar Hale* telescope. Source: Collection of the *Rakow Research Library* (number: 1000093961) 103
- 4.1 Characteristic examples of structures employing cast glass blocks: The *Atocha Memorial* (left), *Crystal Houses* (centre), and the *Crown Fountain* (right). 109
- 4.2 Illustration of the structural systems currently developed for structures using cast glass components. 110
- 4.3 The transition of the light rays through multiple media in a hollow glass block results in much more distortion compared to a solid glass block. 111
- 4.4 The *Optical House*. Source: *Koji Fujii / Nacasa & Partners Inc.* 114
- 4.5 Cast glass block unit of the *Optical House*. Source: *Hiroshi Nakamura & NAP*. 114
- 4.6 Assembly of the *Optical House*. Source: *Hiroshi Nakamura & NAP*. 115
- 4.7 Detail drawings of the *Optical House's* glass block system. Drawing courtesy: *Hiroshi Nakamura & NAP*. 115
- 4.8 The two *Crown Fountain* towers at night. 116
- 4.9 The *Atocha Memorial*. Source: *Esaú Acosta (FAM Arquitectura y Urbanismo)* 117
- 4.10 Plan and details of the *Atocha Memorial* glass structure. Source: *Bellapart*. 118
- 4.11 Glass block unit of the *Atocha Memorial*. 118
- 4.12 Construction of the *Atocha Memorial*. Source: *Bellapart, SAU*. 119
- 4.13 *Crystal Houses* façade, Site elevation. Source: *MVRDV architects* 120
- 4.14 Diagram indicating the properties and dimensional accuracy of a normal-size glass brick for the *Crystal Houses* façade project. Source: *MVRDV architects*. 120
- 4.15 Left: 3D visualization of the *Crystal Houses* façade by *MVRDV Architects*. Right: The realized façade. 121
- 4.16 Solid glass blocks used for the construction of the *Crystal Houses* façade. 122
- 4.17 Qualitative stress analysis through cross polarization. Bricks with clear indication of stresses (left) were discarded. Specimens with no visible strain concentration (right) were employed in the façade. 123
- 4.18 Bonding and curing of the adhesive at the *Crystal Houses* façade. 123
- 4.19 Prototype of a 3 mm thick, cast interlayer from PU70 (Oikonomopoulou et al. 2018). 124
- 4.20 Visualization (top) and a tested glass block prototype (bottom) of the dry-stacked glass arch bridge concept developed by (Snijder et al. 2016). 125
- 4.21 Evolution of interlocking cast glass blocks towards more curved geometries of equal mass distribution. From left to right: interlocking glass brick inspired by the *LEGO®* block by (Barou et al. 2016), osteomorphic block by (Jacobs 2017) and osteomorphic blocks by (Oikonomopoulou et al. 2018a) 126
- 4.22 Physical prototypes of a two-component interlocking geometry by (Oikonomopoulou et al. 2018b). 126

- 4.23 Physical prototypes of different interlocking geometries by (Oikonomopoulou et al. 2018b). 127
- 4.24 Top left to bottom right: Glass block units employed in the *Optical House*, *Atocha Memorial*, *Crystal Houses* façade and the interlocking research. 129
- 5.1 Illustration by MVRDV of the concept behind the *Crystal Houses* façade. 137
- 5.2 Left: 3D visualization of the *Crystal Houses* façade by MVRDV Architects. Right: The realized façade. 138
- 5.3 Schematic illustration of the applied buttress system. 139
- 5.4 Basic structural scheme of the proposed system 139
- 5.5 Schematic illustration of the relation between a stiff adhesive's strength and thickness by (Riewoldt 2014; den Ouden 2009; Wurm 2007). 143
- 5.6 Common flaws occurring in the adhesive layer: air gaps, capillary action and dendritic patterns. 144
- 5.7 Photographs of the three mock-ups. Mock-up A was made with higher tolerances. As a result there were significant offsets in both height and width, as well as open joints between blocks. Mock-up B was made with blocks of higher accuracy that prevented a substantial offset in height. Still, any unevenness up to ± 0.5 mm in flatness resulted to cavities and bubbles in the bond area. In mock-up C all blocks meet the ± 0.25 mm tolerance, resulting in an even spread of the adhesive and thus, in homogeneous bonding and satisfactory visual result without any cavities and bubbles of substantial dimensions. 144
- 5.8 The final (4th) wall mock-up which includes the buttress's construction by interlocking glass blocks 145
- 5.9 Left: the 300 x 200 x 70 mm borosilicate glass block of the *Atocha Memorial* made by press mould. Centre: a 210 x 105 x 65 mm soda-lime glass block of the *Crystal Houses* prior to post-processing. Right: a 210 x 105 x 65 mm soda-lime glass block of the *Crystal Houses* after post-processing. 147
- 5.10 Size and annealing time of the *Crystal Houses* blocks (left and centre) and of the *Atocha Memorial* block (right). 148
- 5.11 Optical transmittance data of a standard *Poesia* brick by (Tijssen 2014). 148
- 5.12 Overview of tests and of the various dimensions, composition and number of specimens. 150
- 5.13 Set-ups of the compression tests on single glass blocks. 151
- 5.14 Dimensions and experimental set-up of the glass pillars. 152
- 5.15 Experimental set-up of the 4-point bending tests 153
- 5.16 Illustration of the 4-point bending experimental set-up 154
- 5.17 Dimensions and experimental set-up of the glass architrave 155
- 5.18 4-point bending set-up of the architrave 155
- 5.19 Schematic illustration of the hard body test set-up. 156
- 5.20 Set-up of the hard body impact and vandalism test 157
- 5.21 Illustration of the four different thermal shock tests 158
- 5.22 Compression tests of glass blocks. Top left: Test set-up for the first two series. Bottom left: Test set-up for the specimens of the third series with plywood as intermediary. Right: Typical initial crack pattern in specimen. 160

- 5.23 Left: B_{NS} column prior to testing. Centre left: Initiation of crack. Centre right: Same specimen at complete failure. Right: Intact piece of the tested specimen after failure: the principal crack essentially propagated vertically, defying the adhesive joints. 162
- 5.24 The glass column specimens after testing. Left two pictures: B_{NS} specimens. Right two: B_{NL} specimens 162
- 5.25 Left: Experimental set-up. Right: Typical failure mode (Specimen C_3) 164
- 5.26 Typical failure mode of specimens, a clear, vertical cut at the middle of the beam. 164
- 5.27 Illustration of the breaking pattern of the tested specimen 165
- 5.28 The architrave specimen after failure. 166
- 5.29 Top: Result of the first vandalism test. Bottom left: Following, the vandalism test was repeated to an adjacent brick. Again, only the aimed block was damaged. Bottom right: The prototype after the replacement of one of the damaged blocks. 168
- 5.30 Specimens of the F_1 and F_2 series tested in thermal shock from 80 °C to 20 °C. Left: Cracks in the specimens immediately after they were removed from the water. Right: Growth of the cracks in the same specimens after approx. one day. 170
- 6.1 Left: The high precision, open steel moulds. Right: Molten glass bricks during the rapid cooling phase from 1200°C to ~700°C degrees. 182
- 6.2 Qualitative analysis of strain concentration by polarization test. Bricks such as the ones shown on the left image, with a clear indication of residual stresses, were discarded. Specimens such as the one on the right, with no visible considerable strain concentration, were employed in the façade. 184
- 6.3 Glass bricks of 210 mm x 210 mm x 65 mm coming out of the annealing oven after circa 36-38 h. The natural shrinkage is visible on the top surface. 184
- 6.4 Glass bricks rapidly cooled down to the annealing point in vertical orientation. The natural shrinkage is evident besides the top surface, also across the larger surfaces. 185
- 6.5 The jig used in the first dimensional control. 186
- 6.6 Set-up of the second control for checking the height and flatness of the components. 186
- 6.7 Left: A minor crack on a brick's bonding surface. Right: The propagation of such a minor crack after the curing of the adhesive. 187
- 6.8 The masonry wall was already constructed prior to the glass elevation. 188
- 6.9 Left: the installed aluminium place holders of the opening. Right: The mast climbing working platform and one of the three mobile elevated platforms. 189
- 6.10 On the left the bolts used for levelling the stainless steel plate, seen on the right. 190
- 6.11 Principle of the developed levelling system. 191
- 6.12 Bricks of a new row laid down prior to bonding (left). Afterwards, a feeler gauge is used for checking the thickness of the resulting seam (right). The blade of the feeler gauge is sufficiently flexible and round not to induce any surface damage on glass. 192
- 6.13 *PURE*® mould used for the application of the adhesive on the final façade wall. 192
- 6.14 Bonding steps from left to the right: 1. Application of the adhesive with the aid of the *PURE*® form. 2. Resulting X pattern. 3. Local hardening of the adhesive by a UV beam light for preventing capillary action. 4. UV-lamp used to cure the adhesive for 60—120 seconds. 193
- 6.15 Left: Sealing of the already bonded bricks. Right: the final, visual result achieved by the novel bonding method. 194
- 6.16 The top connection is completely masked by the ceramic strips. 194

- 6.17 Left: The special rotating fixture for the preassembly of the architraves. Right: The installation of the bonded architraves on site. 195
- 6.18 Practical implications were encountered when combining terracotta and glass blocks. 196
- 6.19 Left: Bonding of the ceramic strips to the shorter bricks. Right: The final visual result. 197
- 6.20 End result of the intermixing, gradient zone. 197
- 6.21 From left to right: Bonding of the steel plate to the corner brick. Positioning of the brick by a suction cup holder. Application of the semi-elastic polymer. 198
- 6.22 The graphite moulds used for the fabrication of the frames. 199
- 6.23 Left: The simultaneous application of the polymer from both sides. Centre and right: The final result of the bonded glass frames. 200
- 6.24 The completed *Crystal Houses* façade. Source: *MVRDV Architects / Image copyright: Daria Scagliola and Stin Brakkee*. 202
- 7.1 Principle of interlocking and topological interlocking systems 213
- 7.2 Interlocking wall made by the Incas at Ollantaytambo, Peru. 213
- 7.3 Proposed type of peripheral constraint by (Dyskin et al. 2019). Left: lateral constraint imposed by a specially built frame. Right: constraint produced by internal tensioned cables 216
- 7.4 Interlocking glass block systems currently explored. Top: Tested prototype of the glass arch bridge by (Snijder et al. 2016). Bottom left: Glass column by (Akerboom 2016). Bottom right: Interlocking glass wall system developed by Oikonomopoulou, Bristogianni and Barou for the *3TU.bouw* project *Restorative Glass*, presented in (Oikonomopoulou et al. 2017a). 218
- 7.5 Overview of the established design criteria. The double arrows indicate the alignment between the two different sets of criteria, due to casting and due to interlocking 221
- 7.6 Developed interlocking designs 221
- 7.7 Step-by-step process of the lost wax technique employed for the casting of the prototypes. 223
- 7.8 Kiln-casting method employed at the lab for the casting of prototypes. 223
- 7.9 Illustration of the kiln-casting method employed to manufacture the glass interlocking prototypes. 223
- 7.10 Osteomorphic blocks. Left: Type A. Right: Type B 224
- 7.11 Type C Prototype. The bone-shaped components are made of recycled coloured glass. 225
- 7.12 Type D prototype made of clear glass, recycled float glass (teal) and recycled Cathode Ray Tube (CRT) screen (black). 226
- 7.13 Prototype using E1 and E2 glass blocks from clear glass and recycled mouth-blown coloured glass. 226
- 7.14 Possible structural geometries using osteomorphic blocks (Type A). 228
- 7.15 Prototype with osteomorphic blocks made using various types of waste glass, exhibited at the *Dutch Design Week 2018* 228
- 7.16 Diagram of the shore hardness scales, including an indication of the shore hardness of common objects 230
- 7.17 Cast PU interlayer following the osteomorphic geometry of the cast blocks. 233
- 7.18 Principle of circular use of glass in dry-assembled interlocking structures by the *Re³ Glass* project. 234
- 7.19 Rough illustration of the current glass recycling scheme in the Netherlands and the *Re³ Glass* proposal. 237

- 7.20 Proposal for a borosilicate recycling scheme by (Scholtens 2019). 238
- 7.21 Prototypes of the Type A osteomorphic topology made of recycled artware glass (blue), CRT screens (black), float glass (light blue) and optical lenses (clear) within the context of the Re³ Glass project. 239
- 7.22 Prototypes of the Type C topology made from the re-melting of different types of glass waste within the context of the Re³ Glass project. 240
- 7.23 Prototypes of the E typology made from the mixing of different colours of recycled art (lead) glass. 242
- 8.1 Firing schedule followed for the kiln-casting and annealing of the osteomorphic blocks. 252
- 8.2 From left to right: Arrangement of the glass-containing flowerpots above the crystal cast moulds and set-up of the kiln; View of the kiln at 970°C; Kiln-cast osteomorphic blocks prior to mould removal. 252
- 8.3 Two-part 3D-printed mould out of PLA for casting the interlayers. 254
- 8.4 Prototype of a 3 mm thick, cast PU interlayer. 254
- 8.5 Experimental set-up 255
- 8.6 Labelling principle of the specimens 255
- 8.7 Schematic illustration and overview of the three series of experiments under compressive load on interlayers. 255
- 8.8 Prototype with 70A interlayer of 3 mm thickness (left) and of 6 mm thickness (right). 256
- 8.9 Typical Y breaking pattern originating at the shortest section of the block (specimen 80A₁) 258
- 8.10 Possible explanation of the cause of failure of the specimens interleaved with *PMC770* (70A) and *Task 16* (80A). 258
- 8.11 75A specimen after the test was aborted due to visible tearing of the interlayer. 260
- 8.12 Typical glass failure originating at the edge of the assembly caused by the perforation/tearing of the interlayer (specimen 60A₁) 260
- 8.13 Specimen 60A₃ after the completion of the test. There is evident plastic deformation. 260
- 8.14 One of the 80A interlayer specimens during (right) and after (left) testing. No visible plastic deformation was observed. 261
- 8.15 Displacement in time graph of 70A_{3,x} and 80A_{3,x} specimens (left) and processed so that only the deformation in time under the static 40 kN load is shown (right) 261
- 8.16 Failure mode of glass specimen without the use of an interlayer. 262
- 8.17 Displacement in time ($u - t$) graph for the 70A and 80A 6 mm thick specimens tested to 40kN load for 900 s (left) and processed so that the deformation in time is shown only during the static 40 kN load (right). 263
- 8.18 Displacement in time ($u - t$) graph for the 80A interlayer specimens of 3 mm and 6 mm thickness tested under 40 kN load for 900s (left) and processed graph so that the deformation in time is shown only during the set 40kN constant load (right). 265
- 8.19 Displacement in time ($u - t$) graph of 70A interlayer specimens of 3 mm and 6 mm thickness tested under a static 40 kN load for 900 s (right) and processed graph so that the deformation in time is shown only during the static 40 kN load (right). 265
- 8.20 Displacement in time ($u-t$) graph for 70A interlayer specimens, 6 mm thick tested under 20 kN (70A_{6,1} - 70A_{6,3}) and 40 kN (70A_{6,4} - 70A_{6,6}) load for 900s (left) and processed graph so that the deformation in time is shown only during the set constant loads (right). 265
- 8.21 A 6 mm thick 70A specimen before (left) and during (right) resting under 40 kN constant load 266

- 8.22** A 6 mm thick 70A specimen, before (left) and during (right) testing under 40 kN constant load. [266](#)
- 8.23** Visible plastic deformation of 70A specimen directly after the completion of the test. [266](#)
- 8.24** Assemblies (without the use of an interlayer) of blocks with the different examined amplitudes. [270](#)
- 8.25** Illustration of the experimental set-up. [271](#)
- 8.26** Experimental set-up [271](#)
- 8.27** Displacement – Standard Force diagram for all specimens [272](#)
- 8.28** Maximum deformation prior to failure of assemblies with blocks of 10 mm (left), 15 mm (center) and 20 mm (right) amplitude. The tests with blocks of 10 mm amplitude were aborted once the assembly reached an apparent deformation of 25 mm. [274](#)
- 8.29** Assembly of block with 10 mm amplitude before (left), during (centre) and after testing (right). It can be seen that upon load removal the assembly is self-realigned towards its original configuration. [274](#)
- 8.30** Specimen out of blocks with 15 mm amplitude before testing (top left); at max. deformation (top right); and after failure (bottom left and right). [276](#)
- 8.31** Specimen out of blocks with 20 mm amplitude before testing (top left); at max. deformation (top right); and after failure (bottom left and right) [276](#)
- 8.32** Specimens out of blocks with 20 mm amplitude after testing. It is evident that the crack in adjacent blocks are not continuous. [277](#)
- 8.33** Numerical model (Type B block) vs experimentally tested block (Type A). [278](#)
- 8.34** Definition of block height and amplitude height. [278](#)
- 8.35** Left: Numerical set up and results for Christensen's failure criterion value of one (SCH=1) of the tested variants. Right: Christensen's output (SCH=1) of middle brick (amplitude 10 mm). Shear capacity at failure is approximately 155 kN. Source:(Jacobs 2017). [280](#)
- 8.36** (left) 2D Full scale principle of the model. Source:(Jacobs 2017). [280](#)
- 8.37** (right) Uplifting principle for interlocking blocks with A=5 mm and A=20 mm. The shear force is depicted as a concentrated force (F) halfway the amplitude. Dead weight and weight of upper structure are not accounted for. The force is conveyed in an uplifting force (Ff) by traction tangent to the steepness at that point and in a force (Fn) by compression normal to the geometry. Source:(Jacobs 2017). [280](#)
- 8.38** Support conditions in a) Z-direction, b) Y-direction and c) X-direction. d) Tied vertexes loaded with a prescribed deformation load. Source: (Jacobs 2017) [283](#)
- 8.39** Shear capacity and deformation at failure of the different variants. Source: (Jacobs 2017) [285](#)
- 8.40** Influence of amplitude on shear capacity, uplifting force (parallel to interlock curvature) and reaction forces. The prediction lines are based on hand calculations described in (Jacobs 2017). [286](#)
- 8.41** Contour plots at failure load for various amplitude variations, demonstrating the stress redistribution of the given geometries. For the failure loads of each amplitude variation refer to Fig. 8.39. Source: (Jacobs 2017) [286](#)
- 8.42** The effect of the height on the shear capacity of the brick plotted together with the expectations from hand calculations. Source: (Jacobs 2017). [287](#)

Curriculum Vitae



- 1984** Born in Athens, Greece
- 2002 - 2008** Diploma of Architect Engineer (MSc), National Technical University of Athens (NTUA)
- 2008 - 2009** Architect Engineer at AR.TE Architecture Studio, Greece / Travel article contributor at GEOTropio Magazine, Greece
- 2010 - 2012** Master of Science in Building Technology (MSc), TU Delft
- 2013** Researcher at Structural Mechanics & Design Chair, TU Delft
- 2014 - present** Researcher/Lecturer at Structural Mechanics & Design Chair, Dept. of Architectural Engineering & Technology, TU Delft

Faidra (*Phaedra*) Oikonomopoulou was born on 1984 in Athens, Greece. In 2009 she graduated with a diploma (*MSc*) of Architect Engineer from the Faculty of Architecture at the *National Technical University of Athens* [NTUA], ranking among the top students in her class. For the coming one year she worked both as an architect engineer in Athens and as a travel article contributor. In 2010 she followed a second master degree in Building Technology at the *Delft University of Technology*. It was her MSc thesis initiative that introduced her to glass as a structural material: "*The design of a fully glass pavilion for the Temple of Apollo Epikourios in Peloponnese*". She proudly presented the findings of her thesis in *Challenging Glass 3 Conference*. Following her graduation in 2012, Faidra embarked on an adventure in Namelok, a Maasai village in Kenya, to work on the use of mud bricks for construction and pursue her other big passions: travelling and wildlife spotting. Many elephants and lions later she returned to Delft as a researcher for a project on *innovative glass joints*, followed by a six-month internship in an engineering office specializing in structural glass applications in Athens.

In 2014 Faidra returned to Delft to work on a glass project that she knew little about: the *Crystal Houses Façade*. Faidra was the lead PhD researcher on the research and development of the applied adhesively bonded system. After approximately one and a half years of research and experimental work, together with colleague Telesilla Bristogianni they supervised the construction of the *Crystal Houses* façade and even built together with the construction crew the first 1.5 meter of the glass wall. For her work in the *Crystal Houses* Faidra has co-received multiple awards, including the *Innovation Award 2016* by the Society of Façade Engineers and the *Talent met Toekomst 2017*. Through the *Crystal Houses* façade project Faidra discovered the architectural potential of cast glass, but also saw the engineering challenges involved. Together with Telesilla they have been awarded two *4TU. Bouw Lighthouse* grants for innovative research on cast glass and their research on recycled cast glass building components was nominated for the New Material Award 2018.

Faidra pursued her PhD degree while working as a Researcher/Lecturer at the *Architectural Engineering + Technology Department* of the *Faculty of Architecture at Delft University of Technology*. Currently Faidra is employed as a Senior Researcher & Lecturer at the same department, where she continues her research on structural cast glass. Faidra has given invited talks and workshops on the structural potential of cast glass in several institutions, universities and companies in Europe and USA. Her vision is to create circular, load-bearing and aesthetically intriguing cast glass structures. Meanwhile she continues pursuing her other big passions as well, by travelling all over the world and encountering rare animals in the wild.

List of Publications

Journal articles

Oikonomopoulou, F., Bristogianni, T., Barou, L., Veer, F., Nijse, R., 2018. The potential of cast glass in structural applications. Lessons learned from large-scale castings and state-of-the art load-bearing cast glass in architecture. *Journal of Building Engineering*, 20, p.213-234.

Oikonomopoulou, F., Bristogianni, T., Barou, L., Jacobs, E., Frigo, G., Veer, F., Nijse, R., 2018. Interlocking cast glass components, exploring a demountable dry-assembly structural glass system. *Heron*, 63 (1/2), p.103-138.

Bristogianni, T., Oikonomopoulou, F., Justino de Lima, C., Veer, F., Nijse, R., 2018. Structural cast glass components manufactured from waste glass: Diverting everyday discarded glass from the landfill to the building industry. *Heron*, 63 (1/2), p.57-102.

Barou, L., Oikonomopoulou, F., Bristogianni, T., Veer, F., Nijse, R., 2018. Structural glass: A new remedial tool for the consolidation of historic structures. *Heron*, 63 (1/2), p. 159-198.

Oikonomopoulou, F., van den Broek, E., Bristogianni, T., Veer, F., Nijse, R., 2017. Design and experimental testing of the bundled glass column. *Journal of Glass Structures & Engineering*, 2 (2), p.183-200.

Oikonomopoulou, F., Bristogianni, T., Veer, F., Nijse, R., 2017. The construction of the Crystal Houses façade: challenges and innovations. *Journal of Glass Structures & Engineering*, 3 (1), p.87-108.

Oikonomopoulou, F., Baardolf, K., Veer, F., Nijse, R., 2014. A completely transparent, adhesively bonded soda-lime glass block masonry system. *Journal of Façade Design and Engineering*, 2 (3-4), p.201-221.

Conference Papers

Oikonomopoulou, F., Bristogianni, T., Louter, C., Veer, F., Nijse, R., 2019. Education on Structural Glass Design: Redefining glass through the design of innovative, full-glass structures. *ICSA 2019 Conference Proceedings, Lisbon, Portugal*.

Oikonomopoulou, F., Bristogianni, T., Barou, L., Veer, F., 2019. Dry interlayers out of cast polyurethane rubber for interlocking cast glass structures: experimental exploration and validation. *SEMC 2019 Proceedings, Cape Town, South Africa*.

Bristogianni, T., Oikonomopoulou, F., Veer, F., Nijse, R., 2019. The effect of manufacturing flaws in the meso-structure of cast glass on the structural performance. *SEMC 2019 Proceedings, Cape Town, South Africa*.

Oikonomopoulou, F., Bristogianni, T., Barou, L., Jacobs, E., Frigo, G., Veer, F., Nijse, R., 2018. A novel, demountable structural glass system out of dry-assembly, interlocking cast glass components. *Challenging Glass 6 Conference Proceedings, Delft, The Netherlands, p.71-82*

Bristogianni, T., Oikonomopoulou, F., Justino de Lima, C., Veer, F., Nijse, R., 2018. Cast Glass Components out of Recycled Glass: Potential and Limitations of Upgrading Waste to Load-bearing structures. *Challenging Glass 6 Conference Proceedings, Delft, The Netherlands, p. 151-174*.

Vitalis, D., Veer, F., Oikonomopoulou, F., 2018. Design and experimental testing of all glass sandwich panels. An experimental and numerical study for the glass floors of the Acropolis museum. *Challenging Glass 6 Conference Proceedings, Delft, The Netherlands, p.251-270*.

Barou, L., Oikonomopoulou, F., Bristogianni, T., Veer, F., Nijse, R., 2018. Dematerialization of the ruins: Glass as a promising restorative material for the consolidation of historic structures. *Challenging Glass 6 Conference Proceedings, Delft, The Netherlands, p. 11-26*.

Oikonomopoulou, F., van den Broek, E., Bristogianni, T., Veer, F., Nijse, R., 2017. Design and experimental testing of the bundled glass columns. *Glass Performance Days 2017 Conference Proceedings, Tampere, Finland, p.141-142*.

Bristogianni, T., Oikonomopoulou, F., Veer, F., Snijder, A., Nijse, R., 2017. Production and Testing of Kiln-cast glass components for an interlocking, dry-assembled

transparent bridge. *Glass Performance Days 2017 Conference Proceedings, Tampere, Finland, p.101-106.*

Oikonomopoulou, F., Karron, K., Bristogianni, T., Groot, C., Veer, F., Nijssse, R., 2016. Restoring and structurally reinforcing historic monuments by glass. *Proceedings of the Sixth International Conference on Structural Engineering, Mechanics and Computation (SEMC), Cape Town, South Africa, p.593-595.*

Bristogianni, T., Oikonomopoulou, F., Veer, F., Nijssse, R., 2016. Design and production of a structural cast glass element for a transparent dome. *Proceedings of the Sixth International Conference on Structural Engineering, Mechanics and Computation (SEMC), Cape Town, South Africa, p.591-593.*

Oikonomopoulou, F., Bristogianni, T., Veer, F., Nijssse, R., 2016. Developing the bundled glass column. *Structures and Architecture - Beyond their limits, Proceedings of the 3rd International Conference on Structures and Architecture (ICSA), Guimaraes, Portugal, p.1014-1021.*

Oikonomopoulou, F., Bristogianni, T., Veer, F., Nijssse, R., 2016. Challenges in the Construction of the Crystal Houses Façade. *Challenging Glass 5 Conference Proceedings, Gent, Belgium.*

Oikonomopoulou, F., Bristogianni, T., Veer, F., Nijssse, R., 2015. Innovative structural applications of adhesively bonded solid glass blocks. *Glass Performance Days 2015 Conference Proceedings, Tampere, Finland, p.256-261.*

Veer, F., Oikonomopoulou, F., Bokel, R., 2012. Designing a glass pavilion to protect an ancient Greek temple. *Challenging Glass 3 Conference Proceedings 2012, Delft, The Netherlands*

Oikonomopoulou, F., Veer, F., Bokel, R., 2012. Pure Transparency / Designing a complete glass shelter for the temple of Apollo Epikourios at Bassae. *COST Structural Glass Training School (TU0905) Proceedings, Gent, Belgium.*

Prizes & Awards related to the PhD research

- 2019** – *Honourable Award by Bouwerend Netherlands* for the contribution to innovative research on structural glass of the *Glass & Transparency Research Group* of TU Delft – as member of the Glass & Transparency Research Group.
- 2018** – *New Material Award 2018 Nominee*, by Het Nieuwe Instituut, Fonds Kwadraat & Stichting Doen for the *Re³ Glass project* - Conjoined award with ir. T. Bristogianni
- *Best Presentation Award* at *ICG Annual Meeting 2018*, Yokohama, Japan.
- 2017** – *Talent met Toekomst - Nederlandse Bouwprijs 2017* (“*Talent with future*” *Dutch construction engineering award*) for the contribution in the engineering and construction of the Crystal Houses façade - Conjoined award with ir. T. Bristogianni
- 2016** – *Outstanding Innovation Award 2016* awarded by the Society of Façade Engineers for the Crystal Houses façade - Conjoined award of TU Delft and ABT
- *Public Award* at *Dutch Design Awards 2016*, for the Crystal Houses façade - Conjoined award of MVRDV, TU Delft, ABT and Poesia
- *Innovation Award* at *Glas Award 2016*, by *Bouwend Nederland*, for the Crystal Houses façade - Conjoined award of MVRDV, TU Delft, ABT and Poesia
- *AE+T Award for Special Achievements*, Faculty of Architecture, TU Delft, for the Crystal Houses façade - Conjoined award with ir. Telesilla Bristogianni, prof. ir. Rob Nijssen, dr. ir. Fred Veer and Kees Baardolf

Unveiling the third dimension of glass

Solid cast glass components and assemblies for structural applications

Faidra Oikonomopoulou

Over the last decades, the perception of glass in the engineering world has changed from that of a brittle, fragile material to a reliable structural component of high compressive load-bearing capacity. Although the structural applications of glass in architecture are continuously increasing, they are dominated by a considerable geometrical limitation: the 2-dimensionality imposed by the prevailing float glass industry. Cast glass can overcome this limitation: solid 3-dimensional glass components of virtually any shape and cross-section can be made. Owing to their monolithic nature, such components can form robust repetitive units for the construction of free-form, all-glass structures that take full advantage of the compressive strength of glass; a solution little explored so far. Subsequently, there is a lack of design guidelines in the use of cast glass as a structural material. Scope of this research is, therefore, to investigate both the potential and the limitations of employing solid cast glass components for the engineering of transparent, 3-dimensional, glass structures in architecture. Accordingly, the design, development, prototyping and experimental validation of two distinct cast glass building systems for self-supporting envelopes, from unit level to the entire structure, are presented. First, an *adhesively-bonded solid glass block* system, using a colourless adhesive as an intermediary, is developed and applied in the *Crystal Houses* façade. Following, a *dry-assembly, interlocking cast glass block system*, employing a colourless dry interlayer, is explored as a reversible, circular solution. The results of this dissertation can serve as design guidelines for future structural applications of cast glass in architecture.